MOLECULAR IMAGING AGENTS FOR CATHEPSIN B

DESIGN, SYNTHESIS, AND EVALUATION OF MOLECULAR IMAGING PROBES FOR CATHEPSIN B

By PATRICIA E. EDEM, B.Sc., M.Sc.

A Thesis Submitted to the School of Graduate Studies in Partial Fulfilment of the Requirements for the Degree of Doctor of Philosophy

Ph.D. Thesis – Patricia Edem; McMaster University – Chemistry & Chemical Biology.

McMaster University DOCTOR OF PHILOSOPHY (2015) Hamilton, Ontario (Chemical Biology)

TITLE: Design, Synthesis, and Evaluation of Molecular Imaging Agents for Cathepsin B AUTHOR: Patricia E. Edem, B.Sc. (Dalhousie University), M.Sc. (McMaster University) SUPERVISOR: John F. Valliant NUMBER OF PAGES: xxx, 266

Abstract

Cathepsin B is a cysteine protease that is overexpressed in cancers that are likely to metastasize. Molecular imaging can be used to non-invassively detect cathepsin B *in vivo* in order to characterize cancer progression and treatment response. This thesis describes the development of four different strategies to develop cathepsin B targeted probes. First, an SAR strategy was used to synthesize and test a number of AOMK inhibitors that incorporated iodine. A high affinity (K_i = 180 nM) lead **2.23a** was converted to its radioactive analogue [^{125}I]**2.23a** by optimizing radiolabelling procedures to maximize radiochemical yields (>26%) and radiochemical purities (> 95%). *In vivo* evaluation showed low tumour uptake (0.05% at 23 h p.i.) due to high *in vivo* deiodination (thyroid = 20% ID/g at 23 h p.i.).

Next, AOMK inhibitors with greater stability were developed using the $[ReCO_3]^+$ core either via a direct linkage or a dendrimer platform. The binding affinities of these probes were lower than **2.23a** (K_i > 350 nM). A pretargeted approach was then developed that could be used to image cathepsin B *in vitro* and *in vivo*.

Third, an affinity label was developed using the AOMK warhead linked to TCO giving **4.5** (K_i = 190 nM). A cell assay was developed and intracellular targeting of cathepsin B was observed, something that has

not been observed previously with a pretargeted agent in nuclear medicine. Of the five tetrazine based bioorthogonal pairs tested with **4.5**, three were sufficient for this approach.

The final approach was to use a cathepsin B substrate to link a radiopharmaceutical such as an iodobenzamide used for melanoma imaging. Synthetic strategies were explored to develop the radioactive and non-radioactive analogues. Challenges were encountered during the development of these probes due to stability, which require further optimization.

Acknowledgements

Over the course of my graduate studies I have come in contact with so many people that have contributed to my success in both a professional and personal capacity. I would like to start by acknowledging my supervisor Dr. John Valliant. When I joined this research group I had very little experience working in a synthetic organic lab and even less experience with biological analysis. Despite this I was entrusted with challenging dynamic project and encouraged to take on a leadership role. This responsibility helped me adopt the strong leadership skills and self-confidence to take on challenging scientific projects. I was also given the opportunity to travel to prestigious international conferences to discuss my work with some of the top scientists in the field, futhering my communication skills and my network. For all of this I would like to thank John.

I would like to acknowledge my supervivory committee members Drs. Alex Adronov, and Paul Harrison their participation. I would also like to thank Dr. Alex Adronov and Lukas Sadowski for their research collaboration, and various scientific discussions.

The Valliant research group has been a great source of support throughout my studies. I have been able to work with numerous undergrads, grad students, and post docs from all over the world, who

have all contributed to my experience. I would like to extend special thanks to Dr. Chitra Sundarajan, Dr. Karin Stephenson, Mike Beer, and Dr. Laura Harrington for their help early on in my graduate studies; Dr. Anika Louie for her countless advice and presentation tips; Dr. Silvia Albu and Salma Al-Karmi for numerous scientific disscussions and support - working on similar projects my research would not have been the same without them; and I would also like to thank Dr. Antonio Toppino, Omid Beiraghi, Reza Yazdani, Teri Gullon, and Justin Hicks not only for their help in the lab but their friendship.

I would like to thank the various members from the Department of Chemistry and Chemical Biology, noteably Tammy Feher, Dr. Fred Capretta, Dr. Kirk Green, Connie Carabs, Nancy McKenzie, Dr. Don Hughes, and Dr. Brian McCarry. And of course the many friends I have made during my time here. I have been very lucky to go through graduate school surrounded by such a great group of people – without you guys it wouldn't have been the same ☺.

I have been lucky to be influenced by a number of educators during my path to a career in chemistry, beginning with my high school chemistry teachers: Mrs McLellan (née Delaney) and Mr. Crosby; to my undergraduate research supervisor: Dr. Neil Burford. I want to thank them

all for helping me develop an interest and passion for chemistry and research.

Most importantly I would like to thank my family. The lessons and beliefs that they have instilled in me from a young age have enabled me to tackle any challenge in life without hesitation or self-doubt. My uncle, Dr. Okechuckwu Ikejiani has been a great influence not only on me, but my entire family. The last piece of advice he gave to me was to persue a doctorate degree. His leadership, wisdom, and kindness will be treasured and missed. Thanks to my little sister Theresa Edem for always reminding me of my Nova Scotian self. And thanks to my mother Dorothy Edem for her everlasting love, encouragement, support, and all of the sacrifices she has made for my sister and I to go forward in life. Nothing was possible without her. Thanks all – You are all amazeballs <3.

Table of Contents

List of Figures

List of Tables

List of Schemes

List of all Abbreviations and Symbols

[^{18}F]FAZA	^{18}F-fluoroazomycin arabinoside
[^{18}F]FDG	2-deoxy-2-[^{18}F]-fluoro-D-glucose
[^{18}F]FMISO	^{18}F-fluoromisonidazole
ABP	activity based probe
AOMK	acyloxymethyl ketone
BLI	bioluminescence imaging
Boc	*tert*-butoxycarbonyl
BODIPY	boron-dipyrromethene
BSGI	breast specific γ-imaging
CA-074	L-3-*trans*-(propylcarbamyl)oxirane-2-carbonyl)-L-isoleucyl-L-proline
CCD	charge-coupled device
CPI	cysteine protease inhibitors
cRGD	cyclic arginine-glycine-aspartic acid
CT	computed tomography
CuAAC	copper catalyzed azide-alkyne cycloaddition
DMAP	4-dimethylaminopyridine
ECM	extracellular matrix
ER	estrogen receptor; endoplasmic reticulum
Fmoc	fluorenylmethyloxycarbonyl
FRET	Förster resonance energy transfer

FSPE	fluorous solid-phase extraction
GCase	β-glucocerebrosidase
GLUT	glucose transporter
HER2	human epidermal growth factor receptor 2
HIF	hypoxia-inducible factor
HPLC	high performance (pressure) liquid chromatography
HRMS	high resolution mass spectrometry
Hz	Hertz
IBCF	isobutyl chloroformate
ID/g	injected dose per gram
IEDDA	inverse electron demand Diels Alder
J	coupling constant
k_{cat}	turnover number
k_i	apparent inactivation rate
K_m	Michaelis-Menten constant
k_{obs}	observed rate constant
mAbs	monoclonal antibodies
MI	molecular imaging
MMP	matrix metalloproteinases
MRI	magnetic resonance imaging

Mtt	4-methyltrityl
NIR	near infrared fluorescence
NMI	nuclear molecular imaging
PABA	para-aminobenzyloxycarbonyl
PDA	photodiode array
PEM	positron emission mammography
PET	positron emission tomography; photoinduced electron transfer
p.i.	post-injection
PyBOP	benzotriazol-1-yl-oxytripyrrolidinophosphonium hexafluorophosphate
qABP	quenched activity based probes
ROS	reactive oxygen species
SAAC	single amino acid chelate
SBP	substrate based probe
SPECT	single photon emission computed tomography
T:NT	target to non-target ratio
TBET	through bond electron transfer
TCO	*trans*-cyclooctene
TFA	trifluoroacetic acid
TIMP	tissue inhibitors of matrix metalloproteinases
Tz	tetrazine

uPA	urokinase plasminogen activator
US	ultrasound
VEGF	vascular endothelial growth factor
Z-RR-pNA	Cbz-Arg-Arg-p-nitroanilide
Z-YA-DMK	Benzyl ((*S*)-1-(((*S*)-4-diazo-3-oxobutan-2-yl)amino)-3-(4-hydroxyphenyl)-1-oxopropan-2-yl)carbamate
α	alpha
β^+	positron
γ	gamma

Declaration of Academic Achievement

During my PhD studies, I started a new research initiative where I develop a nuclear molecular imaging agent that targets the cysteine protease cathepsin B (an enzyme overexpressed in highly aggressive cancers). I developed an SAR strategy to synthesize and test a number of cathepsin B inhibitors that incorporated iodine. Successful leads were converted to their radiolabelled analogues following optimization of the radiolabelling procedures to maximize radiochemical yields (>26%) and radiochemical purities (> 95%). *In vitro* and *in vivo* evaluations were subsequently performed on the radioactive analogues. Despite not being directly involved in the handling of the animals for the *in vivo* evaluation, I was heavily involved in designing the experiments, acquiring and analyzing the data. This work describes the first *in vivo* evaluation of radioiodinated probes for cathepsin B. I have presented this work at internal, national, and international conferences. The success of this work resulted in its publication in the Journal of Medicinal Chemistry and was highlighted in a recent review article.

As an extension of this project, an additional goal was to develop the first class of technetium based imaging probes for cathepsin B. This project involved the SAR development using a dendrimer platform. This project was done in collaboration with Prof. Alex Adronov and Lukas

Sadowski at McMaster University who had experience with polymer chemistry and in particular, dendrimers. Through this collaboration, I was able to facilitate various discussions and meetings in order share our expertise in polymer chemistry, enzymology, and radiochemistry. This work describes the first platform to develop ^{99m}Tc based imaging agents for cathepsin B. My role was to synthesize azide derived AOMK inhibitors and to evaluate the binding affinities of the subsequent dendrimer derivatives. Dr. Adronov, Lukas Sadowski, and myself have discussed this work in oral presentations at national conferences and a manuscript is currently in preparation for submission.

The third project was to develop a pretargeted approach that could be used to image cathepsin B *in vitro* and *in vivo*. The goal was to design a single pretargeting agent that could be used with an imaging partner for either optical or nuclear imaging. Through this work, I was able to develop an *in vitro* assay where I demonstrated intracellular targeting of cathepsin B. This work has recently been presented at an international conference.

Peer Reviewed Articles:

Edem, P. E., Czorny, S., Valliant, J. F. (2014) Synthesis and Evaluation of Radioiodinated Acyloxymethyl Ketone Inhibitors as Activity-Based Probes for Cathepsin B. *Journal of Medicinal Chemistry*, 57, 9564–77.

Peer Reviewed Abstracts:

Edem, P. E., Czorny, S., Valliant, J. F. (2013) Radioiodinated Inhibitors of Cathepsin B as Tumor Imaging Probes. *Journal of Nuclear Medicine 54* (S2), 1135. [Poster presented at the Society of Nuclear Medicine and Molecular Imaging 2013 Annual Meeting; Vancouver, Canada; June 2013.]

Edem, P. E., Valliant, J. F. (2011) Preparation and Evaluation of Halogenated and Metallated Cathepsin B Inhibitors as Molecular Imaging Agents. *Journal of Labelled Compounds and Radiopharmaceuticals* 54 (S1), S576. . [Poster presented at the 19th International Symposium on Radiopharmaceutical Sciences; Amsterdam, The Netherlands; August 2011.]

Edem, P. E., Valliant, J. F. (2010) Technetium-Labelled Cathepsin B Inhibitors as Molecular Imaging Agents. *Nuclear Medicine & Biology* 37, (6), 681. [Poster presented at the International Symposium on Technetium and Other Radiometals in Chemistry and Medicine; Bressanone, Italy; September 2010.]

Edem, P. E., Valliant, J. F. (2009) Discovery and Evaluation of a Potential Molecular Imaging Agent for Cathepsin B. *Journal of Labelled Compounds and Radiopharmaceuticals* 52, (S1), S134. [Poster presented at the 18th International Symposium on Radiopharmaceutical Sciences; Edmonton, Canada; July 2009.]

1 Introduction

1.1 Cancer Prevalence and Treatment

Cancer is the leading cause of death in Canada.[1] As of 2015 it is predicted that 2 in 5 Canadians will develop the disease at some point in their lifetime, while 1 in 4 Canadians with die as a result of the disease. It is predicted that 51% of new cancer cases will be due to lung, colorectal, breast, or prostate cancer.[1] Cancer is generally defined as out of control cellular growth where six criteria have been established to characterize the disease. They are: self-sufficient growth signals, resistance toward to biochemical growth inhibition signals, resistance to programmed cell death, sustained ability to multiply, ability to grow new blood vessels, and the ability to spread to other cells, tissues and organs.[2]

Cancer can have devastating effects on the emotional, physical and personal well being of an individual's life and there is also an economic burden on the healthcare system. It is estimated that cancer accounted for $3.8 billion to Canadian healthcare costs in 2008.[1] The majority of Canadians diagnosed with cancer are over 50 and the proportion of Canadians over 65 is predicted to continue to grow through to 2032.[1] This expected increase in the aging population is driving a greater demand for better cancer diagnostic and treatment tools.

The 5-year survival rate for those diagnosed with cancer is 63%, however this number varies drastically from one cancer to another (8% for pancreatic cancer to 98% for thyroid cancer).[1] Mortality rates for various cancers have declined in Canada since 1988 due to preventative and treatment measures.[1] Lung cancer and breast cancer have seen the strongest decline which can often be attributed to control on tobacco use and increase in breast cancer screening and treatment.[1]

Screening is the process where asymptomatic individuals who are likely to acquire a specific illness are identified. This identification comes at a time where intervention can still result in an improved prognosis.[3] The chance of survival is often related to the stage of the cancer at the time of diagnosis especially for breast and prostate cancers.[3,4] There is some controversy in attributing the decline in breast cancer mortality rates to increased screening because there are some associated biases that should be considered.

First, there is a lead-time bias, which is the time between the initial diagnosis due to screening and the point where the disease would have been present clinically without screening. In instances where intervention does not change the outcome, early prediction only increases the time during which the individual lives with the diagnosis, therefore the apparent

survival time is lengthened.[3] Secondly there is length-time bias where a tumour is detected that may never have been clinically present without screening. Some of these slow growing tumours are often treated despite the fact that they may have never resulted in a health concern.[3]

To avoid unnecessary costs to the healthcare system it is important not to over diagnose or over-treat non-threatening cancers, while the focus should be on cancers that pose the greatest imminent risks. In principle the optimal screening test should lead to a statistical increase in disease occurrence in the early stages, but a decline in the occurrence of the disease at advanced stages due to early intervention.[4]

Another factor often attributed to the decline in cancer mortality rates is the availability of more effective treatments.[5] Breast cancer for example is typically treated by locoregional treatments such as surgery and radiotherapy, systemic treatments such as chemotherapy, endocrine therapy, or targeted therapy, or a combination of locoregional and systemic methods.[5] In the case of endocrine therapy for breast cancer, the estrogen receptor (ER) is targeted with drugs such as tamoxifen.[5] In the case of targeted therapy, human epidermal growth factor receptor 2 (HER2) positive tumours are often treated with drugs derived from monoclonal antibodies (mAbs) such as trastuzumab.[5] For systematic therapy to be effective it is important to confirm target expression and

monitor the treatment response. Typically this is done with biological assays or size-based anatomical imaging; however functional imaging techniques in the field of molecular imaging (MI) are becoming the ideal approach.[5,6]

1.2 Clinical Tools for Cancer Imaging

The most widely used tool for imaging breast cancer is (X-ray) mammography, however this method is only able to detect anatomical changes and therefore gives very little biochemical information. For an imaging technique to be effective the sensitivity (detection of positive results) and specificity (differentiation from negative results) must be high.[3] Mammography has a sensitivity rate between 80-90% and a specificity of up to 95% for breast cancer; however these numbers can vary due to factors such as breast density and the number of views.[3] Any abnormalities that are observed through a mammogram or physical examination are subject to further assessment such as a biopsy or further imaging to confirm that cancer is in fact present.[3] A large proportion of women (70-90%) who have undergone screening and are called for secondary assessment have normal or benign disease and do not require further intervention.[3]

To acquire biochemical information, most tests in diagnostic oncology require sampling tissue. Biopsies make it difficult to monitor a process over time due to the invasive nature of the tests.[7] Equally important, there is a propensity for tissue-sampling errors especially if there is tumour heterogeneity.[7] The ideal approach would involve real time and minimally invasive analysis of key biological processes *in vivo*. This can be achieved through the use of molecular imaging (MI).[8]

MI is a class of techniques used to measure and characterize regional biological processes *in vivo*. MI methods have the advantage of allowing biological changes to be observed before they appear as anatomical changes. This helps in early disease detection and the prompt evaluation of the effectiveness of treatment regimens.[7,9] MI typically utilizes a signalling agent containing a radioactive, fluorescent, or paramagnetic label, or an ultrasound (US) contrast agent that has been administered systemically prior to imaging.[10]

Molecular targeting involves the use of a chemical reporter or a drug-like molecule that interacts with a specific biological/biochemical entity present in specific disease.[10] This differs from perfusion agents which are designed to follow physiological processes that are altered in diseased versus healthy tissue such as blood flow.[10] Since there is a shift to develop

novel drugs that interact with specific biological targets MI is gaining importance as a tool in drug development and treatment management.[9]

Imaging modalities that are commonly used clinically for detection and characterization of different cancers include US and magnetic resonance imaging (MRI).[5] US gives anatomic detail with high resolution especially with the use of targeted microbubbles as contrast agents. The use of this technique of MI studies is limited due to challenges in producing and translating effective microbubble based targeting agents.[7] MRI provides high spacial resolution and image quality with the use of targeted contrast agents using Gd or Fe. Targeted contrast agents are limited however, due to the narrow range of isotopes that can be used as well as the high concentration of contrast agent needed.[7]

Nuclear molecular imaging (NMI) uses specialized cameras to detect the emissions from compounds tagged with radioactive nuclei, which are referred to as radiotracers.[8] Radiotracers are governed by the tracer principle, which is based on the theory proposed by George de Hevesy that small quantities of radioactivity can be detected without perturbing the biological system under investigation. Small quantities (pico to nanomoles) of a radiotracer can be administered to follow biochemical processes and

to measure the expression of specific targets, even at low concentrations.[8,11]

There are generally two modalities for NMI: single photon computed tomography (SPECT) and positron emission tomography (PET). PET provides superior spatial resolution and more accurate image quantification and uses isotopes that are more readily incorporated in to small molecules (e.g. ^{13}N, ^{15}O, ^{18}F) when compared to SPECT.[7] The spatial resolution for NMI is less than that of MRI; however using multimodal imaging systems has helped overcome some of the associated limitations.[7] Dual imaging modalities incorporating computed tomography (CT) or MRI such as SPECT-CT, PET-CT, SPECT-MRI and PET-MRI combine functional imaging with anatomical imaging and can lead to images with improved spatial resolution and sensitivity when compared to just the nuclear or anatomical modality alone.[12,13] These approaches are being used increasingly in oncology for both diagnostic and prognostic applications.

1.3 Nuclear Medicine Techniques in Cancer Management

1.3.1 Single Photon Emission Computed Tomography

SPECT uses radionuclides that emit γ-rays between 70 – 360 keV. The γ-rays are detected by a camera (or cameras) that rotate around the

patient.[14] The most widely used SPECT isotope is ^{99m}Tc, which is used in more than 80% of diagnostic nuclear studies due to its ideal γ–ray emission energy and availablity.[11] Small compact γ–cameras have more recently been used for breast specific γ-imaging (BSGI) with ^{99m}Tc-Sestamibi.[12] The agent accumulates in tissues with high mitochondrial activity, areas exhibiting fat necrosis, fibroadenomas, phyllodes tumours, or benign papillomas however its use is limited by a high false positive rate (low specificity).[12]

1.3.2 Positron Emission Tomography

PET uses radionuclides that emit positrons (β^+), which undergo an annihilation event with a neighbouring electron to produce two 511 keV γ-rays that travel approximately 180º from each other. These γ-rays are detected by a circular array of detectors that use electronic collimation to remove background scatter. This is in contrast to SPECT imaging, which uses lead collimation making the sensitivity and resolution for PET superior.[11] Positron Emission Mammography (PEM) is analogous to x-ray mammography (and BSGI) where PET tracers are used to visualize breast cancers.[15] The most widely used PET radiotracer in oncology is 2-deoxy-2-[^{18}F]-fluoro-D-glucose ([^{18}F]FDG). It is a general purpose agent that is

used for detecting a large array of tumours and its uptake is often correlated with aggressiveness.[10] Further discussion of [^{18}F]FDG and its uptake and retention mechanism in cells is described in Chapter 4. One major limitation of [^{18}F]FDG is that it localizes in areas of inflammation or infection.[11] This makes it difficult to distinguish these areas from cancer consequently there has been an extensive search for more specific cancer imaging probes.

One of the limitations of using NMI for routine screening is the high cost of the instrumentation and the ability to gain access to the necessary isotopes. It is anticipated that routine screening tools such as mammograms or US for example, will not be replaced with NMI for these reasons. These techniques are better suited for cases where high cancer risk is suspected, and biochemical characterization, and monitoring therapy response are needed.

1.4 Targeted Radiotherapy

Another application of radioactive isotopes in oncology is that they can be used for cancer treatment through targeted radiotherapy. This technique uses radiopharmaceuticals that are similar to NMI agents except that the radioisotope emits energy that can irreparably damage

cancer cells. The therapeutic effect is most often achieved through α or β radiation, where the latter is the most commonly used in the clinic.[16]

The negatron (β^-) is able to pass through the tumour tissue and interact with the atoms in water and lose energy. This leads to the production of free radicals and energized/ionized atoms which can then damage cellular DNA.[16] Alpha (α) emitters, which are becoming more widely used with the approval of the prostate cancer therapeutic Xofigo, behave similarly except they have a shorter tissue penetration range and a more profound damage to cellular DNA.[16] Some examples of β-emitters used for targeted radiotherapy in the clinic include: $^{186/188}$Re, ^{131}I, and ^{90}Y and examples of α-emitters include: ^{211}At, ^{225}Ac, and ^{213}Bi.

It is possible to convert a diagnostic imaging agent into a therapeutic radiopharmaceutical by replacing the radioisotope used. An example would be using ^{123}I for SPECT imaging and ^{131}I for targeted radiotherapy. This approach is advantageous because imaging can be used to identify target positive patients for treatment with a pharmaceutical that has identical properties to the diagnostic compound used to identify the disease.

1.5 Imaging Metastatic Potential

Metastasis is the dissemination of tumour cells to distant target sites and it is the leading cause of death in cancer patients.[17] The process involves tumour cells departing from their origin (intravasation), surviving circulation (embolization), arriving at the new site (extravasation), and finally forming new tumours (colonization).[18] The most difficult types of cancer to treat are those that have spread to other organs, therefore preventing this from happening is critical for early cancer management. The likelihood that a primary tumour will form secondary metastases is defined as its metastatic potential.[18] Imaging the metastatic potential would allow for the aggressiveness of the disease and effectiveness of treatment to be assessed non-invasively; for this reason, it is a critical goal in oncology. Cancers where such a tool would have an immediate and profound impact, because of their tendencies to form metastases leading to death, include melanoma, breast, and colorectal cancers.[19]

The metastatic potential of a tumour depends on the ability of the cells to seek distant organs as well as how receptive the site is to colonization. These events are governed by a set of genetic determinants, which can be classified into three groups: metastasis initiating genes, metastasis progression genes, and metastasis virulence genes.[18] Given the importance of metastatic potential characterization, gene expression

markers are under development; however we are only at the early stages of understanding the genetic role in cancer metastasis. Surrogate markers of metastatic potential have also been studied clinically including angiogenesis, hypoxia, glucose metabolism, and protease activity.[18]

1.5.1 Surrogate Markers for Metastatic Potential

In order for tumours to survive outside of their primary site they need to provide their own blood supply. The process where tumours are able to form new capillaries from existing blood vessels is known as angiogenesis. Metastasis is dependent on angiogenesis as most tumours cannot grow larger than a few millimetres without generating new blood vessels.[20] Angiogenesis is therefore an attractive surrogate marker to measure metastatic potential. Two targets that have been widely studied for angiogenesis imaging include vascular endothelial growth factor (VEGF) and the $\alpha_v\beta_3$ integrin.[18,20] Radiopharmaceuticals based on anti-VEGF antibodies such as bevacizumab have been successful for preclinical and clinical imaging of VEGF in tumours.[21,22] Derivatives of the cyclic arginine-glycine-aspartic acid (cRGD) peptide have also shown preclinical and clinical success in imaging the $\alpha_v\beta_3$ integrin receptors in tumours as markers of angiogenesis.[23,24]

When a tumour reaches a critical mass (1-2 mm), it outgrows its blood supply leading to local hypoxia, which induces VEGF expression. [18,20] The hypoxic environment also leads to the expression of the hypoxia-inducible factor (HIF)-1α which has been shown to be highly expressed in malignant tumours.[10,18] Hypoxia is considered a predictor of poor treatment response and metastatic potential.[10,25] HIF-1α has not been targeted directly but since hypoxia occurs when pO_2 and pH levels are below normal physiological levels radiolabeled nitroimidazoles can be used as imaging agents because they are reduced and become trapped within hypoxic cells.[10,25] One example is ^{18}F-fluoromisonidazole ([^{18}F]FMISO) which shows uptake that correlates with poor outcomes following chemotherapy and radiotherapy however one of its drawbacks is that the target:non-target (T:NT) ratios are low due to slow blood clearance.[18] Alternative agents such as ^{18}F-fluoroazomycin arabinoside ([^{18}F]FAZA) have been studied to overcome this challenge. Preclinical studies indicate that the T:NT ratios of [^{18}F]FAZA are superior to [^{18}F]FMISO in general however a recent study indicates that the T:NT ratio of [^{18}F]FMISO improves over time.[26,27]

Increased glucose metabolism is associated with all cancer cells.[28] As stated previously [^{18}F]FDG has gained clinical importance as a tool for cancer diagnosis, staging, and imaging treatment response by measuring

glucose metabolism.[28] Using it as a tool to predict prognosis is also possible. The uptake of [^{18}F]FDG in tumours correlates with high HIF-1α expression and its use has been able to predict poor survival rate in lung cancer patients.[18] Use of [^{18}F]FDG, however, is unable to differentiate between hypoxic and normoxic tumours.[18] Although [^{18}F]FDG is recommended for diagnosis, staging, and reoccurrence any positive finding should be confirmed by secondary tests due to the risk of false positives.[28]

In order for tumours to progress and spread they must develop the ability to degrade the extracellular matrix (ECM), which is a network of proteins surrounding cells that provides structural support.[17] The ECM is primarily made up of collagen, which is a large protein family made up of three polypeptide chains.[17] The ECM makes up the basement membrane and connective tissue matrices for all organs. ECM proteins are resistant to a number of proteases and serve as a barrier for tumour invasion.[17] In cancer, various proteases work together to break down ECM proteins such as collagen.

1.5.2 Proteases as Targets

Proteases are enzymes that are responsible for catalyzing the otherwise slow hydrolysis of amide bonds in proteins and peptides in a

process known as proteolysis.[29] There are more than 670 proteases making up 2% of the human genome, in six general classes: cysteine, serine, threonine, aspartic acid, glutamic acid, and metalloproteinases depending on their mechanism of action.[30–32] Because of the increase in proteolysis associated with a variety of diseases, proteases have been actively investigated as targets for imaging to assist with diagnosis and treatment monitoring.[29]

Proteases are produced from inactive zymogens (pro-enzymes), which are then made active after biochemical processing.[33] Once active, they are involved in a number of normal cellular processes such as bone remodelling, protein turnover, cell death, gene expression, and differentiation.[29,34] Their activity is regulated by endogenous inhibitors however when unregulated, proteolysis can lead to a variety of disease states such as diabetes, thrombosis, hypertension, and cancer.[29]

Many tumours express proteases early in their development where they are involved in angiogenesis and proliferation.[32] Tumour associated proteolysis occurs due to proteases present in tumour cells and tumour associated cells.[34] These processes involve interactions between tumour cells and endothelial, stromal, lymphocytic, and mast cells, and neutrophils.[32,35]

There are three classes of proteases that are typically implicated in

cancer progression: matrixmetalloproteinases (MMPs), serine proteases, and cysteine proteases, although cathepsin D, an aspartic acid protease, has also been shown to have a role in cancer progression.[17,36] Each enzyme class has a different mechanism for proteolysis and provides different functions in tumour progression, so selective targeting is important in understanding their function.

The MMPs are a class of zinc dependent enzymes, 27 of which are known in humans. Many MMPs have been implicated in their role in cancer, however MMP-2, MMP-9, MMP-14, MMP-1, MMP-13, MMP-7, and MMP-11 are associated with metastasis.[17] Their active sites are very similar across the class and they are inhibited by a group of proteins known as tissue inhibitors of matrix metalloproteinases (TIMPs). [^{111}In]DTPA-*N*-TIMP2 is an MMP inhibitor that has been evaluated in patients with Kaposi sarcoma, however tumour uptake was not observed in any of the patients.[37] Other radiolabeled probes for MMPs have been evaluated preclinically but have not shown sufficiently high or selective tumour uptake.[38–41]

The serine protease, urokinase plasminogen activator (uPA) is responsible for converting plasmin to plasminogen (Figure 1.1) and binds to urokinase-type plasminogen activator receptor (uPAR).[17] It is an

important target in oncology that has been well studied since both uPA and uPAR have been shown to be overexpressed in aggressive cancers. Despite this, examples of radiolabelled uPA inhibitors reported in the literature for preclinical cancer imaging have been very limited and still require further development.[42]

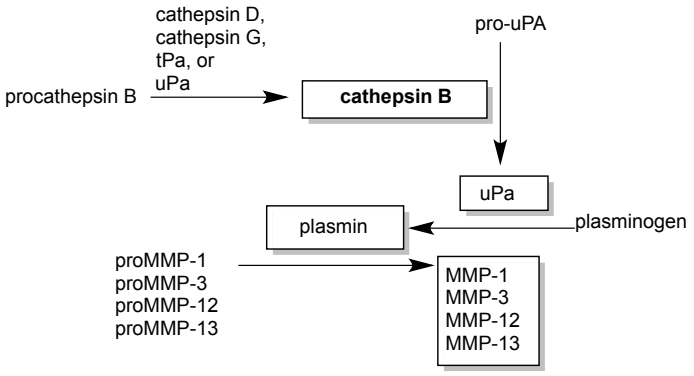

Figure 1.1 Activation of proteolytic enzymes involved in cancer (adapted from[17]).

The most studied cysteine protease is cathepsin B. It is a lysosomal cysteine protease that is found in normal tissues and it is involved in a number a regulatory processes.[43] Cathepsin B is overexpressed in a variety of cancers and its expression correlates with metastatic potential and poor prognosis. Malignancies show greater secretion of cathepsin B in aggressive legions compared to normal or less aggressive tissues.[43–46] Active cathepsin B can convert pro-uPA to uPA, which then produces plasmin, which is involved in regulating various MMPs.[35] As noted above,

cathepsin B alongside the MMPs, uPA, and plasmin are involved in ECM degradation.

The Ets1 transcription factor is known to increase the expression of different proteases in tumours including cathepsin B and it is upregulated by collagen I. Collagen I, cathepsin B, uPA/uPAR, MMP-2, and MMP-14 are colocalized in tumour caveolae which is a lipid raft on the plasma membrane.[34,47] There appears to be a complex network of interactions regarding these proteases mediated by cathepsin B, making it a very important target in monitoring proteolytic activity in tumours (Figure 1.1).

1.5.3 Cysteine Cathepsins and Cathepsin B

The term 'cathepsin' is derived from the Greek word meaning to digest. It was originally used to describe acidic proteases.[48] The cathepsins are comprised of cysteine, serine, and aspartic acid proteases and are generally found within digestive organelles known as lysosomes.[48] The cysteine cathepsins (papain-like thiol proteases) found in the human genome include cathepsins B, L, K, S, V, F, W, H, X, C, and O. Cathepsins B, L, F, H, X, C, and O are ubiquitously expressed.[31,34] Cathepsin B was the first cysteine protease that was isolated and it is the most studied of all cysteine proteases.[48] It has been established that cathepsin B and L are able to hydrolyze ECM proteins such as collagen

IV, laminin, and fibronectin.[34]

All papain-like thiol proteases are comprised of a signal peptide, a propeptide, and a catalytic domain. The signal peptide in cathepsin B is 17 amino acids in length and it is responsible for translocation in to the endoplasmic reticulum (ER) during mRNA translation. The propeptide is 62 amino acids in length and serves three functions. It acts as a scaffold for protein folding, a chaperone for proenzyme transport to the endosomal/lysosomal compartment, and as a reversible inhibitor preventing premature activation of the catalytic domain. Finally the catalytic domain contains the active sites for the cysteine cathepsins, comprising of cysteine, histidine, and asparagine residues. The catalytic domain is 260 amino acids long in cathepsin B and contains only one active site.[49,50]

In the first step in the catalytic cycle, Cys^{25} and His^{125} form an ion pair, which is stabilized by Asn^{175} (Figure 1.2).[51] The resultant nucleophilic attack by the deprotonated cysteine residue leads to a tetrahedral intermediate forming an oxyanion and releasing the carboxy terminus portion of the substrate. This intermediate is then stabilized by hydrogen bonding, within what is known as the oxyanion hole (Figure 1.3). The intermediate then becomes an acyl enzyme or enzyme thioether, which is then hydrolysed by a proximal water molecule giving a second tetrahedral

intermediate. This intermediate then releases the free enzyme and the amino terminus portion of the enzyme.[51]

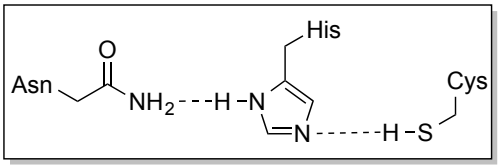

Figure 1.2 Active site residues in cysteine proteases.

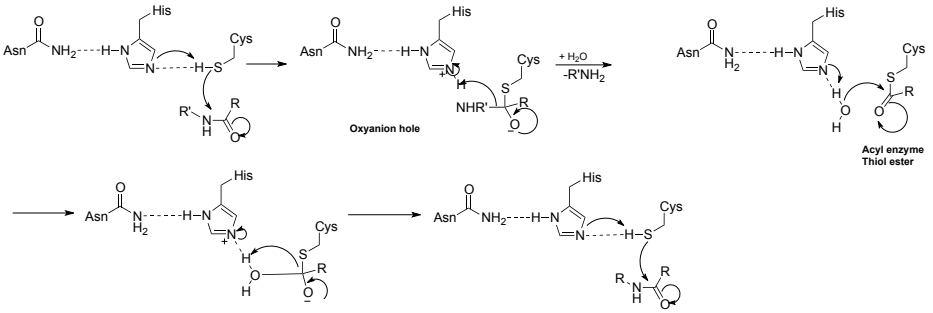

Figure 1.3 Substrate hydrolysis mechanism for cysteine proteases (adapted from[17]).

Proteases hydrolyse substrates at a specific bond known as the scissile bond (Figure 1.4). Residues on the amino end of the scissile bond are labelled P_1, P_2, P_3, P_n, etc. while residues on the carboxy end of the scissile bond are deemed primed sites and they are labelled P_1', P_2', P_3', P_n', etc. (Figure 1.4). The corresponding substrate binding sites are named similarly using S_n or S_n' instead.[17]

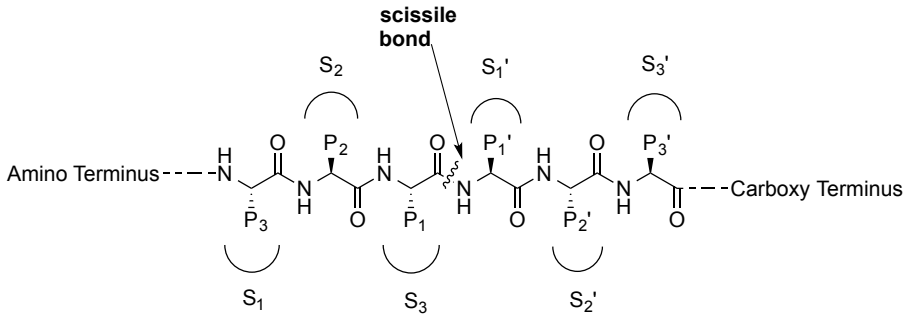

Figure 1.4 General nomenclature for enzyme substrate cleavage.

The first translational product of cathepsin B mRNA is the 44 kDa inactive precursor, which is converted to the 33 kDa single chain form of cathepsin B. It is then further processed to the 27 kDa glycosylated double chain form and the 24 kDa unglycosylated double chain form.[52] The conversion to the double chain form occurs in the lysosomes and this is a cell-type specific process, therefore the ratio of glycosylated to non-glycosylated enzyme can vary.[52] The glycosylated form has reduced activity when compared to the non-glycosylated form.[53] The release of membrane-bound cathepsin B in tumours could be due to a defect in the carbohydrate moieties during post-translational modification.[48]

Cathepsin B is localized on the leading edge of highly invasive tumours and it has been shown that on the surface of breast tumour cells it colocalizes with the annexin II heterotetramer (a calcium dependent phospholipid binding protein), which is also overexpressed in cancer.[54]

There are endogenous cysteine protease inhibitors (CPIs) that can be

classified in to three categories: the cystanins, stefins, and kininogens.[48] The cystanins and stefins are the most potent toward cathepsin B with K_i values in the nanomolar range.[48] CPIs have reduced expression in malignant lesions, for example the expression of stefin A is much lower in brain tumours than benign tissues, based on mRNA profiling and concentration.[55] This further supports the notion that active cathepsin B is important in tumour malignancy.

Cathepsin B is unique among papain like proteases in that it can behave as an endopeptidase (cleaves within the peptide chain) or an exopeptidase/carboxypeptidase (cleaves at the C-terminus of a peptide chain). This is due to the presence of a segment known as the occluding loop that restricts access to the active site.[56] At low pH the occluding loop is held in place by a salt bridge between the histidine and aspartic acid residues, but at higher pH His is deprotonated and the loop opens up allowing exopeptidase activity.[57] In general cathepsin B is most stable at pH < 7.0.[48]

1.6 Preclinical Probe Development for Cathepsin B

Presently there are no MI probes targeting the cathepsins that are used routinely in the clinic; however, there have been numerous examples of cathepsin B targeted probes used for preclinical evaluation of metastatic

cancers. Preclinical studies in animal models are useful because they allow for the evaluation of the specificity and general distribution of new probes in a multicellular system.

1.6.1 Animal Models

Animal models are key to the evaluation of the pharmacokinetic properties (adsorption, distribution, metabolism, excretion) and stability of novel probes *in vivo.* Simple animal models such as healthy rodents serve as good starting points for preclinical evaluation of probes that show affinity for the target of interest. Mice have similar physiology to humans such as organ function and expression level of most molecules in healthy tissues; however it is important to consider some physiological differences between mice and humans when making these evaluations.[58] For example the mouse heart beats faster than the human heart and mice breathe at a faster rate than humans. Also tissue perfusion times are much faster in mice due to their size.[58] Healthy mice can be used to evaluate processes that occur in normal physiological conditions such as blood flow, renal and brain activity, bone metabolism, etc.; however diseases such as cancer require more sophisticated models.

Tumour bearing models fall into separate categories depending on the source of the tumour, the immunocompetance of the animal, and if genetic

modifications are used.[58] Syngeneic models arise when the rodent bears tumours derived from its species. Xenogenic models involve the administration of human cancer cells to immunodeficient mice, which are used to avoid rejection of the cells. Thirdly genetically modified models are cases where the expression of particular target molecules in the transplanted tumours is altered. This is achieved through using transfected cell lines or transgenic mice where the mouse genome is altered.[58] Xenogenic models are the most commonly used in preclinical MI because they allow for the monitoring of targets derived from humans. A main drawback of this approach is that while the tumour cells may be derived from human origins the stromal cells and blood vessels surrounding them are that of the rodent.[58] This is important to consider when testing agents for cathepsin B as it is expressed in various cells surrounding the tumours as well. Although this is addressed with genetically modified models they are much more difficult to obtain than xenogenic models.

1.6.2 Small Animal Imaging

Most non-invasive imaging modalities have been scaled down to create dedicated small animal instruments. An example is optical imaging techniques used for rodents. Optical imaging is less expensive than other MI techniques such as NMI and MRI.[59] It involves the use of fluorescence

or bioluminescence as a means for signal contrast, typically in the form of near infrared fluorescence (NIRF) imaging or bioluminescence imaging (BLI).[60] Near infrared (NIR) light is ideal for imaging biological systems because haemoglobin, water, and lipids have the lowest absorption coefficient in the NIR region (approximately 650-900 nm) and they are the principal absorbers of light in the visible (haemoglobin) or infrared (water, lipids) regions.[60] In fluorescence imaging, light is used to illuminate the fluorophore (excitation) then the fluorophore emits a signal at a different wavelength (emission) that is captured using a camera equipped with an ultrasensitive charge-coupled device (CCD).[59,60] BLI detects photons emitted from cells genetically modified to express luciferase and has very little potential for clinical translation because it requires transgenically modified cells.[59]

1.6.3 Cathepsin B Imaging

There have been a number of near infrared fluorescence (NIRF) imaging agents developed for preclinical imaging of cathepsin B expressing tumours. In general protease targeted probes can be classified in to activity based probes (ABPs) and substrate based probes (SBPs). Because it is the active enzyme that is involved in the cellular processes that regulate cancer, active site targeting molecules are the focus for

probe development as opposed to antibodies.[30]

ABPs are molecules that covalently bind to the active site in a manner that is dependent on the activity of the enzyme.[30] The targets for ABPs include serine, cysteine, threonine, and metalloproteases as well as phosphatases, and other hydrolases.[61] ABPs are typically comprised of a synthetic or natural irreversible inhibitor deemed a warhead that is linked to a tag either for purification (i.e. biotin), or identification (i.e. fluorophores or radioisotopes) (Figure 1.5).[61] The warhead is often the most difficult part of the probe to select and many inhibitors such as epoxides, diazomethylketones, and acyloxymethyl ketones (AOMKs) have been used to develop ABPs for different cysteine proteases (Figure 1.6).[62–71] The AOMKs in particular show exceptional selectivity for cysteine proteases and so have been used to develop ABP for this class.[50]

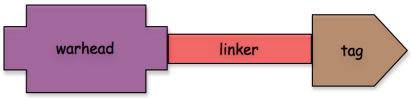

Figure 1.5 General structure of an ABP.

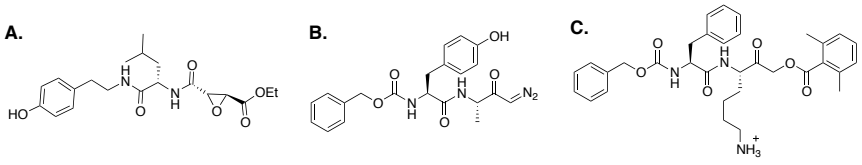

Figure 1.6 Cathepsin B inhibitors used as warheads for ABPs.

Perhaps one of the biggest breakthroughs for preclinical imaging of proteases has been “smart probes.” These probes change their emissive properties after biochemical modification by the protease typically via a quenching-dequenching sequence.[59,72] The probes are optically silent in their native state and then become optically active following enzymatic cleavage.

AOMKs have been modified with fluorophores at the unprimed sites and quenchers at the primed site of the inhibitor. Following enzyme hydrolysis the resultant probe is optically active and bound to the enzyme while the quencher is released with the leaving group.[62,66,73] Cat B 750 FAST and Cat B 680 FAST (PerkinElmer) are examples of commercially available polymeric activatable fluorescent imaging probes that are available for preclinical imaging of cathepsin B.[44,74–77] Additional examples of SBPs are discussed in Chapter 4.

Although NIRF probes are effective in detecting protease activity in small animals they have low potential for clinical translation due to the poor tissue penetration of the NIRF signal.[32] Clinically, optical imaging is only suitable for subcutaneous lesions, endoscopy, and determining surgical margins.[32] The promising results of these optical MI agents have encouraged further investigations towards the development of NMI agents that would have high potential for clinical translation.

1.6.4 Enzyme Target Probe Development

For an enzyme targeted probe there are a number of factors that need to be considered during development. An APB follows the similar principles applied to the receptor-ligand model. The expression level of the active enzyme as well as the binding affinity and specificity of the ABP need to be optimal.[10] The ABP should bind to the enzyme active site with high affinity (low K_i) and high specificity (poor affinity towards other targets). SBPs follow the enzyme-substrate model. To be effective, a probe must have fast turnover rates (high k_{cat}) and high target affinity (low K_m).[10]

Overall the ideal MI probe for cathepsin B would be able to access the target *in vivo* (many protease targets are intracellular), have high affinity and selectivity for the target, show a high T:NT ratio, high stability, and low toxicity (which should be the case for nuclear probes due to the tracer principle).[58] The ideal signalling agent would also exhibit properties specific to the modality used. Nuclear imaging would require an isotope that had appropriate half-life, optimal emission energy, low cost, and high availability.[78] Optical imaging with a fluorescent probe would require a fluorophore with a high quantum yield, resistance to photobleaching, and emission in the NIR region.[79]

1.7 Objectives

Current imaging techniques that identify the presence of a cancer are not sufficient to determine the aggressiveness of the disease and optimal course of treatment; therefore secondary tests are often employed. This typically involves biopsies and biospecimen assays, which can be influenced by sampling biases. Non-invasive *in vivo* MI is an effective tool that allows for disease characterisation and can be used for treatment planning, and monitoring of response. As the use of targeted therapy options emerge, more non-invasive MI methods using probes that target specific markers of tumour aggressiveness are needed. While there has been substantial development of new MI probes for oncologic imaging a number of the targets are not expressed in all cancer and there is still a need to be able to identify high-risk cancers, especially those with high metastatic potential.

Cathepsin B expression is strongly connected to metastatic potential and as one of the most studied of the cysteine proteases there is a wealth of preclinical and clinical data to support its role in cancer metastasis. Despite successful preclinical optical imaging probes for cathepsin B there remains a lack of clinically relevant NMI probes for this important target.

The goal of this thesis was to develop, investigate and assess different strategies for the preparation of cathepsin B targeted probes as the basis

for creating radiopharmaceuticals for NMI of metastatic potential. The initial strategy (Chapter 2) was to incorporate radioiodine into an AOMK scaffold such that the affinity for cathepsin B was maintained for *in vivo* monitoring of cathepsin B activity. Biochemical assays were described and used for later applications of the AOMKs. The second strategy (Chapter 3) was to develop cathepsin B targeted ABPs that incorporate Re/^{99m}Tc in to the AOMK backbone. A dendrimer platform was compared to the single targeting vector approach to determine the effect on cathepsin B binding affinities. In Chapter 4 an alternate strategy is described where the AOMK was functionalized with a reactive group that can be used with a radioiodinated or fluorescent bioorthogonal probe for NMI or optical imaging. Cell assays were established as a means to compare directly labelled probes with the new bioorthogonal pairs. As an alternative to the AOMK inhibitor platform (Chapter 5) a cathepsin B substrate linked to a known tracer was prepared as a potential enzyme activated delivery platform. Synthetic strategies were explored to produce radioactive analogues for this system. Conclusions and future directions are described in Chapter 6.

1.8 References

1. *Canadian Cancer Society's Advisory Committee on Cancer Statistics*, Toronto ON, 2015.

2. D. Hanahan and R. A. Weinberg, *Cell*, 2000, **100**, 57–70.

3. M. Reddy and R. Given-Wilson, *Women's Heal. Med.*, 2006, **3**, 22–27.

4. L. Esserman, Y. Shieh, and I. Thompson, *JAMA*, 2009.

5. J. H. Lee, E. L. Rosen, and D. A. Mankoff, *J. Nucl. Med.*, 2009, **50**, 569–581.

6. J. H. Lee, E. L. Rosen, and D. A. Mankoff, *J. Nucl. Med.*, 2009, **50**, 738–748.

7. D. A. Mankoff, *Breast Cancer Res.*, 2008, **10**, S3.

8. D. S. Wang, M. D. Dake, J. M. Park, and M. D. Kuo, *J. Vasc. Interv. Radiol.*, 2006, **17**, 1405–1423.

9. W. Cai, J. Rao, S. S. Gambhir, and X. Chen, *Mol. Cancer Ther.*, 2006, **5**, 2624–33.

10. S. H. Britz-Cunningham and S. J. Adelstein, *J. Nucl. Med.*, 2003, **44**, 1945–61.

11. C. S. Cutler, H. M. Hennkens, N. Sisay, S. Huclier-Markai, and S. S. Jurisson, *Chem. Rev.*, 2013, **113**, 858–83.

12. M. O. Connor, D. Rhodes, and C. Hruska, *Expert. Rev. Anticancer Ther.*, 2009, **9**, 1073–1080.

13. R. T. M. de Rosales, *J. Labelled Comp. Radiopharm.*, 2014, **57**, 298–303.

14. M. W. Groch and W. D. Erwin, *J. Nucl. Med. Technol.*, 2000, **28**, 233–244.

15. S. B. Glass and Z. A Shah, *Proc. (Bayl. Univ. Med. Cent).*, 2013, **26**, 314–9.

16. M. Hamoudeh, M. Anas, R. Diab, and H. Fessi, *Adv. Drug Deliv. Rev.*, 2008, **60**, 1329–1346.

17. M. Lee, R. Fridmanb, and Shahriar Mobashery, *Chem. Soc. Rev.*, 2004, **33**, 401–409.

18. P. T. Winnard, A. P. Pathak, S. Dhara, S. Y. Cho, V. Raman, and M. G. Pomper, *J. Nucl. Med.*, 2008, **49 Suppl 2**, 96S–112S.

19. C. Jedeszko and B. F. Sloane, *Biol. Chem.*, 2004, **385**, 1017–27.

20. Y. S. Choe and K.-H. Lee, *Curr. Pharm. Des.*, 2007, **13**, 17–31.

21. W. B. Nagengast, E. G. de Vries, G. a Hospers, N. H. Mulder, J. R. de Jong, H. Hollema, A. H. Brouwers, G. a van Dongen, L. R. Perk, and M. N. Lub-de Hooge, *J. Nucl. Med.*, 2007, **48**, 1313–1319.

22. S. B. M. Gaykema, a H. Brouwers, M. N. Lub-de Hooge, R. G. Pleijhuis, H. Timmer-Bosscha, L. Pot, G. M. van Dam, S. B. van der Meulen, J. R. de Jong, J. Bart, J. de Vries, L. Jansen, E. G. E. de Vries, and C. P. Schroder, *J. Nucl. Med.*, 2013, **54**, 1014–1018.

23. O. Jacobson, L. Zhu, G. Niu, I. D. Weiss, L. P. Szajek, Y. Ma, X. Sun, Y. Yan, D. O. Kiesewetter, S. Liu, and X. Chen, *Mol. Imaging Biol.*, 2011, **13**, 1224–1233.

24. H. Choi, J. H. Phi, J. C. Paeng, S. K. Kim, Y. S. Lee, J. M. Jeong, J. K. Chung, D. S. Lee, and K. C. Wang, *Mol. Imaging*, 2013, **12**, 213–217.

25. K. Okuda, Y. Okabe, T. Kadonosono, T. Ueno, B. G. M. Youssif, S. Kizaka-Kondoh, and H. Nagasawa, *Bioconjugate Chem.*, 2012, **23**, 324–9.

26. S. G. J. A. Peeters, C. M. L. Zegers, N. G. Lieuwes, W. van Elmpt, J. Eriksson, G. a. M. S. van Dongen, L. Dubois, and P. Lambin, *Int. J. Radiat. Oncol.*, 2015, **91**, 351–359.

27. G. Reischl, D. S. Dorow, C. Cullinane, A. Katsifis, P. Roselt, D. Binns, and R. J. Hicks, *J. Pharm. Pharm. Sci.*, 2007, **10**, 203–211.

28. J. W. Fletcher, B. Djulbegovic, H. P. Soares, B. a Siegel, V. J. Lowe, G. H. Lyman, R. E. Coleman, R. Wahl, J. C. Paschold, N. Avril, L. H. Einhorn, W. W. Suh, D. Samson, D. Delbeke, M. Gorman, and A. F. Shields, *J. Nucl. Med.*, 2008, **49**, 480–508.

29. B. Law and C.-H. Tung, *Bioconjugate Chem.*, 2009, **20**, 1683–95.

30. L. E. Edgington, M. Verdoes, and M. Bogyo, *Curr. Opin. Chem. Biol.*, 2011, **15**, 798–805.

31. D. Bromme and S. Wilson, *Extracellular Matrix Degradation*, Springer Berlin Heidelberg, Berlin, Heidelberg, 2011.

32. Y. Yang, H. Hong, and Y. Zhang, *Cancer Growth Metastasis*, 2009, **2**, 13–27.

33. B. Turk, *Nat. Rev. Drug Discov.*, 2006, **5**, 785–799.

34. B. F. Sloane, S. Yan, I. Podgorskia, B. E. Linebaugha, M. L. Cherb, J. Maia, M. S. Dora Cavallo-Medveda, J. Dosescua, and Kamiar Moin, *Semin. Cancer Biol.*, 2005, **15**, 149–157.

35. J. E. Koblinski, M. Ahram, and B. F. Sloane, *Clin. Chim. Acta*, 2000, **291**, 113–135.

36. T. T. Lah, M. Cercek, A. Blejec, J. Kos, E. Gorodetsky, R. Somers, and I. Daskal, *Clin. Cancer Res.*, 2000, **6**, 578–584.

37. R. Kulasegaram, B. Giersing, C. J. Page, P. J. Blower, R. a. Williamson, B. S. Peters, and M. J. O'Doherty, *Eur. J. Nucl. Med.*, 2001, **28**, 756–761.

38. S. M. J. van Duijnhoven, M. S. Robillard, K. Nicolay, and H. Grull, *J. Nucl. Med.*, 2011, **52**, 279–286.

39. S. van Duijnhoven, M. Robillard, K. Nicolay, and H. Grüll, *Molecules*, 2015, **20**, 12076–12092.

40. S. M. J. van Duijnhoven, M. S. Robillard, K. Nicolay, and H. Grüll, *Contrast Media Mol. Imaging*, 2015, **10**, 59–66.

41. S. M. J. van Duijnhoven, M. S. Robillard, S. Hermann, M. T. Kuhlmann, M. Schäfers, K. Nicolay, and H. Grüll, *Mol. Pharm.*, 2014, **11**, 1415–23.

42. J. Ides, D. Thomae, L. Wyffels, C. Vangestel, J. Messagie, J. Joossens, F. Lardon, P. Van der Veken, K. Augustyns, S. Stroobants, and S. Staelens, *Nucl. Med. Biol.*, 2014, **41**, 477–487.

43. B. F. Sloane and K. V. Honn, *Cancer Metas. Rev.*, 1984, 249 – 263.

44. C. Bremer, C.-H. Tung, A. J. Bogdanov, and R. Weissleder, *Radiology*, 2002, **222**, 814–8.

45. M. A. Nouh, M. M. Mohamed, M. El-Shinawi, M. A. Shaalan, D. Cavallo-Medved, H. M. Khaled, and B. F. Sloane, *J. Transl. Med.*, 2011, **9**, 1.

46. F. Qian, A. S. Bajkowski, D. F. Steiner, S. J. Chan, and A. Frankfater, *Cancer Res.*, 1989, **49**, 4870–4875.

47. D. Cavallo-Medved, D. Rudy, G. Blum, M. Bogyo, D. Caglic, and B. F. Sloane, *Exp. Cell. Res.*, 2009, **315**, 1234–1246.

48. B. F. Sloane, K. Moin, E. Krepela, and J. Rozhin, *Cancer Metas. Rev.*, 1990, **9**, 333–352.

49. B. Turk, D. Turk, F. Gubensek, and V. Turk, *Biochemistry*, 1994, **33**, 14800– 14806.

50. M. J. Evans and B. F. Cravatt, *Chem. Rev.*, 2006, **106**, 3279–3301.

51. F. Lecaille, J. Kaleta, and D. Bromme, *Chem. Rev.*, 2002, **102**, 4459 – 4488.

52. L. Mach, K. Stuwe, A. Hagen, C. Ballaun, and J. Glossl, *Biochem. J.*, 1992, **282**, 577–582.

53. S. Hasnain, T. Hirama, A. Tam, and J. S. Mort, *J. Biol. Chem.*, 1992, **267**, 4713–4721.

54. J. Mai, D. M. Waisman, and B. F. Sloane, *BBA*, 2000, **1477**, 215–230.

55. T. Strojnik, I. Zajc, A. Bervar, B. Zidanik, R. Golouh, J. Kos, V. Dolenc, and T. Lah, *Pflügers Arch. - Eur. J. Physiol.*, 2000, **439**, R122–123.

56. C. Illy, O. Quraishi, J. Wang, E. Purisima, T. Vernet, and J. S. Mort, *Biochemistry*, 1997, **272**, 1197–1202.

57. I. Redzynia, A. Ljunggren, M. Abrahamson, J. S. Mort, and J. C. Krupa, *J. Biol. Chem.*, 2008, **283**, 22815–22825.

58. S. Mather, *Bioconjug. Chem.*, 2009, **20**, 631–643.

59. R. Weissleder, *Nat. Rev. Cancer*, 2002, **2**, 11–8.

60. K. Shah and R. Weissleder, *NeuroRX*, 2005, **2**, 215–225.

61. A. B. Berger, P. M. Vitorino, and M. Bogyo, *Am. J. Pharmacogenomics*, 2004, **4**, 371–381.

62. G. Blum, G. von Degenfeld, M. J. Merchant, H. M. Blau, and M. Bogyo, *Nat. Chem. Biol.*, 2007, **3**, 668–677.

63. K. B. Sexton, M. D. Witte, G. Blum, and M. Bogyo, *Bioorg. Med. Chem. Lett.*, 2007, **17**, 649–653.

64. D. Kato, K. M. Boatright, A. B. Berger, T. Nazif, G. Blum, C. Ryan, K. A. H. Chehade, G. S. Salvesen, and M. Bogyo, *Nat. Chem. Biol.*, 2005, **1**, 33–38.

65. L. E. Edgington, M. Verdoes, A. Ortega, N. P. Withana, J. Lee, S. Syed, M. H. Bachmann, G. Blum, and M. Bogyo, *J. Am. Chem. Soc.*, 2013, **135**, 174–182.

66. M. G. Paulick and M. Bogyo, *ACS Chem. Biol.*, 2011, **6**, 563–572.

67. K. A. Chehade, A. Baruch, S. H. Verhelst, and M. Bogyo, *Synthesis (Stuttg).*, 2005, **2005**, 240–244.

68. P. E. Edem, S. Czorny, and J. F. Valliant, *J. Med. Chem.*, 2014, **57**, 9564–9577.

69. J. Falgueyret, W. C. Black, W. Cromlish, S. Desmarais, S. Lamontagne, C. Mellon, D. Riendeau, S. Rodan, P. Tawa, G. Wesolowski, K. E. Bass, S. Venkatraman, and M. D. Percival, *Anal. Biochem.*, 2004, **335**, 218–227.

70. G. Ren, G. Blum, M. Verdoes, H. Liu, S. Syed, L. E. Edgington, O. Gheysens, Z. Miao, H. Jiang, S. S. Gambhir, M. Bogyo, and Z. Cheng, *PLoS One*, 2011, **6**, e28029.

71. R. W. Mason, L. T. Bartholomew, and B. S. Hardwick, *Biochem. J.*, 1989, **263**, 945–949.

72. U. Mahmood and R. Weissleder, *Mol. Cancer Ther.*, 2003, **2**, 489 – 496.

73. G. Blum, S. R. Mullins, K. Keren, M. Fonovic, C. Jedeszko, M. J. Rice, B. F. Sloane, and M. Bogyo, *Nat. Chem. Biol.*, 2005, **1**, 203–209.

74. R. Weissleder, C.-H. Tung, U. Mahmood, and A. J. Bogdanov, *Nat. Biotechnol.*, 1999, **17**, 375–378.

75. C. Tung, U. Mahmood, S. Bredow, and R. Weissleder, *Cancer Res.*, 2000, 4953–4958.

76. E. Gounaris, C. H. Tung, C. Restaino, R. Maehr, R. Kohler, J. A. Joyce, H. L. Ploegh, H. L. Plough, T. A. Barrett, R. Weissleder, and K. Khazaie, *PLoS One*, 2008, **3**, e2916.

77. S. Eser, M. Messer, P. Eser, A. von Werder, B. Seidler, M. Bajbouj, R. Vogelmann, A. Meining, J. von Burstin, H. Algül, P. Pagel, A. E.

Schnieke, I. Esposito, R. M. Schmid, G. Schneider, and D. Saur, *P. Natl. Acad. Sci. USA*, 2011, **108**, 9945–50.

78. T. J. Ruth, *Reports Prog. Phys.*, 2009, **72**, 016701.

79. S. Lee, J. Xie, and X. Chen, *Biochemistry*, 2010, **49**, 1364–1376.

2 Synthesis and Evaluation of Radioiodinated Acyloxymethyl Ketones as Activity-Based Probes for Cathepsin B

2.1 Preface

The following describes work that was published in the Journal of Medicinal Chemistry. Patricia Edem performed all experiments (with the exception of animal studies and initial SDS-PAGE studies), data collection, and compound characterization. The manuscript was written by Patricia Edem and edited by Prof. John Valliant.

2.2 Introduction

Cathepsin B is a ubiquitously expressed lysosomal cysteine protease that is involved in normal physiological processes such as protein turnover, wound healing, cell differentiation and growth.[1] The enzyme is overexpressed in a variety of cancers including breast carcinoma, prostate carcinoma, glioblastoma, and melanoma,[2–5] with higher levels of active cathepsin B residing in tumors having high metastatic potential.[6–8] In normal cells cathepsin B is localized in the lysosomes yet in tumors it

distributes throughout the cytoplasm and cell periphery, and is secreted into the extracellular matrix as well.[9–11] These features make cathepsin B an attractive target for developing molecular imaging probes for detecting cancer and assessing metastatic potential.

A number of NIRF probes for cathepsin B have been developed.[12–15] Substrate based probes such as Cat B 750 FAST and Cat B 680 FAST are commercially available and have been used in a number of cancer models.[13,16–19] Most recently substrate based probes incorporating a self-immolative spacer linked to a fluorophore have been developed and used for *in vitro* and *in vivo* imaging of cathepsin B.[12,20,21] Irreversible inhibitors have also been employed to develop ABPs for cathepsin B imaging.[14,15,22–25]

ABPs for cathepsin B have been prepared from a number of different constructs including dipeptidyl AOMKs. The AOMK derivatives are attractive because of their specificity and high affinity for cysteine proteases *in vitro* and *in vivo*.[26–29] These inhibitors inactivate the enzyme by reacting with the active site cysteine resulting in a thioether linkage between the ABP and cathepsin B.[1,27,30,31] Phe-Lys-AOMKs have been fluorescently labeled at the lysine ε-amine and have shown specific tumor uptake *in vivo*.[14,15] Radiolabelled variants have also been developed where ^{64}Cu and the macrocyclic ligand 1,4,7,10-tetraazacyclododecane-

1,4,7,10-tetraacetic acid (DOTA) was also incorporated at the P_1 site.[14,32] This construct exhibited a tumor uptake of 0.35 ± 0.13 % injected dose per gram (ID/g) at 30 min post injection (p.i.) and the activity remained in the tumor at 24 h p.i. (0.27 ± 0.05 % ID/g). High liver and kidney uptake was also observed, which is likely associated with loss of copper *in vivo*.[33]

The present study describes the preparation and *in vivo* evaluation of novel dipeptidyl AOMK cathepsin B inhibitors, bearing different iodine containing prosthetic groups linked to the lysine ε-amine of a Phe-Lys-AOMK derivative. One of the advantages of working with iodine is that a single construct can be used to prepare agents for SPECT, PET or radiotherapy, simply by varying the isotope used (e.g., ^{123}I, ^{124}I, or ^{131}I). This is exemplified by the use of aryl iodides to synthesize diagnostic and therapeutic radiopharmaceuticals for melanoma, glioma, and prostate cancer.[34–38] Radioiodinated AOMKs have been used as ABPs to label diverse families of cysteine proteases *in vitro* but not cathepsin B, and they employed prosthetic groups that are not stable *in vivo*.[29] To evaluate the potential utility of iodinated AOMKs as molecular imaging probes, a library of candidates derived from robust iodine synthons was prepared and screened as inhibitors of cathepsin B. Two compounds were subsequently radiolabeled and tested *in vitro* and *in vivo*.

2.3 Synthesis of Parent Inhibitors (2.6a and 2.6b).

The parent AOMK inhibitors **2.6a** and **2.6b** (Figure 2.1A) were prepared from the protected dipeptide Cbz-Phe-Lys(ε-Boc)-OH (**2.3**). Following modified published procedures, isobutyl chloroformate (IBCF) (Scheme 2.1, Route A) or benzotriazole (Scheme 2.1, Route B) were used to couple the protected phenylalanine and lysine amino acids giving **2.3**.[39–41] The dipeptide **2.3** was activated with IBCF and treated with ethereal diazomethane to generate the diazomethylketone *in situ*. Treatment with HBr gave the bromomethyl ketone **2.4**, which was then converted to **2.5a** or **2.5b**, following the method of Blum *et al.*[14] The amount of potassium fluoride used in the final step was reduced to help minimize epimerization of the lysine residue, which was evident by both HPLC and ^{1}H NMR in most compounds.[27,40] The *tert*-butoxycarbonyl (Boc) group was subsequently removed using trifluoroacetic acid (TFA) giving **2.6a** or **2.6b** as TFA salts.

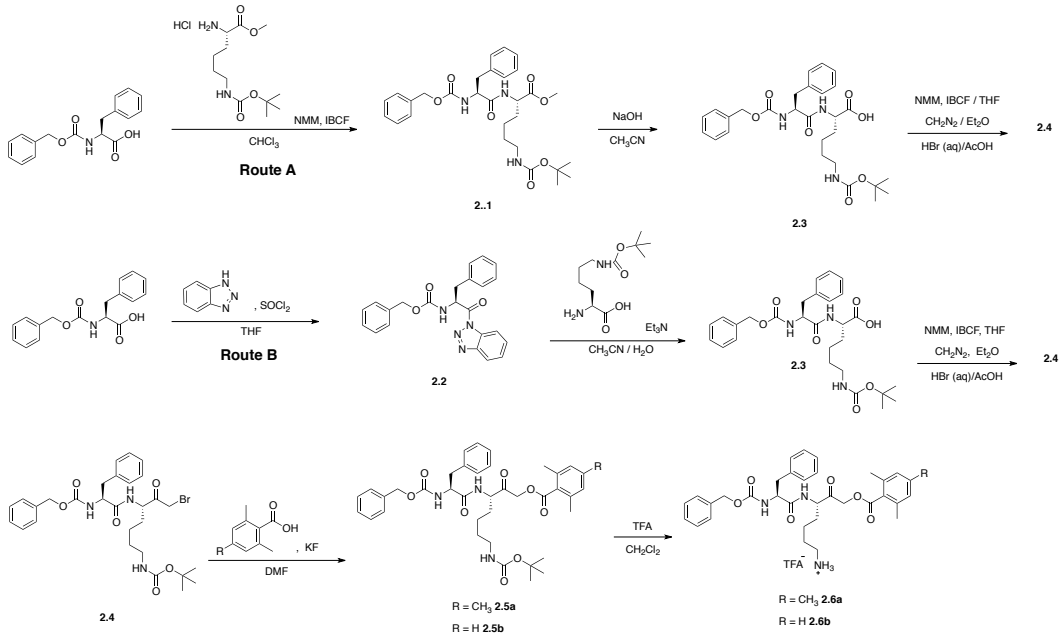

Scheme 2.1 Synthesis of **2.6a**/**2.6b**.

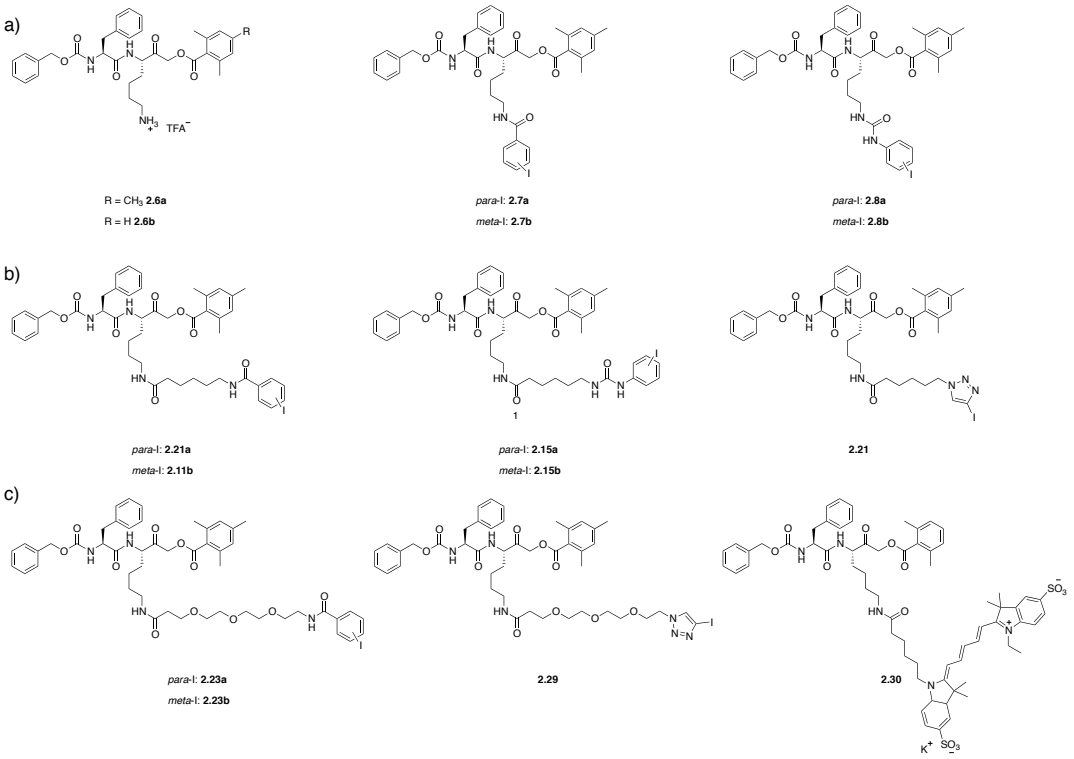

Figure 2.1. Structures of AOMK cathepsin B inhibitors. (a) Structures of the parent AOMKs (**2.6a**/**b**) and initial iodinated AOMKs: iodobenzamides (**2.7a**/**b**) and iodophenyl ureas (**2.8a**/**b**). (b) Structures of AOMKs with alkyl spacer: iodobenzamides (**2.11a**/**b**), iodophenyl ureas (**2.15**) and iodotriazole (**2.21**). (c) Structures of AOMKs with PEG spacer: iodobenzamides (**2.23a**/**b**) and iodotriazole (**2.29**) and the known optical probe: GB123 (**2.30**).

2.4 Synthesis of Initial Iodinated AOMKs

The first series of iodinated inhibitors prepared involved linking aryl iodides to the free amine of **2.6a** giving iodobenzamides (**2.7a**/**b**) and

iodophenylureas (**2.8a**/**b**) (Figure 2.1A). Compound **2.6a** was coupled to 3- or 4-iodobenzoic acid using IBCF in the presence of N-methylmorpholine (NMM) (Scheme 2.2). The desired products **2.7a** and **2.7b** were isolated following simple extraction in yields of 29% and 45% respectively. To generate the ureas, **2.6a** was combined with 3- or 4- iodophenyl isocyanate in the presence of triethylamine giving **2.8a** and **2.8b** in 9% and 14% yields respectively following silica gel chromatography (Scheme 2.3).

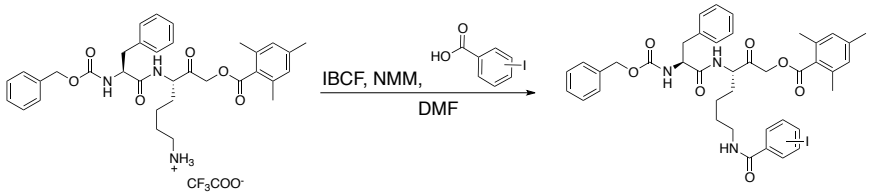

2.6a

para-I: **2.7a**
meta-I: **2.7b**

Scheme 2.2 Synthesis of **2.7a**/**b**.

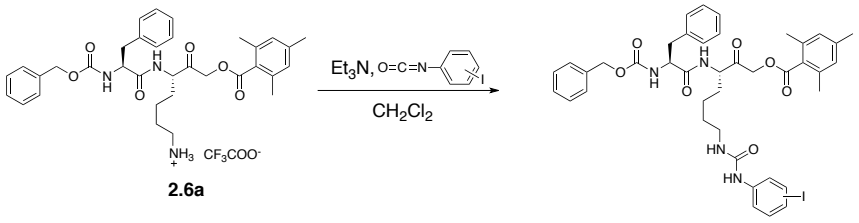

2.6a

para-I: **2.8a**
meta-I: **2.8b**

Scheme 2.3 Synthesis of **2.8a**/**b**.

It has been reported that inhibitors containing bulky amino acids at the P_1 position exhibit reduced affinity for cathepsin B.[43] To minimize possible steric interactions a six-carbon spacer was also used to incorporate the

aryl iodides (Figure 2.1B). 6-Aminohexanoic acid was combined with the active esters **2.9a** or **2.9b** giving the aryl iodide spacers **2.10a** and **2.10b** in 82% and 87% yields respectively (Scheme 2.3). These were linked to **2.6a** using benzotriazol-1-yl-oxytripyrrolidinophosphonium hexafluorophosphate (PyBOP) in the presence of triethylamine to generate compounds **2.11a** and **2.11b** in 45% and 30% yields respectively. For the urea derivatives it was necessary to use the protected methyl 6-aminohexanoate **2.12** and combine it with 3- or 4-iodophenyl isocyanate (Scheme 2.5). Following deprotection, **2.14a** or **2.14b** was coupled with **2.6a** using IBCF in the presence of NMM to give **2.15a** and **2.15b** in 35% and 30% yields respectively.

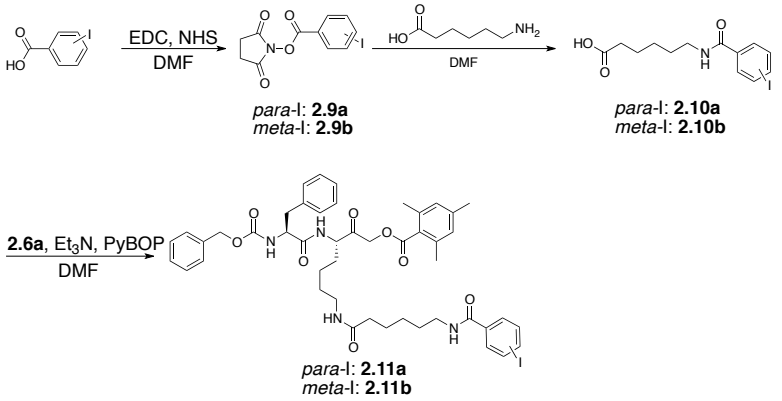

Scheme 2.4 Synthesis of **2.11a**/**b**.

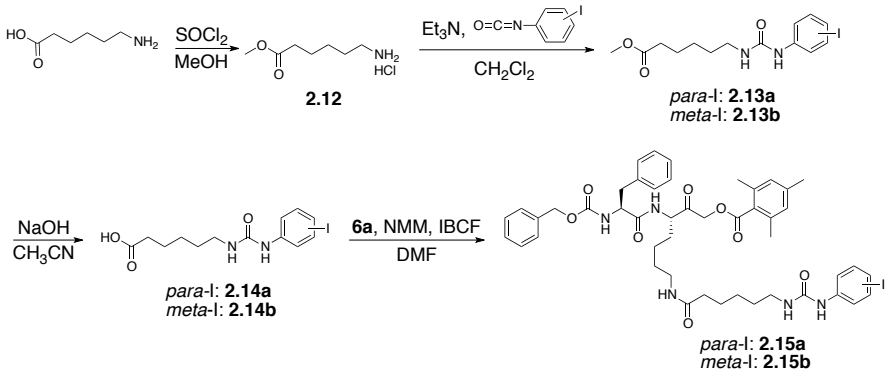

Scheme 2.5 Synthesis of **2.15a**/**b**.

We have shown that iodinated triazoles are more polar than iodobenzene-based derivatives, have minimal non-specific binding *in vivo*, and can clear readily via renal excretion.[44] To prepare a triazole-derived synthon to derivatize **2.6a**, ethynyl tributyltin was used in a 1,3-dipolar cycloaddition with **2.17** giving the triazole **2.18** (Scheme 2.6). ^{1}H and ^{13}C NMR spectroscopy confirmed that a single isomer was obtained, which is consistent with the literature.[45] Iododestanylation was achieved by treating **2.18** with molecular iodine to give **2.19** in 69% yield.[45] Following hydrolysis, compound **2.20** was coupled to **2.6a** using PyBOP in the presence of triethylamine to generate **2.21** in 33% yield.

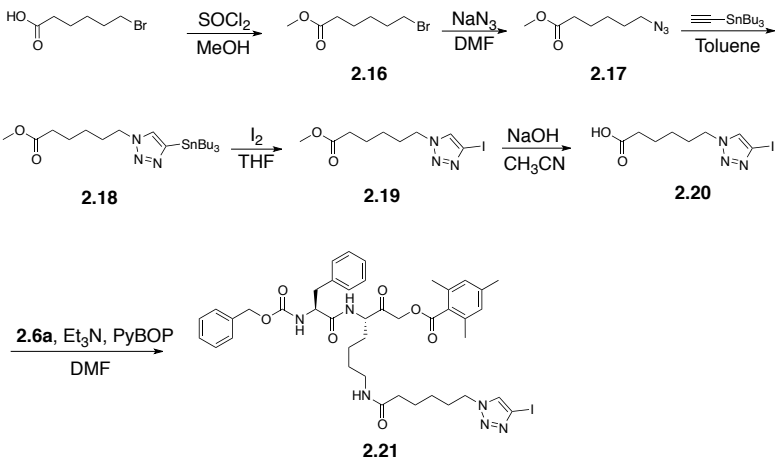

Scheme 2.6 Synthesis of **2.21**.

2.5 Inhibition of Cathepsin B by Iodinated AOMKs.

The binding affinity of the iodinated AOMKs was determined using a kinetic assay similar to that reported by Krantz *et al*.[27], employing Cbz-Arg-Arg-p-nitroanilide (Z-RR-pNA) as the substrate and human liver cathepsin B (Calbiochem). Optimal enzyme concentration range and linearity was determined by monitoring the substrate hydrolysis over time in the presence of various amounts of enzyme (Figure 2.2A). The rate of hydrolysis (ν_0) was linear when the enzyme concentration [E] was between 5 and 15 nM ($R^2 > 0.99$) (Figure 2.2B). The reaction rate (ν_0) was also monitored when varying the substrate concentration in order to determine the Michaelis-Menten constant (K_m) (Figure 2.3). A value of 390 ± 20 μM was found, which is lower than the previously reported value of

900 ± 60 μM.[46] The variance is likely due to differences in amount of DTT used to activate the enzyme, the incubation time for this activation, as well as the enzyme source, which can influence the observed K_m for this substrate.[46,47]

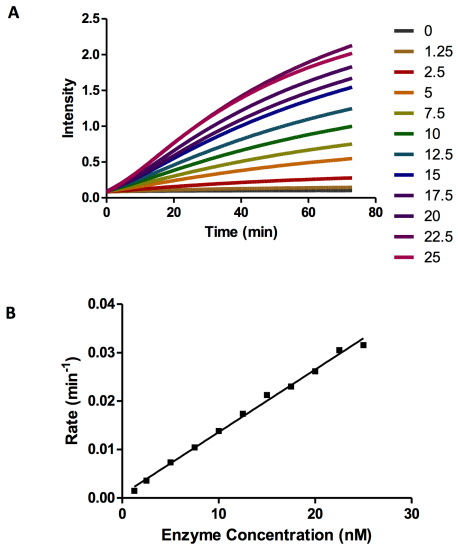

Figure 2.2 Optimization of enzyme concentration. (a) Time course of substrate (Z-Arg-Arg-pNA) hydrolysis; The legend shows enzyme concentration from 1.25 – 25 nM. (b) Initial rate (t < 10 min) vs. [enzyme].

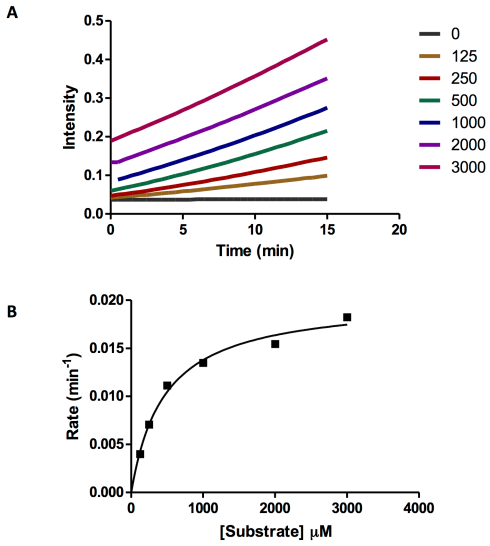

Figure 2.3 Determination of the Michaelis-Menten constant (K_m). (a) Time course of substrate hydrolysis; The legend shows substrate concentration from 125 μM- 3 mM. (b) Initial rate (t < 10 min) vs [substrate]. K_m = 390 ± 20 μM.

Inhibition constants (K_i) were determined by monitoring the substrate hydrolysis over time in the presence of 0 – 1 μM of inhibitor (Figure 2.4A). The observed rate constant (k_{obs}) was determined and plotted against the inhibitor concentration (Figure 2.4B). Using non-linear regression, K_i values were determined where possible. In cases where full inhibition was not observed, only the second-order rate constant (k_i/K_i) was determined (Table 2.1).

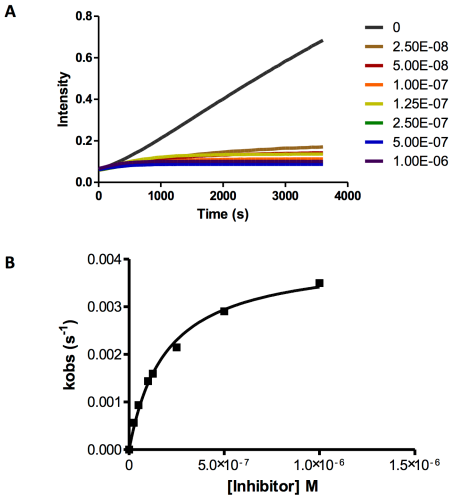

Figure 2.4 Determination of Binding Affinity (K_i) and Second Order Rate Constants (k_i/K_i). Representative example for **2.23a**. (a) Time course of substrate hydrolysis; The legend indicates inhibitor concentration from 0 – 1 μM. (b) Observed rate constants (k_{obs}) vs. [inhibitor]. K_i = 181 ± 9 nM. k_i/K_i = 21 000 ± 300 $M^{-1}s^{-1}$.

Table 2.1. Inhibitory Activities of Iodinated AOMK Derivatives[a]

Compound	K_i (nM)	k_i/K_i ($s^{-1}M^{-1}$)
2.6a	80 ± 10	40 000 ± 3 000
2.6b	52 ± 6	40 000 ± 6 000
2.7a	2 000 ± 1 000	810 ± 80
2.7b	n.d.[b]	630 ± 10
2.8a	n.d.	0.013 ± 0.002

2.8b	n.d.	0.0035 ± 0.0002
2.11a	n.d.	310 ± 20
2.11b	n.d.	280 ± 20
2.15a	n.i.[c]	n.i.
2.15b	n.i.	n.i.
2.21	1 000 ± 50	4 430 ± 70
2.23a	181 ± 9	21 100 ± 300
2.23b	370 ± 25	12 700 ± 600
2.29	350 ± 40	9 900 ± 200
2.30	120 ± 20	19 000 ± 2 000

[a] Inhibition constants were determined at 37 °C and pH 6.0 with human liver cathepsin B. [b] n.d.: full inhibition was not observed therefore the value was not determined. [c] n.i.: no inhibition observed.

The known inhibitor **2.6a** was evaluated as reference point to compare all iodinated derivatives. The measured K_i value was 80 ± 10 nM, which differed from the reported value (K_i = 170 ± 50 nM) again likely due to difference in enzyme sources.[27] The simple aryl iodide derivatives (**2.7a**/**b**–**2.8a**/**b**) showed poor affinity for the protease where a K_i value could only be determined for **2.7a** (K_i = 2 ± 1 μM) and the ureas (**2.8a**/**b**) exhibited no detectable inhibition. Incorporation of the alkyl spacer did not show an improvement for the iodophenyl ureas (**2.15a**/**b)** or the iodobenzamides (**2.11a/b)**. These compounds formed heterogeneous

solutions when added to the assay buffer indicating poor solubility, which in turn made it difficult to obtain accurate measures of the binding constants. The iodotriazole derivative **2.21** had improved solubility and showed improved binding affinity (K_i = 1.00 ± 0.05 μM) but was over 10 times less potent than the parent compound and was therefore regarded as a poor candidate.

2.6 Synthesis of Iodinated AOMKs Containing a Hydrophilic Linker

A more hydrophilic linker was used in an attempt to improve the solubility of the inhibitors and enhance their binding affinities. This was achieved by replacing the six-carbon spacer with a 3-unit polyethylene glycol linker (Figure 2.1C). Using similar methods, compounds **2.9a** and **2.9b** were coupled to the triethylene glycol bifunctional linker giving the iodobenzamide-PEG derivatives **2.22a** and **2.22b** (Scheme 2.7). Compound **2.6a** was coupled to the new linkers using PyBOP in the presence of triethylamine, giving **2.23a** and **2.23b** in 22% and 37% yields respectively.

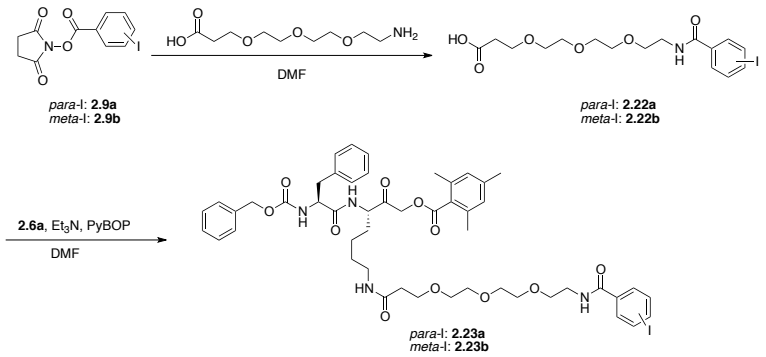

Scheme 2.7 Synthesis of **2.23a**/**b**.

To prepare the bifunctional triazole linker, triethylene glycol was combined with *tert*-butyl acrylate, generating the protected carboxylic acid **2.24** (Scheme 2.8). Compound **2.24** was converted to the mesylate and combined with sodium azide to generate **2.25**. Ethynyl tributyltin was used in a 1,3-dipolar cycloaddition with **25** producing the triazole **2.26** as a single isomer. Treatment of **2.26** with iodine gave the iodinated triazole **2.27**, which was deprotected to generate **2.28**. The resultant iodotriazole PEG linker **2.28** was then coupled to **2.6a** using PyBOP in the presence of triethylamine giving **2.29** in 37% yield.

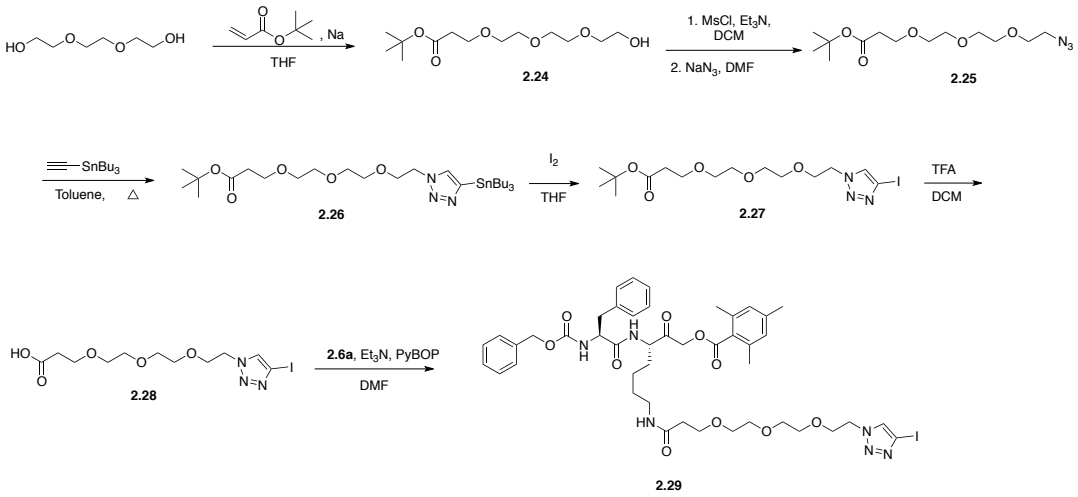

Scheme 2.8 Synthesis of **2.29**.

2.7 Inhibition of Cathepsin B by Iodinated-PEG-AOMKs

Inhibitors containing the PEG spacer (**2.23a**, **2.23b**, and **2.29**) showed improved binding affinities over their alkyl counter parts (**2.11a**, **2.11b** and **2.21**) with nanomolar K_i values (Table 2.1). The *para*-iodobenzamide **2.23a** exhibited the best affinity with a K_i of 181 ± 9 nM (Table 2.1). As an additional comparison, a known Cy5-labeled AOMK, GB123 (**2.30**, Figure 2.1C), was synthesized and tested (Scheme 2.9). Reports of GB123 have shown good visualization of cathepsin B positive tumors through optical imaging.[3–5] A K_i value of 120 ± 20 nM was determined for **2.30** suggesting that the K_i value for **2.23a** was sufficient to proceed to radiolabeling and biodistribution studies.

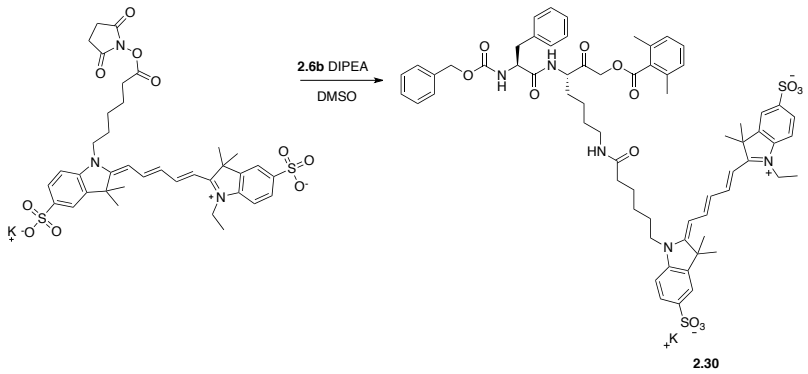

Scheme 2.9 Synthesis of **2.30**.

2.8 Synthesis of Radioiodinated AOMKs.

To compare the effect of the hydrophilic spacer *in vitro* and *in vivo*, **2.11a** was selected alongside **2.23a** for radiolabeling and further testing. We have previously demonstrated that fluorous tin benzamides and phenyl ureas can be used to radioiodinate small molecules and the products can be isolated without HPLC via a simple fluorous solid-phase extraction (FSPE).[50,51] To convert the selected cathepsin B inhibitors to their radioactive analogues, the iodobenzamide precursors **2.10a** and **2.22a** were converted to the corresponding arylstannanes using a fluorous distannane and a Pd-catalyzed cross coupling reaction (Scheme 2.10 & Scheme 2.11).[52] The addition of the fluorous tin moiety was performed on the prosthetic group as opposed to the iodinated inhibitors to avoid degradation of the peptide backbone due to the harsh reaction conditions. The fluorous tin groups **2.31** and **2.33** were coupled to **2.6a** using PyBOP

in the presence of triethylamine giving the precursors for radiolabeling **2.32** and **2.34** in 14% and 12% yields respectively (Scheme 2.10 & Scheme 2.11).

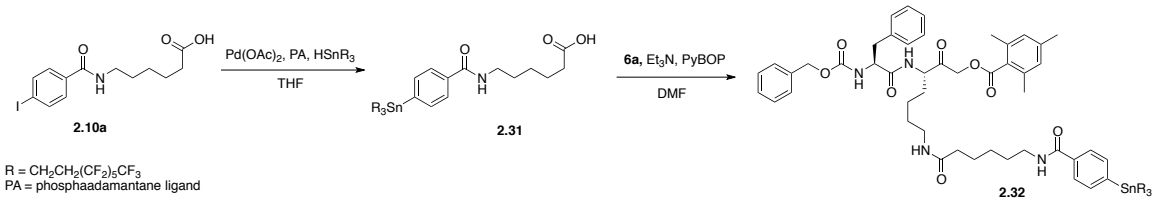

Scheme 2.10 Synthesis of **2.32**.

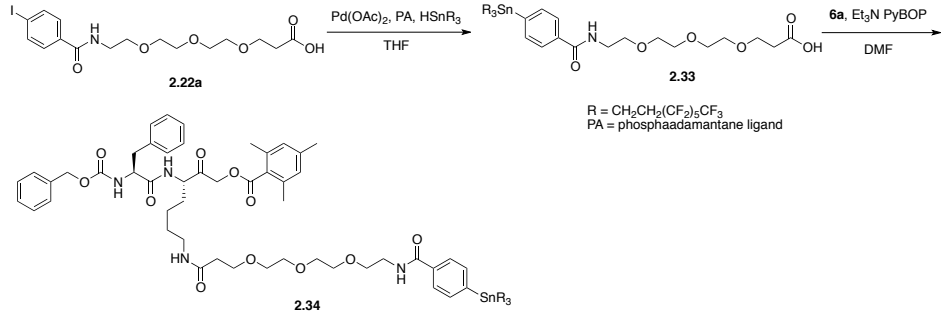

Scheme 2.11 Synthesis of **2.34**.

Radiolabeling was performed by treating **2.32** and **2.34** with [^{125}I]NaI in the presence of iodogen (Scheme 2.12). Following FSPE purification, isolated radiochemical yields ranged from 32 - 36% (*n* = 3) for [^{125}I]**2.11a** and 26 - 35% (*n* = 3) for [^{125}I]**2.23a**. The modest radiochemical yields can be attributed to non-specific binding of the inhibitors to the reaction vessel and to the FSPE cartridge. The identities of the radiolabeled compounds

were confirmed by co-injection with the non-radioactive standards and correlating the retention times of the peaks in the gamma and UV-chromatograms (Figure 2.5 & Figure 2.6). Because of the long reaction times needed to couple the arylstannane spacers to **2.6a**, the precursors **2.32** and **2.34** underwent some extent of epimerization. Consequently [^{125}I]**2.11a** and [^{125}I]**2.23a** also contained the associated epimers (~7 and 20% respectively, Figure 2.5 & Figure 2.6), similar to what has been observed for other AOMK derivatives.[28]

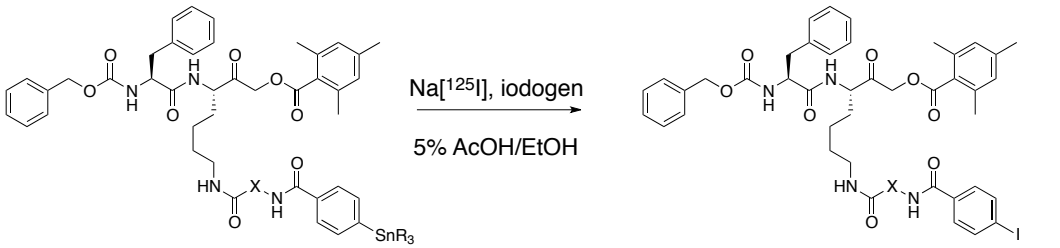

Scheme 2.12 Synthesis of [^{125}I]**2.11a** and [^{125}I]**2.23a**.

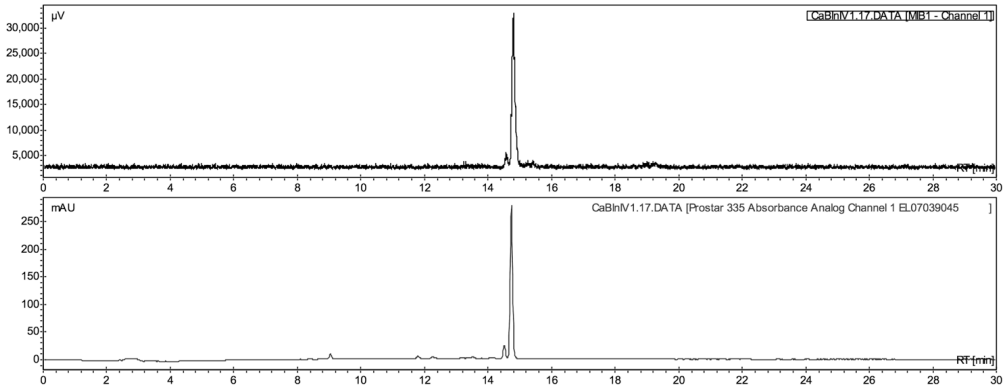

Figure 2.5 HPLC Chromatograms of [^{125}I]**2.11a** coinjected with the reference standard **2.11a**. Radiochromatogram (upper trace) and UV-visible (λ = 254 nm) chromatogram (lower trace).

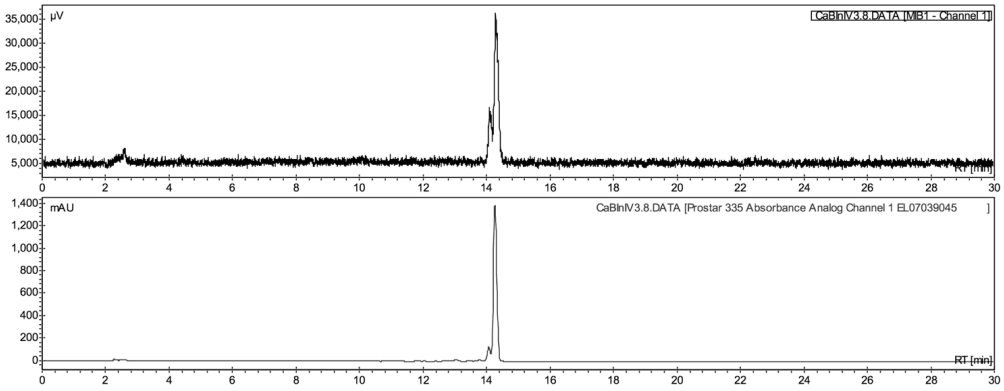

Figure 2.6 Radiochromatogram (upper trace) and UV-visible (λ = 254 nm) chromatogram of [^{125}I]**2.23a** co-injected with the reference standard **2.23a**.

2.9 Activity-Based Labeling of Cathepsin B.

The affinity of the radiolabeled inhibitors for cathepsin B was evaluated using SDS-PAGE. Equivalent amounts of cathepsin B were pretreated with saturating amounts of the known cathepsin B specific inhibitor L-3-*trans*-(propylcarbamyl)oxirane-2-carbonyl)-L-isoleucyl-L-proline (CA-074)[53] or with the vehicle (DMSO). The samples were then treated with [^{125}I]**2.11a** or [^{125}I]**2.23** and subjected to SDS-PAGE then autoradiography. Despite different binding affinities cathepsin B labeling was observed with both [^{125}I]**2.11a** and [^{125}I]**2.23** (Figure 2.7). The activity in each band was

blocked quantitatively by the addition of CA-074 indicating site-specific labeling of cathepsin B. It has be established that Phe-Lys-AOMKs can inactivate other cysteine cathepsins such as cathepsin L and cathepsin S.[14,22,23,32] It is therefore expected that the iodine derivatives described here would show similar inhibition and selectivity.

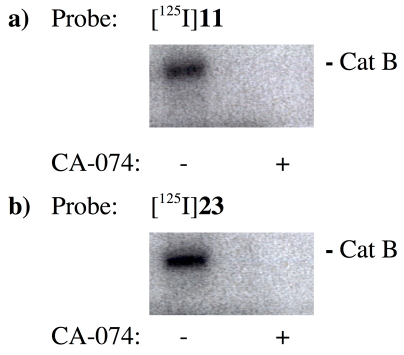

Figure 2.7 Phosphor images of an SDS-PAGE gel showing the specific labeling of active cathepsin B. Solutions of cathepsin B were pretreated with CA-074 (+) or DMSO (-) followed by (a) [^{125}I]**2.11a** or (b) [^{125}I]**2.23a**.

2.10 Biodistributions of ABPs in Tumor Bearing Mice.

The labeled probes, [^{125}I]**2.11a** and [^{125}I]**2.23a** were administered intravenously into CD1 nu/nu mice bearing the MDA-MB-231 xenograft. MDA-MB-231 cells are known to express cathepsin B and the xenografts have been used to evaluate other AOMK based ABPs.[14,54] After 0.5 h, 5 h, and 23 h p.i., animals were sacrificed and the percent injected dose per

gram (% ID/g) in various tissues, organs, and fluids was determined (Table 2.2).

Table 2.2. Biodistribution of [^{125}I]**2.11a** and [^{125}I]**2.23a** in MDA-MB-231 Tumor Bearing Mice[a]

	[^{125}I]**2.11a**[b]			[^{125}I]**2.23a**[c]		
Organs	30 min	5 h	23 h	30 min	5 h	23 h
blood	1.14 ±0.09	0.43 ±0.05	0.030 ±0.003	2.3 ±0.2	0.28 ±0.03	0.04 ±0.00
heart	0.68 ±0.06	0.19 ±0.02	0.030 ±0.004	0.9 ±0.2	0.11 ±0.01	0.02 ±0.00
lungs	2.2 ±0.2	0.84 ±0.09	0.21 ±0.02	3.5 ±0.5	0.59 ±0.08	1 ±1
liver	16 ±1	4.5 ±0.4	1.6 ±0.2	3.4 ±0.3	0.71 ±0.07	0.29 ±0.04
gall bladder	170 ±30	60 ±20	0.4 ±0.1	42 ±7	5 ±1	0.17 ±0.09
spleen	8 ±2	1.3 ±0.2	0.6 ±0.1	1.5 ±0.2	0.37 ±0.04	0.13 ±0.01

kidneys	2.9	0.80	0.20	6	0.55	0.4
	±0.3	±0.05	±0.02	±1	±0.06	±0.1
stomach	3.8	4.2	0.15	11	2.2	0.09
	±0.7	±0.6	±0.06	±3	±0.2	±0.01
small intestine	12	10	1.6	5.9	0.7	0.07
	±1	±1	±0.2	±0.2	±0.2	±0.02
large intestine	0.30	21	0.63	0.7	4.9	0.12
	±0.02	±2	±0.07	±0.1	±0.1	±0.02
tumor	0.58	0.5	0.040	1.12	0.27	0.05
	±0.06	±0.1	±0.002	±0.08	±0.07	±0.01
thyroid/	3.2	19	17	11	21	20
trachea	±0.8	±5	±9	±3	±9	±10
adipose	0.22	0.100	0.030	1.1	0.03	0.01
	±0.05	±0.004	±0.005	±0.9	±0.01	±0.00
bone	0.52	0.15	0.030	0.55	0.09	0.01
	±0.07	±0.01	±0.004	±0.07	±0.01	±0.00
skeletal muscle	0.25	0.11	0.010	0.5	0.05	0.01
	±0.03	±0.02	±0.001	±0.2	±0.00	±0.00
brain	0.09	0.04	0.003	0.19	0.01	0.00
	±0.01	±0.01	±0.001	±0.02	±0.00	±0.00
bladder & urine	90	38	0.9	400	31	0.7
	±20	±9	±0.2	±200	±3	±0.2

[a] Values are the mean % ID/g ± standard error from the mean [b] n = 5 or [c] n = 3.

After 30 min p.i., the bladder/urine (90 ± 20 % ID/g), gall bladder (170 ± 30 % ID/g), and liver (16 ± 1 % ID/g) showed the highest uptake for [^{125}I]**2.11a**, which was reduced after 23 h p.i. (0.9 ± 0.2, 0.4 ± 0.1, and 1.6 ± 0.2 % ID/g respectively). The areas with the highest uptake at 23 h p.i. were the thyroid/trachea (17 ± 9 % ID/g), small intestine (1.6 ± 0.2 % ID/g) and liver (1.6 ± 0.2 % ID/g). The accumulation in the thyroid/trachea is indicative of deiodination as the sample did not contain any free iodide at the time of administration.[55] The initial tumor uptake was (0.58 ± 0.06 % ID/g at 30 min p.i.) and decreased over time. Despite this, the tumor:blood ratios increased from 0.5 reaching a maximum of 1.6 after 23 h p.i. (Figure 2.8A). Similarly the tumor:muscle ratios increased from 2.3 reaching a peak value of 4 at 5 h p.i.

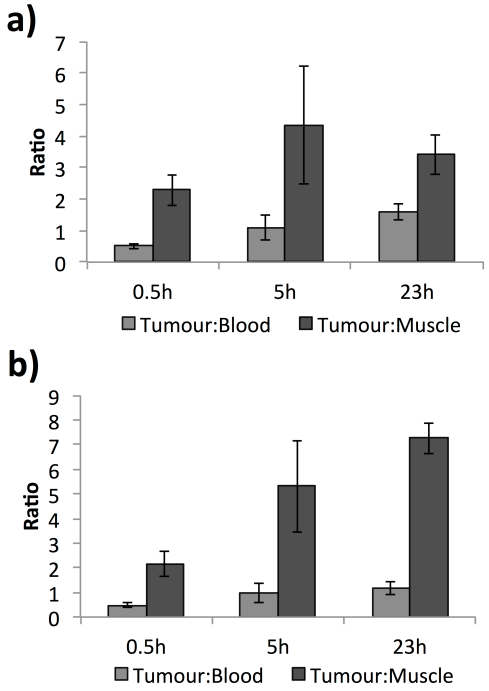

Figure 2.8 Average tumor-to-blood and tumor-to-muscle ratios for (a) [^{125}I]**2.11a** (*n* = 5) and (b) [^{125}I]**2.23a** (*n* = 3).

In the case of the more potent and hydrophilic derivative [^{125}I]**2.23a**, the bladder/urine (400 ± 200 % ID/g) and gall bladder (42 ± 7 % ID/g) showed the highest uptake after 30 min p.i. The liver uptake was lower in comparison to [^{125}I]**2.11a** (3.4 ± 0.3 % ID/g vs. 16 ± 1 % ID/g, 30 min p.i.) and the radioactivity was cleared from the majority of the tissues after 23 h p.i. Again, accumulation in the thyroid/trachea was observed, indicating *in vivo* deiodination. The observed tumor uptake was higher for [^{125}I]**2.23a** (1.12 ± 0.08 % ID/g) than that of [^{125}I]**2.11a** at 30 min., and the

tumor:blood ratios showed an increase from 0.5 to 1.2 after 23 h p.i. (Figure 2.8B). In addition the tumor:muscle ratios increased from 2.1 to 7.3 for **2.23a** reaching a maximum at 23 h.

Compound [^{125}I]**2.23a** showed lower accumulation in non-target tissues in comparison with the previously reported ^{64}Cu AOMK deriviative.[32] When tested in MDA-MB-435 xenografts it exhibited < 0.5% ID/g tumor uptake, a tumor-to-blood ratio of 0.61, and a tumor-to-muscle ratio of 3.03 at 2 h p.i. Compound [^{125}I]**2.23a** exhibited similar tumor uptake at 5 h p.i. (0.27% ID/g) in the MDA-MB-231 xenografts, which have comparable levels of cathepsin B activity as the MDA-MB-435 model,[14] while the tumor-to-blood (0.98) and tumor-to-muscle (5.31) ratios were higher for [^{125}I]**2.23a**.

2.11 Summary and Conclusion

This work explored the utility of the AOMK construct as a targeting vector to develop radioiodinated ABPs for cathepsin B. Attachment of bulky aromatic groups to the lysine side-chain with and without an aliphatic spacer had a detrimental impact on cathepsin B binding when compared to the parent ligand. However, inhibitors containing a PEG spacer showed high affinity for the enzyme. Despite different binding affinities and lipophilicities [^{125}I]**2.11a** and [^{125}I]**2.23a** were able to label cathepsin B *in vitro*, which was blocked in the presence of a known cathepsin B inhibitor.

Evaluation of [^{125}I]**2.23a** in a human MDA-MB-231 breast cancer model showed improved tumor-to-non-tumor ratios in comparison to other P_1 radiolabelled AOMKs but modest total tumor uptake.

2.12 Experimental

General. All chemicals, unless otherwise stated, were purchased from Sigma-Aldrich, Novabiochem, or Bachem and used without further purification. The Cy5 succinimidyl ester was obtained from GE Healthcare. (Tris(1H,1H,2H,2H-perfluorooctyl)tin hydride was obtained from Fluorous Technologies Inc. Diazomethane was prepared using the Diazald® Glassware Set with System 45® connections (Aldrich) following the procedures provided by the supplier. As this is a toxic and explosive substance the appropriate precautions should be exercised. 1,3,5,7-Tetramethyl-6-(2,4-dimethoxyphenyl)-2,4,8-trioxa-6-phosphaadamantane was provided by the Capretta research group (McMaster University). [^{125}I]NaI (specific activity, 629 GBq/mg was provided by the McMaster Nuclear Reactor. As this is a radioactive isotope, appropriate facilities, licenses, and procedures should be in place prior to use.

For screening studies, human liver cathepsin B and Cbz-Arg-Arg-pNA were purchased from Calbiochem and Enzo Life Sciences respectively. Reagents used in the assay buffer were from Sigma-Aldrich. Inhibitors

were dissolved in biological grade DMSO and diluted in the assay buffer. Black, clear bottom 96-well plates were obtained from BD Biosciences. L-3-*trans*-(propylcarbamyl)oxirane-2-carbonyl)-L-isoleucyl-L-proline (CA-074) was obtained from EMD Biosciences, precast gels were from Bio-Rad, and the gel drying kit was from Promega. 1,3,4,6-Tetrachloro-3a,6a-diphenyl-glycoluril (iodogen) was obtained from Thermo Scientific. According to HPLC analysis, supported by ^{1}H and ^{13}C NMR spectroscopy and HRMS, the chemical purity of all compounds screened for cathepsin B inhibition was > 95%.

Microwave reactions were performed using a Biotage Initiator Microwave Synthesizer. Automated flash chromatography was performed using a Biotage SP1 Flash Purification System. Analytical TLC was performed on silica gel plates with fluorescent indicator UV_{254} (Macherey-Nagel) and visualized using UV light and ninhydrin or vanillin in EtOH. ^{1}H, ^{13}C, and 2D NMR spectra were recorded using either a Bruker AV500 or AV600 spectrometer. ^{1}H NMR signals are reported in ppm measured relative to the residual proton signal of the deuterated solvent. Coupling constants (J) are reported in Hertz (Hz). ^{13}C signals are reported in ppm relative to the carbon signal from the solvent. High-resolution mass spectrometry (HRMS) was preformed using a Waters/Micromass Q-Tof

Ultima Global spectrometer. Analytical HPLC was performed using an Agilent/Varian Pro Star model 330 PDA detector, model 230 solvent delivery system and a Phenomenex Gemini (L × ID = 100 × 4.6 mm) column (5 μm C18). Semi-preparative HPLC was performed using an Agilent/Varian Pro Star model 325 PDA detector, model 24 solvent delivery system and a Phenomenex Gemini (L × ID = 250 × 10 mm) column (5 μm C18). The elution conditions were as follows: **Method A**: Solvent A = CH_3CN with 0.1% TFA, B = H_2O with 0.1% TFA: Gradient: 30% A to 100% A, 0 – 12 min; 100% A, 12 – 24 min; 100% A, to 90% A, 24 – 28 min; 90% A, to 30% A, 28 – 30 min. **Method B**: Solvent A = CH_3CN, B = H_2O: Gradient: 30% A to 100% A, 0 – 12 min; 100% A, 12 – 24 min; 100% A to 90% A, 24 – 28 min; 90% A to 30% A, 28 – 30 min. **Method C**: Solvent A = CH_3CN B = H_2O: Gradient: 10% A, 0 – 2 min; 10% A – 90% A, 2 – 20 min; 90% A, 20 – 22 min; 90% A, to 10% A, 22 – 23 min; 10% A, 23 – 25 min. The flow rate was set at 1 mL/min for analytical methods and 4 mL/min for semi-preparative methods; monitoring occurred at 254 nm. Autoradiography was measured using a GE Storm 840 phosphor imager and absorbance readings were performed using a BioRad EL 808 plate reader. Radioactivity measurements for biodistribution and LogP studies were made using a Wizard 1470 Automated Gamma Counter (PerkinElmer, Woodbridge ON).

Synthetic Methods

(*S*)-Methyl 2-((*S*)-2-(((benzyloxy)carbonyl)amino)-3-phenylpropanamido)-6-((*tert*-butoxycarbonyl)amino)hexanoate (2.1). Z-Phe-OH (3.0 g, 10 mmol) was dissolved in $CHCl_3$ (14 mL) at -20 °C and *N*-methylmorpholine (NMM) (1.1 mL, 10 mmol) was added. After 15 min. isobutylchloroformate (IBCF) (1.3 mL, 10 mmol) was added the temperature was maintained at -20 °C. After 10 min H-Lys(ε-Boc)-OMe·HCl (2.9 g, 9.9 mmol) and N-methylmorpholine (1.1 mL, 10 mmol) were added and the solution was stirred overnight. The solvent was removed by rotary evaporation and the resultant residue was dissolved in EtOAc (100 mL) and extracted with water (3 × 30 mL), sat. $NaHCO_3$ (3 × 30 mL), 5% (w/v) citric acid (3 × 30 mL), water (3 × 25 mL), and brine (3 × 30 mL). The organic layer was dried over $MgSO_4$ and the solvent was removed by rotary evaporation. The product was isolated following recrystalization from $CHCl_3$/hexanes, giving a white powder. Yield (4.1 g, 76%). TLC (1:1 EtOAc:Hex): R_f = 0.47; ^{1}H NMR (600.13 MHz, $(CD_3)_2SO$): δ 8.41 (d, J = 7.4 Hz, 1H, N***H***CHCOCH$_3$), 7.50 (d, J = 8.7 Hz, 1H, N***H***CHCONH), 7.34-7.20 (m, 10H Ph), 6.80 (t, J = 5.3 Hz, 1H, CH$_2$N***H***COO^{t}Bu), 4.93 (s, 2H, PhC***H***$_2$O), 4.31 (dt, J = 9.7, 3.7 Hz, 1H, HNC***H***CO Phe), 4.21-4.25 (m, 1H, HNC***H***CO Lys), 3.62 (s, 3H OC***H***$_3$),

2.99 (dd, J = 13.8, 3.5 Hz, 1H, CHC***H***HPh), 2.88-2.91 (m, 2H, $CH_2CH_2C\boldsymbol{H}_2NCO$), 2.72 (dd, J = 13.7, 11.1 Hz, 1H, CHC***H***HPh), 1.73-1.68 (m, 1H, CHC***H***HCH_2CH_2), 1.62 (dtd, J = 14.2, 9.5, 4.6 Hz, 1H, CHC***H***HCH_2CH_2), 1.36 (m, 11H, $C(C\boldsymbol{H}_3)_3$ and $CH_2C\boldsymbol{H}_2CH_2NHCO$), 1.32-1.26 (m, 2H, $C\boldsymbol{H}_2CH_2CH_2NHCO$); ^{13}C NMR (150.92 MHz, $(CD_3)_2SO$) δ 172.4, 171.8, 155.8, 155.5, 138.0, 137.0, 129.2, 128.2, 128.0, 127.6, 127.4, 126.2, 77.3, 65.2, 55.8, 52.0, 51.8, 39.6, 37.4, 30.6, 29.1, 28.2, 22.6; HRMS Calcd. for $C_{29}H_{40}N_3O_7$ $[M+H]^+$: 542.2866. Found 542.2872. mp: 115-118 °C.

(*S*)-Benzyl (1-(1*H*-benzo[*d*][1,2,3]triazol-1-yl)-1-oxo-3-phenylpropan-2-yl)carbamate (2.2) 1H-benzotriazole (4.8 g, 40 mmol) was dissolved in anhydrous THF (30 mL) under a stream of Ar. Thionyl chloride (10 mmol, 730 μL) was added to the solution and stirred for 30 min at 35°C. Z-Phe-OH (3.0 g, 10 mmol) was dissolved in anhydrous THF (10 mL) at 0°C and added dropwise to the reaction mixture at 0 °C. After 3 h of stirring the white percipitate that formed was removed by filtration. THF was removed by rotary evaporation and the solid residue was dissolved in EtOAc (100 mL), extracted with 6 N HCl (3 × 50 mL) and brine (3 × 50 mL) and dried over $MgSO_4$. The solvent removed by rotary evaporation and the residue was recrystalized from $CHCl_3$/hexanes giving **2.2** as a white powder. Yield (3.0 g, 74%). TLC (1:2 EtOAc:Hex): R_f = 0.52; ^1H NMR (600.13 MHz;

CD_2Cl_2): δ 8.23 (d, J = 8.2 Hz, 1H Ar***H***), 8.16 (d, J = 8.2 Hz, 1H Ar***H***), 7.72-7.69 (m, 1H Ar***H***), 7.58-7.55 (m, 1H Ar***H***), 7.37-7.15 (m, 10H Ph), 6.05-6.01 (m, 1H, NHC***H***CO), 5.57 (d, J = 7.6 Hz, 1H, N***H***CHCO), 5.06 (s, 2H, PhC***H***$_2$O), 3.46 (dd, J = 14.0, 4.7 Hz, 1H, CHC***H***$_2$Ph), 3.20 (dd, J = 14.0, 8.1 Hz, 1H, CHC***H***$_2$Ph); ^{13}C NMR (150.92 MHz; CD_2Cl_2): δ 171.3, 156.0, 146.5, 136.7, 135.7, 131.4, 131.2, 129.6, 129.0, 128.8, 128.5, 128.3, 127.7, 126.9, 120.7, 114.6, 67.4, 56.1, 39.1; HRMS Calcd. for $C_{23}H_{21}N_4O_3$ $[M+NH_4]^+$: 418.1879. Found 418.1891. mp: 112-114 °C.

(*S*)-2-((*S*)-2-(((Benzyloxy)carbonyl)amino)-3-phenylpropanamido)-6-((*tert*-butoxycarbonyl)amino)hexanoic acid (2.3) ROUTE A: To a solution of **2.1** (3.69 mmol, 2.00 g) in CH_3CN (10 mL), NaOH (1N, 4 mL) was added and left to stir for 5 h. The organic solvent was then removed by rotary evaporation, water (20 mL) was then added and excess started material was extracted with EtOAc (3 × 20 mL). The aqueous layer was neutralized with 1 N HCl (4 mL) at 0 °C. The precipitated product was extracted with EtOAc (3 × 20 mL) and dried over $MgSO_4$. The solvent was removed by rotary evaporation and the oily residue was recrystalized from EtOAc/hexanes giving a white solid. Yield (1.5 g, 76%). ROUTE B: To a solution of Et_3N (0.83 mL, 6 mmol) and H-Lys(ε-Boc)-OH (1.2 g, 5 mmol) in 5:2 v/v CH_3CN-water (49 mL), **2.2** (2.2 g, 5.5 mmol) was added and the

solution was stirred for 3 h, after which the organic solvent was removed by rotary evaporation. The resultant residue was dissolved in water (25 mL) and 6N HCl was added dropwise until a precipitate formed, which was then extracted with EtOAc (3 × 20 mL). The organic layers were combined and extracted with 4 N HCl (3 × 20 mL), brine (3 × 20 mL) and dried over $MgSO_4$. The solvent was removed by rotary evaporation and the product was isolated from recystalization from EtOAc/hexanes and white solid. Yield (2.19 g, 83%). TLC (1:1 EtOAc:Hex): R_f = 0.36; ^{1}H NMR (500.13 MHz; $(CD_3)_2SO$): δ 12.58 (s, 1H, O***H***), 8.21 (d, J = 7.6 Hz, 1H, N***H***CHCOOH), 7.46 (d, J = 8.7 Hz, 1H, N***H***CHCONH), 7.34-7.18 (m, 10H, Ph), 6.76-6.75 (m, 1H, CH_2N***H***CO), 4.93 (s, 2H, PhC***H***$_2$O), 4.30 (dt, J = 9.7, 3.4 Hz, 1H, HNC***H***CO Phe), 4.15-4.20 (m, 1H, HNC***H***CO Lys), 3.01 (dd, J = 13.8, 3.1 Hz, 1H, CHC***H***HPh), 2.88-2.92 (m, 2H, CH_2CH_2C***H***$_2$NHCO), 2.72 (dd, J = 13.5, 11.3 Hz, 1H, CHC***H***HPh), 1.76-1.66 (m, 1H, CHC***H***HCH_2CH_2), 1.64-1.54 (m, 1H, CHC***H***HCH_2CH_2), 1.36 (m, 11H, C(C***H***$_3)_3$ and CH_2C***H***$_2CH_2$NHCO), 1.33-1.26 (m, 2H, C***H***$_2CH_2CH_2$NHCO). ^{13}C NMR (125.77 MHz, $(CD_3)_2SO$): δ 173.5, 171.7, 155.8, 155.5, 138.1, 137.0, 129.2, 128.3, 128.0, 127.6, 127.4, 126.2, 77.3, 65.2, 55.9, 51.9, 40.0, 37.4, 30.8, 29.1 28.3, 22.8; HRMS Calcd. for $C_{28}H_{38}N_3O_7$ $[M+H]^+$: 528.2710. Found 528.2704. mp: 104 – 105 °C.

ZPheLys(ε-Boc)CH_2Br (2.4) To a solution of **2.3** (2.0 g, 3.8 mmol) in anhydrous THF (20 mL) at -20 °C, NMM (0.52 mL, 4.8 mmol) and IBCF (0.57 mL, 4.4 mmol) were added and stirred for 20 min under a stream of Ar. A solution of CH_2N_2 in Et_2O was added to the reaction mixture dropwise until a bright yellow color persisted after warming to room temperature. The stream of Ar was removed and the solution was left to stir 3 h while warming to room temperature. A solution of 11:22:17 v/v/v HBr/AcOH/water (12.1 mL) was added dropwise at 0 °C and the solution stirred for 3 min. EtOAc (100 mL) was addded and the solution was extracted with water (3 × 30 mL), sat. $NaHCO_3$ (3 × 30 mL), brine (3 × 30 mL) and dried over $MgSO_4$. Removal the solvent gave **2.4** as a pale yellow solid. Yield (2.0 g, 89%). TLC (1:1 EtOAc:Hex): R_f = 0.47; ^{1}H NMR (500.13 MHz; $(CD_3)_2SO$): δ 8.48 (d, J = 7.3 Hz, 1H, N***H***CHCOCH_2Br), 7.59 (d, J = 8.2 Hz, 1H, N***H***CHCONH), 7.35-7.20 (m, 10H Ph), 6.75 (t, J = 5.1 Hz, 1H, CH_2N***H***CO), 4.96 (s, 2H, PhC***H***$_2$O), 4.36 (dt, J=11.4, 4.5 Hz, 1H HNC***H***CO Lys), 4.31-4.28 (m, 1H, HNC***H***CO Phe), 4.26 (d, J = 4.6 Hz, 2H, COC***H***$_2$Br), 2.99 (dd, J = 13.7, 5.0 Hz, 1H, CHC***H***HPh), 2.88-2.91 (m, 2H, CH_2CH_2C***H***$_2$NCO), 2.78 (dd, J = 13.6, 10.1 Hz, 1H, CHC***H***HPh), 1.74 (ddt, J = 14.0, 9.3, 5.0 Hz, 1H, CHC***H***HCH_2CH_2), 1.54-1.56 (m, 1H, CHC***H***HCH_2CH_2), 1.32 (m 11H, C(C***H***$_3$)$_3$ and CH_2C***H***$_2CH_2$NHCO), 1.24-

1.18 (m, 2H, C***H***$_2$CH$_2$CH$_2$NHCO). ^{13}C NMR (125.77 MHz; $(CD_3)_2SO$): δ 200.4, 171.9, 155.9, 155.5, 137.8, 136.9, 129.2, 128.3, 128.1, 127.7, 127.5, 126.3, 77.3, 65.3, 56.5, 56.0, 37.2, 35.1, 29.2, 29.1, 28.3, 28,1, 22.5; HRMS Calcd. for $C_{29}H_{39}N_3O_6Br$ $[M+H]^+$: 604.2022. Found 604.2003. mp: 125-135 °C.

(*S*)-3-((*S*)-2-(((Benzyloxy)carbonyl)amino)-3-phenylpropanamido)-7-((*tert*-butoxycarbonyl)amino)-2-oxoheptyl 2,4,6-trimethylbenzoate (2.5a) To a solution of **2.4** (1.9 g, 3.2 mmol) in anhydrous DMF (20 mL), anhydrous KF (0.56 g, 9.6 mmol) and 2,4,6-trimethylbenzoic acid (0.58 g, 3.5 mmol) were added and the solution left to stir for 3 d under a stream of Ar. Water (30 mL) was added and the product was extracted with CH_2Cl_2 (3 × 20 mL) and the combined organic layers extracted with brine (3 × 20 mL), water (5 × 20 mL), sat $NaHCO_3$ (3 × 20 mL), and dried over Na_2SO_4. The solvent was removed by rotary evaporation and the product was precipitated from CH_2Cl_2/hexanes giving **2.5a** as a white powder. Yield (1.5 g, 69%). TLC (1:1 EtOAc:Hex): R_f = 0.64; ^{1}H NMR (600.13 MHz; $(CD_3)_2SO$): δ 8.49 (d, J = 7.4 Hz, 1H, N***H***CHCOCH$_2$), 7.63 (d, J = 8.1 Hz, 1H, N***H***CHCONH), 7.34-7.18 (m, 10H Ph), 6.92 (s, 2H, Me$_3$C$_6$***H***$_2$CO), 6.74 (m, 1H, CH$_2$N***H***CO), 4.97 (s, 2H, PhC***H***$_2$O), 4.90 (d, J = 17.2 Hz, 1H, COC***H***HOCO), 4.80 (d, J = 17.1 Hz, 1H, COC***H***HOCO), 4.33 (m, 2H, HNC***H***CO Phe and Lys), 3.02 (dd, J=13.5, 5.1 Hz, 1H, CHC***H***HPh), 2.89-

2.91 (m, 2H, $CH_2CH_2C\boldsymbol{H}_2NHCO$), 2.81 (dd, J=13.3, 10.0 Hz, 1H $CHC\boldsymbol{H}HPh$), 2.27 (s, 6H, 2,6-$(C\boldsymbol{H}_3)_3C_6H_2CO$), 2.25 (s, 3H, 4-$(C\boldsymbol{H}_3)_3C_6H_2CO$), 1.82-1.75 (m, 1H, $CHC\boldsymbol{H}HCH_2CH_2$), 1.58-1.51 (m, 1H, $CHC\boldsymbol{H}HCH_2CH_2$), 1.36 (m, 12H, $C(C\boldsymbol{H}_3)_3$, $CH_2C\boldsymbol{H}_2CH_2NHCO$, and $C\boldsymbol{H}HCH_2CH_2NHCO$), 1.27-1.23 (m, 1H, $C\boldsymbol{H}HCH_2CH_2NHCO$); ^{13}C NMR (150.92 MHz, $((CD_3)_2SO)$ δ 202.6, 171.9, 168.2, 155.8, 155.5, 139.1, 137.8, 136.9, 134.9, 129.9, 129.2, 128.2, 128.1, 128.0, 127.7, 127.5, 126.3, 77.3, 66.6, 65.3, 56.0, 55.9, 39.9, 37.2, 29.1, 29.1, 28.2, 22.3, 20.7, 19.3; HRMS Calcd. for $C_{39}H_{50}N_3O_8$ $[M+H]^+$: 688.3598. Found 688.3622. mp: 140-144°C.

(*S*)-3-((*S*)-2-(((Benzyloxy)carbonyl)amino)-3-phenylpropanamido)-7-((*tert*-butoxycarbonyl)amino)-2-oxoheptyl 2,6-dimethylbenzoate (2.5b)

To a solution of **2.4** (180 mg, 0.29 mmol) in anhydrous DMF (10 mL), anhydrous KF (51 mg, 0.87 mmol) and 2,6-dimethylbenzoic acid (48 mg, 0.32 mmol) were added and the solution left to stir for 3 d under a stream of Ar. Water (15 mL) was added and the product was extracted with CH_2Cl_2 (3 × 15 mL) and the combined organic layers extracted with brine (3 × 15 mL), sat $NaHCO_3$ (3 × 15 mL), and dried over $MgSO_4$. The solvent was removed by rotary evaporation and the product was recrystallized from $CHCl_3$/hexanes giving **2.5b** as a white powder. Yield (150 mg, 74%).

TLC (2:1 EtOAc:Hex): R_f = 0.56; ^{1}H NMR (600.13 MHz; $(CD_3)_2SO$): δ 8.52 (d, J = 7.5 Hz, 1H, N***H***CHCOCH$_2$), 7.66 (d, J = 8.3 Hz, 1H, N***H***CHCONH), 7.35-7.19 (m, 11 Ar***H***), 7.11 (d, J = 7.6 Hz, 2H, 3,5-Me$_2$C$_6$***H***$_3$CO), 6.78 (dd, J = 7.2, 3.6 Hz, 1H, CH$_2$N***H***CO), 4.98 (s, 2H, PhC***H***$_2$O), 4.93 (d, J = 17.2 Hz, 1H, COC***H***HOCO), 4.83 (d, J = 17.2 Hz, 1H, COC***H***HOCO), 4.34 (m, 2H, NC***H***CO Phe and Lys), 3.03 (dd, J = 13.6, 5.4 Hz, 1H, CHC***H***HPh), 2.92-2.88 (m, 2H, CH$_2$CH$_2$C***H***$_2$NHCO), 2.82 (dd, J = 13.6, 9.7 Hz, 1H, CHC***H***HPh), 2.31 (s, 6H, (C***H***$_3$)$_2$C$_6$H$_3$CO), 1.83-1.77 (m, 1H, CHC***H***HCH$_2$CH$_2$), 1.59-1.53 (m, 1H, CHC***H***HCH$_2$CH$_2$), 1.34-1.32 (m 12H, C(C***H***$_3$)$_3$, CH$_2$C***H***$_2$CH$_2$NHCO, and C***H***HCH$_2$CH$_2$NHCO), 1.27-1.24 (m, 1H, C***H***$_2$CH$_2$CH$_2$NHCO); ^{13}C NMR (150.92 MHz; $(CD_3)_2SO$): δ 202.6, 172.0, 168.1, 155.8, 155.6, 137.8, 136.9, 134.7, 132.9, 129.6, 129.2, 128.26, 128.08, 127.69, 127.51, 126.3, 77.4, 66.7, 65.3, 56.04, 55.93, 37.2, 29.14, 29.10, 28.2, 22.3, 19.3. HRMS Calcd. for $C_{39}H_{48}N_3O_8$ $[M+H]^+$: 673.3441. Found 674.3460. mp: 149-151 °C.

(*S*)-5-((*S*)-2-(((Benzyloxy)carbonyl)amino)-3-phenylpropanamido)-6-oxo-7-((2,4,6-trimethylbenzoyl)oxy)heptan-1-ammonium trifluoroacetate (2.6a) To a solution of **2.5a** (1.1 g, 1.6 mmol) in CH_2Cl_2 (33 mL) TFA (22 mL) was added dropwise at 0 °C. The solution was left to stir for 3 h warming to room temperature after which the solvent was removed by rotary evaporation. The residue was dissolved in CH_2Cl_2 and

added to cold Et_2O forming a white powder, which was then collected using centrifugation. Yield (1.0 g, 94%). TLC (20% MeOH:CH_2Cl_2): R_f = 0.66; HPLC (Method A): ^tR = 12.8 min; ^1H NMR (600.13 MHz; $(CD_3)_2SO$): δ 8.53 (d, J = 7.7, 1H, N***H***CHCOCH$_2$), 7.67-7.65 (m, 4H, CH_2CH_2N***H***$_3$, and N***H***CHCONH), 7.35-7.19 (m, 10H Ph), 6.92 (s, 2H, Me_3C_6***H***$_2$CO), 4.97 (s, 1H, PhC***H***HO), 4.97 (s, 1H, PhC***H***HO), 4.89 (d, J = 17.2 Hz, 1H, COC***H***$_2$O), 4.78 (d, J = 17.2 Hz, 1H, COC***H***$_2$O), 4.39-4.35 (m, 1H, HNC***H***CO Phe), 4.34-4.30 (m, 1H, HNC***H***CO Lys), 3.03 (dd, J = 13.7, 5.4, 1H, CHC***H***HPh), 2.83 (dd, J = 13.4, 9.7, 1H, CHC***H***HPh), 2.78-2.73 (m, 2H, CH_2CH_2C***H***$_2NH_3$), 2.27 (s, 6H, 2,6-(C***H***$_3)_3C_6H_2CO$), 2.25 (s, 3H, 4-(C***H***$_3)_3C_6H_2CO$), 1.85-1.80 (m, 1H, CHC***H***HCH$_2$CH$_2$), 1.60-1.47 (m, 3H CHC***H***HCH$_2$CH$_2$ and CH_2C***H***$_2CH_2NH_3$), 1.39-1.23 (m, 2H, C***H***$_2CH_2CH_2NH_3$); ^{13}C NMR (150.92 MHz; $(CD_3)_2SO$): δ 202.6, 172.0, 168.3, 158.2 ($J_{(C,F)}$ = 30.8 Hz), 155.9, 139.2, 137.7, 136.9, 134.9, 129.9, 129.3, 128.31, 128.25, 128.12, 127.8, 127.5, 126.4, 66.6, 65.3, 56.1, 55.7, 38.6, 37.2, 28.8, 26.5, 21.9, 20.7, 19.3; HRMS Calcd. for $C_{34}H_{42}N_3O_6$ $[M]^+$: 588.3074. Found 588.3083. mp: 119-123 °C.

(*S*)-5-((*S*)-2-(((Benzyloxy)carbonyl)amino)-3-phenylpropanamido)-7-((2,6-dimethylbenzoyl)oxy)-6-oxoheptan-1-aminium (2.6b) To a solution of **2.5b** (89 mg, 130 μmol) in CH_2Cl_2 (9 mL), TFA (3 mL) was

added dropwise at 0 °C. The solution was left to stir for 3 h warming to room temperature after which the solvent was removed by rotary evaporation. The residue was dissolved in CH_2Cl_2 (1 mL) and added to cold Et_2O (30 mL) forming a white powder, which was then collected using centrifugation. Yield (84 mg, 93%). TLC (20% MeOH:CH_2Cl_2): R_f = 0.60; HPLC (Method A): ^tR = 12.6 min; ^1H NMR (600.13 MHz; $(CD_3)_2SO$): δ 8.56 (d, J = 7.7 Hz, 1H, N***H***CHCOCH$_2$), 7.71-7.67 (m, 3H, CH_2CH_2N***H***$_3$, and m, 1H, N***H***CHCONH), 7.35-7.19 (m, 11 Ar***H***), 7.11 (d, J = 7.6 Hz, 3,5-Me_2C_6***H***$_3$CO), 4.97 (s, 2H, PhC***H***$_2$O), 4.92 (d, J = 17.2, 1H, COC***H***HO), 4.81 (d, J = 17.2, 1H, COC***H***HO), 4.38 (td, J = 8.6, 3.9 Hz, 1H, HNC***H***CO Phe), 4.34-4.30 (m, 1H, HNC***H***CO Lys), 3.03 (dd, J = 13.7, 5.5 Hz, 1H, CHC***H***HPh), 2.84 (dd, J = 13.6, 9.7, 1H, CHC***H***HPh), 2.79-2.74 (m, 2H, CH_2CH_2C***H***$_2NH_3$), 2.31 (s, 6H, (C***H***$_3)_2C_6H_3CO$), 1.86-1.80 (m, 1H, CHC***H***HCH_2CH_2), 1.54 (m, 3H CHC***H***HCH_2CH_2 and CH_2C***H***$_2CH_2NH_3$), 1.40-1.26 (m, 2H, C***H***$_2CH_2CH_2NH_3$); ^{13}C NMR (150.92 MHz; $(CD_3)_2SO$): δ 202.5, 172.0, 168.1, 155.9, 137.7, 136.9, 134.7, 132.8, 129.6, 129.3, 128.29, 128.11, 127.7, 127.5, 126.4, 66.6, 65.3, 56.1, 55.6, 38.6, 37.2, 28.8, 26.5, 21.8, 19.3. HRMS Calcd. for $C_{33}H_{39}N_3O_6$ $[M+Na]^+$: 596.2737. Found 596.2715. mp: 117-124 °C.

(*S*)-3-((*S*)-2-(((Benzyloxy)carbonyl)amino)-3-phenylpropanamido)-7-(3-iodobenzamido)-2-oxoheptyl 2,4,6-trimethylbenzoate (2.7a). To a

solution of 4-iodobenzoic acid (72 mg, 290 μmol) in DMF (12 mL) at -16 °C, NMM (32 μL, 290 μmol) and IBCF (38 μL, 290 μmol) were added and left to stir until dissolved. To this, **2.6a** (204 mg, 290 μmol) was added and the solution was left to stir overnight while warming to room temperature. The reaction mixture was diluted to 25 mL with water and extracted with EtOAc (3 × 50 mL), and the combined organic layers extracted with water (5 × 20 mL), sat. Na_2CO_3 (3 × 20 mL), water (20 mL), 5% (w/v) citric acid (3 × 20 mL), water (20 mL), brine (3 × 20 mL), and dried over $MgSO_4$. The solvent was removed by rotary evaporation and the product was isolated as a white powder. Yield (68 mg, 29%). TLC (2:1 EtOAc:Hex): R_f = 0.53; HPLC (Method B): ^{t}R = 18.1 min; ^{1}H NMR (600.13 MHz; $(CD_3)_2SO$): 8.51-8.48 (m, 2H, N***H***CHCONH and $CH_2CH_2CH_2N$***H***), 7.79 (d, J = 8.2 Hz, 2H, 2,6-C_6***H***$_2H_2I$), 7.63-7.60 (m, 1H, N***H***$CHCOCH_2$), 7.61 (d, J = 8.5 Hz, 2H, 3,5-C_6***H***$_2H_2I$), 7.33-7.18 (m, 10H Ph), 6.91 (s, 2H, Me_3C_6***H***$_2CO$), 4.95 (s, 2H, PhC***H***$_2OCO$), 4.91 (d, J = 17.4, 1H, COC***H***HO), 4.82 (d, J = 17.2, 1H, COC***H***HO), 4.38-4.31 (m, 2H, HNC***H***CO Phe and Lys), 3.25-3.22 (m, 2H, CH_2CH_2C***H***$_2NH$), 3.01 (dd, J = 13.4, 5.0 Hz, 1H, CHC***H***HPh), 2.80 (dd, J = 13.1, 10.4 Hz, 1H, CHC***H***HPh), 2.26 (s, 6H, 2,6-(C***H***$_3)_3C_6H_2CO$), 2.25 (s, 3H, 4-(C***H***$_3)_3C_6H_2CO$), 1.84-1.82 (m, 1H, CHC***H***HCH_2CH_2), 1.62-1.56 (m, 1H, CHC***H***HCH_2CH_2), 1.55-1.47 (m, 2H, CH_2C***H***$_2CH_2NH$), 1.40-1.30 (m,

2H, C***H***$_2$CH$_2$CH$_2$NH); ^{13}C NMR (150.92 MHz, $(CD_3)_2SO$) δ 202.7, 172.0, 168.2, 165.4, 155.8, 139.1, 137.8, 137.0, 136.9, 134.9, 134.1, 129.9, 129.2, 129.1, 128.3, 128.2, 128.1, 127.7, 127.5, 126.3, 98.5, 66.6, 65.3, 56.0, 55.9, 54.9, 37.3, 29.2, 28.6, 22.4, 20.7, 19.3; HRMS Calcd. For $C_{41}H_{45}N_3O_7I$ $[M+H]^+$: 818.2302. Found: 818.2280. mp: 163-165 °C.

(*S*)-3-((*S*)-2-(((Benzyloxy)carbonyl)amino)-3-phenylpropanamido)-7-(3-iodobenzamido)-2-oxoheptyl 2,4,6-trimethylbenzoate (2.7b). To a solution of 3-iodobenzoic acid (72 mg, 290 μmol) in DMF (12 mL) at -24 °C, NMM (33 μL, 300 μmol) and IBCF (39 μL, 300 μmol) were added stirred until dissolved. To this, **2.6a** (180 mg, 260 μmol) was added and the solution was left to stir overnight while warming to room temperature. The reaction mixture was diluted to 25 mL with water and extracted with EtOAc (3 × 20 mL), and the combined organic layers extracted with water (5 ×10 mL), sat. Na_2CO_3 (3 × 10 mL), water (20 mL), 5% (w/v) citric acid (3 × 10 mL), water (20 mL), brine (3 × 10 mL), and dried over $MgSO_4$. Yield (95 mg, 45%). TLC (2:1 EtOAc:Hex): R_f = 0.83; HPLC (Method B): ^tR = 18.0 min; ^{1}H NMR (600.23 MHz; $(CD_3)_2SO$): δ 8.52 (m, 2H, N***H***CHCONH and $CH_2CH_2CH_2N$***H***), 8.18 (s, 1H, 2-C_6***H***H_3I), 7.86-7.83 (m, 2H, 4,6-C_6***H***$_2H_2I$), 7.63 (d, J = 8.2, 1H, N***H***$CHCOCH_2$), 7.33-7.18 (m, 10H Ph), 6.91 (s, 2H, Me_3C_6***H***$_2CO$), 4.95 (s, 2H, PhC***H***$_2OCO$), 4.91 (d, J = 17.2 Hz, 1H,

COC***H***HO), 4.81 (d, J = 17.2 Hz, 1H, COC***H***HO), 4.39-4.32 (m, 2H, HNC***H***CO Phe and Lys), 3.24 (m, 2H, $CH_2CH_2C\boldsymbol{H}_2NH$), 3.02 (dd, J = 13.7, 5.3 Hz, 1H, CHC***H***HPh), 2.81 (dd, J = 13.5, 10.0 Hz, 1H, CHC***H***HPh), 2.26 (s, 6H, 2,6-$(C\boldsymbol{H}_3)_3C_6H_2CO$), 2.25 (s, 3H, 4-$(C\boldsymbol{H}_3)_3C_6H_2CO$), 1.87-1.78 (m, 1H, CHC***H***HCH_2CH_2), 1.64-1.56 (m, 1H, CHC***H***HCH_2CH_2), 1.56-1.47 (m, 2H, $CH_2C\boldsymbol{H}_2CH_2NH$), 1.41-1.29 (m, 2H, $C\boldsymbol{H}_2CH_2CH_2NH$); ^{13}C NMR (150.92 MHz, $(CD_3)_2SO$) δ 202.6, 172.0, 168.2, 164.5, 155.8, 139.5, 139.1, 137.8, 136.9, 136.6, 135.6, 134.9, 130.4, 129.9, 129.2, 128.2, 128.2, 128.1, 127.7, 127.5, 126.6, 126.3, 94.6, 66.6, 65.2, 56.0, 55.9, 40.0, 37.2, 29.1, 28.6, 22.5, 20.7, 19.3; HRMS Calcd. For $C_{41}H_{45}N_3O_7I$ $[M+H]^+$: 818.2302. Found: 818.2291. mp: 135-140 °C.

(*S*)-3-((*S*)-2-(((Benzyloxy)carbonyl)amino)-3-phenylpropanamido)-7-(3-(3-iodophenyl)ureido)-2-oxoheptyl 2,4,6-trimethylbenzoate (2.8a). To a solution of 4-iodophenyl isocyanate (42 mg, 170 μmol) in anhydrous CH_2Cl_2 (5 mL), Et_3N (24 mL, 170 mmol) and **2.6a** (119 mg, 170 mmol) was added and the solution left to stir 3 h under a stream of Ar. The solvent was removed by rotary evaporation and the residue was dissolved in DMF (1 mL). This solution was then added dropwise to rapidly stirring cold water (approx. 100 mL) forming a white powder that was collected using centrifugation. The product was isolated as a white powder following flash

chromatography (2:1, EtOAc/Hex). Yield (13 mg, 9%). TLC (2:1 EtOAc:Hex): R_f = 0.72; HPLC (Method B): ^{t}R = 17.3 min; ^{1}H NMR (600.13 MHz; $(CD_3)_2SO$): δ 8.55 (s, 1H, CON***H***C_6H_4I), 8.51 (d, J = 7.5 Hz, 1H CON***H***CHCO), 7.63 (d, J = 8.3 Hz, 1H, CON***H***CHCO), 7.51-7.48 (m, 2H, CONHC$_6$***H***$_2$H$_2$I), 7.33-7.19 (m, 12H, Ar***H***), 6.91 (s, 2H, Me_3C_6***H***$_2$CO), 6.20 (t, J = 5.4 Hz, 1H, $CH_2CH_2CH_2N$***H***), 4.96 (s, 2H, PhC***H***$_2$OCO), 4.91 (d, J = 17.2 Hz, 1H, COC***H***$_2$O), 4.81 (d, J = 17.2 Hz, 1H, COC***H***HO), 4.38-4.31 (m, 2H, HNC***H***CO Phe and Lys), 3.07-3.01 (m, 3H, CH_2CH_2C***H***$_2$NH, CHC***H***HPh), 2.81 (dd, J = 13.7, 9.8 Hz, 1H, CHC***H***HPh), 2.27 (s, 6H, 2,6-(C***H***$_3$)$_3C_6H_2CO$), 2.25 (s, 3H, 4-(C***H***$_3$)$_3C_6H_2CO$), 1.85-1.78 (m, 1H, CHC***H***HCH_2CH_2), 1.62-1.54 (m, 1H, CHC***H***HCH_2CH_2), 1.46-1.39 (m, 2H, CH_2C***H***$_2CH_2$NH), 1.39-1.33 (m, 1H, C***H***HCH_2CH_2NH), 1.32-1.25 (m, 1H, C***H***HCH_2CH_2NH); ^{13}C NMR (150.92 MHz; $(CD_3)_2SO$): δ 202.7, 172.0, 168.2, 155.9, 154.9, 140.5, 139.1, 137.8, 137.1, 134.9, 129.9, 129.2, 128.3, 128.3, 128.2, 128.1, 127.7, 127.5, 126.3, 119.9, 83.3, 66.6, 65.3, 56.1, 55.9, 38.9, 37.2, 29.3, 29.2, 22.4, 20.7, 19.3. HRMS Calcd. for $C_{41}H_{46}N_4O_7I$ $[M+H]^+$: 833.2411. Found 833.2451. mp: 149-159 °C.

(*S*)-3-((*S*)-2-(((Benzyloxy)carbonyl)amino)-3-phenylpropanamido)-7-(3-(4-iodophenyl)ureido)-2-oxoheptyl 2,4,6-trimethylbenzoate (2.8b). Synthesized in a similar manner as **2.8a** using 3-iodophenyl isocyanate in place of 4-iodophenyl isocyanate. Yield (20 mg, 14%). TLC (2:1

EtOAc:Hex): R_f = 0.85; HPLC (Method B): ^{t}R = 18.0 min; ^{1}H NMR (600.13 MHz; $(CD_3)_2SO$): δ 8.60 (s, 1H, CON***H***C_6H_4I), 8.53 (d, J = 7.4 Hz, 1H, CON***H***CHCO), 7.96 (dd, J = 1.8, 1,8 Hz, 1H, 5-NHC_6***H***$_2H_2I$), 7.65 (d, J = 8.2 Hz, 1H, CON***H***CHCO), 7.34-7.20 (m, 12H, Ar***H***), 6.99 (dd, J = 8.0, 1H, 2-NHC_6***H***$_2H_2I$), 6.92 (s, 2H, Me_3C_6***H***$_2$CO), 6.25 (t, J = 4.6 Hz, 1H, $CH_2CH_2CH_2N$***H***), 4.96 (s, 2H, PhC***H***$_2$OCO), 4.92 (d, J = 17.2 Hz, 1H, COC***H***HO), 4.81 (d, J = 17.2 Hz, 1H, COC***H***HO), 4.39-4.32 (m, 2H, HNC***H***CO Phe and Lys), 3.08-3.02 (m, 3H, CH_2CH_2C***H***$_2$NH and CHC***H***$_2$HPh), 2.82 (dd, J = 13.6, 9.8 Hz, 1H, CHC***H***HPh), 2.27 (s, 6H, 2,6-(C***H***$_3)_3C_6H_2$CO), 2.25 (s, 3H, 4-(C***H***$_3)_3C_6H_2$CO), 1.85-1.80 (m, 1H, CHC***H***HCH_2CH_2), 1.63-1.55 (m, 1H, CHC***H***HCH_2CH_2), 1.47-1.40 (m, 2H, CH_2C***H***$_2CH_2$NH), 1.39-1.33 (m, 1H, C***H***HCH_2CH_2NH), 1.32-1.27 (m, 1H, C***H***HCH_2CH_2NH); ^{13}C NMR (150.92 MHz; $(CD_3)_2SO$): δ 202.7, 172.0, 168.2, 155.9, 154.9, 142.1, 139.1, 137.8, 134.9, 130.6, 129.3, 129.3, 129.2, 128.3, 128.2, 128.1, 127.7, 127.7, 127.5, 126.3, 125.6, 116.8, 94.7, 66.6, 65.3, 56.1, 55.9, 38.9, 37.2, 29.3, 29.2, 22.4, 20.7, 19.4. HRMS Calcd. for $C_{41}H_{46}N_4O_7I$ $[M+H]^+$: 833.2411. Found 833.2416. mp: 166-169 °C.

2,5-Dioxopyrrolidin-1-yl 4-iodobenzoate (2.9a) 4-Iodobenzoic acid (992 mg, 4 mmol), *N*-(3-dimethylaminopropyl)-*N*′-ethylcarbodiimide

hydrochloride (3.83 g, 20 mmol), and *N*-hydroxysuccinimide (2.30 g, 20 mmol) were dissolved in anhydrous DMF (20 mL) and left to stir for 3 h under a stream of Ar. Water (30 mL) was then added and the product was isolated following filtration as a white powder. Yield (1.38 g, >99%). TLC (2:1 EtOAc:Hex): R_f = 0.61. ^{1}H NMR (600.13 MHz; $(CD_3)_2SO$): δ 8.06 (d, J = 8.4 Hz, 2H, Ar***H***), 7.83 (d, J = 8.4 Hz, 2H, Ar***H***), 2.89 (s, 4H, C***H***$_2$C***H***$_2$); ^{13}C NMR (150.92 MHz, $(CD_3)_2SO$) δ 170.2, 161.6, 138.6, 131.3, 123.8, 104.9, 25.5; HRMS Calcd. for $C_{11}H_8NO_4INa$ $[M+Na]^+$: 367.9396. Found: 367.9393. mp: 134-139 °C.

2,5-Dioxopyrrolidin-1-yl 3-iodobenzoate (2.9b) Synthesized in a similar manner as **9a** using 3-iodobenzoic acid instead of 4-iodobenzoic acid. Yield (1.35 g, 98%). TLC (1:2 EtOAc:Hex): R_f = 0.46; ^{1}H NMR (600.13 MHz; CD_2Cl_2): δ 8.46 (s, 1H, NHC_6***H***H_3I), 8.10 (dd, J = 7.8, 0.9 Hz, 1H, NHC_6***H***H_3I), 8.04 (dd, J = 7.9, 0.9 Hz, 1H, NHC_6***H***H_3I), 7.29 (dd, J = 7.9, 7.9 Hz, 1H, NHC_6***H***H_3I), 2.87 (s, 4H, C***H***$_2$C***H***$_2$); ^{13}C NMR (150.92 MHz, CD_2Cl_2) δ 169.6, 161.2, 144.4, 139.6, 131.1, 130.1, 127.6, 94.4, 26.3. HRMS Calcd. for $C_{11}H_8NO_4INH_4$ $[M+NH_4]^+$: 362.9842. Found: 363.0068. mp: 225-231 °C.

6-(4-Iodobenzamido)hexanoic acid (2.10a) 6-Aminocaproic acid (951 mg, 7.25 mmol) and **9a** (500 mg, 1.45 mmol) were added to DMF (5 mL) in a 5 mL microwave vial. The solution was heated by microwave

irradiation at 120 °C for 8 min. Afterwards water (5 mL) was added and the mixture was extracted with CH_2Cl_2 (3 × 10 mL) and the combined organic layers extracted with water (5 × 10 mL), brine (3 × 10 mL) and dried over $MgSO_4$. The solvent was then removed under reduced pressure affording a white powder. Yield (431 mg, 82%). TLC (5% MeOH/CH_2Cl_2): R_f = 0.44; ^{1}H NMR (600.13 MHz; $(CD_3)_2SO$): δ 11.99 (s, 1H, $CH_2CH_2CH_2COO\boldsymbol{H}$), 8.49 (t, J = 5.4 Hz, 1H, $N\boldsymbol{H}CH_2CH_2CH_2$), 7.84 (d, J = 8.2 Hz, 2H, $NHCOC_6\boldsymbol{H}H_3I$), 7.61 (d, J = 8.2 Hz, 2H, $NHCOC_6\boldsymbol{H}H_3I$), 3.24-3.21 (m, 2H, $NHC\boldsymbol{H}_2CH_2CH_2$), 2.20 (t, J = 7.3 Hz, 2H, $CH_2CH_2C\boldsymbol{H}_2COOH$), 1.54-1.48 (m, 4H, $NHCH_2C\boldsymbol{H}_2CH_2C\boldsymbol{H}_2$), 1.32-1.27 (m, 2H, $NHCH_2CH_2C\boldsymbol{H}_2$); ^{13}C NMR (150.92 MHz; $(CD_3)_2SO$) δ 174.8, 165.7, 137.4, 134.4, 129.5, 98.8, 39.4, 33.9, 29.1, 26.4, 24.6; HRMS Calcd. for $C_{13}H_{17}NO_3I$ $[M+H]^+$: 362.0253. Found: 362.0271. mp: 134-139 °C.

6-(3-Iodobenzamido)hexanoic acid (2.10b) 6-Aminocaproic acid (14.5 mmol, 1.90 g) and **9b** (1.0 g, 15 mmol) were added to DMF (5 mL) in a 2 – 5 mL microwave vial. The solution was heated in a microwave at 120 °C for 8 min. Afterwards water (5 mL) was added and the mixture was extracted with CH_2Cl_2 (3 × 10 mL) and the combined organic layers extracted with water (5 × 10 mL), brine (3 × 10 mL) and dried over $MgSO_4$. The solvent was then removed under reduced pressure affording a white

powder. Yield (910 mg, 87%). TLC (5% MeOH/CH_2Cl_2): R_f = 0.23; ^{1}H NMR (500.13 MHz; MeOD): δ 8.54 (br s, N***H***$CH_2CH_2CH_2$), 8.17 (s, 1H, $NHCOC_6$***H***H_3I), 7.88 (d, J = 7.6 Hz, 1H, $NHCOC_6$***H***H_3I), 7.80 (d, J = 7.6 Hz, 1H, $NHCOC_6$***H***H_3I), 7.23 (dd, J = 7.8, 7.8 Hz, 1H, $NHCOC_6$***H***H_3I), 3.36 (t, J = 6.8 Hz, 2H, NHC***H***$_2CH_2CH_2$), 2.31 (t, J = 7.3 Hz, 2H, CH_2CH_2C***H***$_2COOH$), 1.69-1.61 (m, 4H, $NHCH_2C$***H***$_2CH_2C$***H***$_2$), 1.45-1.39 (m, 2H, $NHCH_2CH_2C$***H***$_2$); ^{13}C NMR (125.76 MHz, MeOD) δ 177.7, 168.6, 141.6, 138.1, 137.5, 131.5, 127.7, 94.8, 41.1, 35.0, 30.3, 27.7, 25.9; HRMS Calcd. for $C_{13}H_{17}NO_3I$ $[M+H]^+$: 362.0253. Found: 362.0246. mp: 127-132 °C.

(*S*)-3-((*S*)-2-(((Benzyloxy)carbonyl)amino)-3-phenylpropanamido)-7-(6-(4-iodobenzamido)hexanamido)-2-oxoheptyl 2,4,6-trimethylbenzoate (2.11a). To a solution of **2.10a** (49 mg, 137 μmol) in anhydrous DMF (2 mL), benzotriazol-1-yl-oxytripyrrolidinophosphonium hexafluorophosphate (PyBOP) (71 mg, 140 μmol) was added and dissolved at 0 °C under a stream of Ar. Et_3N (38 μL, 270 μmol) was then added and allowed to stir 5 min. Afterwards **2.6a** (96 mg, 140 μmol) and Et_3N (19 mL, 140 μmol) were added and the solution was stirred overnight at room temperature. The reaction mixture was diluted to 25 mL with water and extracted with CH_2Cl_2 (3 × 15 mL), the organic layers were combined

and further extracted with water (5 × 15 mL), brine (30 mL), and dried over Na_2SO_4. The solvent was removed by rotary evaporation leaving an oily residue, which was then purified by flash chromatography (1%-10% MeOH/CH_2Cl_2). The product was isolated as white powder following lyophilization. Yield (57 mg, 45%). TLC (5% MeOH/CH_2Cl_2): R_f = 0.44; HPLC (Method B): ^{t}R = 17.3 min; ^{1}H NMR (600.13 MHz; $(CD_3)_2SO$): d 8.48 (m, 2H, N***H***CHCONH and CH_2N***H***COAr), 7.83 (d, J = 8.4, 2H, COC_6***H***$_2H_2I$), 7.71 (t, J = 5.7, 1H, CH_2N***H***$COCH_2$), 7.63 (d, J = 8.4, 1H, N***H***$CHCOCH_2$), 7.61 (d, J = 8.4, 2H, COC_6***H***$_2H_2I$), 7.34-7.19 (m, 10H Ph), 6.91 (s, 2H, Me_3C_6***H***$_2CO$), 4.97 (s, 2H, PhC***H***$_2OCO$), 4.91 (d, J = 17.2, 1H, COC***H***HO), 4.81 (d, J = 17.2, 1H, COC***H***HO), 4.36-4.32 (m, 2H HNC***H***CO Phe and Lys), 3.23-3.19 (m, 2H, C***H***$_2$NHCOAr), 3.04-2.97 (m, 3H, CHC***H***HPh and C***H***$_2$NHCOCH$_2$), 2.84-2.79 (m, 1H, CHC***H***HPh), 2.27 (s, 6H, 2,6-(C***H***$_3)_3C_6H_2CO$), 2.25 (s, 3H, 4-(C***H***$_3)_3C_6H_2CO$), 2.04 (t, J = 7.5, 2H, CH_2NHCOC***H***$_2$), 1.82-1.76 (m, 1H, CHC***H***HCH_2CH_2), 1.60-1.54 (m, 1H, CHC***H***HCH_2CH_2), 1.49 (m, J = 7.4, 5H, $CHCH_2$C***H***HC***H***$_2$ and $NHCOCH_2$C***H***$_2$), 1.40-1.30 (m, 3H, $CHCH_2$C***H***HCH_2 and C***H***$_2CH_2$NHCO Lys), 1.28-1.22 (m, 2H, $COCH_2CH_2$C***H***$_2$); ^{13}C NMR (150.92 MHz; $(CD_3)_2SO$): d 202.6, 172.0, 171.8, 168.2, 165.3, 155.8, 139.1, 137.8, 137.1, 136.9, 134.9, 134.1, 129.9, 129.2, 129.1, 128.3, 128.2, 128.1,

127.7, 127.5, 126.3, 98.5, 66.6, 65.3, 56.0, 55.9, 38.1, 38.1, 37.2, 35.4, 29.1, 28.8, 28.8, 26.2, 25.1, 22.4, 20.7, 19.3; HRMS Calcd. for $C_{47}H_{56}N_4O_8I$ $[M+H]^+$: 931.3143. Found 931.3104. mp: 190-196 °C.

(*S*)-3-((*S*)-2-(((Benzyloxy)carbonyl)amino)-3-phenylpropanamido)-7-(6-(3-iodobenzamido)hexanamido)-2-oxoheptyl 2,4,6-trimethylbenzoate (2.11b). Synthesized in a similar manner as **2.11a** using **2.10a** in place of **2.10b**. Yield (38 mg, 30%). TLC (5% MeOH/CH_2Cl_2): R_f = 0.46; HPLC (Method B): ^tR = 17.4 min; ^1H NMR (600.13 MHz; $(CD_3)_2SO$): d 8.54-8.51 (m, 2H, N***H***CHCONH and CH_2N***H***COAr), 8.17 (s, 1H, $NHCOC_6$***H***H_3I), 7.87 (d, J = 7.8, 1H, $NHCOC_6$***H***H_3I), 7.83 (d, J = 7.9, 1H, $NHCOC_6$***H***H_3I), 7.74 (t, J = 5.5, 1H, N***H***$CHCOCH_2$), 7.67 (d, J = 8.3, 1H, CH_2N***H***$COCH_2$), 7.33-7.18 (m, 11H, Ph and $NHCOC_6$***H***H_3I), 6.91 (s, 2H, Me_3C_6***H***$_2CO$), 4.96 (s, J = 6.7, 2H, Ph***C*****H**$_2OCO$), 4.90 (d, J = 17.3, 1H, COC***H***HO), 4.80 (d, J = 17.2, 1H, COC***H***HO), 4.35-4.31 (m, 2H, HNC***H***CO Phe and Lys), 3.22-3.19 (m, 2H, C***H***$_2$NHCOAr), 3.04-2.99 (m, 3H, CHC***H***HPh and C***H***$_2NHCOCH_2$), 2.80 (dd, J = 13.6, 9.8, 1H, CHC***H***HPh), 2.27 (s, 6H, 2,6-(C***H***$_3)_3C_6H_2CO$), 2.24 (s, 3H, 4-(C***H***$_3)_3C_6H_2CO$), 2.04 (t, J = 7.4, 2H, CH_2NHCOC***H***$_2$), 1.82-1.75 (m, 1H, CHC***H***HCH_2CH_2), 1.59-1.52 (m, 1H, CHC***H***HCH_2CH_2), 1.52-1.46 (m, 5H, $CHCH_2C$***H***HC***H***$_2$ and $NHCOCH_2C$***H***$_2$), 1.39-1.30 (m, 3H, $CHCH_2C$***H***HCH_2 and C***H***$_2CH_2NHCO$ Lys), 1.28-1.22 (m, 2H,

$COCH_2CH_2C\boldsymbol{H}_2$); ^{13}C NMR (125.77 MHz; $(CD_3)_2SO$): δ 202.8, 172.15, 172.02, 168.4, 164.7, 156.0, 139.7, 139.3, 138.0, 137.1, 136.8, 135.7, 135.1, 130.6, 130.1, 129.4, 128.41, 128.39, 128.25, 127.86, 127.68, 126.8, 126.5, 94.8, 66.8, 65.5, 56.24, 56.09, 38.28, 38.25, 37.4, 35.5, 29.3, 28.9, 26.3, 25.2, 22.6, 20.8, 19.5, 19.1; HRMS Calcd. for $C_{47}H_{56}N_4O_8I$ $[M+H]^+$: 931.3143. Found 931.3161. mp: 159-162 °C.

Methyl 6-aminohexanoate hydrochloride (2.12) 6-Aminocaproic acid (3.3 g, 25 mmol) was stirred in MeOH (50 mL) at -10 °C under a stream of Ar. Thionyl chloride (4.0 mL, 55 mmol) was added dropwise and the solution was stirred at -10 °C for 10 min and then left to stir 18 h warming to room temperature. The organic solvent was removed by rotary evaporation and the yellow/white solid was dissolved in MeOH (20 mL) and added to cold Et_2O (100 mL). The product was isolated as a white powder following filtration. Yield (4.0 g, 87%). TLC (25% MeOH/CH_2Cl_2): R_f = 0.69; ^1H NMR (600.13 MHz; CD_2Cl_2): δ 8.25 (br s, $N\boldsymbol{H}_3CH_2CH_2CH_2$), 3.63 (s, 3H, $CH_2CH_2COOC\boldsymbol{H}_3$), 2.99 (br s, $NH_3C\boldsymbol{H}_2CH_2CH_2$), 2.32 (t, J = 7.4 Hz, 2H, $CH_2CH_2C\boldsymbol{H}_2COOMe$), 1.81-1.76 (m, 2H, $NH_3CH_2C\boldsymbol{H}_2CH_2$), 1.66-1.61 (m, 2H, $NH_3CH_2CH_2CH_2C\boldsymbol{H}_2$), 1.46-1.41 (m, 2H, $NH_3CH_2CH_2C\boldsymbol{H}_2$); ^{13}C NMR (150.92 MHz; CD_2Cl_2): δ 174.1, 51.8, 40.0,

33.9, 27.5, 26.2, 24.6. HRMS Calcd. For $C_7H_{16}NO_2$ $[M]^+$: 146.1181. Found: 146.1196. mp: 114-119 °C.

Methyl 6-(3-(4-iodophenyl)ureido)hexanoate (2.13a) To a solution of **2.12** (74 mg, 410 μmol) in anhydrous CH_2Cl_2 (10 mL), Et_3N (110 μL, 820 μmol) and 4-iodophenyl isocyanate (100 mg, 410 μmol) were added and left to stir for 3 h under a stream of Ar. The reaction solvent was removed by rotary evaporation and the residue was dissolved in CH_2Cl_2 (25 mL) with heating. The solution was extracted with 1 N HCl (3 × 10 mL). The organic solvent was removed by rotary evaporation giving a white powder. Yield (147 mg, 92%). TLC (1:1 EtOAc:Hex): R_f = 0.70; ^{1}H NMR (600.13 MHz; $(CD_3)_2SO$): δ 8.53 (s, 1H, CON***H***C_6H_4I), 7.51 (d, J = 8.8 Hz, 2H, CONHC$_6$***H***$_2$H$_2$I), 7.23 (d, J = 8.8 Hz, 2H, CONHC$_6$***H***$_2$H$_2$I), 6.16 (t, J = 5.6 Hz, 1H, N***H***$CH_2CH_2CH_2$), 3.58 (s, 3H, CH_2CH_2COOC***H***$_3$), 3.06-3.03 (m, 2H, NHC***H***$_2CH_2CH_2$), 2.30 (t, J = 7.4 Hz, 2H, CH_2CH_2C***H***$_2$COOMe), 1.56-1.51 (m, 2H, $NHCH_2CH_2CH_2C$***H***$_2$), 1.43-138 (m, 2H, $NHCH_2C$***H***$_2CH_2CH_2$), 1.29-124 (m, 2H, $NHCH_2CH_2C$***H***$_2$). ^{13}C NMR (150.92 MHz; $(CD_3)_2SO$): δ 173.3, 154.9, 140.5, 137.1, 119.9, 83.4, 51.2, 38.9, 33.2, 29.4, 25.8, 24.2. HRMS Calcd. For $C_{14}H_{20}N_2O_3I$ $[M+H]^+$: 391.0519. Found: 391.0503. mp: 139 -142 °C.

Methyl 6-(3-(3-iodophenyl)ureido)hexanoate (2.13b) Synthesized in a similar manner as **2.13a** using 3-iodophenyl isocyanate in place of 4-iodophenyl isocyanate. Yield (101 mg, 63%). TLC (1:1 EtOAc:Hex): R_f = 0.65; ^{1}H NMR (500.13 MHz; CD_2Cl_2): δ 7.76 (dd, J = 1.7, 1.7 Hz, 1H, $CONHC_6\boldsymbol{H}H_3I$), 7.33 (d, J = 7.8 Hz, 1H, $CONHC_6\boldsymbol{H}H_3I$), 7.29 (dd, J = 7.9, 1.6 Hz, 1H, $CONHC_6\boldsymbol{H}H_3I$), 6.98 (dd, J = 8.0, 8.0 Hz, 1H, $CONHC_6\boldsymbol{H}H_3I$), 6.71 (s, 1H, $CON\boldsymbol{H}C_6H_4I$), 5.00 (br s, $N\boldsymbol{H}CH_2CH_2CH_2$), 3.63 (s, 3H, $CH_2CH_2COOC\boldsymbol{H}_3$), 3.20 (t, J = 6.4 Hz, 2H, $NHC\boldsymbol{H}_2CH_2CH_2$), 2.29 (t, J = 7.4 Hz, 2H, $CH_2CH_2C\boldsymbol{H}_2COOMe$), 1.64-1.57 (m, 2H, $NHCH_2CH_2CH_2C\boldsymbol{H}_2$), 1.53-1.47 (m, 2H, $NHCH_2C\boldsymbol{H}_2CH_2CH_2$), 1.36-130 (m, 2H, $NHCH_2CH_2C\boldsymbol{H}_2$); ^{13}C NMR (150.92 MHz; $(CD_3)_2SO$): δ 174.4, 155.6, 141.0, 132.0, 130.8, 128.5, 119.0, 94.4, 51.7, 40.4, 34.2, 30.0, 26.7, 24.8. HRMS Calcd. For $C_{14}H_{20}N_2O_3I$ $[M+H]^+$: 391.0519. Found: 391.0511. mp: 109-112 °C.

6-(3-(4-Iodophenyl)ureido)hexanoic acid (2.14a) To a solution of **2.13a** (98 mg, 250 μmol,) in CH_3CN (20 mL), 1 M NaOH (2.5 mL) was added and the solution was left to stir overnight at room temperature, then at 40 °C for 1 h. The solvent was removed by rotary evaporation and the residue was dissolved in warm water (12 mL). To this 1 N HCl (5 mL) was added at 0 °C. The product was collected as a white precipitate following filtration. Yield (85 mg, 90%). TLC (5% MeOH/CH_2Cl_2): R_f = 0.29; ^{1}H NMR

(600.13 MHz; $(CD_3)_2SO$): δ 11.99 (s, 1H, $CH_2CH_2COO\boldsymbol{H}$), 8.53 (s, 1H, $CON\boldsymbol{H}C_6H_4I$), 7.51 (d, J = 8.2 Hz, 2H, $CONHC_6\boldsymbol{H}_2H_2I$), 7.23 (d, J = 8.2 Hz, 2H, $CONHC_6\boldsymbol{H}_2H_2I$), 6.17 (br s, $N\boldsymbol{H}CH_2CH_2CH_2$), 3.06-3.03 (m, 2H, $NHC\boldsymbol{H}_2CH_2CH_2$), 2.20 (t, J = 7.1 Hz, 2H, $CH_2CH_2C\boldsymbol{H}_2COOH$), 1.53-1.48 (m, 2H, $NHCH_2CH_2CH_2C\boldsymbol{H}_2$), 1.42-1.39 (m, 2H, $NHCH_2C\boldsymbol{H}_2CH_2CH_2$), 1.29-1.26 (m, 2H, $NHCH_2CH_2C\boldsymbol{H}_2$); ^{13}C NMR (150.92 MHz; $(CD_3)_2SO$): δ 174.4, 154.9, 140.5, 137.1, 119.9, 83.3, 38.9, 33.7, 29.4, 25.9, 24.3 HRMS Calcd. for $C_{13}H_{18}N_2O_3I$ $[M+H]^+$: 377.0362. Found: 377.0356. mp: 187-194 °C.

6-(3-(3-Iodophenyl)ureido)hexanoic acid (2.14b) To a solution of **2.13b** (38 mg, 98 μmol) in warm CH_3CN (10 mL), water (5 mL) and 1 M NaOH (2 mL) were added and the solution was left to stir overnight at room temperature. The solvent was removed by rotary evaporation and the residue was dissolved in water (12 mL). To this 1 M HCl (2 mL) was added dropwise at 0 °C. The product was collected as a white precipitate following filtration. Yield (35 mg, 95%). TLC (5% MeOH/CH_2Cl_2): R_f = 0.10; ^1H NMR (600.13 MHz; $(CD_3)_2SO$): δ 11.99 (s, 1H, $CH_2CH_2COO\boldsymbol{H}$), 8.53 (s, 1H, $CON\boldsymbol{H}C_6H_4I$), 7.97 (dd, J = 1.9, 1.9 Hz, 1H, $CONHC_6\boldsymbol{H}H_3I$), 7.25 (ddd, J = 8.2, 1.0, 1.0 Hz, 1H, $CONHC_6\boldsymbol{H}H_3I$), 7.23 (ddd, J = 7.8, 1.6, 0.9 Hz, 1H, $CONHC_6\boldsymbol{H}H_3I$), 7.01 (dd, J = 8.0, 8.0 Hz, 1H, $CONHC_6\boldsymbol{H}H_3I$), 6.18 (t, J = 5.7 Hz, 1H, $N\boldsymbol{H}CH_2CH_2CH_2$), 3.06 (dt, J = 10.1, 4.9 Hz, 2H,

NHC***H***$_2$CH$_2$CH$_2$), 2.21 (t, J = 7.4 Hz, 2H, CH$_2$CH$_2$C***H***$_2$COOH), 1.55-1.49 (m, 2H, NHCH$_2$CH$_2$CH$_2$C***H***$_2$), 1.45-1.40 (m, 2H, NHCH$_2$C***H***$_2$CH$_2$CH$_2$), 1.31-1.26 (m, 2H, NHCH$_2$CH$_2$C***H***$_2$). ^{13}C NMR (150.92 MHz; (CD$_3$)$_2$SO): δ 174.1, 154.6, 141.8, 130.3, 129.1, 125.3, 116.5, 94.4, 38.6, 33.3, 29.1, 25.6, 24.0; HRMS Calcd. for $C_{13}H_{18}N_2O_3I$ $[M+H]^+$: 377.0362. Found: 377.0351. mp: 144-146 °C.

((S)-3-((S)-2-(Benzyloxycarbonyl)-3-phenylpropanamido)-7-(6-(3-(4-iodophenyl)ureido)hexanamido)-2-oxoheptyl 2,4,6-trimethylbenzoate (2.15a). To a solution of **2.14a** (56 mg, 150 μmol) in anhydrous DMF (5 mL), NMM (17 μL, 150 μmol) and IBCF (21 μL, 150 μmol) were added and the mixture stirred at -10 °C under a stream of Ar. After 1 min **2.6a** (95 mg, 140 μmol) and NMM (17 μL, 150 μmol) were added and the solution was left to stir overnight warming to room temperature. The reaction mixture was diluted to 25 mL with water and extracted with EtOAc (3 × 25 mL). The combined extracts were extracted with sat. Na_2CO_3 (3 × 25 mL), water (25 mL), 5% (w/v) citric acid (3 × 25 mL), water (25 mL), brine (3 × 25 mL), and dried over $MgSO_4$. The solvent was removed by rotary evaporation leaving an oily residue which was then purified by flash chromatography (1:1 EtOAc:Hex). The product was isolated as white powder following lyophilization. Yield (45 mg, 35%). TLC (1:1 EtOAc:Hex):

R_f = 0.60; HPLC (Method B): ^{t}R = 16.8 min; ^{1}H NMR (600 MHz; $(CD_3)_2SO$): δ 8.54-8.47 (m, 2H, NHCON***H***Ar and N***H***CHCONH), 7.73-7.70 (m, 1H, CH_2N***H***$COCH_2$), 7.65-7.61 (m, 1H, N***H***$CHCOCH_2$), 7.50 (d, J = 8.7, 1H $NHCOC_6$***H***$_2H_2I$), 7.34-7.18 (m, 12H, Ph and $NHCOC_6$***H***$_2H_2I$), 6.91 (s, 2H, Me_3C_6***H***$_2CO$), 6.20-6.16 (m, 1H, N***H***CONHAr), 4.96 (s, 2H, PhC***H***$_2OCO$), 4.90 (d, J = 16.7, 1H, COC***H***HO), 4.80 (d, J = 17.4, 1H, COC***H***HO), 4.35-4.30 (m, 2H, HNC***H***CO Phe and Lys), 3.04-3.00 (m, 3H, CHC***H***HPh and C***H***$_2NHCOCH_2$), 2.99-2.93 (m, 1H,), 2.83-2.80 (m, 1H, CHC***H***HPh), 2.27 (s, 6H, 2,6-(C***H***$_3)_3C_6H_2CO$), 2.25 (s, 3H, 4-(C***H***$_3)_3C_6H_2CO$), 2.04-2.02 (m, 2H, CH_2NHCOC***H***$_2$), 1.79-1.78 (m, 1H, CHC***H***HCH_2CH_2), 1.58-1.54 (m, 1H, CHC***H***HCH_2CH_2), 1.49-1.47 (m, 2H, $NHCOCH_2C$***H***$_2$), 1.40-1.33 (m, 6H, $CHCH_2C$***H***$_2C$***H***$_2$ and C***H***$_2CH_2NHCO$), 1.25-1.21 (m, 2H, $COCH_2CH_2C$***H***$_2$); ^{13}C NMR (150.92 MHz; $(CD_3)_2SO$): d 156.8, 154.9, 142.2, 137.1, 135.4, 134.9, 130.6, 129.3, 129.3, 128.3, 128.2, 128.1, 125.6, 119.8, 116.8, 109.1, 94.7, 65.3, 40.1, 33.99, 33.79, 29.5, 26.0, 24.3, 18.9; HRMS Calcd. for $C_{47}H_{57}N_5O_8I$ $[M+H]^+$: 946.3252. Found 946.3266.

(S)-3-((S)-2-(Benzyloxycarbonyl)-3-phenylpropanamido)-7-(6-(3-(3-iodophenyl)ureido)hexanamido)-2-oxoheptyl 2,4,6-trimethylbenzoate (2.15b). To a solution of **2.14b** (47 mg, 125 μmol) in anhydrous DMF (5 mL), NMM (25 μL, 250 μmol) and IBCF (16 μL, 125 μmol) were added and

allowed to stir at -10 °C under a stream of Ar. After 1 min **2.6a** (106 mg, 150 μmol) and NMM (13 μL, 125 μmol) were added and the solution was left to stir overnight warming to room temperature. The reaction mixture was made up to 25 mL with water and extracted with EtOAc (4 × 25 mL). The combined extracts were extracted with sat. Na_2CO_3 (3 × 25 mL), water (25 mL), 5% (w/v) citric acid (3 × 25 mL), water (25 mL), brine (3 × 25 mL), and dried over $MgSO_4$. The solvent was removed by rotary evaporation leaving an oily residue, which was purified by flash chromatography (12%-100% EtOAc/Hex). The product was isolated as white powder following lyophilization. Yield (0.047 g, 30%). TLC (1:1 EtOAc:Hex): R_f = 0.60; HPLC (Method B): ^{t}R = 17.0 min; ^{1}H NMR (600 MHz; $(CD_3)_2SO$): δ 8.54 (s, 1H, NHCON***H***Ar), 8.49 (d, J = 7.3, 1H, N***H***CHCONH), 7.96 (s, 1H, CONHC$_6$***H***H$_3$I), 7.72-7.70 (m, 1H, CH$_2$N***H***COCH$_2$), 7.64-7.62 (m, 1H, N***H***CHCOCH$_2$), 7.33-7.19 (m, 12H, Ph and NHCOC$_6$***H***$_2$H$_2$I), 7.01-6.98 (m, 1H, NHCOC$_6$***H***H$_3$I), 6.92 (s, 2H, Me$_3$C$_6$***H***$_2$CO), 6.20-6.17 (m, 1H, N***H***CONHAr), 4.97 (s, 2H, PhC***H***$_2$OCO), 4.91 (d, J = 17.2, 1H, COC***H***HO), 4.81 (d, J = 17.3, 1H, COC***H***HO), 4.36-4.31 (m, 2H, HNC***H***CO Phe and Lys), 3.07-3.01 (m, 6H, C***H***$_2$NHCONH, CHC***H***HPh, C***H***$_2$NHCOCH$_2$, and CHC***H***HCH$_2$CH$_2$), 2.83-2.79 (m, 1H, CHC***H***HPh), 2.28 (s, 6H, 2,6-(C***H***$_3$)$_3$C$_6$H$_2$CO), 2.25 (s, 3H, 4-

($C\boldsymbol{H}_3)_3C_6H_2CO$), 2.21 (t, J = 7.4, 2H, $CH_2NHCOC\boldsymbol{H}_2$), 2.06-2.03 (m, 1H, $CHC\boldsymbol{H}HCH_2CH_2$), 1.52-1.49 (m, 1H, $CHC\boldsymbol{H}HCH_2CH_2$), 1.43-1.37 (m, 6H, $CHCH_2C\boldsymbol{H}_2C\boldsymbol{H}_2$ and $C\boldsymbol{H}_2CH_2NHCO$), 1.31-1.25 (m, 2H, $COCH_2CH_2C\boldsymbol{H}_2$); ^{13}C NMR (151 MHz; $(CD_3)_2SO$): d 174.8, 174.8, 142.5, 139.5, 138.2, 135.3, 133.5, 131.0, 129.7, 129.7, 128.7, 128.6, 128.5, 128.5, 128.1, 127.9, 126.0, 117.2, 95.1, 67.0, 65.7, 65.7, 56.3, 38.5, 37.7, 35.8, 34.1, 29.9, 29.8, 26.5, 26.3, 25.5, 24.7, 22.8, 20.1, 19.8; HRMS Calcd. for $C_{47}H_{57}N_5O_8I$ $[M+H]^+$: 946.3252. Found 946.3223.

Methyl 6-bromohexanoate (2.16) To a solution of 6-bromohexanoic acid (7.8 g, 40 mmol) dissolved in MeOH (50 mL), thionyl chloride (8.7 mL, 120 mmol) was added and the solution was stirred for 12 h. The solvent was evaporated and EtOAc (50 mL) was added and extracted with sat. $NaHCO_3$ (3 × 40 mL), brine (30 mL), and dried over Na_2SO_4. The product was isolated as a yellow oil. Yield (8.3 g, >99%). TLC (5% MeOH/CH_2Cl_2): R_f = 0.55; ^1H NMR (600.13 MHz; $CDCl_3$): δ 3.62 (s, 3H, $CH_2CH_2COOC\boldsymbol{H}_3$), 3.36 (t, J = 6.8 Hz, 2H, $BrC\boldsymbol{H}_2CH_2CH_2$), 2.28 (t, J = 7.5 Hz, 2H, $CH_2CH_2C\boldsymbol{H}_2COOMe$), 1.85-1.80 (m, 2H, $BrCH_2CH_2CH_2C\boldsymbol{H}_2$), 1.63-1.58 (m, 2H, $BrCH_2C\boldsymbol{H}_2CH_2CH_2$), 1.43 (m, 2H, $NHCH_2CH_2C\boldsymbol{H}_2$); ^{13}C NMR (150.92 MHz; $CDCl_3$): δ 173.8, 51.5, 33.8, 33.4, 32.4, 27.6, 24.0; HRMS Calcd. for $C_7H_{14}O_2Br$ $[M+H]^+$: 209.0177. Found 209.0179.

Methyl 6-azidohexanoate (2.17) Sodium azide (30 mmol, 2.0 g) and **2.16** (15 mmol, 3.1 g) were dissolved in DMF (10 mL) and water (2.5 mL) and stirred 24 h at 60°C. The solution was diluted with water (25 mL) and extracted with EtOAc (50 mL). The organic layer was extracted with sat. $NaHCO_3$ (3 × 20 mL), water (3 × 20 mL), brine (30 mL), and dried over Na_2SO_4. Following rotary evaporation, the product was isolated as a pale yellow oil. Yield (2.2 g, 84%). TLC (1:1 EtOAc:Hex): R_f = 0.82; ^{1}H NMR (600.13 MHz; $CDCl_3$): δ 3.68 (s, 3H, $CH_2CH_2COOC\boldsymbol{H}_3$), 3.28 (t, J = 6.9 Hz, 2H, $N_3C\boldsymbol{H}_2CH_2CH_2$), 2.33 (t, J = 7.5 Hz, 2H, $CH_2CH_2C\boldsymbol{H}_2COOMe$), 1.69-1.65 (m, 2H, $N_3CH_2CH_2CH_2C\boldsymbol{H}_2$), 1.64-1.60 (m, 2H, $N_3CH_2C\boldsymbol{H}_2CH_2CH_2$), 1.44-1.39 (m, 2H, $N_3CH_2CH_2C\boldsymbol{H}_2$); ^{13}C NMR (150.92 MHz; $CDCl_3$): δ 173.9, 51.5, 51.2, 33.8, 28.6, 26.2, 24.4. HRMS Calcd. for $C_7H_{13}N_3O_2Na$ $[M+Na]^+$: 194.0905 Found 194.0900.

Methyl 6-(4-(tributylstannyl)-1*H*-1,2,3-triazol-1-yl)hexanoate (2.18). Tributyl(ethynyl)stannane (680 mg, 2.2 mmol) and **2.16** (310 mg, 1.8 mmol) were combined in toluene (2 mL) and heated to reflux at 120 °C for 14 hr. The solvent was evaporated and the product was isolated as a colourless oil following flash chromatography (8%-66% EtOAc/hexanes). Yield (680 mg, 78%). TLC (1:2 EtOAc:Hex): R_f = 0.55 ^{1}H NMR (600.13 MHz; $CDCl_3$): δ 7.41 (s, 1H, triazole-H), 4.36 (t, J = 7.2 Hz, 2H,

NC***H***$_2$CH$_2$CH$_2$), 3.63 (s, 3H, CH$_2$CH$_2$COOC***H***$_3$), 2.28 (t, J = 7.4 Hz, 2H, CH$_2$CH$_2$C***H***$_2$COOMe), 1.93-1.88 (m, 2H, NCH$_2$C***H***$_2$CH$_2$CH$_2$), 1.67-1.60 (m, 2H, NCH$_2$CH$_2$CH$_2$C***H***$_2$), 1.59-1.47 (m, 6H, Sn(CH$_2$C***H***$_2$CH$_2$)$_3$), 1.37-1.27 (m, 8H, NCH$_2$CH$_2$C***H***$_2$ and Sn(CH$_2$CH$_2$C***H***$_2$)$_3$), 1.15-1.06 (m, 6H, Sn(C***H***$_2$CH$_2$CH$_2$)$_3$), 0.86 (t, J = 7.3 Hz, 9H, (CH$_2$CH$_2$CH$_2$C***H***$_3$)$_3$); ^{13}C NMR (150.92 MHz; CDCl$_3$): δ 173.8, 144.3, 129.7, 51.5, 49.3, 33.7, 30.2, 29.0, 27.2, 26.0, 24.3, 13.7, 9.9; HRMS Calcd. for $C_{21}H_{42}N_3O_2Sn$ $[M+H]^+$: 488.2303. Found: 488.2280.

Methyl 6-(4-iodo-1*H*-1,2,3-triazol-1-yl)hexanoate (2.19). To a solution of **2.18** (490 g, 1.0 mmol) in THF (8 mL), I_2 (280 g, 1.1 mmol) was added and left to stir for 2 h. The solution was diluted to 25 mL with EtOAc and extracted with sat. $Na_2S_2O_3$ (3 × 20 mL), brine (20 mL) and dried over $MgSO_4$. The solvent was removed by rotary evaporation and the product was isolated as a white solid following flash chromatography (8%-66% EtOAc/hexanes). Yield (220 mg, 69%). TLC (1:2 EtOAc:Hex): R_f = 0.23; ^{1}H NMR (600.13 MHz; CDCl$_3$): δ 7.64 (s, 1H, triazole-H), 4.30 (t, J = 7.1 Hz, 2H, NC***H***$_2$CH$_2$CH$_2$), 3.55 (s, 3H, CH$_2$CH$_2$COOC***H***$_3$), 2.21 (t, J = 7.4 Hz, 2H, CH$_2$CH$_2$C***H***$_2$COOMe), 1.85-1.80 (m, 2H, NCH$_2$C***H***$_2$CH$_2$CH$_2$), 1.58-1.53 (m, 2H, NCH$_2$CH$_2$CH$_2$C***H***$_2$), 1.28-1.22 (m, 2H, NCH$_2$CH$_2$C***H***$_2$); ^{13}C NMR (150.92 MHz; CDCl$_3$): δ 173.6, 129.1, 86.9, 51.5, 50.4, 33.6, 29.8, 25.8,

24.1; HRMS Calcd. for $C_9H_{15}N_3O_2I$ $[M+H]^+$: 324.0209. Found: 324.0218. mp: 49-51 °C.

6-(4-Iodo-1*H*-1,2,3-triazol-1-yl)hexanoic acid (2.20) To **2.19** (190 mg, 600 μmol) dissolved in CH_3CN (30 mL), 1 N NaOH (6 mL) was added and the solution was left to stir overnight. After the solvent was evaporated, the residue was dissolved in water (25 mL), and 1 N HCl (6 mL) added. The product was then extracted with CH_2Cl_2 (3 × 20 mL), and the combined organic layers extracted with brine (20 mL) and dried over Na_2SO_4. The product was obtained as a white wax following rotary evaporation. Yield (150 g, 80%). TLC (5% MeOH:CH_2Cl_2): R_f = 0.52; ^{1}H NMR (600.13 MHz; $CDCl_3$): δ 7.62 (s, 1H, triazole-H), 4.40 (t, J = 7.1 Hz, 2H, NC***H***$_2$$CH_2CH_2$), 2.38 (t, J = 7.3 Hz, 2H, CH_2CH_2C***H***$_2$COOH), 1.97-1.92 (m, 2H, NCH_2C***H***$_2$$CH_2CH_2$), 1.72-1.67 (m, 2H, $NCH_2CH_2CH_2C$***H***$_2$), 1.42-1.37 (m, 2H, NCH_2CH_2C***H***$_2$). ^{13}C NMR (150.92 MHz; $CDCl_3$): δ 178.5, 128.8, 86.9, 50.3, 33.4, 29.8, 25.7, 23.8; HRMS Calcd. for $C_8H_{13}N_3O_2I$ $[M+H]^+$: 310.0052. Found: 310.0045. mp: 73-77 °C.

(*S*)-3-((*S*)-2-(((Benzyloxy)carbonyl)amino)-3-phenylpropanamido)-7-(6-(4-iodo-1*H*-1,2,3-triazol-1-yl)hexanamido)-2-oxoheptyl 2,4,6-trimethylbenzoate (2.21) To a solution of **2.20** (42 mg 140 mmol) anhydrous DMF (10 mL), PyBOP (71 mg, 140 μmol) was added and

allowed to dissolve while the reaction mixture was kept at 0 °C under a stream of Ar. Et_3N (38 μL, 270 μmol) was added and the solution was left to stir for 5 min. Afterwards, **2.6a** and Et_3N (19 μL 140 μmol) were added and the reaction mixture was allowed to warm to room temperature overnight with stirring. The solution was made up to 25 mL with water and extracted with CH_2Cl_2 (5 × 15 mL), and the combined organic layers extracted with water (5 × 15 mL) and brine (3 × 25 mL). The solvent was evaporated and the product was obtained following flash chromatography (1%-10% MeOH/CH_2Cl_2) as a white solid. Yield (40 mg, 33%). TLC (5% MeOH/CH_2Cl_2): R_f = 0.15; ^{1}H NMR (600.13 MHz; $(CD_3)_2SO$): δ 8.48 (d, J = 7.5, 1H, N***H***CHCONH), 8.33 (s, 1H, triazole-H), 7.71 (t, J = 5.5, 1H, CH_2N***H***$COCH_2$), 7.62 (d, J = 8.3, 1H, N***H***$CHCOCH_2$), 7.33-7.18 (m, 10H Ph) 6.91 (s, 2H, Me_3C_6***H***$_2CO$), 4.96 (s, 2H, PhC***H***$_2OCO$), 4.91 (d, J = 17.3, 1H, COC***H***HO), 4.80 (d, J = 17.3, 1H, COC***H***HO), 4.36-4.31 (m, 4H, C***H***$_2N_3C_2HI$ and HNC***H***CO Phe and Lys), 3.04-2.99 (m, 4H C***H***$_2$NHCOCH_2 and CHC***H***HPh), 2.81 (dd, J = 13.8, 9.8, 1H, CHC***H***HPh), 2.26 (s, 6H 2,6-(C***H***$_3)_3C_6H_2CO$), 2.25 (s, 3H, 4-(C***H***$_3)_3C_6H_2CO$), 2.02 (t, J = 7.4, 2H, CH_2NHCOC***H***$_2$), 1.79-1.72 (m, 3H, CHC***H***HCH_2CH_2 and C***H***$_2CH_2N_3C_2HI$), 1.58-1.55 (m, 1H, CHC***H***HCH_2CH_2), 1.51-1.46 (m, 2H, $NHCOCH_2$C***H***$_2$), 1.40-1.23 (m, 4H $CHCH_2$C***H***$_2$C***H***$_2$), 1.18-1.12 (m, 2H, $COCH_2CH_2$C***H***$_2$); ^{13}C NMR (150.91 MHz; $(CD_3)_2SO$): d 202.6, 172.0, 171.7, 168.2, 155.9, 139.1,

137.8, 136.9, 136.1, 134.9, 129.9, 129.2, 128.26, 128.22, 128.08, 127.69, 127.50, 126.3, 88.3; HRMS Calcd. for $C_{42}H_{52}N_6O_7I$ $[M+H]^+$: 879.2943. Found 879.2915. mp: 102-109 °C.

1-(4-Iodophenyl)-1-oxo-5,8,11-trioxa-2-azatetradecan-14-oic acid (2.22a). 3-(2-(2-(2-aminoethoxy)ethoxy)ethoxy)propanoic acid (332 mg, 1.5 mmol) and **9a** (173 mg, 500 μmol) were added to DMF (2 mL) in a 2 – 5 mL microwave vial. The solution was heated in a microwave at 120 °C for 8 min. Afterwards, water (5 mL) was added and the mixture was extracted with CH_2Cl_2 (3 × 10 mL), the organic layers combined and then extracted with water (5 × 10 mL), brine (3 × 10 mL) and dried over Na_2SO_4. The product was isolated as a white solid following flash chromatography (1%-10% MeOH/CH_2Cl_2 (with 0.1% AcOH)). Yield (150 mg, 67%). TLC (5% MeOH/CH_2Cl_2 (with AcOH)): R_f = 0.25; ^{1}H NMR (600.13 MHz; $CDCl_3$): δ 7.77 (d, J = 8.3 Hz, 2H, $NHCOC_6\boldsymbol{H}_2H_2I$), 7.56 (d, J = 8.4 Hz, 2H, $NHCOC_6\boldsymbol{H}_2H_2I$), 7.04 (br s, $N\boldsymbol{H}CH_2CH_2O$), 3.74 (t, J = 6.0 Hz, 2H, $NHC\boldsymbol{H}_2CH_2O$), 3.69-3.63 (m, 12H, $(C\boldsymbol{H}_2OC\boldsymbol{H}_2)_3$), 2.59 (t, J = 5.7 Hz, 2H, $CH_2C\boldsymbol{H}_2COOH$); ^{13}C NMR (150.92 MHz; $CDCl_3$): δ 167.3, 137.6, 133.7, 129.0, 98.5, 70.36, 70.26, 70.21, 70.08, 69.9, 66.6, 58.1, 40.0. HRMS Calcd. For $C_{16}H_{23}NO_6$ $[M+H]^+$: 452.0570. Found: 452.0555. mp: 56-64 °C.

1-(3-Iodophenyl)-1-oxo-5,8,11-trioxa-2-azatetradecan-14-oic acid (2.22b). 3-(2-(2-(2-aminoethoxy)ethoxy)ethoxy)propanoic acid (120 mg 540 μmol) and **2.9b** (620 mg 180 μmol) were added to DMF (1.5 mL) in a 0.5 – 2 mL microwave vial. The solution was heated in a microwave at 120 °C for 8 min. Afterwards water (5 mL) was added and the mixture was extracted with CH_2Cl_2 (3 × 10 mL) the organic layers were combined then extracted with water (5 × 10 mL), brine (10 mL) and dried over Na_2SO_4. The solvent was removed by rotary evaporation and the product was isolated as white wax. Yield (34 mg, 42%). TLC (5% MeOH/CH_2Cl_2): R_f = 0.30; ^{1}H NMR (600.13 MHz; $CDCl_3$): δ 8.16 (dd, J = 1.5, 1.5 Hz, 1H, $NHCOC_6\boldsymbol{H}H_3I$), 7.79-7.77 (m, 2H, $NHCOC_6\boldsymbol{H}_2H_2I$), 7.24 (br s, $N\boldsymbol{H}CH_2CH_2O$), 7.14 (dd, J = 7.8. 7.8 Hz, 1H, $NHCOC_6\boldsymbol{H}H_3I$), 3.71 (t, J = 6.1 Hz, 2H, $NHC\boldsymbol{H}_2CH_2O$), 3.67-3.60 (m, 12H, $(C\boldsymbol{H}_2OC\boldsymbol{H}_2)_3$, 2.57 (t, J = 6.1 Hz, 2H, $CH_2C\boldsymbol{H}_2COOH$); ^{13}C NMR (151 MHz; $CDCl_3$): δ 175.5, 166.9, 140.8, 136.97, 136.82, 130.7, 127.0, 94.7, 71.08, 70.92, 70.80, 70.75, 70.4, 67.0, 40.6, 35.5. HRMS Calcd. For $C_{16}H_{23}NO_6$ $[M+H]^+$: 452.0570. Found: 452.0566.

(*S*)-20-((*S*)-2-(((Benzyloxy)carbonyl)amino)-3-phenylpropanamido)-1-(4-iodophenyl)-1,14,21-trioxo-5,8,11-trioxa-2,15-diazadocosan-22-yl 2,4,6-trimethylbenzoate (2.23a). To a solution **2.22a** (36 mg 80 μmol) in

anhydrous DMF (5 mL), PyBOP (42 mg, 80 μmol) was added and dissolved at 0 °C under a stream of Ar. Et_3N (33 mL, 240 μmol) was added the solution was left to stir for 5 min. Afterwards, **2.6a** (56 mg, 80 μmol) was added and the reaction mixture was stirred warming to room temperature overnight. The solution was made up to 25 mL with water and extracted with CH_2Cl_2 (3 × 10 mL), and the organic layers were combined then extracted with water (5 × 15 mL) and brine (5 × 10 mL). The solvent was evaporated and the product was obtained as a white solid following flash chromatography (2%-20% MeOH/CH_2Cl_2) as a white wax. Yield (18 mg, 22%). TLC (5% MeOH/CH_2Cl_2): R_f = 0.22; HPLC (Method B): ^tR = 16.7 min; ^1H NMR (600.13 MHz; $(CD_3)_2SO$): δ 8.58 (t, J = 5.6, 1H, $CH_2N\boldsymbol{H}COAr$), 8.50 (d, J = 7.4, 1H, $N\boldsymbol{H}CHCONH$), 7.85 (d, J = 8.5, 2H, $NHCOC_6\boldsymbol{H}_2H_2I$), 7.79 (t, J = 5.6, 1H, $CH_2N\boldsymbol{H}COCH_2$), 7.65-7.62 (m, 3H, $NHCOC_6\boldsymbol{H}_2H_2I$ and $N\boldsymbol{H}CHCOCH_2$), 7.35-7.20 (m, 10H Ph), 6.92 (s, 2H, $Me_3C_6\boldsymbol{H}_2CO$), 4.98 (s, 2H, $PhC\boldsymbol{H}_2OCO$), 4.92 (d, J = 17.2, 1H, $COC\boldsymbol{H}HO$), 4.81 (d, J = 17.2, 1H, $COC\boldsymbol{H}HO$), 4.37-4.32 (m, 2H, $HNC\boldsymbol{H}CO$ Phe and Lys), 3.57 (t, J = 6.5, 2H, $COC\boldsymbol{H}_2CH_2O$), 3.53-3.39 (m, 12H, $C\boldsymbol{H}_2C\boldsymbol{H}_2OC\boldsymbol{H}_2C\boldsymbol{H}_2OC\boldsymbol{H}_2C\boldsymbol{H}_2$), 3.05-3.01 (m, 3H, $CHC\boldsymbol{H}HPh$ and $C\boldsymbol{H}_2NHCOCH_2$), 2.82 (dd, J = 13.6, 9.7, 1H, $CHC\boldsymbol{H}HPh$), 2.30 (m, 2H, $COCH_2C\boldsymbol{H}_2O$), 2.28 (s, 6H, 2,6-$(C\boldsymbol{H}_3)_3C_6H_2CO$), 2.26 (s, 3H, 4-

($C\boldsymbol{H}_3)_3C_6H_2CO$), 1.83-1.77 (m, 1H, CHC***H***HCH_2CH_2), 1.61-1.53 (m, 1H, CHC***H***HCH_2CH_2), 1.41-1.24 (m, 4H, $CHCH_2C\boldsymbol{H}_2C\boldsymbol{H}_2$); ^{13}C NMR (150.92 MHz; $(CD_3)_2SO$): d 202.6, 172.0, 169.8, 168.2, 165.6, 155.8, 139.1, 137.8, 137.1, 136.9, 134.9, 133.8, 129.9, 129.2, 129.1, 128.3, 128.2, 128.1, 127.7, 127.5, 126.3, 98.8, 69.7, 69.6, 69.6, 69.5, 68.8, 66.8, 66.6, 65.3, 56.0, 55.9, 40.1, 38.2, 37.2, 36.1, 29.1, 28.7, 22.3, 20.7, 19.3; HRMS Calcd. for $C_{50}H_{62}N_4O_{11}I$ $[M+H]^+$: 1021.3460. Found 1021.3456.

(*S*)-20-((*S*)-2-(((Benzyloxy)carbonyl)amino)-3-phenylpropanamido)-1-(3-iodophenyl)-1,14,21-trioxo-5,8,11-trioxa-2,15-diazadocosan-22-yl 2,4,6-trimethylbenzoate (2.23b). To a solution **2.22b** (26 mg 57 μmol) in anhydrous DMF (5 mL), PyBOP (30 mg, 57 μmol) was added and dissolved at 0 °C under a stream of Ar. Et_3N (8 mL, 57 μmol) was added and the solution was left to stir for 5 min. Afterwards, **2.6a** (40 mg, 57 μmol) and Et_3N (16 mL, 114 μmol) were added and the reaction mixture was stirred and allowed to warm to room temperature overnight. The solution was made up to 25 mL with water and extracted with CH_2Cl_2 (3 × 10 mL), the organic layers were combined then extracted with water (5 × 15 mL) and brine (5 × 10 mL). The solvent was evaporated and the product was obtained as a white solid following flash chromatography (5% MeOH/CH_2Cl_2). Yield (216 mg, 37%). TLC (10% MeOH/CH_2Cl_2): R_f = 0.51;

HPLC (Method B): ^{t}R = 16.7 min. ^{1}H NMR (600.13 MHz; $(CD_3)_2SO$): δ 8.61 (t, J = 5.5, 1H, $CH_2N\boldsymbol{H}COAr$), 8.50 (d, J = 7.4, 1H, $N\boldsymbol{H}CHCONH$), 8.19 (m, 1H $NHCOC_6\boldsymbol{H}H_3I$), 7.89-7.87 (m, 1H, $NHCOC_6\boldsymbol{H}H_3I$), 7.86-7.85 (m, 1H, $NHCOC_6\boldsymbol{H}H_3I$), 7.79 (t, J = 5.7, 1H, $CH_2N\boldsymbol{H}COCH_2$), 7.64 (d, J = 8.2, 1H, $N\boldsymbol{H}CHCOCH_2$), 7.34-7.18 (m, 11H Ph and $NHCOC_6\boldsymbol{H}H_3I$), 6.92 (s, 2H, $Me_3C_6\boldsymbol{H}_2CO$), 4.97 (d, J = 5.2, 2H, $PhC\boldsymbol{H}_2OCO$), 4.91 (d, J = 17.2, 1H, $COC\boldsymbol{H}HO$), 4.80 (d, J = 17.2, 1H, $COC\boldsymbol{H}HO$), 4.36-4.33 (m, 2H, $HNC\boldsymbol{H}CO$ Phe and Lys), 3.57 (t, J = 6.5, 2H, $COC\boldsymbol{H}_2CH_2O$), 3.53-3.38 (m, 12H, $C\boldsymbol{H}_2C\boldsymbol{H}_2OC\boldsymbol{H}_2C\boldsymbol{H}_2OC\boldsymbol{H}_2C\boldsymbol{H}_2$), 3.05-3.01 (m, 3H, $CHC\boldsymbol{H}HPh$ and $C\boldsymbol{H}_2NHCOCH_2$), 2.82 (dd, J = 13.6, 9.7, 1H, $CHC\boldsymbol{H}HPh$), 2.29 (d, J = 6.5, 1H, $COCH_2C\boldsymbol{H}HO$), 2.27 (s, 6H, 2,6-$(C\boldsymbol{H}_3)_3C_6H_2CO$), 2.25 (s, 3H, 4-$(C\boldsymbol{H}_3)_3C_6H_2CO$), 1.82-1.78 (m, 1H, $CHC\boldsymbol{H}HCH_2CH_2$), 1.60-1.53 (m, 1H, $CHC\boldsymbol{H}HCH_2CH_2$), 1.40-1.24 (m, 4H, $CHCH_2C\boldsymbol{H}_2C\boldsymbol{H}_2$);. ^{13}C NMR (150.92 MHz; $(CD_3)_2SO$): δ 202.6, 172.0, 172.0, 169.8, 168.2, 155.8, 139.6, 139.1, 137.8, 136.9, 136.4, 135.6, 134.9, 130.5, 129.9, 129.2, 128.3, 128.2, 128.1, 127.7, 127.5, 126.6, 126.3, 94.6, 69.7, 69.7, 69.6, 69.5, 68.7, 66.8, 66.6, 65.3, 56.0, 55.9, 40.0, 38.2, 37.2, 36.1, 29.1, 28.7, 22.4, 20.7, 19.3; HRMS Calcd. for $C_{50}H_{62}N_4O_{11}I$ $[M+H]^+$: 1021.3460. Found 1021.3484. mp: 79-86 °C.

tert*-Butyl 3-(2-(2-(2-hydroxyethoxy)ethoxy)ethoxy)propanoate (2.24)** To a solution of triethylene glycol (25.1 mL, 188 mmol) in anhydrous THF (85 mL), sodium (40 mg, 1.74 mmol) was added and the solution was left to stir for 40 min. After which, *tert*-butyl acrylate (9.6 mL, 66 mmol) was added and the solution was allowed to stir for 20 h. 1N HCl (1.6 mL) was added (pH ≈ 6) and the solvent was removed by rotary evaporation. Brine (70 mL) was added to the residue and the product was extracted with EtOAc (3 × 50 mL), and the combined organic layers extracted with brine (50 mL) and dried over $MgSO_4$. The solvent was removed by rotary evaporation giving the product as a clear colorless oil. Yield (14 g, 76%). TLC (10% MeOH:CH_2Cl_2): R_f = 0.58; ^{1}H NMR (600.13 MHz; $CDCl_3$): d 3.61-3.48 (m, 14H, CH***$_2$ in PEG-3), 2.97 (s, 1H, O***H***), 2.39 (t, J = 6.5, 2H ^{t}BuOOCC***H***$_2$), 1.33 (s, 9H C(C***H***$_3$)$_3$); ^{13}C NMR (150.92 MHz; $CDCl_3$): δ 171.3, 80.9, 72.9, 71.0, 70.9, 70.7, 67.3, 62.1, 36.6, 28.5; HRMS Calcd. For $C_{13}H_{26}O_6Na$ $[M+Na]^+$: 301.1627. Found: 301.1619.

***tert*-Butyl 3-(2-(2-(2-azidoethoxy)ethoxy)ethoxy)propanoate (2.25)** To a solution of **2.24** (1.25 g, 4.50 mmol) in anhydrous CH_2Cl_2 (5 mL) and Et_3N (1.53 mL, 10.9 mmol), $MeSO_2Cl$ (720 μL, 9.3 mmol) was added dropwise at 0 °C and the solution left to stir for 3 h warming to room temperature. After which the solution was filtered through celite, and extracted with ice water (2 × 20 mL), brine (2 × 20 mL) and dried over

$MgSO_4$. The solvent was removed by rotary evaporation, the residue was dissolved in anhydrous DMF (30 mL), and sodium azide (293 mg, 4.5 mmol) was added and the solution stirred for 14 h under a stream of Ar. The solvent was then removed and the residue was dissolved in water (20 mL) and extracted with Et_2O (5 × 20 mL) and the organic layers combined and dried over $MgSO_4$. The solvent was evaporated and the product was obtained as a clear golden oil following flash chromatography (12%-66% EtOAc/hexanes). Yield (0.771 g, 56%). TLC (1:2 EtOAc:Hex): R_f = 0.28; ^{1}H NMR (600.13 MHz; $CDCl_3$): δ 3.71-3.59 (m, 12H, C***H***$_2$OC***H***$_2$), 3.37 (t, J = 5.1 Hz, 2H, N_3C***H***$_2CH_2O$), 2.49 (t, J = 6.6 Hz, 2H, CH_2C***H***$_2COO^t$Bu), 1.43 (s, 9H, (C***H***$_3)_3COOC$); ^{13}C NMR (150.92 MHz; $CDCl_3$): δ 171.0, 80.6, 70.83, 70.78, 70.72, 70.5, 70.2, 67.0, 50.8, 36.4, 28.2. HRMS Calcd. For $C_{13}H_{29}N_4O_5$ $[M+Na]^+$: 326.1692. Found: 326.1687.

***tert*-Butyl 3-(2-(2-(2-(4-(tributylstannyl)-1*H*-1,2,3-triazol-1-yl)ethoxy)ethoxy)ethoxy)-propanoate (2.26).** Tributyl(ethynyl)stannane (432 mg, 1.37 mmol) and **2.25** (308 mg, 1.80 mmol) were combined in toluene (3 mL) and heated to reflux at 120 °C for overnight. The solvent was evaporated and the product was isolated as a colourless oil following flash chromatography (12%-100% EtOAc/hexanes). Yield (468 mg, 66%); TLC (1:1 EtOAc:Hex): R_f = 0.33; ^{1}H NMR (600 MHz; $CDCl_3$): δ 7.60 (s, 1H,

triazole-H), 4.57 (t, J = 5.3 Hz, 2H, NC***H***$_2$CH$_2$O), 3.87 (t, J = 5.3 Hz, 2H, NC***H***$_2$CH$_2$O), 3.70 (t, J = 6.6 Hz, 2H, C***H***$_2$CH$_2$COO^{t}Bu), 3.59-3.58 (m, 8H, (OC***H***$_2$C***H***$_2$)$_2$), 2.49 (t, J = 6.7 Hz, 2H, CH$_2$C***H***$_2$COO^{t}Bu), 1.58-1.52 (m, 6H, Sn(CH$_2$C***H***$_2$CH$_2$)$_3$), 1.44 (s, 9H, (C***H***$_3$)$_3$COOC), 1.32 (m, 6H, Sn(CH$_2$CH$_2$C***H***$_2$)$_3$), 1.12-1.09 (m, 6H, Sn(C***H***$_2$CH$_2$CH$_2$)$_3$), 0.88 (t, J = 7.3 Hz, 9H, (CH$_2$CH$_2$CH$_2$C***H***$_3$)$_3$). ^{13}C NMR (150.92 MHz; $CDCl_3$): δ 171.2, 144.5, 131.3, 80.9, 70.96, 70.89, 70.73, 70.1, 67.3, 49.9, 36.6, 29.4, 28.4, 27.6, 10.2. HRMS Calcd. For $C_{27}H_{53}N_3O_5Sn$ $[M+H]^+$: 620.3091. Found: 620.3077.

tert*-Butyl 3-(2-(2-(2-(4-iodo-1*H*-1,2,3-triazol-1-yl)ethoxy)ethoxy)ethoxy)propanoate (2.27).** To a solution of **2.26** (303 mg, 490 μmol) in THF (10 mL), iodine (137 mg, 540 μmol) was added and left to stir for 2 h. The solution volume was made up to 25 mL with EtOAc and extracted with sat. $Na_2S_2O_3$ (3 × 20 mL), brine (20 mL) and dried over $MgSO_4$. The solvent was removed by rotary evaporation and the product was isolated a clear colorless oil following flash chromatography (12%-100% EtOAc/hexanes). Yield (0.187 mg, 84%). TLC (1:1 EtOAc:Hex) R_f = 0.18; ^{1}H NMR (600.13 MHz; $CDCl_3$): δ 7.90 (s, 1H, triazole-H), 4.57 (t, J = 4.9 Hz, 2H, NCH***$_2$CH$_2$O), 3.85 (t, J = 4.9 Hz, 2H, NC***H***$_2$CH$_2$O), 3.72 (t, J = 6.5 Hz, 2H, C***H***$_2$CH$_2$COO^{t}Bu), 3.62-3.60 (m, 8H, (OC***H***$_2$C***H***$_2$)$_3$), 2.50 (t, J = 6.5 Hz, 2H, CH$_2$C***H***$_2$COO^{t}Bu), 1.44 (s, 9H, (C***H***$_3$)$_3$COOC); ^{13}C NMR

(150.92 MHz; $CDCl_3$): δ 171.2, 130.6, 87.2, 80.9, 70.91, 70.80, 70.79, 69.6, 67.3, 51.0, 36.6, 28.5. HRMS Calcd. For $C_{15}H_{27}N_3O_5I$ $[M+H]^+$: 456.0995. Found: 456.0981.

3-(2-(2-(2-(4-Iodo-1*H*-1,2,3-triazol-1-yl)ethoxy)ethoxy)ethoxy)propanoic acid (2.28). To a solution of **2.27** (150 mg, 330 μmol) in CH_2Cl_2 (10 mL), TFA (5 mL) was added dropwise at at 0 °C and the reaction mixture was left to stir for 3 h. The solvent was coevaporated with Et_2O giving the product as a clear colorless oil. Yield (161 mg, >99%). TLC (5% MeOH/CH_2Cl_2): R_f = 0.23; ^{1}H NMR (600 MHz; $CDCl_3$): d 11.02 (br s, $CH_2COO\boldsymbol{H}$), 7.94 (s, 1H, triazole-H), 4.60 (t, J = 4.9 Hz, 2H, $NC\boldsymbol{H}_2CH_2O$), 3.87 (t, J = 4.9 Hz, 2H, $NC\boldsymbol{H}_2CH_2O$), 3.80 (t, J = 6.1 Hz, 2H, $C\boldsymbol{H}_2CH_2COOH$), 3.68-3.67 (m, 2H, $C\boldsymbol{H}_2$), 3.64-3.60 (m, 6H, $C\boldsymbol{H}_2$), 2.67 (t, J = 6.1 Hz, 2H, $CH_2C\boldsymbol{H}_2COOH$). ^{13}C NMR (150.92 MHz; $CDCl_3$): δ 176.4, 131.1, 86.0, 70.5, 70.4, 70.4, 70.3, 69.1, 66.4, 50.9, 34.8; HRMS Calcd. for $C_{11}H_{19}N_3O_5I$ $[M+H]^+$: 400.0370. Found: 400.0368.

(*S*)-18-((*S*)-2-(((Benzyloxy)carbonyl)amino)-3-phenylpropanamido)-1-(4-iodo-1*H*-1,2,3-triazol-1-yl)-12,19-dioxo-3,6,9-trioxa-13-azaicosan-20-yl 2,4,6-trimethylbenzoate (2.29). To a solution of **2.28** (37 mg, 91 μmol) in anhydrous DMF (10 mL), PyBOP (47 mg, 91 μmol) was added and dissolved at 0 °C under a stream of Ar. Et_3N (20 μL, 182 μmol) was added

the solution was left to stir for 5 min. Afterwards, **2.6a** (40 mg, 57 μmol) was added and the reaction mixture was stirred and allowed warm to room temperature overnight. The solution was made up to 25 mL with water and extracted with CH_2Cl_2 (3 × 20 mL), and the combined organic layers extracted with water (5 × 10 mL) and brine (3 × 20 mL). The solvent was evaporated and the product was obtained as a white solid following flash chromatography (1%-20% MeOH/CH_2Cl_2). Yield (220 mg, 37%). TLC (10% MeOH/CH_2Cl_2): R_f = 0.67; HPLC (Method B): ^{t}R = 17.1 min; ^{1}H NMR (600.13 MHz; $(CD_3)_2SO$): δ 8.50 (d, J = 7.5, 1H, N***H***CHCONH), 7.79 (t, J = 5.6, 1H, CH_2N***H***$COCH_2$), 7.64 (d, J = 8.2, 1H, N***H***$CHCOCH_2$), 7.34-7.18 (m, 10H, Ph), 6.91 (s, 2H, Me_3C_6***H***$_2CO$), 4.97 (s, 2H, PhC***H***$_2OCO$), 4.91 (d, J = 17.2, 1H, COC***H***HO), 4.80 (d, J = 17.2, 1H, COC***H***HO), 4.36-4.32 (m, 2H, HNC***H***CO Phe and Lys), 3.63-3.56 (m, 4H, COC***H***$_2$C***H***$_2$O), 3.47 (m, 12H, C***H***$_2$C***H***$_2$OC***H***$_2$C***H***$_2$OC***H***$_2$C***H***$_2$), 3.03-2.99 (m, 3H, CHC***H***HPh and C***H***$_2NHCOCH_2$), 2.82-2.81 (m, 1H, CHC***H***HPh), 2.27 (s, 6H, 2,6-(C***H***$_3)_3C_6H_2CO$), 2.25 (s, 3H, 4-(C***H***$_3)_3C_6H_2CO$), 1.63-1.54 (m, 2H, CHC***H***$_2CH_2CH_2$), 1.40-1.32 (m, 4H, $CHCH_2$C***H***$_2$C***H***$_2$); ^{13}C NMR (150.92 MHz; $(CD_3)_2SO$): d 202.8, 172.1, 169.9, 168.4, 156.0, 139.3, 137.9, 137.1, 135.1, 130.6, 130.1, 128.41, 128.37, 128.23, 128.14, 127.84, 127.66, 126.5, 88.5, 69.85, 69.80, 69.77, 69.71, 69.68, 69.65, 69.62, 67.0, 65.4,

56.20, 56.05, 38.3, 37.4, 36.3, 30.9, 29.2, 28.9, 20.8, 19.5; HRMS Calcd. for $C_{45}H_{58}N_6O_{10}I$ $[M+H]^+$: 969.3259. Found: 969.3243. mp: 91-95 °C.

2-((1*E*,3*E*,5*E*)-5-(1-((5*S*,8*S*)-5-Benzyl-8-(2-((2,6-dimethylbenzoyl)oxy)acetyl)-3,6,14-trioxo-1-phenyl-2-oxa-4,7,13-triazanonadecan-19-yl)-3,3-dimethyl-5-sulfonato-3,3a-dihydro-1*H*-indol-2(7a*H*)-ylidene)penta-1,3-dien-1-yl)-1-ethyl-3,3-dimethyl-3*H*-indol-1-ium-5-sulfonate (2.30). To a solution of **2.6b** (3 mg, 5 μmol) in DMSO (500 μL) Cy5-OSu (4 mg, 5 μmol) in DMSO (100 μL) was added. *N*,*N*-Diisopropylethylamine (2 μL, 14 μmol) was added and solution was left to stir for 3 h at room temperature. Water was added and the solvent was removed by lyophilization and the product isolated by semi-preparative HPLC (Method C). ^tR = 8.1 min. HRMS Calcd. for $C_{66}H_{77}N_5O_{13}S_2$ $[M-2H]/2^+$: 604.7407. Found: 604.7429.

6-(4-(Tris(3,3,4,4,5,5,6,6,7,7,8,8,8-tridecafluorooctyl)stannyl)benzamido)hexanoic acid (2.31). 1,3,5,7-Tetramethyl-6-(2,4-dimethoxyphenyl)-2,4,8-trioxa-6-phosphaadamantane (8.0 mg, 27 μmol) and $Pd(OAc)_2$ (3.0 mg, 13 μmol), each dissolved in degassed THF (1 mL) were added to a 2 – 5 mL microwave vial purged with Ar and mixed together for 15 min. Tris(1H,1H,2H,2H-perfluorooctyl)tin hydride (850 mg, 730 μmol) dissolved in THF (1 mL) was added and the

solution stirred for 15 min. A solution of **2.10a** (120 mg, 332 μmol) dissolved in THF (1 mL) was then added and the reaction mixture was heated by microwave irradiation at 85 °C for 30 min. The mixture was filtered through silica/KF (3:1) and then further purified by column chromatography (1%-5% MeOH/CH_2Cl_2 (with 1% AcOH). The desired fractions were then diluted with water and the product, a white wax, was obtained following rotary evaporation. Yield (117 mg, 35%). TLC (5% MeOH/CH_2Cl_2): R_f = 0.57; ^{1}H NMR (600.13 MHz; $CDCl_3$): ^{1}H NMR (600 MHz; $CDCl_3$): d 7.77 (d, J = 8.1, 2H Ar***H***), 7.51-7.42 (m, 2H, Ar***H***), 6.25 (t, J = 5.8, 1H, N***H***CH_2CH_2), 3.48-3.45 (m, J = 6.6, 2H, NHC***H***$_2CH_2$), 2.37 (t, J = 7.3, 2H, CH_2C***H***$_2$COOH), 2.62-2.35 (m, 6H, Sn(CH_2C***H***$_2)_3$), 1.71-1.67 (m, 2H, C***H***$_2CH_2$COOH), 1.66-1.62 (m, 2H, NHCH$_2$C***H***$_2$), 1.48-1.42 (m, 2H, C***H***$_2CH_2CH_2$COOH), 1.38-1.33 (m, 6H, Sn(C***H***$_2CH_2)_3$); ^{13}C NMR (150.92 MHz; $CDCl_3$): d 167.6, 141.5, 136.4, 135.8, 127.1, 40.1, 33.9, 29.5, 27.8, 26.6, 24.5, -1.0; HRMS Calcd. for $C_{37}H_{29}NO_3F_{39}Sn$ $[M+H]^+$: 1396.0554. Found: 1396.0468.

(*S*)-3-((*S*)-2-(((Benzyloxy)carbonyl)amino)-3-phenylpropanamido)-2-oxo-7-(6-((4-(tris(3,3,4,4,5,5,6,6,7,7,8,8,8-tridecafluorooctyl)stannyl)phenyl)amino)hexanamido)heptyl 2,4,6-trimethylbenzoate (2.32) To a solution of **2.31** (42 mg, 30 μmol) in anhydrous DMF (5 mL), PyBOP (16 mg, 30 μmol) was added and the

solids allowed to dissolve at 0 °C under a stream of Ar. Et_3N (4.0 mL, 30 μmol) was added the solution was left to stir for 5 min. Afterwards, **2.6a** (21 mg, 30 μmol) and Et_3N (8 μL, 60 μmol) were added and the solution was stirred and allowed to warm to room temperature overnight. Water (20 mL) was added and the solution was extracted with CH_2Cl_2 (3 × 10 mL), and the combined organic layers extracted with water (5 × 10 mL) and brine (3 × 10 mL) and dried over Na_2SO_4. The solvent was evaporated and the product was obtained as a white wax following semi preparative HPLC (Method B). Yield (8 mg, 14%); TLC (5% MeOH/CH_2Cl_2): R_f = 0.36; HPLC (Method B): ^{t}R = 25.1 min. ^{1}H NMR (500.13 MHz; $(CD_3)_2SO$): δ 8.48 (d, J = 7.3, 1H N***H***CHCONH), 8.40 (t, J = 4.8, 1H, CH_2N***H***COAr), 7.80 (d, J = 7.8, 2H, COC_6***H***$_2H_2Sn$), 7.70 (t, J = 5.4, 1H, CH_2N***H***$COCH_2$), 7.63-7.59 (m, 3H, N***H***$CHCOCH_2$ and COC_6***H***$_2H_2Sn$), 7.33-7.18 (m, 10H Ph), 6.90 (s, 2H, Me_3C_6***H***$_2CO$), 4.96 (d, J = 4.4, 2H, PhC***H***$_2OCO$), 4.90 (d, J = 17.5, 1H, COC***H***HO), 4.80 (d, J = 17.0, 1H, COC***H***HO), 4.35-4.32 (m, 2H, HNC***H***CO Phe and Lys), 3.24-3.20 (m, 2H, C***H***$_2$NHCOAr), 3.04-2.99 (m, 3H, CHC***H***HPh and C***H***$_2NHCOCH_2$), 2.83-2.79 (m, 1H, CHC***H***HPh), 2.47-2.36 (m, 6H $Sn(CH_2C$***H***$_2)_2$), 2.26 (s, 6H, 2,6-(C***H***$_3)_3C_6H_2CO$), 2.24 (s, 3H, , 4-(C***H***$_3)_3C_6H_2CO$), 2.04 (t, J = 7.3, 2H, CH_2NHCOC***H***$_2$), 1.82-1.75 (m, 1H, CHC***H***HCH_2CH_2), 1.57-1.46 (m, 4H, CHC***H***HC***H***HCH_2 and

NHCOCH$_2$C***H***$_2$), 1.39-1.21 (m, 11H, CHCH$_2$C***H***HCH$_2$, C***H***$_2$C***H***$_2$NHCO, and Sn(C***H***$_2$CH$_2$)$_3$); HRMS Calcd. for $C_{71}H_{68}N_4O_8Sn$ $[M+H]^+$: 1965.3455. Found 1965.2988.

1-Oxo-1-(4-(tris(3,3,4,4,5,5,6,6,7,7,8,8,8-tridecafluorooctyl)stannyl)phenyl)-5,8,11-trioxa-2-azatetradecan-14-oic acid (2.33). 1,3,5,7-tetramethyl-6-(2,4-dimethoxyphenyl)-2,4,8-trioxa-6-phosphaadamantane (4 mg, 15 μmol) and $Pd(OAc)_2$ (2 mg, 7 μmol), each dissolved in degassed THF (1 mL) were added to a 2 – 5 mL microwave vial purged with Ar and mixed together for 15 min. Tris(1H,1H,2H,2H-perfluorooctyl)tin hydride (470 mg, 400 μmol) dissolved in THF (1 mL) was added and the solution stirred for 15 min. A solution of **2.22a** (82 mg, 182 μmol) dissolved in THF (1 mL) was then added and the solution was heated by microwave irradiation at 80 °C for 20 min. The mixture was filtered through celite and the product was isolated as a white wax following reverse phase flash chromatography (30%-100% CH_3CN/H_2O; 100% THF). Yield (0.095 g, 35%). TLC (5% $MeOH/CH_2Cl_2$): R_f = 0.58; ^{1}H NMR (600.13 MHz; $CDCl_3$): δ 7.79 (d, J = 8.1, 2H, Ar***H***), 7.46 (d, J = 8.1, 2H, Ar***H***), 6.91 (t, J = 0.5, 1H, N***H***CH$_2$CH$_2$O), 3.76-3.56 (m, 14H NHC***H***$_2$CH$_2$O and (C***H***$_2$OC***H***$_2$)$_3$), 2.55 (t, J = 6.4, 2H, CH$_2$C***H***$_2$COOH), 2.35-2.29 (m, 6H, Sn(CH$_2$C***H***$_2$)$_3$), 1.32 (t, J = 8.2, 6H, Sn(C***H***$_2$CH$_2$)$_3$); HRMS Calcd. for $C_{49}H_{35}NO_6F_{39}Sn$ $[M+H]^+$:1486.0873. Found: 1486.0826.

(S)-20-((S)-2-(((Benzyloxy)carbonyl)amino)-3-phenylpropanamido)-1,14,21-trioxo-1-(4-(tris(3,3,4,4,5,5,6,6,7,7,8,8,8-tridecafluorooctyl)stannyl)phenyl)-5,8,11-trioxa-2,15-diazadocosan-22-yl 2,4,6-trimethylbenzoate (2.34) To a solution of **2.33** (38 mg, 26 μmol) in anhydrous DMF (5 mL), PyBOP (140 mg, 26 μmol) was added and the solids allowed to dissolve at 0 °C under a stream of Ar. Et_3N (7 μL, 52 μmol) was added and the solution left to stir for 5 min. Afterwards, **2.6a** (21 mg, 30 μmol) and Et_3N (4 μL, 26 μmol) were added and the solution was stirred warming to room temperature overnight. Water (20 mL) was added and the solution was extracted with CH_2Cl_2 (3 × 10 mL), and the combined organic layers extracted with water (5 × 10 mL) and brine (3 × 10 mL) and dried over Na_2SO_4. The solvent was evaporated and the product was obtained as a white wax following semi preparative HPLC (Method B). Yield (6 mg, 12%); TLC (5% MeOH/CH_2Cl_2): R_f = 0.09; HPLC (Method B): ^{t}R = 25 min; ^{1}H NMR (600.13 MHz; $(CD_3)_2SO$): δ 8.51-8.47 (m, 2H, $CH_2N\boldsymbol{H}COAr$ and $N\boldsymbol{H}CHCONH$), 7.81 (d, J = 8.1, 2H, $NHCOC_6\boldsymbol{H}_2H_2Sn$), 7.77 (t, J = 5.6, 1H, $CH_2N\boldsymbol{H}COCH_2$), 7.62 (d, J = 8.2, 1H, $N\boldsymbol{H}CHCOCH_2$), 7.60-7.55 (m, 2H, $NHCOC_6\boldsymbol{H}_2H_2Sn$), 7.32-7.18 (m, 10H Ph), 6.89 (s, 2H, $Me_3C_6\boldsymbol{H}_2CO$), 4.96 (s, 2H, $PhC\boldsymbol{H}_2OCO$), 4.90 (d, J = 17.2, 1H, $COC\boldsymbol{H}HO$), 4.79 (d, J = 17.3, 1H, $COC\boldsymbol{H}HO$), 4.35-4.31 (m, 2H,

HNC***H***CO Phe and Lys), 3.55 (t, J = 6.5, 2H, COC***H***$_2$CH$_2$O), 3.51-3.39 (m, 12H, C***H***$_2$C***H***$_2$OC***H***$_2$C***H***$_2$OC***H***$_2$C***H***$_2$), 3.04-3.00 (m, 3H, CHC***H***HPh and C***H***$_2$NHCOCH$_2$), 2.81 (dd, J = 13.6, 9.5, 1H, CHC***H***HPh), 2.46-2.37 (m, 6H, Sn(CH$_2$C***H***$_2$)$_3$), 2.28 (d, J = 6.5, 2H, COCH$_2$C***H***$_2$O), 2.24 (s, 6H, 2,6-(C***H***$_3$)$_3$C$_6$H$_2$CO), 2.23 (s, 3H, 4-(C***H***$_3$)$_3$C$_6$H$_2$CO), 1.80-1.77 (m, 1H, CHC***H***HCH$_2$CH$_2$), 1.59-1.52 (m, 1H, CHC***H***HCH$_2$CH$_2$), 1.38-1.22 (m, 10H, CHCH$_2$C***H***$_2$C***H***$_2$ and Sn(C***H***$_2$CH$_2$)$_3$); HRMS Calcd. for $C_{74}H_{77}F_{39}N_5O_{11}Sn$ $[M+NH_4]^+$: 2072.4038. Found 2072.3989.

Screening Studies

Optimization of Enzyme Concentration. Cathepsin B (500 nM) was preincubated for 30 min at room temperature in a solution of 5 mM dithiothreitol (DTT) and 0.01% (v/v) Tween-20. Cathepsin B was added the wells of a 96-well microplate containing the assay buffer (25 mM K_2PO_4, 1 mM EDTA, 250 mM NaCl, and 3% (v/v) DMSO, pH = 6.0), and Cbz-Arg-Arg-pNA (50 mL) was added resulting in enzyme concentrations from 1.25 to 25 nM and a substrate concentrations of 1 mM. Formation of the p-nitroanilide (p-NA) product was monitored for 73 min at 405 nm at 37 °C. Measurements were obtained in triplicate. Initial rates (ν_0) were measured from the slope obtained during the first 10 min.

Determination of K_m. Cathepsin B (200 nM) was preincubated for 30 min at 37 °C in a solution of 5 mM DTT and 0.01% (v/v) Tween-20. Cathepsin

B (5 μL) was added to the wells of a 96-well microplate containing the assay buffer. Cbz-Arg-Arg-pNA (50 μL) was then added resulting in an enzyme concentration of 5 nM and substrate concentrations from 125 μM to 3 mM. Formation of the p-NA product was monitored for 15 min at 405 nm at 37 °C. Measurements were obtained in triplicate. Initial rates (ν_0) were measured from the slope obtained during the first 10 min. K_m was determined in accordance to: $\nu_0 = \frac{Vmax[S]}{Km+[S]}$ and solved using GraphPad Prism Software.

Determination of Inhibition Constants. Cathepsin B (200 nM) was preincubated for 30 min at 37 °C in a solution of 5 mM DTT and 0.01% (v/v) Tween-20. The substrate, Cbz-Arg-Arg-pNA (25 or 40 μL), and the AOMKs (50 μL) were added the wells of a 96-well microplate containing the assay buffer. The reaction was initiated by the addition of cathepsin B, resulting in substrate concentrations of 500 or 800 μM, inhibitor concentrations from 25 nM to 1 μM, and an enzyme concentration of 5 nM. Formation of the p-NA product was monitored for 60 min at 405 nm at 37 °C. Measurements were obtained in triplicate. Absorbance vs. time measurements were analyzed using non-linear regression to determine the pseudo first-order rate constant (k_{obs}) in accordance to: Absorbance =

Ae^{-kobst} + B. The second-order rate constant, (k_i/K_i), the apparent inactivation rate (k_i), and the inhibition constant (K_i) (where possible) were determined in accordance to: $k_{obs} = \frac{ki[I]}{Ki+[I]}$ for hyperbolic relationships or $k_{obs} = \frac{ki}{Ki}[I]$ for linear relationships. Equations were solved using GraphPad Prism software.

Radiochemical Methods

^{125}I-(*S*)-3-((*S*)-2-(((benzyloxy)carbonyl)amino)-3-phenylpropanamido)-7-(6-(4-iodobenzamido)hexanamido)-2-oxoheptyl 2,4,6-trimethylbenzoate ([^{125}I]2.11a). To a tube containing iodogen (5 μg, 0.01 μmol) in EtOH (25 μL), **2.32** (100 μg, 0.05 μmol) in EtOH (100 μL) was added. AcOH (5 μL) and [^{125}I]NaI (18.5 MBq) in 0.1% NaOH (10 mL) were added and after 10 min the reaction was quenched with 0.1 M $Na_2S_2O_5$ (25 μL). The reaction mixture was diluted with water (1.5 mL) and loaded unto a F-SPE cartridge (1 g). The F-SPE cartridge was pre-activated by washing with dimethylformamide (1 mL) and water (6 mL). Unreacted [^{125}I]NaI was eluted with water (10 mL), the pure product eluted with 80% EtOH (10 mL), while the excess precursor remained on the cartridge. RCY = 32 - 36% (*n* = 3); specific activity > 23.6 GBq/mmmol; HPLC ^{t}R = 14.8 min; LogP (pH 7.4) = 1.05 ± 0.01.

^{125}I-(*S*)-20-((*S*)-2-(((benzyloxy)carbonyl)amino)-3-phenylpropanamido)-1-(4-iodophenyl)-1,14,21-trioxo-5,8,11-trioxa-2,15-diazadocosan-22-yl 2,4,6-trimethylbenzoate ([^{125}I]2.23a). To a tube containing iodogen (2.5 μg, 0.005 μmol) in EtOH (25 μL), **2.34** (100 μg, 0.05 μmol) in EtOH (100 μL) was added. AcOH (5 μL) and [^{125}I]NaI (18.5 MBq) in 0.1% NaOH (10 μL) were added and after 10 min the reaction was quenched with 0.1 M $Na_2S_2O_5$ (25 μL). The reaction mixture was diluted with water (1.5 mL) and loaded unto a F-SPE cartridge (1 g). The F-SPE cartridge was preactivated by washing with dimethylformamide (1 mL) and water (6 mL). Unreacted [^{125}I]NaI was eluted with water (10 mL) and the pure product eluted with 50% EtOH (10 mL), while the excess precursor remained on the cartridge. RCY = 26 - 35% (*n* = 3); specific activity > 23.1 GBq/mmmol; HPLC: ^{t}R = 14.1 min; LogP (pH 7.4) = 0.95 ± 0.01.

Determination of Log P (pH 7.4). A solution of [^{125}I]**23** or [^{125}I]**11** (444 kBq) in 10% EtOH in PBS (300 μL) was added to a 1:1 mixture of *n*-octanol:PBS (pH 7.4) (2 mL), vortexed for 20 min and centrifuged for 30 min at 6000 rpm. Aliquots (60 μL) were removed from each layer in triplicate and added to pre-weighed tubes. The tubes were re-weighed and the amount of radioactivity was measured using a gamma counter. The

partition coefficient, P, was calculated using the following: $P = \frac{activity\ concentration\ in\ n-octanol}{activity\ concentration\ in\ aqueous\ buffer}$.

Labeling of Cathepsin B with ABPs. Human liver cathepsin B (1 μg) was incubated in 1× binding buffer (5mM Tris pH = 5.5, 5 mM $MgCl_2$, 2 mM DTT) containing RIPA buffer (100 mM Tris, pH = 8, 50 mM NaCl, 1% IGEPAL® CA-630, 0.5% sodium deoxycholate, 0.1% SDS) in the presence of either of CA-074 or DMSO for 1 h on ice. **[^{125}I]2.11a** or **[^{125}I]2.23a** (approx. 1 × 10^6 cpm) was added to each sample to give a total volume of 30 mL and the mixtures were incubated for 2 h at 0 °C. The assay was stopped by the addition of 6× sample buffer (9% SDS; 60% glycerol; 375 mM Tris pH 6.8; 0.015% bromophenol blue, 12% β-mercaptoethanol) to a final concentration of 1× and incubated at room-temperature for 30 min. Following incubation aliquots (30 μL) of the mixtures were loaded onto a 10% Mini-Protean TGX precast gel and analyzed by SDS-PAGE. Gels were incubated overnight in gel-shrinking solution (65% methanol; 0.5% glycerol) while shaking, at 4°C. Gels were dried for 2 h at room temperature using a commercial gel drying kit, and exposed to a phosphor imaging screen for 72 h.

Animal Model. MDA-MB-231 cells were purchased from the ATCC and cultured in accordance to the supplier guidelines. Animal studies were

approved by the Animal Research Ethics Board at McMaster University in accordance with Canadian Council on Animal Care (CCAC) guidelines. Female CD1 nu/nu mice (5-6 weeks old) were obtained from Charles River Laboratories (Senneville QC) and were maintained under SPF conditions with 12 hour light/dark cycles and given food and water ad libitum. To create the tumor xenograft model, CD1 nu/nu female mice were injected with 2.0×10^6 MDA-MB-231 cells in 100 µL of PBS/Matrigel/ (1:1; BD Biosciences, Mississauga, ON, and Invitrogen, Burlington, ON, respectively) subcutaneously into the right flank. Tumors were allowed to grow for approximately 2-3 weeks prior to biodistribution studies.

Biodistribution studies

[^{125}I]**2.11a.** CD1 nu/nu mice (*n* = 15) were administered approximately 259 kBq of [^{125}I]**2.11a** (3.7 GBq/mL) in 10% EtOH in sterile PBS via tail vein injection. Following 30 min, 5 h, and 23 h groups of mice (*n* = 5) were anesthetized with 3% Isoflurane, euthanized via exsanguination, and the indicated organs and tissues were collected by dissection and weighed. Activities were measured using a gamma counter and reported as the percent injected dose per gram (% ID/g) of each organ, tissue, or fluid. [^{125}I]**2.23a.** Performed in a similar manner as [^{125}I]**2.11a** except CD1 nu/nu

mice (*n* = 9) were administered approximately 74 kBq of [^{125}I]**2.23a** (3.7 GBq/mL).

2.13 References

1. J. C. Powers, J. L. Asgian, Ö. D. Ekici, and K. E. James, *Chem. Rev.*, 2002, **102**, 4639–4750.

2. C. Jedeszko and B. F. Sloane, *Biol. Chem.*, 2004, **385**, 1017–27.

3. B. F. Sloane, K. Moin, E. Krepela, and J. Rozhin, *Cancer Metas. Rev.*, 1990, **9**, 333–352.

4. B. Sloan, S. Yan, I. Podgorski, B. Linebaugh, M. Cher, J. Mai, D. Cavallo-Medved, M. Sameni, J. Dosescu, and K. Moin, *Semin. Cancer Biol.*, 2005, **15**, 149–157.

5. S. Roshy, B. F. Sloane, and K. Moin, *Cancer Metas. Rev.*, 2003, **22**, 271–86.

6. F. Qian, A. S. Bajkowski, D. F. Steiner, S. J. Chan, and A. Frankfater, *Cancer Res.*, 1989, **49**, 4870–4875.

7. B. Sloane, K. Honn, J. Sadler, W. Turner, J. Kimpson, and J. D. Taylor, *Cancer Res.*, 1981, **42**, 980–986.

8. B. F. Sloane, J. R. Dunn, and K. V Honn, *Science*, 1981, **212**, 1151–3.

9. A. D. Recklies, K. J. Tiltman, and T. A. M. Stoker, *Cancer Res.*, 1980, **40**, 550–556.

10. J. A. Joyce, A. Baruch, K. Chehade, N. Meyer-Morse, E. Giraudo, F.-Y. Tsai, D. C. Greenbaum, J. H. Hager, M. Bogyo, and D. Hanahan, *Cancer Cell*, 2004, **5**, 443–453.

11. D. Cavallo-Medved, D. Rudy, G. Blum, M. Bogyo, D. Caglic, and B. F. Sloane, *Exp. Cell. Res.*, 2009, **315**, 1234–46.

12. E. Kisin-Finfer, S. Ferber, R. Blau, R. Satchi-Fainaro, and D. Shabat, *Bioorg. Med. Chem. Lett.*, 2014, **24**, 2453–8.

13. R. Weissleder, C.-H. Tung, U. Mahmood, and A. J. Bogdanov, *Nat. Biotechnol.*, 1999, **17**, 375–378.

14. G. Blum, G. von Degenfeld, M. J. Merchant, H. M. Blau, and M. Bogyo, *Nat. Chem. Biol.*, 2007, **3**, 668–77.

15. M. Verdoes, K. Oresic Bender, E. Segal, W. A. van der Linden, S. Syed, N. P. Withana, L. E. Sanman, and M. Bogyo, *J. Am. Chem. Soc.*, 2013, **135**, 14726–14730.

16. U. Mahmood, C. H. Tung, A. Bogdanov, and R. Weissleder, *Radiology*, 1999, **213**, 866–70.

17. A. A. Bogdanov Jr., C. P. Lin, M. Simonova, L. Matuszewski, and R. Weissleder, *Neoplasia*, 2002, **4**, 228–36.

18. V. Ntziachristos, C. Bremer, E. E. Graves, J. Ripoll, and R. Weissleder, *Mol. Imaging*, 2002, **1**, 82–8.

19. K. Marten, C. Bremer, K. Khazaie, M. Sameni, B. Sloane, C. Tung, and R. Weissleder, *Gastroenterology*, 2002, **122**, 406–414.

20. X. Tian, K.-H. Baek, and I. Shin, *Chem. Sci.*, 2013, **4**, 947.

21. M. A. Chowdhury, I. A. Moya, S. Bhilocha, C. C. McMillan, B. G. Vigliarolo, I. Zehbe, and C. P. Phenix, *J. Med. Chem.*, 2014, **57**, 6092–104.

22. M. G. Paulick and M. Bogyo, *ACS Chem. Biol.*, 2011, **6**, 563–72.

23. G. Blum, S. R. Mullins, K. Keren, M. Fonovic, C. Jedeszko, M. J. Rice, B. F. Sloane, and M. Bogyo, *Nat. Chem. Biol.*, 2005, **1**, 203–209.

24. M. R. Pratt, M. D. Sekedat, K. P. Chiang, and T. W. Muir, *Chem. Biol.*, 2009, **16**, 1001–12.

25. H. C. Hang, J. Loureiro, E. Spooner, A. W. M. van der Velden, Y. Kim, A. M. Pollington, R. Maehr, M. N. Starnbach, and H. L. Ploegh, *ACS Chem. Biol.*, 2006, **1**, 713–23.

26. R. A. Smith, L. J. Copp, P. J. Coles, H. W. Pauls, V. J. Robinson, R. W. Spencer, S. B. Heard, and A. Krantz, *J. Am. Chem. Soc.*, 1988, **110**, 4429–4431.

27. A. Krantz, L. J. Copp, P. J. Coles, R. A. Smith, and S. B. Heard, *Biochemistry*, 1991, 4678–4687.

28. B. M. Wagner, R. A. Smith, P. J. Coles, L. J. Copp, M. J. Ernest, and A. Krantz, *J. Med. Chem.*, 1994, **37**, 1833–40.

29. D. Kato, K. M. Boatright, A. B. Berger, T. Nazif, G. Blum, C. Ryan, K. A. H. Chehade, G. S. Salvesen, and M. Bogyo, *Nat. Chem. Biol.*, 2005, **1**, 33–38.

30. L. E. Edgington, M. Verdoes, and M. Bogyo, *Curr. Opin. Chem. Biol.*, 2011, **15**, 798–805.

31. M. Lee, R. Fridmanb, and Shahriar Mobashery, *Chem. Soc. Rev.*, 2004, **33**, 401–409.

32. G. Ren, G. Blum, M. Verdoes, H. Liu, S. Syed, L. E. Edgington, O. Gheysens, Z. Miao, H. Jiang, S. S. Gambhir, M. Bogyo, and Z. Cheng, *PLoS One*, 2011, **6**, e28029.

33. M. Shokeen and C. J. Anderson, *Accounts Chem. Res.*, 2009, **42**, 832–41.

34. K. P. Maresca, S. M. Hillier, F. J. Femia, D. Keith, C. Barone, J. L. Joyal, A. P. Kozikowski, J. A. Barrett, W. C. Eckelman, J. W. Babich, and C. N. Zimmerman, *J. Med. Chem.*, 2009, **52**, 347 – 357.

35. Y. Chen, C. a Foss, Y. Byun, S. Nimmagadda, M. Pullambhatla, J. J. Fox, M. Castanares, S. E. Lupold, J. W. Babich, R. C. Mease, and M. G. Pomper, *J. Med. Chem.*, 2008, **51**, 7933–7943.

36. D. M. Wieland, J. Wu, L. E. Brown, T. J. Mangner, D. P. Swanson, and W. H. Beierwaltes, *J. Nucl. Med.*, 1980, **21**, 349–353.

37. A. R. Wafelman, M. C. P. Konings, C. A. Hoefnagel, R. A. A. Maes, and J. H. Beijnen, *Appl. Radiat. Isot.*, 1994, **45**, 997–1007.

38. J. M. Michelot, M. F. Moreau, P. G. Labarre, J. C. Madelmont, a J. Veyre, J. M. Papon, D. F. Parry, J. F. Bonafous, J. Y. Boire, and G. G. Desplanches, *J. Nucl. Med.*, 1991, **32**, 1573–80.

39. C. Spezzacatena, A. Pepe, L. M. Green, L. B. Sandberg, B. Bochicchio, and A. M. Tamburro, *Eur. J. Org. Chem.*, 2005, 1644–1651.

40. A. R. Katritzky, G. Meher, and P. Angrish, *Chem. Biol. Drug. Des.*, 2006, **68**, 326–33.

41. A. R. Katritzky, K. Suzuki, and S. K. Singh, *Synthesis (Stuttg).*, 2004, 2645–2652.

42. J. H. Clark and J. M. Miller, *Tetrahedron Lett.*, 1977, 599–602.

43. D. Musil, D. Zucic, D. Turk, R. A. Engh, I. Mayr, R. Huber, T. Popovic, V. Turk, T. Towatari, and N. Katunuma, *EMBO J.*, 1991, **10**, 2321–30.

44. A. Darwish, M. Blacker, N. Janzen, S. M. Rathmann, S. Czorny, S. M. Hillier, J. L. Joyal, J. W. Babich, and J. F. Valliant, *ACS Med. Chem. Lett.*, 2012, **3**, 313–316.

45. S. Ito, A. Satoh, Y. Nagatomi, Y. Hirata, G. Suzuki, T. Kimura, A. Satow, S. Maehara, H. Hikichi, M. Hata, H. Kawamoto, and H. Ohta, *Bioorg. Med. Chem.*, 2008, **16**, 9817–9829.

46. K. Moin, N. A. Day, M. Sameni, S. Hasnain, T. Hiramat, and B. F. Sloane, *Biochem. J.*, 1992, **285**, 427–434.

47. S. Hasnain, T. Hirama, A. Tam, and J. S. Mort, *J. Biol. Chem.*, 1992, **267**, 4713–4721.

48. G. Blum, R. M. Weimer, L. E. Edgington, W. Adams, and M. Bogyo, *PLoS One*, 2009, **4**, e6374.

49. J. L. Cutter, N. T. Cohen, J. Wang, A. E. Sloan, A. R. Cohen, A. Panneerselvam, M. Schluchter, G. Blum, M. Bogyo, and J. P. Basilion, *PLoS One*, 2012, **7**, e33060.

50. A. Donovan, J. Forbes, P. Dorff, P. Schaffer, J. Babich, and J. F. Valliant, *J. Am. Chem. Soc.*, 2006, **128**, 3536–7.

51. A. C. Donovan and J. F. Valliant, *J. Org. Chem.*, 2009, **74**, 8133–8.

52. J. W. McIntee, C. Sundararajan, A. C. Donovan, M. S. Kovacs, A. Capretta, and J. F. Valliant, *J. Org. Chem.*, 2008, **73**, 8236–8243.

53. T. Towatari, T. Nikawa, M. Murata, C. Yokoo, M. Tamai, K. Hanada, and N. Katunuma, *FEBS Lett.*, 1991, **280**, 311 – 315.

54. I. Zajc, L. Frangež, and T. T. Lah, *Radiol. Oncol.*, 2003, **37**, 233–240.

55. D. S. Wilbur, S. W. Hadley, M. D. Hylarides, P. G. Abrams, P. A. Beaumier, A. C. Morgan, J. M. Reno, and A. R. Fritzberg, *J. Nucl. Med.*, 1989, **30**, 216–26.

3 Synthesis and Evaluation of Re-ABPs

3.1 Introduction

Radioiodinated AOMKs (Chapter 2) have shown promise as agents for detecting cathepsin B activity *in vitro*. One of the challenges in using these probes for *in vivo* detection was the loss of the radionuclide prior to accumulation at the tumour site.[1] In a study by Ren *et al.* DOTA was incorporated into the AOMK scaffold to enable labelling to be performed with ^{64}Cu (Figure 3.1). Although the probes were able to detect cathepsin B activity *in vitro*, visualization of enzyme activity using PET was of limited quality due to low tumour uptake and high accumulation in non-target tissues such as the liver and kidneys.[2] The authors postulated that it is the release of free copper *in vivo* that contributed to high background signal and difficulty in tumour detection using PET. This is a reasonable assertion as the Cu-DOTA chelate is known to have limited stability *in vivo*, which has led to the creation of other macrocycle chelates for ^{64}Cu.[3]

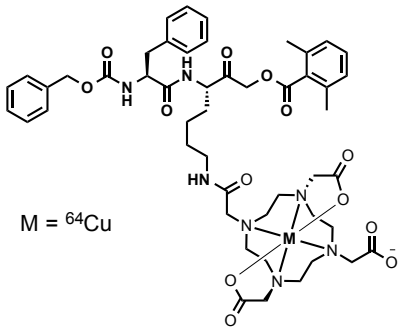

Figure 3.1 Z-FK(^{64}Cu-DOTA)-AOMK, Radiolabelled AOMK derivative for PET imaging.

To address the instability of the current AOMK based NMI probes alternate prosthetic groups can be explored. An established and stable class of prosthetic groups are derived from Re(I)/Tc(I) tridentate chelate complexes. The [$M(CO)_3^+$] core (where M = technetium-99m or rhenium) is known to react with nitrogen based tridentate ligands yielding a stable complex that has been used to label a variety of biomolecules (carbohydrates, vitamins, peptides, nucleosides, etc.) for imaging different biological processes and targets.[4]

Technetium-99m is the most widely used radionuclide in nuclear medicine, in that it is used to prepare nearly 80% of clinically available radiopharmaceuticals.[5] Its ideal nuclear properties (6.02 h half-life, 141 keV γ-ray) and wide availability make it an attractive isotope for diagnostic imaging applications. For instance, the half-life of ^{99m}Tc is long enough to

prepare most radiotracers and to allow it to accumulate at the target site, while being short enough that the patient's radiation dose is minimized. Furthermore, the γ-ray energy is suitable for imaging with most γ-cameras yet low enough such that the dose to the patient is also minimized.[4]

There are two general classes of Tc radiopharmaceuticals: technetium essential and technetium-tagged agents.[4] In the case of technetium essential agents, the Tc atom is required to achieve the desired distribution and target localization. In the case of technetium-tagged molecules the targeting portion of the probe is linked to Tc through a stable prosthetic group involving a chelating ligand. The targeting portion is responsible for directing localization *in vivo* while the Tc-chelate ensures the radionuclide remains bound. Tc tagged molecules are prepared using bifunctional chelates which are so named as one set of functional groups are used to securely bind to the metal while at least one other is used for bioconjugation.[4]

One example of a bifunctional chelate is the single amino acid chelate (SAAC) system (Figure 3.2a).[6] By functionalising the amino side chain of lysine it is possible to form a robust complex with the $[M(CO)^{3+}]$ core, while the amino acid functionality allows for the incorporation of the ligand into peptides. Although the original SAAC is able to form stable complexes

with the radiometal core, the products are generally lipophilic which promotes hepatobiliary excretion and non-specific binding when attached to a bioactive molecule.[7] This is an issue because uptake in the liver and other non-target organs can occlude tumour visualization. To address this issue the bis(pyridyl) group found in SAAC was replaced with bis(carboxymethylimidazole) donor groups giving the second generation derivative or SAACII (Figure 3.2B).[7] This more polar derivative exhibited greater hydrophilicity resulting in more rapid clearance via the kidneys and reduced non-specific binding when compared to the bis(pyridyl) derivative.[7]

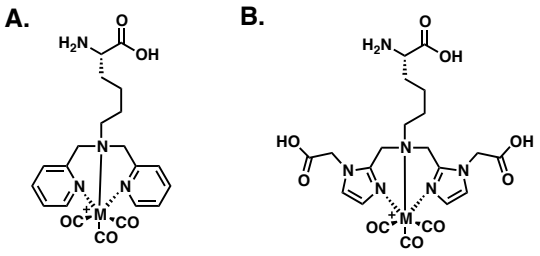

Figure 3.2 Single Amino Acid Chelate Derivatives. (a) Generation 1 - SAAC. (b) Generation 2 - SAACII (M = ^{99m}Tc and Re).

3.2 Objectives

The next class of AOMK based imaging agents that were explored involved the incorporation of Re/Tc chelates to the targeting vector. Because Tc does not have any stable isotopes its non-radioactive congener Re was initially used to prepare the library of derivatives and to

determine cathepsin B binding constants. The first strategy was to use a bifunctional hexanoic acid spacer to incorporate Re into the AOMK scaffold building off the experience from the work on radioiodine derivatives. Although use of this spacer led to decreased water solubility for the iodobenzamide AOMKs,[1] it is expected that the bis(carboxymethylimidazole) chelate would not experience such issues due to its high water solubility.

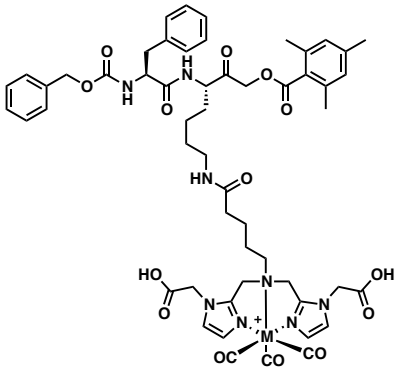

M = Re/^{99m}Tc

Figure 3.3 AOMK based Re/^{99m}Tc Derivative.

3.3 Synthesis and Testing of Rhenium Linked AOMKs

To incorporate Re into the AOMK scaffold the six-carbon spacer previously employed in the development of ^{125}I and cyanine labelled inhibitors was employed. 2-Imidazole carboxyaldehyde was combined with ^{t}butyl bromoacetate giving the protected carboxylic acid derivative (**3.1**)

(Scheme 3.1). 6-Aminohexanoic acid was reacted with **3.1** in a reductive amination reaction, giving the desired ligand **3.2** which was then coordinated with the [$Re(CO)_3^+$] core giving **3.3** in 41% yield. This prosthetic group was coupled to the parent AOMK **2.6a** using PyBOP in the presence of triethylamine giving the protected inhibitor **3.4** in 37% yield. Following deprotection with TFA the desired polar inhibitor **3.5** was obtained.

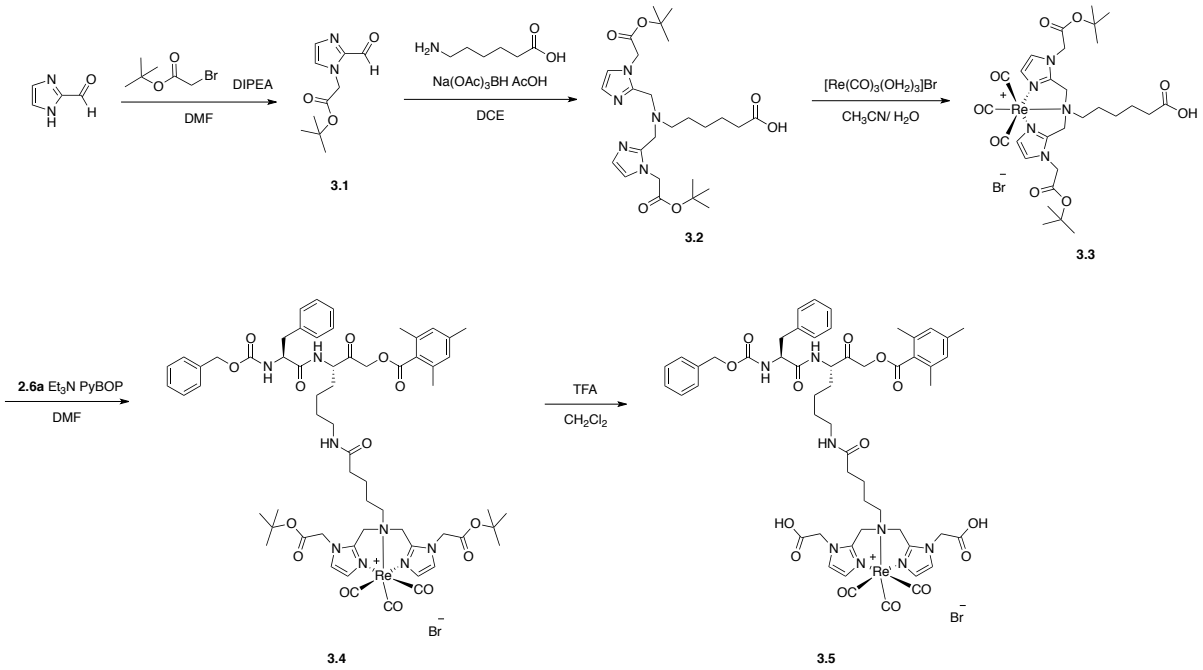

Scheme 3.1. Synthesis of **3.5**.

The binding affinities of **3.4** and **3.5** were measured in a similar fashion as the iodinated AOMKs previously described.[1] The *t*butyl protected analogue (**3.4**) exhibited poor affinity and the K_i value could not be

determined. This result was not surprising due to the increased steric bulk at the P_1 site. Removal of this protecting group resulted in enhanced affinity with a K_i value of 710 nM and k_i/K_i of 4 900 $s^{-1}M^{-1}$ (Table 3.1). Unfortunately these values were not close enough to what was observed for the previous lead compounds (i.e. K_i below 200 nM and k_i/K_i above 10 000 $s^{-1}M^{-1}$) and thus was not explored for *in vivo* applications.

Table 3.1. Inhibitory Activities of Rhenium-AOMK Derivatives.[a]

Compound	K_i (nM)	k_i/K_i ($s^{-1}M^{-1}$)
3.4	n.d.[b]	1 680 ± 30
3.5	710 ± 30	4 900 ± 100

[a] Inhibition constants were determined at 37 °C and pH 6.0 with human liver cathepsin B. [b] ND: full inhibition was not observed therefore the value was not determined. [c] NI: no inhibition observed.

3.4 Dendrimers as a Platform for Multimeric Imaging Probes

An AOMK probe with higher affinity for cathepsin B is desired in order to achieve high T:NT ratios *in vivo*. As an alternative to SAR modifications on monomeric targeting vectors, increasing the number of targeting vectors is a potential means to enhance binding affinity. This can be done with a dendrimer to generate a multimeric MI probe. Dendrimers are

molecules with highly branched units that are symmetrical about a central core that can be used as a bifunctional linker where the core can be functionalized with a signalling agent such as a radiometal chelate and the periphery with multiple targeting vectors.[8]

The multimeric dendrimer approach was exemplified by Almutairi *et al.*, where a dendritic positron-emitting probe for imaging angiogenesis was developed.[9] Multiple cRGD peptides were conjugated to the periphery of a dendrimer, which contained radiohalogens at the core for PET imaging of $\alpha_v\beta_3$ integrin receptors. To observe the effect of the multivalent probe binding affinities for the $\alpha_v\beta_3$ integrin were compared. A 50-fold enhancement in the binding affinity was observed (IC_{50} improved from 10.4 nM to 0.18 nM) for the multimeric probe *vs.* the monovalent probe. The goal was to leverage this approach to develop a ^{99m}Tc-AOMK based dendritic probe with enhanced binding affinity.

Parrot *et al.* reported a strategy to incorporate ^{99m}Tc into the core of a polyester dendrimer using a bis(pyridyl) chelator. These compounds exhibited high *in vivo* stability and very little non-specific binding. The same platform was used to conjugate multiple AOMKs to its periphery. To achieve this, the AOMK used previously was functionalized with azide linkers of varying lengths so that it could be coupled to the appropriately functionalized dendrimer. In this respect the periphery of the polyester

dendrimer was functionalized with alkynes in order to enable coupling with the AOMK-azide through a copper catalyzed azide-alkyne cycloaddition (CuAAC).

3.5 Synthesis and Testing of Dendrimer Based AOMKs

To functionalize the AOMK, two-carbon, four-carbon, six-carbon, or PEG-3 spacers were linked to the ε-nitrogen of lysine in **2.6a** (Figure 2.1). In the case of the two-carbon **3.6** and six-carbon **3.7** derivatives the bifunctional linker was synthesized through a nucleophilic substitution of the corresponding bromo aliphatic acid with sodium azide (Scheme 3.2).

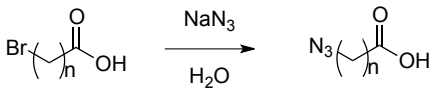

n = 1 **3.6**
n = 5 **3.7**

Scheme 3.2. Synthesis of **3.6** and **3.7**.

The linker groups were then coupled to **2.6a** using IBCF or PyBOP giving **3.8**-**3.11** (Scheme 3.3) in 15 to 66% yield. In the case of **3.10** PyBOP was the better reagent because using IBCF resulted in formation of the isobutyl carbamate derivative. This was observed by ^{1}H NMR (

Figure 3.4), which showed peaks at 3.70 ppm and 0.85 ppm representing the isobutyl protons.

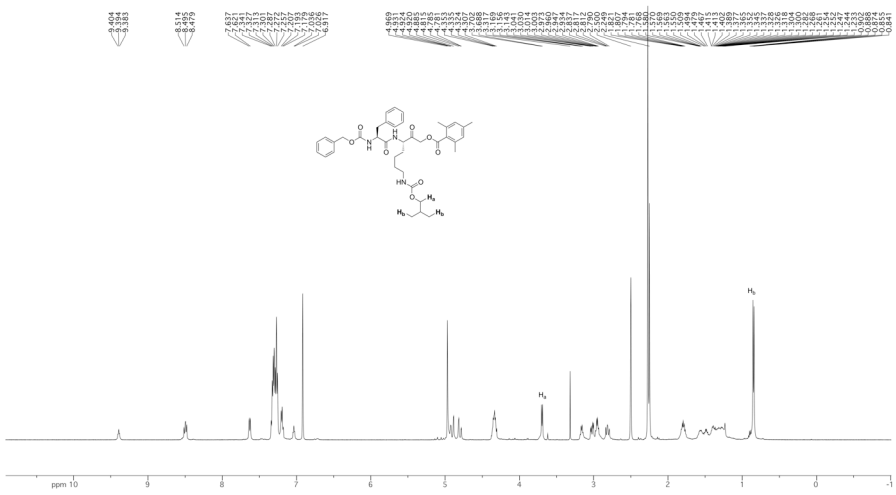

Figure 3.4 ^{1}H NMR ($(CD_3)_2SO$) of (*S*)-3-((*S*)-2-(((benzyloxy)carbonyl)amino)-3-phenylpropanamido)-7-((isobutoxycarbonyl)amino)-2-oxoheptyl 2,4,6-trimethylbenzoate.

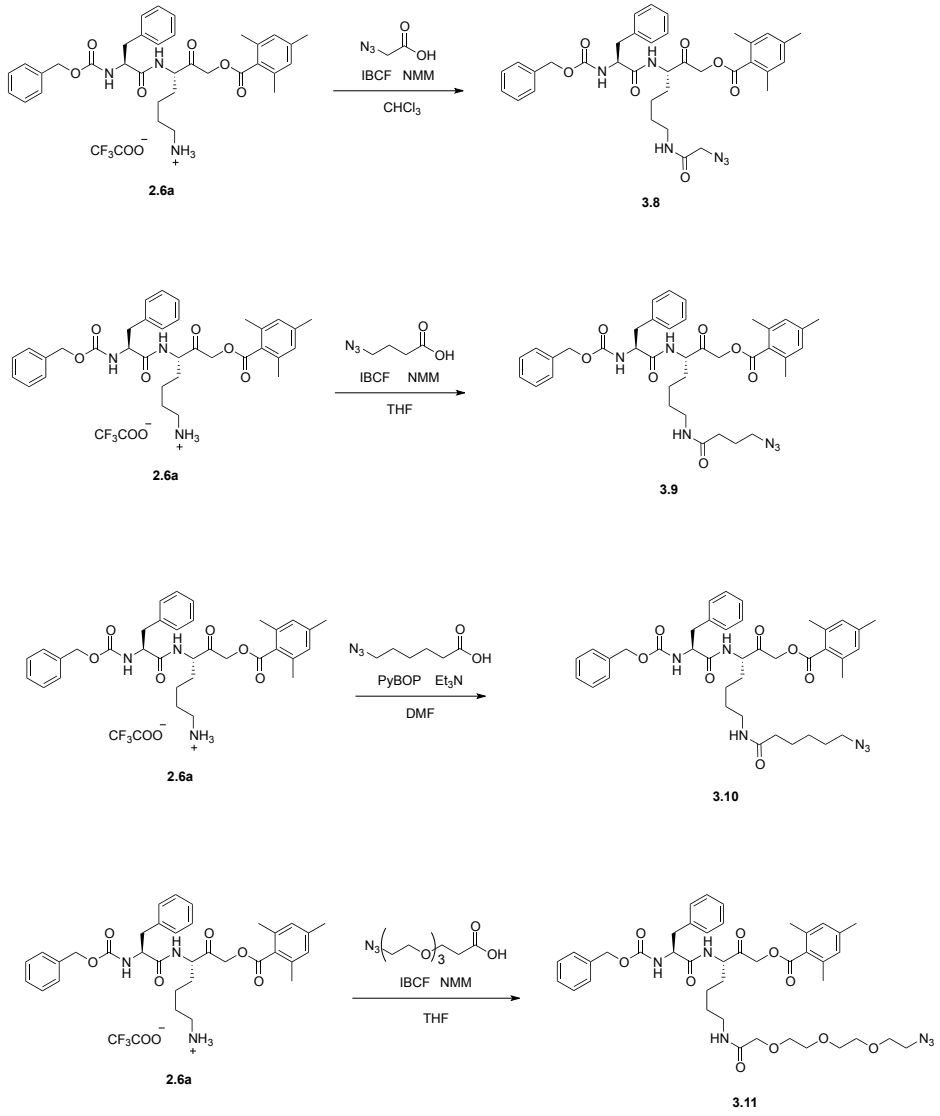

Scheme 3.3. Synthesis of **3.8**-**3.11** (4-azidobutyric acid was synthesized by Lukas Sadowski – Adronov Research Group).

Compounds **3.8**-**3.11** were then used in CuAAC reactions with alkyne functionalized dendrimers containing the $[Re(CO)_3]$-bis(pyridyl) group at

the core (Figure 3.5). Generation 1 (G1) dendrimers containing 2 targeting vectors and generation 2 (G2) dendrimers containing 4 targeting vectors were initially synthesized. As a comparison, generation zero (G0) dendrimers were synthesized where only one targeting vector was incorporated.

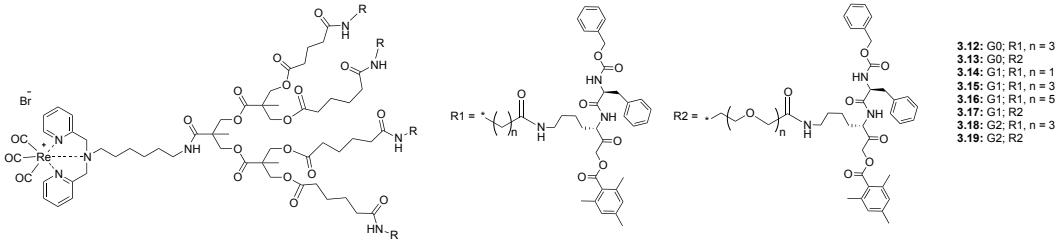

Figure 3.5 General Structures of Dendrimer Linked AOMKs (*note: alkyne and AOMK functionalized dendrimers were synthesized by Lukas Sadowski – Adronov Research Group).

The G1 derivative featuring the two-carbon spacer (**3.14**) was the first construct tested. This compound exhibited very little inhibition and a K_i value could not be accurately determined. Although two targeting vectors are incorporated here the linkage at the P_1 site could result in steric crowding thus lowering the affinity for the cathepsin B. To circumvent this issue increasing the spacer length with the four-carbon (**3.15**), six-carbon (**3.16**), or PEG-3 (**3.17**) spacer was completed. The products only showed improved affinity in the case of **3.15** (K_i = 1.8 μM, k_i/K_i = 1 670 ± 80 Table 4). This was a surprising result as derivatives with a longer spacer (**3.16**

and **3.17**) were expected to show further improvements in affinity. One possible explanation was that higher generation AOMK-dendrimers underwent epimerization during the CuAAC reaction. This was indicated by a split peak appearing in HPLC representing compounds of the same mass as determined by ESI-MS (Figure 3.6).

Table 3.2. Inhibitory Activities of Dendrimer-AOMK Derivatives.[a]

Compound	K_i (nM)	k_i/K_i ($s^{-1}M^{-1}$)
3.12	350 ± 40	13 400 ± 700
3.13	440 ± 20	11 300 ± 400
3.14	n.d.[b]	764 ± 8
3.15	1 800 ± 300	1 670 ± 80
3.16	n.i.[c]	n.i.
3.17	n.d.	20 ± 4
3.18	n.d.	560 ± 10
3.19	n.i.[c]	26 ± 3

[a] Inhibition constants were determined at 37 °C and pH 6.0 with human liver cathepsin B. [b] n.d.: full inhibition was not observed therefore the value was not determined. [c] n.i.: no inhibition observed.

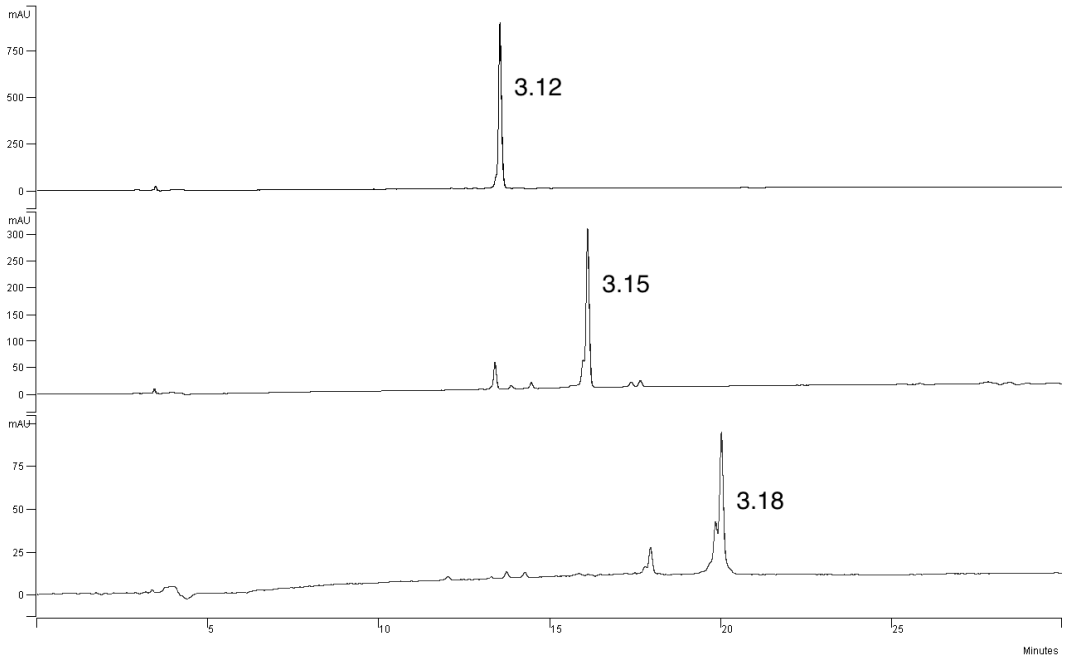

Figure 3.6 UV−visible (λ = 254 nm) HPLC chromatogram of **3.13** (upper trace) **3.15** (middle trace) and **3.18** (lower trace).

To observe the effect of increasing the number of targeting vectors, G2 dendrimers featuring the four-carbon and PEG-3 spacer were tested. Unfortunately these compounds did not exhibit substantial inhibition of the protease again likely due to steric crowding and epimerization. As a comparison, G0 dendrimers featuring the four-carbon (**3.12**) and PEG-3 (**3.13**) spacer were synthesized and tested. K_i values of 350 (k_i/K_i = 13 400 $s^{-1}M^{-1}$) and 440 nM (k_i/K_i = 11 300 $s^{-1}M^{-1}$) were found, which were not improved when moving to G1 or G2 dendrimers. Of the compounds

reported, **3.12** exhibited the best binding affinity and there is the potential to further optimize the construct as an imaging probe.

3.6 Summary and Conclusions

The first examples of Re based AOMK derivatives as model compounds for developing cathepsin B targeted radioimaging probes were described. Initial attempts involved linking a bifunctional chelate of the $[Re(CO)_3^+]$ core to AOMK. This modification did not result in a high affinity probe and was therefore not pursued further.

In an attempt to further enhance affinity, a dendrimer approach was employed where spacers of varying lengths and polarities were used to link multiple AOMK targeting vectors to the metal core. There was an enhancement in binding affinity when longer spacers were employed when comparing **3.12** and **3.13** to **3.5** but this effect was not observed with higher generation constructs. The prevailing hypothesis is that increased steric hindrance at the P_1 site as well as epimerization that occurred during the synthesis of the higher generation dendrimers impacted affinity. Although this strategy was successful in producing higher affinity probes for an RGD based system[9] it is not universal. Yim *et al.* describe multimeric octreotide probes that were labelled with ^{111}In and evaluated *in vivo*.[11] When moving from a monomeric, dimeric, to a tetrameric probe,

improved binding affinity was not observed, similar to the case reported here. When tested *in vivo*, the dimeric ^{111}In probe exhibited lower initial tumour uptake when compared to the monomeric probe, yet better tumour retention. Although this strategy may not yield improvements for *in vitro* analysis it has potential for improvements for *in vivo* applications notably improvement of the clearance rate from non-target organs which is a critical issue for many targeted Tc-based agents.

3.7 Experimental

General. All chemicals, unless otherwise stated, were purchased from Sigma−Aldrich, Novabiochem, or Bachem and used without further purification. $[Re(CO)_3(H_2O)_3][Br]$ was synthesized by Reza Yazdani according to literature procedures.[12] For screening studies, human liver cathepsin B and Cbz-Arg-Arg-pNA were purchased from Calbiochem and Enzo Life Sciences, respectively. Reagents used in the assay buffer were from Sigma−Aldrich. Inhibitors were dissolved in biological-grade DMSO and diluted in the assay buffer. Black, clear-bottom 96-well plates were obtained from BD Biosciences.

Microwave reactions were performed by use of a Biotage Initiator microwave synthesizer. Automated flash chromatography was performed on a Biotage SP1 flash purification system. Analytical thin-layer

chromatography (TLC) was performed on silica gel plates with fluorescent indicator UV254 (Macherey-Nagel) and visualized by use of UV light and ninhydrin or vanillin in EtOH. ^{1}H, ^{13}C, and two- dimensional NMR spectra were recorded on either a Bruker AV500 or AV600 spectrometer. ^{1}H NMR signals are reported in parts per million (ppm) measured relative to the residual proton signal of the deuterated solvent. Coupling constants (J) are reported in Hertz (Hz). ^{13}C signals are reported in ppm relative to the carbon signal from the solvent. HRMS was performed on a Waters/Micromass Q-Tof Ultima Global spectrometer. Analytical high-performance liquid chromatography (HPLC) was performed by use of an Agilent/Varian Pro Star model 330 photodiode array (PDA) detector, model 230 solvent delivery system, and Phenomenex Gemini (L × i.d. = 100 × 4.6 mm) column (5 μm C18). Semipreparative HPLC was performed by use of an Agilent/Varian Pro Star model 325 PDA detector, model 24 solvent delivery system, and Phenomenex Gemini (L × i.d. = 250 × 10 mm) column (5 μm C18). The elution conditions were as follows: **Method A:** Solvent A = CH_3CN, solvent B= H_2O. Gradient: 30% A to 100% A, 0−12 min; 100% A, 12−24 min; 100% A to 90% A, 24−28 min; 90% A to 30% A, 28−30 min. **Method B:** Solvent A = CH_3CN with 0.1% TFA, solvent B= H_2O with 0.1% TFA. Gradient: 30% A to 100% A, 0−12 min; 100% A,

12−24 min; 100% A to 90% A, 24−28 min; 90% A to 30% A, 28−30 min. The flow rate was set at 1 mL/min; monitoring occurred at 254 nm.

***Tert*-butyl 2-(2-formyl-1*H*-imidazol-1-yl)acetate (3.1).** 2-Imidazole carboxaldehyde (2.00 g, 20.8 mmol) and *t*-butyl bromoacetate (3.69 mL, 24.9 mmol) were added to anhydrous DMF (100 mL) containing DIPEA (10.8 mL, 62.3 mmol). The solution was stirred for 1.5 h at 85°C. The solvent was removed under reduced pressure and the product was isolated as a yellow oil following flash chromatography using a gradient of 12% - 100% EtOAc/hexanes. Yield (3.34 g, 76%). TLC (1:1 EtOAc/Hex): R_f = 0.25; ^{1}H NMR (600 MHz; $CDCl_3$): δ 9.73 (s, 1H), 7.25 (d, J = 0.8, 1H), 7.06 (m, 1H), 4.95 (s, 2H), 1.40 (s, 9H); ^{13}C NMR (151 MHz; $CDCl_3$): δ 181.9, 165.9, 143.4, 131.3, 127.0, 83.1, 49.3, 27.8. HRMS Calcd. for $C_{10}H_{15}N_2O_3$ [M+H]+: 211.1083. Found: 211.1076.

6-(Bis((1-(2-(*tert*-butoxy)-2-oxoethyl)-1*H*-imidazol-2-yl)methyl)amino)hexanoic acid (3.2). 6-Amino hexanoic acid (145 mg, 1.10 mmol) and **3.1** (578 mg, 2.75 mmol) were added to dichloroethane (DCE) (20 mL) containing acetic acid (112 μL, 1.96 μmol) and the mixture heated to reflux at 85 °C for 1.5 h under Ar. The reaction was cooled to 0 °C and $NaBH(OAc)_3$ (583 mg, 2.75 mmol) was added. The reaction was allowed to stir overnight at room temperature. The solvent was removed under reduced pressure and the product was isolated as a white powder

following flash chromatography using a gradient of 1% - 30% MeOH/CH_2Cl_2. Yield (380 mg, 66%). TLC (5% MeOH/CH_2Cl_2): R_f = 0.23. ^{1}H NMR (600 MHz; $CDCl_3$): δ 6.96 (m, 2H), 6.79 (d, J = 1.1, 2H), 4.56 (s, 4H), 3.61 (s, 4H), 2.49 (t, J = 7.6, 2H), 2.28 (t, J = 7.5, 2H), 1.63-1.58 (m, 2H), 1.54-1.49 (m, 2H), 1.41 (s, 18H), 1.30-1.23 (m, 2H). ^{13}C NMR (151 MHz; $CDCl_3$): δ 176.9, 166.8, 145.4, 127.1, 121.4, 83.2, 54.6, 49.8, 48.1, 35.1, 28.1, 27.1, 25.5, 25.1. HRMS Calcd. for $C_{26}H_{42}N_5O_6$ $[M+H]^+$: 520.3135. Found: 520.3125.

Compound 3.3. Re[$(CO)_3(H_2O)_3$]Br (142 mg, 350 μmol) and **3.2** (116 mg, 320 μmol) and were added to a 2 mL microwave vial and CH_3CN/H_2O (2:1) (1 mL) was added. The reaction was heated by microwave irradiation for 20 min at 80 °C. The product was isolated following flash chromatography with a gradient of 2% - 20% MeOH/CH_2Cl_2. The product was obtained as a white powder. Yield (113 mg, 41%). TLC (10% MeOH/CH_2Cl_2): R_f = 0.25. ^{1}H NMR (600 MHz; $CDCl_3$): δ 6.95 (s, 2H), 6.72 (s, 2H), 5.67-5.63 (m, 3H), 4.60 (d, J = 18.0, 2H), 4.16 (d, J = 16.3, 2H), 3.69-3.66 (m, 2H), 2.41 (t, J = 7.0, 3H), 1.95-1.94 (m, 3H), 1.77 (t, J = 7.1, 2H), 1.52 (s, 2H), 1.48 (s, 18H). ^{13}C NMR (151 MHz; $CDCl_3$): δ 196.2, 194.8, 166.3, 151.6, 127.7, 123.0, 84.3, 71.1, 58.8, 50.9, 33.8, 28.0, 26.3,

24.9, 24.3. HRMS Calcd. for $C_{29}H_{41}N_5O_9Re$ $[M]^+$: 790.2462. Found: 790.2449.

Compound 3.4. PyBOP (42 mg, 80 μmol) and **3.3** (70 mg, 80 μmol) were dissolved in anhydrous DMF (8 mL) under Ar at 0 °C. Et_3N (22 μL, 160 μmol) was added and the reaction was left to stir for 5 min. Et_3N (11 μL, 80 μmol) and **2.6a** (56 mg, 80 μmol) were then added and the reaction was stirred at room temperature for 8 h. Water (25 mL) was added and the mixture was extracted with CH_2Cl_2 (3 × 15 mL). The combined organic fractions were extracted with water (5 × 25 mL). The solvent was removed under reduced pressure and the product was isolated following flash chromatography using a gradient of 2% - 30% MeOH/CH_2Cl_2 as a white solid. Yield (42 mg, 37%). TLC (5% MeOH/CH_2Cl_2): R_f = 0.23. HPLC (method A) R^t = 11.6 min. ^{1}H NMR (600 MHz; $(CD_3)_2SO$): δ 8.60-8.47 (m, 1H), 7.72-7.60 (m, 2H), 7.37-7.19 (m, 14H), 6.97-6.91 (m, 2H), 5.16-5.03 (m, 1H), 5.00-4.97 (m, 2H), 4.96-4.87 (m, 4H), 4.51 (d, J = 16.7, 1H), 4.44 (d, J = 16.3, 1H), 4.39-4.31 (m, 2H), 3.66-3.63 (m, 1H), 3.05-2.96 (m, 3H), 2.86-2.81 (m, 1H), 2.77-2.73 (m, 1H), 2.63-2.54 (m, 1H), 2.30 (s, 6H), 2.27 (s, 3H), 2.24 (s, 2H), 2.12-2.08 (m, 1H), 1.79-1.74 (m, 2H), 1.59-1.49 (m, 4H), 1.44 (s, 18H), 1.38-1.32 (m, 2H), 1.32-1.26 (m, 2H), 1.19 (s, 1H). ^{13}C NMR (151 MHz; $(CD_3)_2SO$): δ 206.4, 196.6, 172.17, 172.00, 168.2, 166.2,

151.4, 139.1, 137.7, 136.9, 134.9, 129.9, 129.3, 128.24, 128.09, 127.95, 127.70, 127.53, 127.39, 126.3, 124.0, 82.8, 72.3, 68.9, 66.6, 65.3, 57.9, 56.07, 55.89, 48.8, 38.2, 37.2, 35.4, 29.1, 28.8, 27.6, 26.5, 25.9, 25.2, 24.8, 22.39, 22.32, 21.8, 20.7, 19.3. HRMS Calcd. for $C_{63}H_{80}N_8O_{14}Re$ $[M]^+$: 1359.5356. Found: 1359.5352.

Compound 3.5. Compound **3.4** (42 mg, 29 μmol) was dissolved in CH_2Cl_2 (5 mL) at 0 °C and TFA (5 mL) was added dropwise. The reaction was stirred for 3 h at room temperature. The solution was concentrated and the residue was added to cold Et_2O. The product was isolated as a white powder following centrifugation. Yield (23 mg, 61%). TLC (10% MeOH/CH_2Cl_2): R_f = 0.13. HPLC (method B) R^t = 12.6 min. HRMS Calcd. for $C_{63}H_{80}N_8O_{14}Re$ $[M]^+$: 1474.5985. Found: 1474.5968.

2-Azidoacetic acid (3.6). Sodium azide (1.63 g, 25 mmol) dissolved in water (10 mL) and added to a solution of 2-bromoacetic acid (1.39 g, 10 mmol) in water (10 mL) at 0°C. The solution was left to stir overnight at room temperature and then 1N HCl (5 mL *c.a.*) was added. The solution was extracted with EtOAc (5 × 20 mL) and dried over $MgSO_4$. Following rotary evaporation, the product was isolated as a yellow oil. Yield (495 mg, 49%). ^1H NMR (500 MHz; CD_2Cl_2): δ 7.31 (br s, 1H), 3.97 (s, 2H). ^{13}C

NMR (126 MHz; CD_2Cl_2): δ 173.5, 50.2. HRMS Calcd. for $C_2H_3N_3O_2$ $[M-H]^-$: 100.0153. Found: 100.0153.

6-Azidohexanoic acid (3.7). Sodium azide (1.85 g, 28.5 mmol) and 6-bromohexanoic acid (1.11 g, 5.70 mmol) were dissolved in DMF (20 mL) and water (10 mL) and stirred 24 h at 60 °C. The solvent was removed under reduced pressure. To the resultant residue water (10 mL) and 6N HCl (5 mL) was added and extracted with CH_2Cl_2 (3 × 20 mL). The organic layer was extracted with water (3 × 20 mL), brine (3 × 20 mL) and dried over Na_2SO_4. Following rotary evaporation, the product was isolated as a yellow oil. Yield (561 mg, 63%). TLC (2:1 EtOAc/Hex): R_f = 0.73. ^{1}H NMR (600 MHz; $CDCl_3$): δ 3.31 (t, J = 6.9, 2H), 2.40 (t, J = 7.4, 2H), 1.72-1.67 (m, 2H), 1.67-1.62 (m, 2H), 1.49-1.44 (m, 2H). ^{13}C NMR (151 MHz; $CDCl_3$): δ 179.8, 51.3, 33.9, 28.7, 26.3, 24.3. HRMS Calcd. for $C_6H_{11}N_3O_2$ $[M-H]^-$: 156.0779. Found: 156.0780.

(S)-7-(2-azidoacetamido)-3-((S)-2-(((benzyloxy)carbonyl)amino)-3-phenylpropanamido)-2-oxoheptyl 2,4,6-trimethylbenzoate (3.8). To a solution of **3.6** (35.4 mg, 350 μmol) in $CHCl_3$ (5 mL) at -20 °C, NMM (38 μL, 350 μmol) and IBCF (45 μL, 350 μmol) were added and left to stir 1 min. To this, **2.6a** (246 mg, 350 μmol) and NMM (38 μL, 350 μmol) were added and the solution was left to stir overnight while warming to room

temperature. The solvent was removed under reduced pressure, EtOAc (25 mL) was added, and then extracted with sat. $NaHCO_3$ (3 × 15 mL), water (20 mL), 5% (w/v) citric acid (3 × 15 mL), water (20 mL), brine (20 mL) and dried over Na_2SO_4. The solvent was removed by rotary evaporation and the product was isolated as a white solid following column chromatography using EtOAc/hexanes (2:1). Yield (35.1 mg, 15%). TLC (2:1 EtOAc/Hex): R_f = 0.28. ^{1}H NMR (500 MHz; $(CD_3)_2SO$): δ 8.50 (d, J = 7.5, 1H), 8.06 (t, J = 5.3, 1H), 7.64 (d, J = 8.2, 1H), 7.34-7.18 (m, 10H), 6.92 (s, 2H), 4.97 (s, 2H), 4.90 (d, J = 17.2, 1H), 4.80 (d, J = 17.2, 1H), 4.37-4.31 (m, 2H), 3.79 (s, 2H), 3.10-3.01 (m, 3H), 2.82 (dd, J = 13.5, 9.8, 1H), 2.27 (s, 6H), 2.25 (s, 3H), 1.84-1.77 (m, 1H), 1.61-1.53 (m, 1H), 1.46-1.36 (m, 2H), 1.35-1.23 (m, 2H). ^{13}C NMR (126 MHz; $(CD_3)_2SO$): δ 202.5, 171.8, 168.0, 166.8, 155.7, 138.9, 137.6, 136.8, 134.8, 129.8, 129.1, 128.10, 128.06, 127.92, 127.53, 127.35, 126.2, 66.4, 65.1, 55.9, 55.7, 50.6, 38.2, 37.1, 28.9, 28.3, 22.1, 20.5, 19.2.

(S)-7-(4-azidobutanamido)-3-((S)-2-(((benzyloxy)carbonyl)amino)-3-phenylpropanamido)-2-oxoheptyl 2,4,6-trimethylbenzoate (3.9). To a solution of 4-azidobutanoic acid (35.4 mg, 350 μmol) in THF (12 mL) at -30 °C, NMM (63 mL, 570 μmol) and IBCF (75 mL, 570 μmol) were added and left to stir 20 min. under Ar. To this, **2.6a** (400 mg, 570 μmol) and

NMM (126 μL, 1.14 μmol) were added and the solution was left to stir overnight while warming to room temperature. The solvent was removed under reduced pressure, CH_2Cl_2 (50 mL) was added, and then extracted with sat. $NaHCO_3$ (3 × 20 mL), water (30 mL), 5% (w/v) citric acid (3 × 20 mL), water (30 mL), brine (3 × 20 mL) and the organic layer dried over Na_2SO_4. The solvent was removed by rotary evaporation and the product was isolated as a white solid following flash chromatography using a gradient of 50%-66% EtOAc/hexanes (2:1). Yield (187 mg, 47%). TLC (5% MeOH/CH_2Cl_2): R_f = 0.46. ^{1}H NMR (600 MHz; $(CD_3)_2SO$): δ 8.49 (d, J = 7.5, 1H), 7.81 (t, J = 5.4, 1H), 7.63 (d, J = 8.3, 1H), 7.34-7.18 (m, 10H), 6.92 (s, 2H), 4.96 (s, 2H), 4.90 (d, J = 17.2, 1H), 4.80 (d, J = 17.2, 1H), 4.36-4.31 (m, 2H), 3.29 (t, J = 6.8, 2H), 3.04-3.01 (m, 3H), 2.83-2.79 (m, J = 13.7, 9.9, 1H), 2.27 (s, 6H), 2.25 (s, 3H), 2.13 (t, J = 7.4, 2H), 1.81-1.77 (m, 1H), 1.76-1.70 (m, 2H), 1.58-1.53 (m, 1H), 1.42-1.23 (m, 4H). ^{13}C NMR (151 MHz; $(CD_3)_2SO$): δ 202.6, 172.0, 170.9, 168.2, 155.8, 139.1, 137.8, 136.9, 134.9, 129.9, 129.24, 129.20, 128.26, 128.22, 128.08, 127.69, 127.50, 126.3, 66.6, 65.3, 56.04, 55.88, 50.3, 38.2, 37.2, 32.2, 29.1, 28.7, 24.5, 22.4, 20.7, 19.3. HRMS Calcd. for $C_{38}H_{46}N_6O_7$ $[M+H]^+$: 721.3326. Found: 721.3312.

(S)-7-(6-Azidohexanamido)-3-((S)-2-(((benzyloxy)carbonyl)amino)-3-phenylpropanamido)-2-oxoheptyl 2,4,6-trimethylbenzoate (3.10).

PyBOP (291 mg, 520 μmol) and **3.7** (88 mg, 560 μmol) were dissolved in anhydrous DMF (10 mL) under Ar at 0 °C. Et_3N (78 μL, 560 μmol) was added the reaction was left to stir for 5 min. Et_3N (156 μL, 1.12 μmol) and **2.6a** (393 mg, 560 μmol) were added and the reaction was stirred at room temperature for 16 h. Water (15 mL) was added and the mixture was extracted with CH_2Cl_2 (3 × 15 mL). The combined organic fractions were extracted with sat. $NaHCO_3$ (3 × 15 mL), brine (3 × 15 mL) and dried over $MgSO_4$. The solvent was removed under reduced pressure and the product was isolated following flash chromatography using a gradient of 1% - 20% MeOH/CH_2Cl_2 as a white solid. Yield (250 mg, 66%). TLC (5%MeOH/CH_2Cl_2): R_f = 0.49. ^{1}H NMR (600 MHz; $(CD_3)_2SO$): δ 8.50 (d, J = 7.5, 1H), 7.74 (t, J = 5.7, 1H), 7.64 (d, J = 8.3, 1H), 7.35-7.19 (m, 10H), 6.93 (s, 2H), 4.98 (d, J = 6.7, 2H), 4.92 (d, J = 17.2, 1H), 4.81 (d, J = 17.2, 1H), 4.37-4.33 (m, 2H), 3.30-3.27 (m, 3H), 2.85-2.82 (m, 1H), 2.28 (s, 6H), 2.26 (s, 3H), 2.07-2.04 (m, 2H), 1.84-1.77 (m, 1H), 1.61-1.56 (m, 1H), 1.53-1.49 (m, 5H), 1.41-1.30 (m, 3H), 1.30-1.26 (m, 4H). ^{13}C NMR (151 MHz; ; $(CD_3)_2SO$): δ 202.6, 172.0, 171.7, 168.2, 155.9, 139.1, 137.8, 136.9, 134.9, 129.9, 129.2, 128.26, 128.22, 128.08, 127.69, 127.50, 126.3, 66.6, 65.3, 56.05, 55.90, 50.5, 38.1, 37.2, 35.2, 29.1, 28.8, 28.0,

25.8, 24.8, 22.4, 20.7, 19.3. HRMS Calcd. for $C_{40}H_{51}N_6O_7$ $[M+H]^+$: 727.3819. Found: 727.3844.

(S)-1-azido-17-((S)-2-(((benzyloxy)carbonyl)amino)-3-phenylpropanamido)-11,18-dioxo-3,6,9-trioxa-12-azanonadecan-19-yl 2,4,6-trimethylbenzoate (3.11). To a solution of 11-azido-3,6,9-trioxoundecanoic acid (70 mg, 300 μmol) in THF (12 mL) at -18 °C, NMM (33 mL, 300 μmol) and IBCF (40 mL, 300 μmol) were added and left to stir 20 min. To this, **2.6a** (211 mg, 300 μmol) was added and the solution was left to stir overnight while warming to room temperature. The solvent was removed under reduced pressure, CH_2Cl_2 (25 mL) was added, and then extracted with water (10 mL), sat. $NaHCO_3$ (3 × 10 mL), water (10 mL), 5% (w/v) citric acid (3 × 10 mL), water (10 mL), brine (3 × 10 mL) and dried over Na_2SO_4. The solvent was removed by rotary evaporation and the product was isolated as a yellow oil following flash chromatography using a gradient of 1% - 10% MeOH/CH_2Cl_2. Yield (154 mg, 64%). TLC (5%MeOH/CH_2Cl_2): R_f = 0.33. ^{1}H NMR (600 MHz; $(CD_3)_2SO$): δ 8.50 (t, J = 6.8, 1H), 7.67-7.64 (m, 1H), 7.64-7.62 (m, 1H), 7.35-7.19 (m, 10H), 6.93 (s, 2H), 4.98 (s, 2H), 4.92 (d, J = 17.2, 1H), 4.82 (d, J = 17.2, 1H), 4.37-4.32 (m, 2H), 3.87 (s, 2H), 3.61-3.55 (m, 10H), 3.39 (t, J = 4.9, 2H), 3.12-3.08 (m, 2H), 3.05-3.02 (m, 1H), 2.84-2.80 (m, 1H), 2.28 (s, 6H), 2.26 (s, 3H), 1.84-1.78 (m, 1H), 1.62-1.55 (m, 1H), 1.47-1.37 (m, 2H), 1.38-1.24

(m, 2H). HRMS Calcd. for $C_{42}H_{55}N_6O_{10}$ $[M+H]^+$: 803.3980. Found: 803.3964.

Determination of Inhibition Constants. Cathepsin B (200 nM) was preincubated for 30 min at 37 °C in a solution of 5 mM DTT and 0.01% (v/v) Tween-20. The substrate, Cbz-Arg-Arg-pNA (25 or 40 mL), and the AOMKs (50 mL) were added to the wells of a 96-well microplate containing the assay buffer. The reaction was initiated by the addition of cathepsin B, resulting in substrate concentrations of 500 or 800 mM, inhibitor concentrations from 25 nM to 1 mM, and an enzyme concentration of 5 nM. Formation of the p-NA product was monitored for 60 min at 405 nm at 37 °C. Measurements were obtained in triplicate. Absorbance vs. time measurements were analyzed using non-linear regression to determine the pseudo first-order rate constant (k_{obs}) in accordance to: Absorbance = $Ae^{-kobs(t)}$ + B. The second-order rate constant, (k_i/K_i), the apparent inactivation rate (k_i), and the inhibition constant (K_i) (where possible) were determined in accordance to: $k_{obs} = \frac{ki[I]}{Ki+[I]}$ for hyperbolic relationships or $k_{obs} = \frac{ki}{Ki}[I]$ for linear relationships. Equations were solved using GraphPad Prism software.

3.8 References

1. P. E. Edem, S. Czorny, and J. F. Valliant, *J. Med. Chem.*, 2014, **57**, 9564–9577.

2. G. Ren, G. Blum, M. Verdoes, H. Liu, S. Syed, L. E. Edgington, O. Gheysens, Z. Miao, H. Jiang, S. S. Gambhir, M. Bogyo, and Z. Cheng, *PLoS One*, 2011, **6**, e28029.

3. M. Shokeen and C. J. Anderson, *Accounts Chem. Res.*, 2009, **42**, 832–41.

4. M. Bartholomä, J. Valliant, K. P. Maresca, J. Babich, and J. Zubieta, *Chem. Commun.*, 2009, **7345**, 493–512.

5. S. Liu, *Adv. Drug Deliv. Rev.*, 2008, **60**, 1347–1370.

6. M. K. Levadala, S. R. Banerjee, K. P. Maresca, J. W. Babich, and J. Zubieta, *Synthesis (Stuttg).*, 2004, **2004**, 1759–1766.

7. K. P. Maresca, J. C. Marquis, S. M. Hillier, G. Lu, F. J. Femia, C. N. Zimmerman, W. C. Eckelman, J. L. Joyal, and J. W. Babich, *Bioconjug. Chem.*, 2010, **21**, 1032–1042.

8. M. Hamoudeh, M. Anas, R. Diab, and H. Fessi, *Adv. Drug Deliv. Rev.*, 2008, **60**, 1329–1346.

9. A. Almutairi, R. Rossin, M. Shokeen, A. Hagooly, A. Ananth, B. Capoccia, S. Guillaudeu, D. Abendschein, C. J. Anderson, M. J. Welch, and J. M. J. Fréchet, *P. Natl. Acad. Sci. USA*, 2009, **106**, 685–90.

10. M. C. Parrott, S. Rahima Benhabbour, C. Saab, J. a Lemon, S. Parker, J. F. Valliant, and A. Adronov, *J. Am. Chem. Soc.*, 2009, **131**, 2906–2916.

11. C.-B. Yim, I. Dijkgraaf, R. Merkx, C. Versluis, A. Eek, G. E. Mulder, D. T. S. Rijkers, O. C. Boerman, and R. M. J. Liskamp, *J. Med. Chem.*, 2010, **53**, 3944–53.

12. N. Lazarova, S. James, J. Babich, and J. Zubieta, *Inorg. Chem. Commun.*, 2004, **7**, 1023–1026.

4 Development and Testing of Bioorthogonal Reactive Pairs for Cathepsin B Targeting

4.1 Introduction

Multimodal imaging involving nuclear and fluorescent probes has the potential to advance clinical cancer care in that it can allow clinicians to take advantage of the strengths of each technology. Nuclear probes can be used to generate target specific whole body images, while fluorescent probes allow for real time monitoring of target expression in tissue during surgery.[1] Although there are some cases where radio-guided surgery can be effective, it is not an optimal technique for tumour delineation during surgery. The method relies on an acoustic signal (i.e. listening to the signal using a hand held gamma probe) which is not particularly accurate for small lesions.[1] Fluorescent probes are better suited for intraoperative imaging because their signal can be visualized, and surgeons do not have to be concerned with radiation dose, but they do have to be cognisant of the low penetration depth of the optical signal.[1]

Hybrid probes also have an impact in proteomics and preclinical research. For instance, a protease ABP tagged with a radioisotope can be used for protein profiling in tissues, lysates, and whole cells by gel electrophoresis and then translated for small animal imaging with SPECT

or PET.[1,2] Conversely, fluorescently labelled ABPs can be used for protein profiling and fluorescence microscopy as well as small animal optical imaging.

AOMK based ABPs have been used in various applications such as PET imaging,[3] intraoperative imaging,[4] protein profiling,[3,5–12] and microscopy.[5,8–10,12,13] Typically this involves functionalizing an inhibitor with a prosthetic group carrying the fluorophore or radiolabel. The challenge with this approach is that these modifications can lead to variations in the pharmacodynamic and pharmacokinetic properties of the probe, even when they are derived from the same inhibitor.

Previously an AOMK was modified with a boron-dipyrromethene (BODIPY) dye at the P_1 site and a QSY7 quencher at the P_1` site to develop a class of quenched activity based probes (qABPs).[13] Due to steric hindrance, the resultant probe lost affinity for cathepsin B and increased affinity for cathepsin L. A subsequent derivative involved a cyanine dye at $P_1$ and a QSY21 quencher at $P_1$` attached through a spacer group.[12] This reduced unfavourable steric interactions with the protein and as a result affinity for cathepsin B was preserved.

There is often a lack of connection between the biological data reported for radiolabelled and fluorescently labelled AOMKs. For example,

the Cy5 labelled AOMK inhibitor **2.30** (Figure 2.1) exhibited higher overall tumour uptake and much lower non-target binding than ^{64}Cu-DOTA AOMK (Figure 3.1). These variations make it difficult to compare cathepsin B activity measured with a fluorescent probe with that measured from a nuclear probe.[3,12] In order to use fluorescent based and radiometric methods for complementary applications the signal emitted should show similar representations of the biological environment being tested.

A way to address these issues is to employ a tandem labelling/pre-targeting strategy, where the inhibitor is functionalized with a reactive group to give a chemical reporter. The chemical reporter becomes bound to the target site and can undergo a ligation with a reactive pair carrying the signalling agent.[2,14] This approach is advantageous because the signalling agent is not directly linked to the inhibitor and thus has no influence on the pharmacodynamic and pharmacokinetic properties.

This type of pre-targeting strategy exploits bioorthogonal chemistry.[15] For a reaction to be considered bioorthogonal it must have fast kinetics under physiological conditions, proceed without any interference from the surrounding environment, and have no interference on biological functions.[14] Because these reactions follow second order kinetics their reaction rates are dependent on the concentration of the reactive pairs.

Since *in vivo* reactions occur at low concentrations the second order rate constant is often reported as a measure of efficiency for these reactions.[14]

AOMK[16] and epoxide[17] based inhibitors have been functionalized with azides or alkynes and paired with fluorophores or affinity tags (such as biotin) bearing an alkyne, azide, or phosphine group. These chemical reporters were used to measure enzyme activity and as a means to isolate proteins in cancer cell and tumour lysates though 1,3-dipolar cycloadditions or Staudinger Ligations. Although these reactions have been successful for *in vitro* applications the signalling agents require long incubation times (1-2 h)[16,17] due to the slow reaction rates. Although this can be improved through the use of metal catalysts, this approach is not ideal for imaging in multicellular organisms due to toxicity associated with the catalysts.[14] A viable alternative is the use of the inverse-electron demand Diels-Alder (IEDDA) reaction between a tetrazine (Tz) and a strained alkene.

Strained ring systems can undergo an IEDDA reaction with tetrazines with very fast kinetics under biologically relevant conditions.[18,19] Ring systems such as bicyclononyne,[20,21] norbornene,[22,23] cyclopropene,[24,25] and *trans*-cyclooctene (TCO)[26,27] have all been used for bioorthogonal reactions in living systems; however the TCO-Tz ligation exhibits the

fastest rates (~10^3 $M^{-1}s^{-1}$), making it the most suitable candidate for *in vivo* imaging.

Radiolabelled tetrazines with indium-111,[28] copper-64,[29] gallium-68,[30] fluorine-18,[31] and lutetium-177[32] have been used in preclinical applications with pre-targeted TCO functionalized mAb. Because the Tz is able to clear faster than the directly labelled mAb there is a reduced dose burden using this system.[29,32] T:NT ratios do tend to be lower because the Tz-TCO ligation can occur with residual circulating mAb. This has been improved using Tz-linked clearing agents that help increase the blood clearance rate of the mAbs.[32,33] Small molecules clear much faster than mAbs therefore pre-targeting might lead to improved T:NT ratios when compared to the direct targeting.

Fluorescent tetrazines have been used for live cell imaging creating a class of bioorthogonal turn-on probes.[27,34–37] The fluorophore is quenched by the tetrazine and upon ligation with a TCO derivative the fluorescence signal is "turned-on."[34] Fluorophores that emit light between *ca.* 500 - *ca.* 600 nm are most efficiently quenched by the Tz, which typically has an absorption maximum between 500-525 nm.[22,27,34–37] The exact quenching mechanism can vary from Förster resonance energy transfer (FRET),[27,34] photoinduced electron transfer (PET),[34] and through bond energy transfer (TBET)[27,37] depending on the system.

An advantage for bioorthogonal turn-on probes is that the fluorescence signal is only prominent when the probe is at the target site. This can lead to increased signal-to-noise ratios and hence better quality images for *in vitro* and *in vivo* applications. Washing and clearing steps can be eliminated which is helpful in cases where removal of residual dye is slow or problematic.[27,34] To take full advantage of these potential benefits, the turn-on ratio for the probe should be maximized by ensuring the quenched probe has minimal fluorescence.[37] Early Tz-quenched fluorophores exhibited turn-on ratios ranging from 3.3 – 20-fold; however recent reports describe derivatives having up to 11 000-fold turn-on ratios.[27,36,37]

4.2 Objectives

The objective was to apply a TCO-Tz based bioorthogonal strategy as a means to create a new class of optical-nuclear probes for cathepsin B. The first goal was to synthesize a chemical reporter that displays good affinity for cathepsin B and then to identify appropriate fluorescent and radioactive Tz partners to visualize the target. A key step was to in parallel assess different cell lines in parallel, which would be used to evaluate the emerging constructs for cathepsin B activity. ABPs that were previously developed were tested as points of comparison for the hitherto unknown bioorthogonal probes.

4.3 Target Validation Using a Fluorogenic Substrate

Using a commercially available assay kit (Abcam) a collection of cancer cell lines (MDA-MB231, u87-MG, MIA PaCa-2, BxPC-3, and MeWo) were tested for cathepsin B activity. Cell lysates and tumour homogenates were incubated with the fluorogenic cathepsin B substrate, Ac-Arg-Arg-AFC. First the total protease activity was evaluated by measurement the amount of AFC released. The u87MG samples had the highest level of cathepsin B activity while the MDA-MB231 and the MIA PaCa-2 samples had the lowest (Figure 4.1). Protease activity was generally higher in the tumour homogenates than the cell lysates.

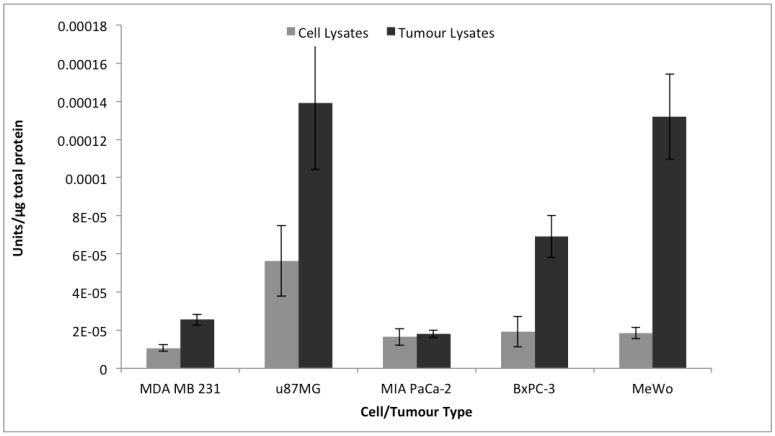

Figure 4.1 Cathepsin B activity: AMC liberated (experiment performed by Nancy Janzen).

Mechanistic release was confirmed by pre-treating the BxPC-3 cell lysates and the u87-MG tumour homogenates with the cathepsin B/L

inhibitor, Z-Phe-Phe-FMK. Fluorescence was supressed when the inhibitor was added indicating the AFC fluorescence signals were due to active cathepsin B/L (Figure 4.2).

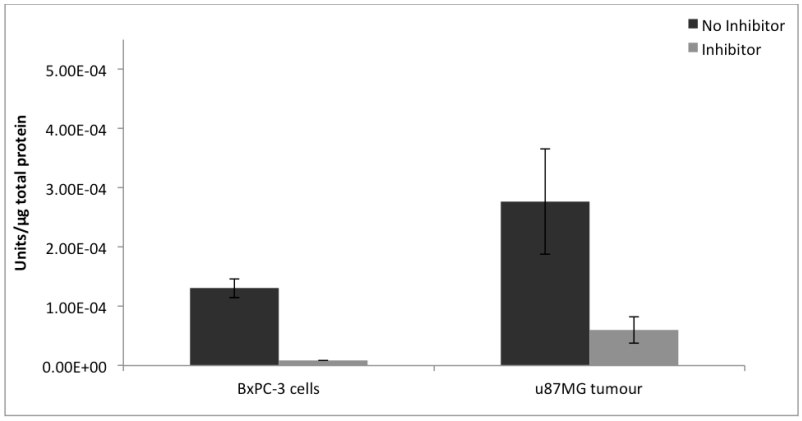

Figure 4.2 Cathepsin B activity: blocking active enzyme.

4.4 Target Validation Using a Fluorescent ABP

A simple fluorescence cell assay was established to test ABPs using **2.30** (Figure 2.1) as the model probe. MeWo and MDA-MB231 cells were seeded in a 96-well plate and pre-treated with the cathepsin B specific inhibitor, CA-074, or the vehicle. Afterwards the cells were treated with **2.30** alone or as a mixture with CA-074. CA-074 is a cell impermeable inhibitor of cathepsin B however at high concentrations (> 10 μM) it can permeate cells and deactivate intracellular cathepsin B over long time periods (> 12h).[8] The cells were washed and fluorescence measurements were made. Again fluorescent signals were higher in the MeWo cells than

the MDA-MB231 cells (Figure 4.3). When CA-074 was used the signal was reduced by 88 or 73%, indicating that the observed fluorescence signal was related to cathepsin B activity.

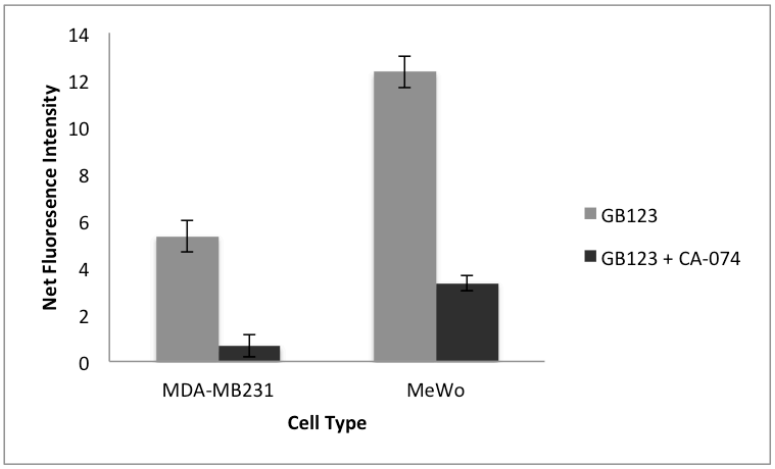

Figure 4.3 Cathepsin B activity assay: GB123 (**2.30**).

4.5 Target Validation Using a Radioiodinated ABP

Methods for affinity profiling were also established to test our probes. A known cysteine protease inhibitor, Z-Tyr-Ala-DMK, was radiolabelled with ^{125}I and used as a control probe. The labelled and unlabelled forms are non-specific inhibitors of cysteine cathepsins.[39,40] The tyrosine residue at the P_1 site can be radioiodinated in an electrophilic aromatic substitution giving the labelled product **4.1** (Scheme 4.1).

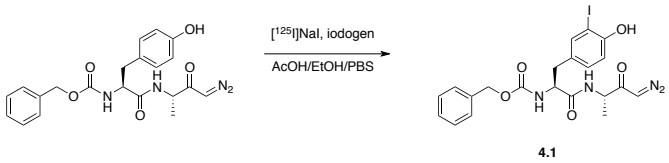

4.1

Scheme 4.1 Radioiodination of **4.1**.

Z-Tyr-Ala-DMK was treated with [^{125}I]NaI in the presence of iodogen in PBS and ethanol. Following HPLC purification **4.1** was obtained with a radiochemical purity >95% and isolated radiochemical yields between 25 – 40% (n = 3) (Figure 4.4). As **4.1** has been previously reported and the precursor was obtained from a commercial source in small quantities the non-radioactive iodinated analogue was not prepared.

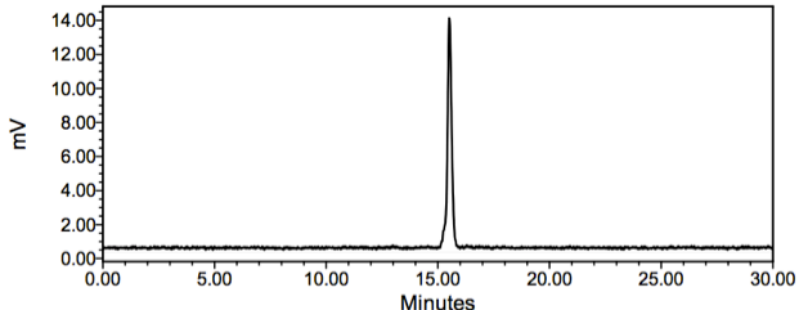

Figure 4.4 UV−visible (λ = 254 nm) HPLC chromatogram (upper trace) and radiochromatogram (lower trace) of **4.1** following purification.

Tumour homogenates (MDA-MB231, u87-MG, and MeWo) and human liver cathepsin B were pre-treated with the cathepsin inhibitor Z-Tyr-Ala-DMK or vehicle. The samples were treated with **4.1** and equal amounts of protein were separated by SDS-PAGE and visualized using autoradiography. Numerous low molecular weight (< 37 kDa) proteins were observed and the bands were blocked by the addition of Z-Tyr-Ala-DMK, indicating the presence of active cathepsins. More intense bands were observed in the MeWo and u87MG samples, likely due to higher cathepsin activity.

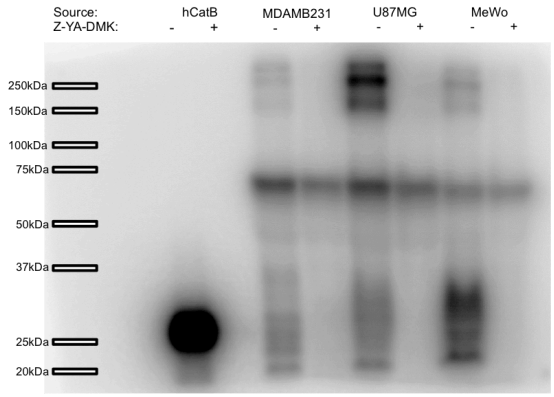

Figure 4.5 Analysis of protease labelling with **4.1** (experiment performed by Nancy Janzen).

The same procedure was applied to the labelled inhibitor ^{125}I-CaBInIV-3 ([^{125}I]**2.23a**) with the tumour homogenates. Due to experimental error, the results regarding the MeWo sample were inconclusive and therefore not shown. The most prominent protein bands were above 50 kDa and only faint bands were present below 37 kDa in the u87-MG sample (Figure 4.6). This was somewhat unexpected as the 2nd order rate constants for [^{125}I]**2.23a** (k_i/K_i = 21 000 ± 300 $s^{-1}M^{-1}$)[41] and **4.1** (27 800 ± 2 480 $s^{-1}M^{-1}$)[42] for cathepsin B inhibition are quite similar.

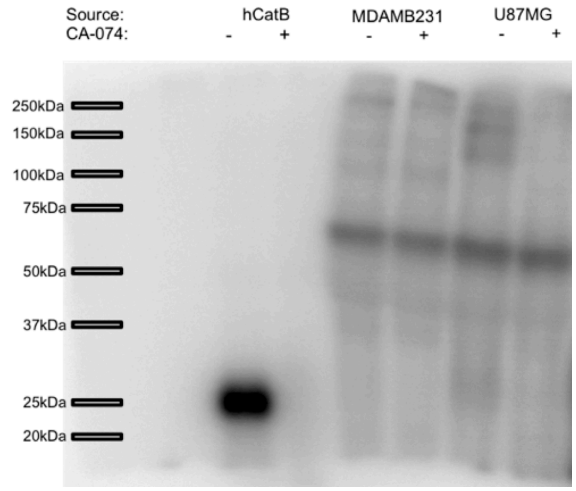

Figure 4.6 Analysis of protease labelling with [^{125}I]**2.23** (experiment performed by Nancy Janzen).

With this information in hand [^{125}I]**2.23** was tested in a CD1 nu/nu mice bearing the u87-MG xenograft. The biodistribution pattern was nearly identical to the previously tested MDA-MB231 model (Chapter 2).[41] The highest uptake was observed in the bladder/urine (600 ± 100 %ID/g) and the gall bladder (50 ± 10 %ID/g) 30 min p.i (Figure 4.7). High uptake was also observed in the thyroid (16 ± 2 %ID/g) and stomach (17 ± 2 %ID/g) indicative of *in vivo* deiodination. The overall tumour uptake was higher in this model (2.2 ± 0.1 %ID/g) in comparison to the MDA-MB231 model (1.12 ± 0.08 %ID/g) 30 min p.i. There was also a slight increase in the tumour:blood (0.5 *vs* 0.6) and tumour:muscle ratios (2.1 *vs* 3.4) 30 min p.i.

Using these methods for *in vitro* and *in vivo* testing, **2.30** and [^{125}I]**2.23** did not produce similar results. However these methods serve as a way to test and compare the bioorthogonal probes described in Section 4.6.

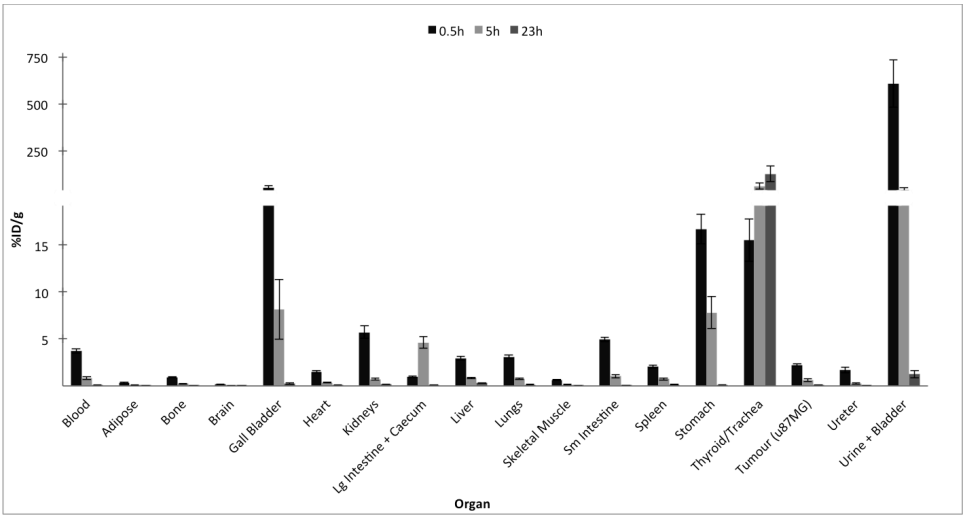

Figure 4.7 Biodistribution of [^{125}I]**2.23** in u87MG mouse xenografts (tumour preparation and data analysis performed by Nancy Janzen).

4.6 Fluorescent Bioorthogonal Reactive Pairs for Cathepsin B

4.6.1 Synthesis and Screening of Transcyclooctene Linked AOMK

The initial approach to prepare TCO derived AOMK was to use the six-carbon spacer previously employed for the development of the directly labelled inhibitors (Chapters 2 and 3). Given that the TCO succinimidyl carbonate ester was commercially available at a high cost, a synthetic strategy was developed such that the TCO was incorporated at the last

possible step. Boc-6-aminohexanoic acid was coupled to the free amine of **2.6b** giving the inhibitor with the Boc protected spacer (**4.2**) (Scheme 4.2). Following deprotection with TFA the spacer linked inhibitor (**4.3**) was coupled with the TCO active ester to give the desired inhibitor CaBInIX-1 (**4.4**).

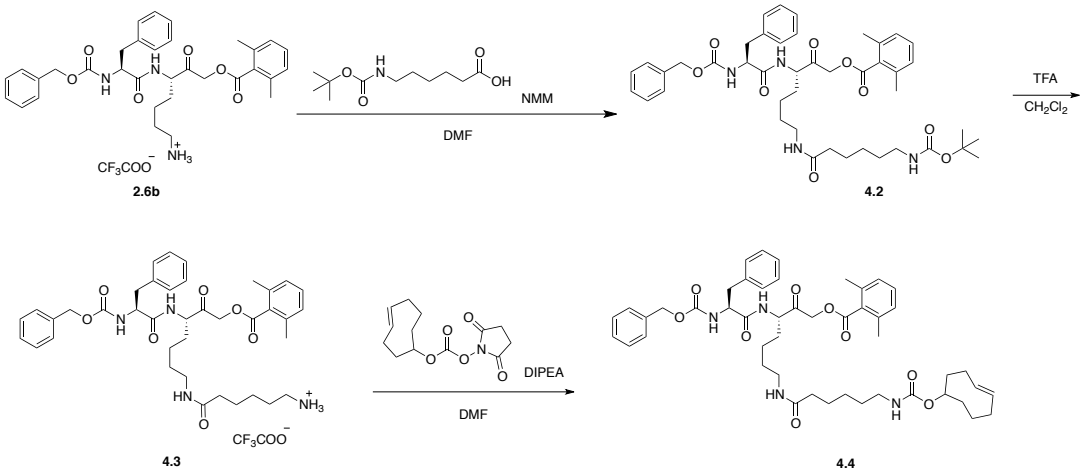

Scheme 4.2 Synthesis of **4.4**.

Upon HPLC analysis it was revealed that **4.3** was also present in the sample after semipreparative HPLC purification (Figure 4.8). It was unclear if the TCO carbamate was undergoing decomposition due to the TFA present in the eluent or if residual **4.3** was not completely removed. Due to the availability of other TCO linkers and the lipophilicity issues discovered when developing iodine based AOMKs with this linker, this strategy was not pursued further.

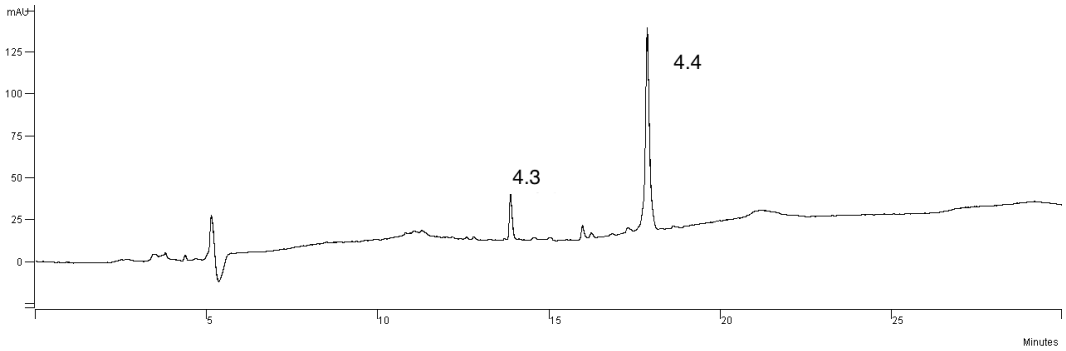

Figure 4.8 UV−visible (λ = 254 nm) HPLC chromatogram of **4.4** following semi-preparative HPLC purification.

While work was underway to prepare **4.4**, PEG linked TCOs became commercially available. This was advantageous since PEG based linkers led to improved cathepsin B affinity as well as a favourable *in vivo* distribution pattern when developing AOMK ABPs.[41] The next TCO linked AOMK involved a simpler synthetic strategy where **2.6b** was combined with the TCO PEG-4 succinimidyl carbonate giving CaBInIX-2 (**4.5**). Semipreparative purification was also employed and after analysis by HPLC a single peak for **4.5** was observed (Figure 4.9).

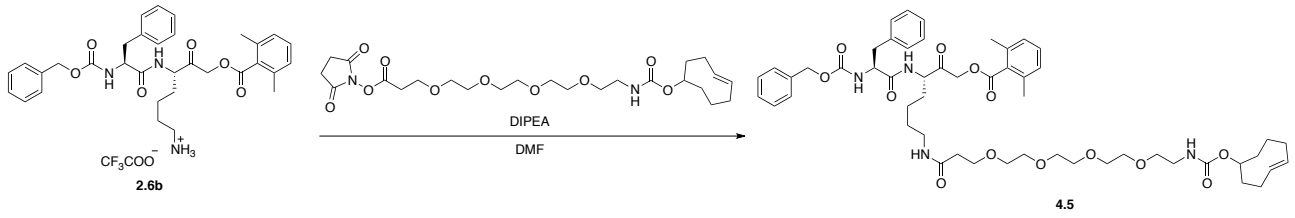

Scheme 4.3 Synthesis of **4.4**.

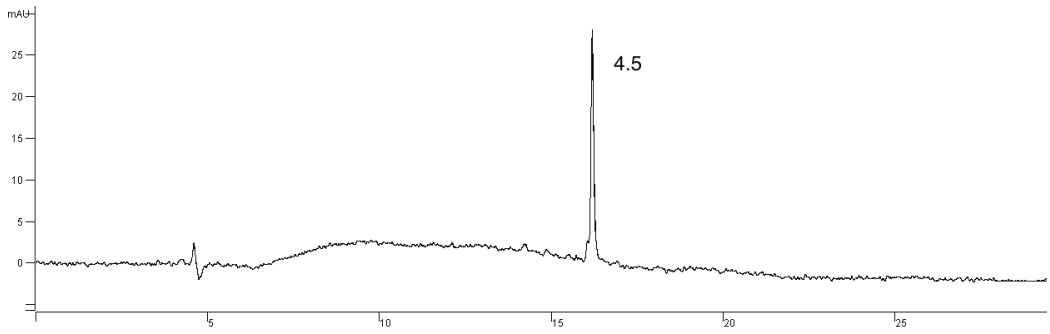

Figure 4.9 UV−visible (λ = 254 nm) HPLC chromatogram of **4.5** following semi-preparative purification.

The binding affinity of **4.5** was measured using the same method previously described in Chapter 2.[41] The TCO derivative exhibited good affinity for cathepsin B with a K_i of 190 ± 20 nM and a second order rate constant (k_i/K_i) of 13 000 ± 600 $s^{-1}M^{-1}$. These values were similar to other high affinity AOMK ABPs **2.30** (K_i = 120 ± 20, k_i/K_i = 19 000 ± 2000)[12,41] and **2.23a** (K_i = 181 ± 9, k_i/K_i = 21 100 ± 300)[41] consequently **4.5** was selected as the chemical reporter for pretargeting. The next step was to prepare the corresponding tetrazine derivatives.

4.6.2 Synthesis of Fluorescent Turn-On Tetrazine Derivatives

The first tetrazine derivative that was tested with **4.5** was BODIPYmTz (**4.8**), a known bioorthogonal turn on probe.[43] It was selected because of its exceptional turn-on ratio (1600-fold) and its ability to label both

intracellular and extracellular targets. Initially the synthetic strategy towards **4.8** was to follow the published procedure.[43]

To obtain the BODIPY core, 3-formylbenzonitrile was combined with 2,4-dimethylpyrrole in the presence of TFA. This was followed by oxidation with 2,3-dichloro-5,6-dicyano-p-benzoquinone and coordination to boron using boron trifluoride diethyl etherate in the presence of DIPEA (Scheme 4.4). The BODIPY nitrile derivative (**4.6**) was obtained in 20% yield. Nitriles can be converted to tetrazines using transition metal catalysts such nickel or zinc triflate in the presence of hydrazine.[27,44] This method was attempted to convert **4.6** to the tetrazine derivate **4.8** however the major product observed was the dipyrromethene core **4.7**. Boron trifluoride diethyl etherate was then added to a solution of **4.7** to produce **4.8** (Scheme 4.4). This synthetic route was not ideal because of the lengthy procedure and so alternative routes were explored. Loss of boron when converting BODIPY nitriles to tetrazines was reported as a problem when using a nickel catalyst but not zinc.[43] This was not the case in our hands and so after a number of attempts, sulfur was used to convert **4.7** to the dihydrotetrazine which was then oxidized to **4.8** in one step following established methods (Scheme 4.5).[45,46]

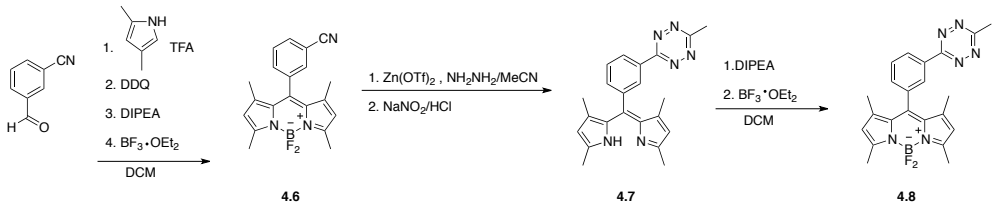

Scheme 4.4 Synthesis of **4.8** using $Zn(OTf)_2$.

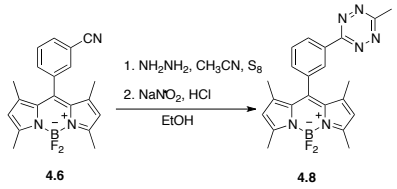

Scheme 4.5 Synthesis of **4.8** using sulfur.

Turn-on ratios that resulted from combining **4.8** with **4.5** were measured following semipreparative purification of **4.8** (Figure 4.10). When 2.5 eq of **4.5** was added to **4.8** in PBS there was a 2.3-fold enhancement in fluorescence intensity (Figure 4.11). When 250 eq of **4.5** was used a 40-fold enhancement was observed. The measured turn-on ratios varied from the literature although authors did report variations in their turn-on ratios (>500-fold) and so used mass guided HPLC to optimize the tetrazine purity and turn-on ratio. Another possible factor affecting the turn-on ratios is the reactivity of the dienophile. Tetrazine based turn-on probes show higher turn-on ratios when activated with TCO compared to the less reactive cyclopropene (e.g. 400 *vs* 135-fold).[36] Tz-TCO reaction

rates can decrease over time due to any amount of isomerization of the TCO to the non-reactive *cis*-cyclooctene.[47] This is a possible reason for the reduced turn-on ratios observed here for **4.5** if the Tz was not fully converted.

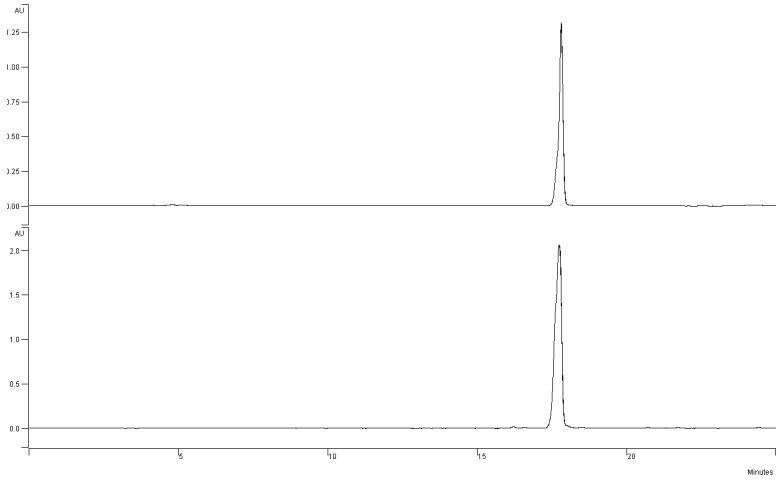

Figure 4.10 UV−visible (λ = 254 nm) HPLC chromatogram (upper trace) and UV−visible (λ = 500 nm) HPLC chromatogram (lower trace) of **4.8**.

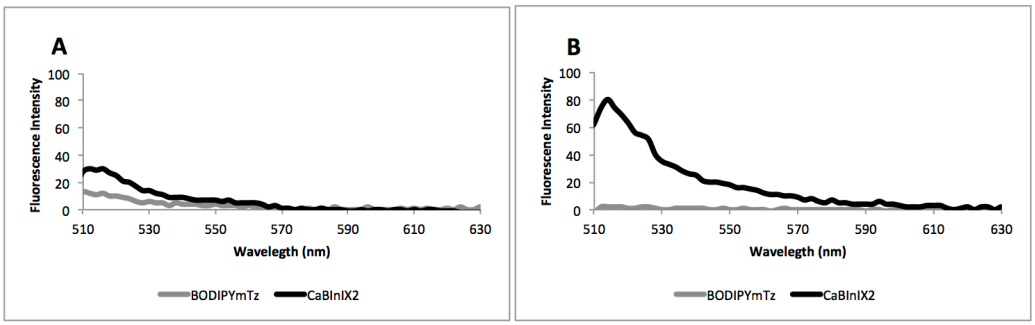

Figure 4.11 Emission spectra for **4.8** at baseline (grey) and after the addition of (a) 2.5 fold or (b) 250-fold excess **4.5**.

Given that the goal was to analyse this pair in a biological setting to see if the strategy could be used to image cathepsin B, further optimization of turn-on ratios was not pursued. We did show however that **4.8** did undergo rapid ligation with **4.5**, which is sufficient to pursue preliminary *in vitro* studies.

To complement the use of a cell permeable bioorthogonal turn-on probe, a tetrazine derivative based on Oregon Green® was used as a cell impermeable probe. The probe of choice was prepared by reacting the commercially available benzylamino tetrazine with the succinimidyl ester of Oregon Green® (Scheme 4.6).[48] The desired product **4.9** was obtained in 34% yield following semipreparative HPLC (Scheme 4.6). It was selected because at the time, it exhibited the highest turn-on ratio (18.5-fold) among tetrazine probes that solely labelled extracellular targets. Other derivatives have since been reported with much higher ratios (400-fold).[36]

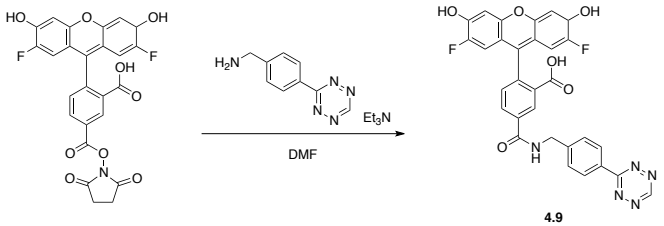

Scheme 4.6 Synthesis of **4.9**.

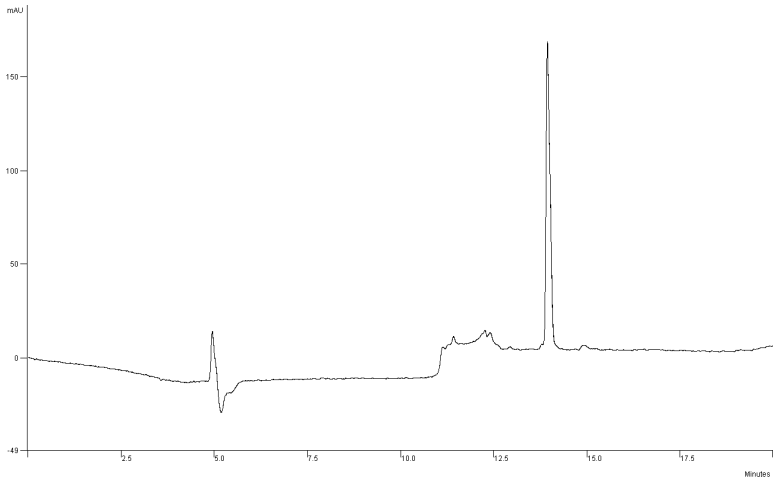

Figure 4.12 UV−visible (λ = 254 nm) HPLC chromatogram of **4.8**.

4.6.3 Evaluation of Fluorescent Turn-On Tetrazines for Cathepsin Targeting

Tetrazines **4.8** and **4.9** were tested for cathepsin targeting in a cell assay similar to what was described in section 4.4. MDA-MB231 and u87-MG cells were seeded in a 96-well plate and pre-treated with CA-074 or the vehicle. Afterwards the cells were treated with **4.5**, the unfunctionalized AOMK inhibitor (**2.6b**), TCO-OH, or the vehicle. After washing, cells were treated with **4.8** or **4.9** and the fluorescence measured.

In the case of **4.8** the pre-targeted reaction performed similarly in the presence or absence of the MDA-MB231 cells (Figure 4.13). The fluorescence signals were lower when tested in u87-MG cells. This result

did not correlate with the previous result showing that u87-MG cells have higher cathepsin activity (Figure 4.1). When the cells were treated with **2.6b**, TCO-OH, or the vehicle there was a reduction in the fluorescence intensity, indicating that **4.5** is necessary for fluorescent enhancement. When cathepsin B was blocked with CA-074 the fluorescence was not reduced. This is likely a result of non-specific binding of **4.5**, which would also explain the higher signal in the MDA-MB231 cells, compared to the u87-MG cells.

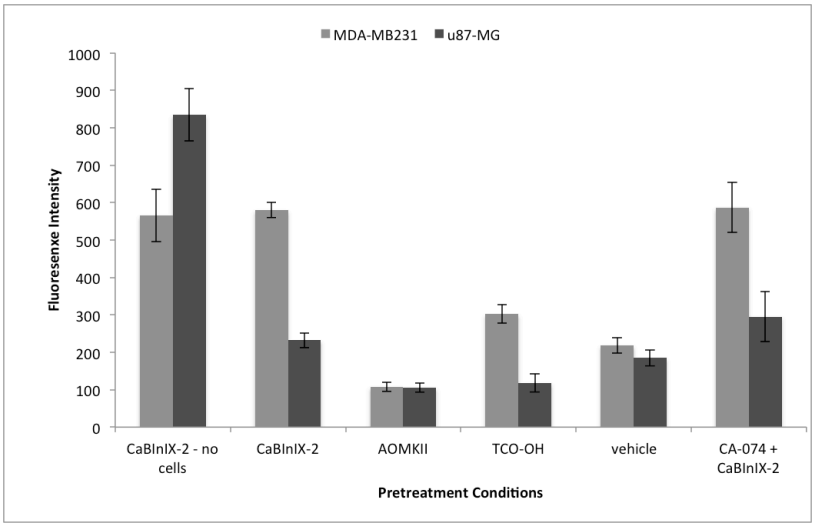

Figure 4.13 Cell assay with **4.7**.

In the case of Oregon Green® the pre-targeted reaction proceeded much better in the absence of the cells (Figure 4.14). When the cells were treated with **4.5**, **2.6b**, TCO-OH, CA-074 or the vehicle there was no substantial difference in the fluorescence intensity. This indicates that the

turn-on reaction does not proceed in the cellular environment. Since **4.9** is cell impermeable it is possible that the majority **4.5** is intracellular and inaccessible for the bioorthogonal reaction.

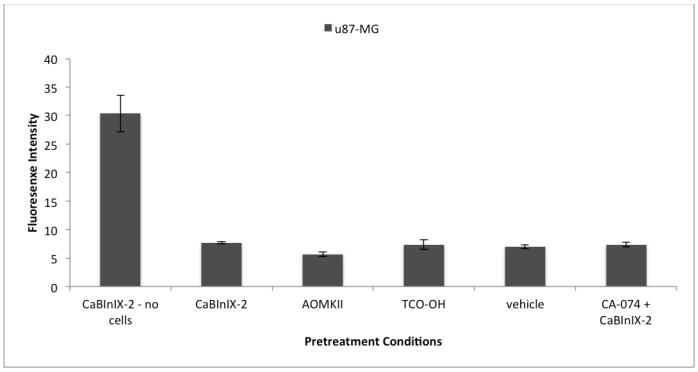

Figure 4.14 Cell assay with **4.8**.

4.6.4 Evaluation of Fluorescent Tetrazines for Cathepsin Targeting

To explore this system further the commercially available tetrazine-Cy5 and tetrazine-5-FAM were tested as well (Figure 4.15). Each fluorophore-Tz was tested in a similar fashion as described in section 4.6.3; however a washing step was added after Tz incubation because the far red/infrared emitting cyanine dyes are not typically quenched by tetrazines and fluorescein is only minimally quenched.[22,48]

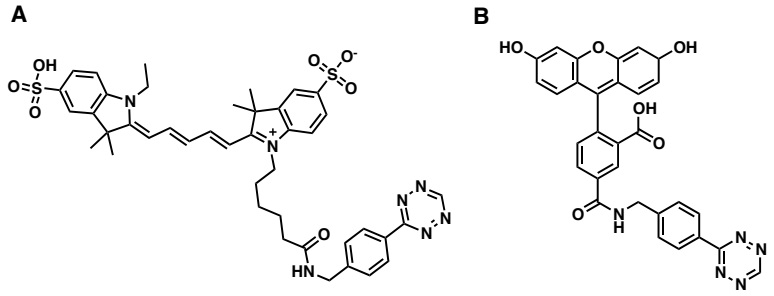

Figure 4.15 Commercially available tetrazine dyes: (A) tetrazine-Cy5 and (B) tetrazine-5-FAM.

Tetrazine-Cy5 behaved similarly to **4.8** in that the pre-targeted reaction proceeded in the presence of cells and there was no binding when **4.5** was not used (Figure 4.16). When cathepsin B was blocked with CA-074 or the cell permeable cathepsin B/L inhibitor, CA-074Me the fluorescence signal remained, likely due to non-specific binding of **4.5**. Although the tetrazine-Cy5 is not expected to permeate cell membranes, sulfonated Cy5 derivatives have been able to label intracellular targets possibly due to endocytosis.[3,49]

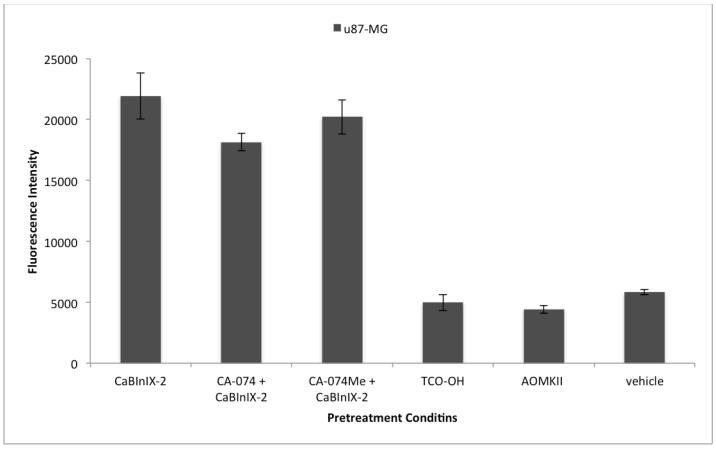

Figure 4.16 Cell assay with tetrazine-Cy5.

Tetrazine-5-FAM behaved similarly to **4.9** in that when the cells were treated with **4.5**, **2.6b**, TCO-OH, CA-074 or the vehicle there was no substantial difference in fluorescence intensity, indicating that the bioorthogonal reaction does not proceed in the cellular environment, likely due to an inability of tetrazine-5-FAM to enter the cells. To further explore the hypotheses stated here a radioiodinated tetrazine derivative was employed for further cell assays and affinity labelling.

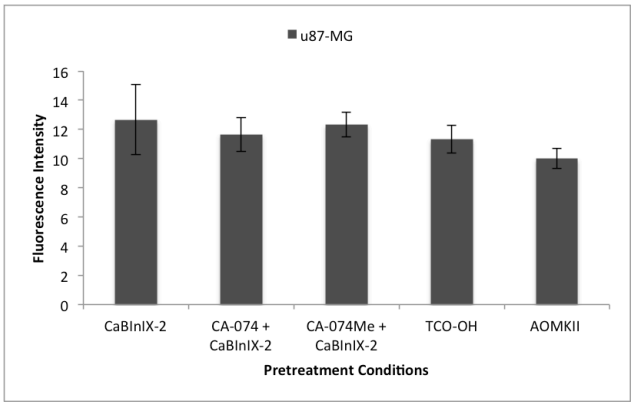

Figure 4.17 Cell assay tetrazine-5-FAM.

4.7 Radioiodinated Bioorthogonal Reactive Pairs for Cathepsin B

4.7.1 Preparation of Radioiodinated Tetrazine

The radioactive tetrazine derivative used was an iodinated dipyridyl derivative, 3-(5-iodopyridin-2-yl)-6-(pyridin-2-yl)-1,2,4,5-tetrazine (**4.10**). This derivative was developed in the Valliant and Capretta research groups and readily reacts with TCO.[46] The trimethyl tin dihydrotetrazine derivative was treated with [^{125}I]NaI in the presence of iodogen resulting in an iododestanylation and subsequent oxidation giving **4.10** (Scheme 4.7). Following HPLC purification **4.10** was obtained with a radiochemical purity >95% and the isolated radiochemical yields were 22-25% (n = 2) (

Figure 4.18).

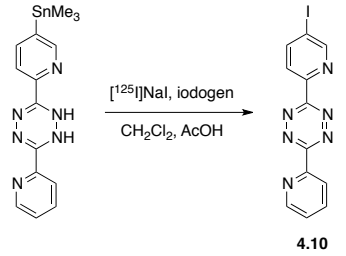

Scheme 4.7 Radioiodination of **4.10**.

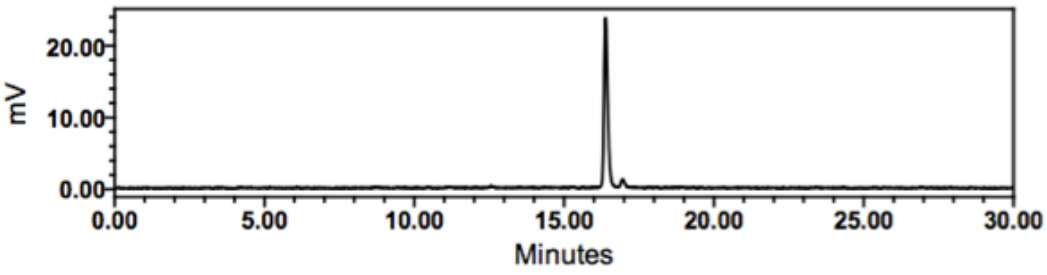

Figure 4.18 Radiochromatogram of **4.10** following purification (initial radiolabelling performed by Dr. Denis Beckford-Vera; subsequent radiolabelling performed by Patricia Edem).

4.7.2 Evaluation of Radioiodinated Tetrazine for Cathepsin Targeting

Using a similar cell assay described for the fluorescent tetrazines, **4.10** was tested for cathepsin B binding. MDA-MB231 and u87-MG cells were seeded in 6-well plates and pre-treated with CA-074Me or the vehicle. Afterwards the cells were treated with **4.5**, **2.6b**, or TCO-OH. After washing, cells were treated with **4.10**, washed, and lysed. Radioactivity

and protein content was measured and plotted as a ratio of radioactivity/protein content for each sample (Figure 4.19).

During the pre-targeted reaction with **4.10** there was a radioactive signal observed in the the MDA-MB231 samples and the u87-MG samples (Figure 4.19). When **4.5** was not present there was a reduction in the radioactive signal. Using CA-074Me as a block did not result in reduction of the radioactive signal. These trends were identical to those observed with the fluorescent tetrazines, **4.8** and tetrazine-Cy5. This result indicates that **4.10** may be able to react with intracellular **4.5** as well. Because blocking was not observed when pre-incubating with the cathepsin B inhibitors further studies were performed to assess the extent of cathepsin B binding.

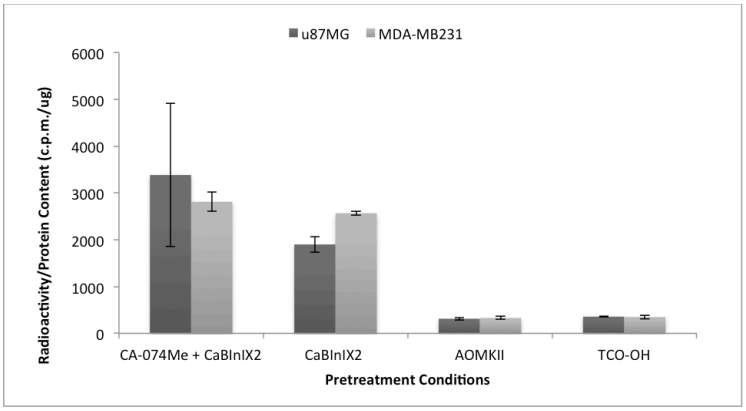

Figure 4.19 Cell assay with **4.10**.

In an experiment similar to that described above, plated cells were pre-treated with **4.5** or **2.6b** and then **4.10**. The cells were removed from the

plate using a cell dissociation buffer, then concentrated and lysed. Equal amounts of protein were separated using SDS-PAGE (Figure 4.20). The cell dissociation buffer was chosen because it can dislodge cells without stripping them. The lysis buffer was prepared with CHAPS because it is the optimal detergent for this enzyme family.[50]

Protein bands were visualized using autoradiography. Following the pre-targeted reaction with **4.5** and **4.10** protein bands between 20 – 30 kDa were observed. These likely represent cathepsin B (~27 kDa) and another protease such as cathepsin L.[3,9.13] A strong band was observed at the gel front likely representing ligation of **4.10** with residual **4.5**. It is important to note that this band was not present when the cells were treated with the unfunctionalized inhibitor **2.6b** indicating that the non-specific binding was not due to **4.10**. The activity observed at the gel front serves as an explanation for the high signals measured in the cell assays when a blocking agent was used.

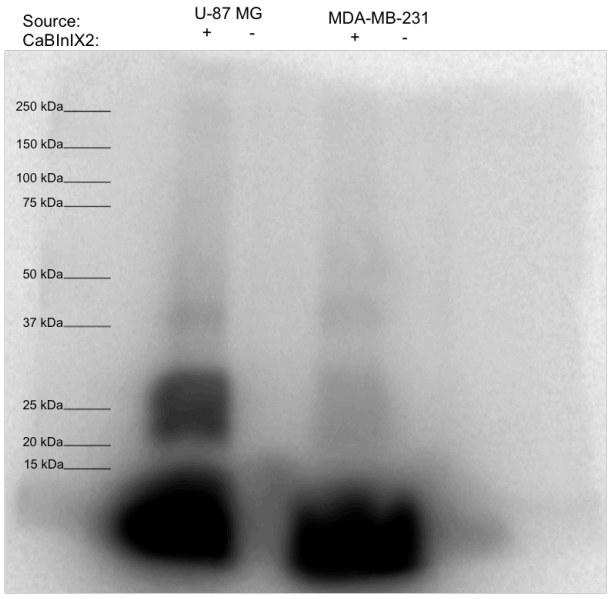

Figure 4.20 Affinity labelling with **4.10**.

To confirm labelling of cathepsin B/L and intracellular ligation an additional blocking experiment was performed. MDA-MB231 cells were pre-treated with CA-074, CA-074Me, or vehicle and then treated as described above. Again bands corresponding to cathepsin B/L were observed following the pre-targeted reaction along with a strong band at the gel front (Figure 4.21). Cathepsin B/L bands were blocked in samples pre-treated with CA-074Me yet the strong band at the gel front was still present. Cathepsin B/L bands were not blocked in samples pre-treated with CA-074.

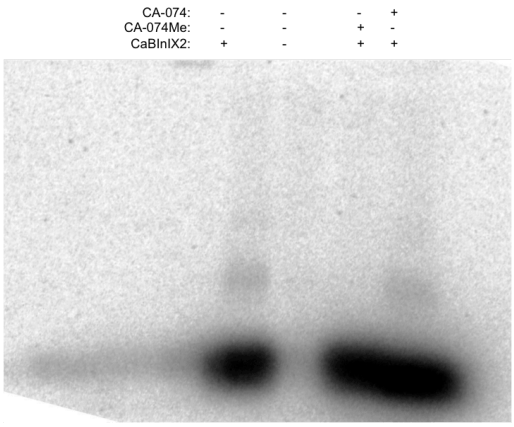

Figure 4.21 Target validation with **4.10** in MDA-MB231 cells.

CA-074, which is a cell impermeable inhibitor of cathepsin B should prevent any **4.5** from binding to extracellular cathepsin B. CA-074Me, which is a cell permeable inhibitor of cathepsin B and L should prevent any **4.5** from binding to intra/extracellular cathepsin B/L. These results indicate that the bioorthogonal reaction between **4.5** and **4.10** occurs when **4.5** is bound to intracellular cathepsin B. This is of great significance as there are no radiolabelled tetrazines reported in the literature for intracellular targets. Also this is important for cancer management as it is reported that it is an intracellular form of cathepsin B that contributes to the invasiveness of cancer.[51]

4.8 Summary and Conclusions

A disconnect was observed when comparing results for the fluorescent ABP (**2.30**) and the nuclear ABP (**2.23a**) in direct targeting; however there was agreement with the pre-targeted approach using fluorescent (**4.8** and tetrazine-Cy5) or nuclear (**4.10**) probes. This early data indicates that the pretargeting strategy is a promising route for cathepsin B imaging and that the AOMK-TCO platform can be used to create complementary optical and nuclear imaging probes.

Biochemical assays were established as a tool to measure cathepsin B activity yielding consistent results across platforms (fluorescent, radiochemical, direct targeting, pre-targeting). The first example of TCO-Tz based bioothorgonal pairs for cathepsin B targeting was described. Modifying a known AOMK inhibitor with a TCO linker led to a high affinity chemical reporter that was able to label active cathepsin B in metastatic cancer cells when paired with a tetrazine probe capable of intracellular labelling. These experiments led us to establish a radioactive tetrazine capable of labelling intracellular targets, thus achieving a goal that has not been reported in the literature. Cell permeable tetrazines are advantageous because the scope of TCO modified reporters can be expanded to those that are cell permeable or internalized.

With the probe in hand, the next steps, should include fluorescence microscopy and comparing optical imaging, and nuclear imaging in different cathepsin B expressing xenogratfs. In addition affinity purification can also be explored in order to evaluate this platform as a means for protein isolation.

4.9 Experimental

General. All chemicals, unless otherwise stated, were purchased from Sigma−Aldrich. (*E*)-2,5-Dioxopyrrolidin-1-yl 1-(cyclooct-4-en-1-yloxy)-1-oxo-5,8,11,14-tetraoxa-2-azaheptadecan-17-oate (TCO-PEG_4-NHS Ester) was obtained from Click Chemistry Tools. 5-((4-(1,2,4,5-Tetrazin-3-yl)benzyl)carbamoyl)-2-(3,6-dihydroxy-3*H*-xanthen-9-yl)benzoic acid (Tetrazine-5-FAM) and 1-(6-((4-(1,2,4,5-tetrazin-3-yl)benzyl)amino)-6-oxohexyl)-2-((1*E*,3*E*,5*Z*)-5-(1-ethyl-3,3-dimethyl-5-sulfoindolin-2-ylidene)penta-1,3-dien-1-yl)-3,3-dimethyl-3*H*-indol-1-ium-5-sulfonate (Tetrazine-Cy5) were obtained from MJS BioLynx Inc. 3-(Pyridin-3-yl)-6-(5-(trimethylstannyl)pyridin-2-yl)-1,2-dihydro-1,2,4,5-tetrazine was synthesized by Silvia Albu. Benzyl ((*S*)-1-(((*S*)-4-diazo-3-oxobutan-2-yl)amino)-3-(4-hydroxyphenyl)-1-oxopropan-2-yl)carbamate (Z-YA-DMK) was obtained from MP Biomedicals. 1,3,4,6-Tetrachloro-3α,6α-diphenyl-glycoluril (iodogen) was obtained from Thermo Scientific. L-3-trans-

(propylcarbamyl)oxirane-2-carbonyl)-L-isoleucyl-L-proline (CA-074) and L-3-*trans*-(Propylcarbamyl)oxirane-2-carbonyl)-L-isoleucyl-L-proline methyl ester (CA-074Me) were obtained from EMD Biosciences.

^{1}H, ^{13}C, and 2D NMR spectra were recorded using a Bruker AV600 spectrometer. ^{1}H NMR signals are reported in ppm measured relative to the residual proton signal of the deuterated solvent. Coupling constants (J) are reported in Hertz (Hz). ^{13}C signals are reported in ppm relative to the carbon signal from the solvent. High-resolution mass spectrometry (HRMS) was performed using a Waters/Micromass Q-Tof Ultima Global spectrometer. Analytical high performance liquid chromatography (HPLC) for non-radioactive compounds was performed using an Agilent/Varian Pro Star model 330 PDA detector, model 230 solvent delivery system. Analytical HPLC for radioactive compounds was performed using a Waters 1525 Binary (Midford, MA, USA) monitored simultaneously with 2489 UV/Visible detector and in-line radioactivity Bioscan gamma detector with NaI(Tl) scintillator. Analytical HPLC were preformed using a Phenomenex Gemini (L × ID = 100 × 4.6 mm) column (5 μm C18). Semi-preparative HPLC was performed using an Agilent/Varian Pro Star model 325 PDA detector, model 24 solvent delivery system and a Phenomenex Gemini (L × ID = 250 × 10 mm) column (5 μm C18). The elution conditions were as follows: **Method A**: Solvent A = CH_3CN (with 0.1% TFA), B = H_2O

(with 0.1% TFA): Gradient: 10% A to 100% A, 0 – 12 min; 100% A, 12 – 16 min; 100% A to 90% A, 16 – 29 min; 90% A to 10% A, 29 – 30 min. **Method B:** Solvent A = CH_3CN B = H_2O: Gradient: 50% A – 100% A, 0 – 17 min; 100% - 100% A, 17 – 18, 100% A – 50% A, 18 - 20 min, 50% A 20 – 25 min. **Method C**: Solvent A = CH_3CN B = H_2O: Gradient: 1% A, 0 – 3 min; 1% - 100% A, 3 – 10 min; 100% A, 10 – 15 min; 100 – 1% A, 15 – 20 min. **Method D**: Solvent A = CH_3CN B = H_2O: Gradient: 20% A – 100% A, 0 – 25 min; 100% - 80% A, 25 – 30 min. **Method E**: Solvent A = CH_3CN B = H_2O: Gradient: 10% - 95% A, 0 – 30 min. The flow rate was set at 1 mL/min for analytical and 4 mL/min for semi-preparative methods; UV detection was done at 254 nm or 500 nm.

[^{125}I]NaI (specific activity, 629 GBq/mg) was provided by the McMaster Nuclear Reactor. As this is a radioactive isotope, appropriate facilities, licenses, and procedures should be in place prior to use. Radioactivity measurements were made using a Wizard 1470 Automated Gamma Counter (PerkinElmer, Woodbridge ON). Autoradiography was measured using a GE Storm 840 phosphor imager.

MDA-MB-231, u87-MG, MIA PaCa-2, BxPC-3, MeWo cells were purchased from the ATCC and cultured in accordance with the supplier guidelines. Cathepsin B Activity Assay Kit was obtained from Abcam

(ab65300). Black, clear bottom 96-well plates were obtained from BD Biosciences. 6-Well plates were obtained from BD Falcon. Precast gels were from Bio-Rad, and the gel drying kit was from Promega. Fluoresence readings were performed using a Tecan infinite M1000 plate reader.

Synthetic Methods

(S)-3-((S)-2-(((Benzyloxy)carbonyl)amino)-3-phenylpropanamido)-7-(6-((tert-butoxycarbonyl)amino)hexanamido)-2-oxoheptyl 2,6-dimethylbenzoate (4.2). To a solution of Boc-6-Ahx-OH (35 mg, 150 μmol) in DMF (5 mL) at -25 °C, NMM (16.5 μL, 150 μmol) and IBCF (20 μL, 150 μmol) were added and left to stir until dissolved. To this, **2.6b** (100 mg, 150 μmol) and NMM (33 μL, 300 μmol) were added and the solution was left to stir overnight while warming to room temperature. The reaction mixture was diluted to 25 mL with water and extracted with CH_2Cl_2 (3 × 10 mL), and the combined organic layers extracted with water (5 × 10 mL), brine (3 × 10 mL), and dried over Na_2CO_3. The solvent was removed by rotary evaporation and the product was isolated as a white powder. Yield (81 mg, 68%). TLC (5% MeOH/CH_2Cl_2): R_f = 0.18. ^{1}H NMR (600 MHz; $(CD_3)_2SO$): δ 8.49 (d, J = 7.3, 1H), 7.71 (t, J = 5.5, 1H), 7.64 (d, J = 8.2, 1H), 7.35-7.19 (m, 11H), 7.12-7.09 (m, 2H), 6.75-6.73 (m, 1H), 4.98 (s, 2H), 4.94 (d, J = 17.2, 1H), 4.84 (d, J = 17.1, 1H), 4.38-4.33 (m, 2H), 3.05-

2.98 (m, 4H), 2.89-2.85 (m, 3H), 2.85-2.81 (m, 1H), 2.30 (s, 6H), 2.03 (dd, J = 9.5, 5.5, 3H), 1.82-1.79 (m, 1H), 1.60-1.56 (m, 2H), 1.49-1.42 (m, 4H), 1.41-1.39 (m, 11H), 1.34-1.29 (m, 4H), 1.29-1.23 (m, 3H), 1.23-1.17 (m, 3H). ^{13}C NMR (151 MHz; $(CD_3)_2SO$): δ 202.6, 171.8, 171.8, 137.8, 134.7, 129.6, 129.2, 128.3, 128.1, 128.0, 127.7, 127.5, 126.3, 72.6, 66.7, 65.3, 56.1, 55.9, 39.9, 38.1, 37.2, 35.4, 29.28, 29.1, 28.8, 28.3, 26.0, 25.0, 22.4, 19.3. HRMS Calcd. for $C_{44}H_{59}N_4O_9$ $[M]^+$: 787.4282. Found: 787.4277.

(5S,8S)-5-Benzyl-8-(2-((2,6-dimethylbenzoyl)oxy)acetyl)-3,6,14-trioxo-1-phenyl-2-oxa-4,7,13-triazanonadecan-19-aminium 2,2,2-trifluoroacetate (4.3) To a solution of **4.2** (52 mg, 66 μmol) in CH_2Cl_2 (20 mL), TFA (5 mL) was added dropwise at 0 °C. The solution was left to stir for 3 h warming to room temperature after which the solvent was removed by rotary evaporation. The desired product was isolated following trituration with Et_2O and lyophilization to yield a sticky film. Yield (19 mg, 42%). TLC (50% MeOH/CH_2Cl_2): R_f = 0.39. HRMS Calcd. for $C_{39}H_{51}N_4O_7$ $[M]^+$: 687.3758. Found: 687.3769.

(3*S*)-3-((*S*)-2-(((Benzyloxy)carbonyl)amino)-3-phenylpropanamido)-7-(6-((((*E*)-cyclooct-4-en-1-yloxy)carbonyl)amino)hexanamido)-2-oxoheptyl 2,6-dimethylbenzoate (4.4) Diisopropylethylamine (DIPEA) (3.3 μL, 19 μmol) was added to a solution of **4.3** (9.2 mg, 13 μmol) and

TCO-*N*-hydroxysuccinimidyl carbonate (1.5 mg, 5.6 μmol) in DMF (900 μL) and left to stir for 1 h at room temperature. Following semipreparative HPLC (Method A) purification a mixture of **4.3** and **4.4** was present. HPLC (Method A) R_t = 17.8 min. ^{1}H NMR (600 MHz; $(CD_3)_2SO$): δ 8.50 (d, J = 7.5, 1H), 7.70 (d, J = 5.7, 1H), 7.63 (d, J = 8.2, 1H), 7.34-7.25 (m, 11H), 7.21-7.19 (m, 3H), 7.11 (t, J = 3.8, 3H), 7.02 (s, 1H), 6.90 (s, 1H), 5.76 (s), 5.58-5.54 (m, 1H), 5.45-5.40 (m, 1H), 4.97-4.96 (m, 2H), 4.93 (d, J = 17.2, 1H), 4.83 (d, J = 17.2, 1H), 4.37-4.32 (m, 3H), 4.20-4.18 (m, 2H), 3.04-3.00 (m, 3H), 2.90-2.88 (m, 3H), 2.84-2.80 (m, 1H), 2.73 (s, 1H), 2.31 (s, 6H), 2.28-2.23 (m, 3H), 2.02 (t, J = 7.5, 2H), 1.90-1.81 (m, 5H), 1.58-1.52 (m, 5H), 1.46-1.42 (m, 3H), 1.40-1.36 (m, 2H), 1.36-1.31 (m, 4H), 1.26-1.24 (m, 2H), 1.19-1.16 (m, 3H). ^{13}C NMR (151 MHz; $(CD_3)_2SO$): δ 202.6, 172.0, 172.0, 168.1, 137.8, 136.9, 134.9, 134.7, 132.8, 132.5, 129.6, 129.2, 128.3, 128.1, 127.7, 127.5, 126.3, 78.8, 66.7, 65.3, 56.1, 55.9, 40.7, 40.0, 38.2, 38.1, 37.2, 35.4, 33.7, 32.1, 30.6, 29.3, 29.1, 28.8, 26.0, 25.0, 22.4, 19.3.

(23S)-23-((S)-2-(((Benzyloxy)carbonyl)amino)-3-phenylpropanamido)-1-((E)-cyclooct-4-en-1-yloxy)-1,17,24-trioxo-5,8,11,14-tetraoxa-2,18-diazapentacosan-25-yl 2,6-dimethylbenzoate (4.5). DIPEA (3.3 μL, 19 μmol) and a solution of TCO-PEG_4-NHS Ester (4.9 mg, 9.5 μmol) in dimethylformamide (DMF) (97.2 μL) were added to a vial containing **2.6b**

(13 mg, 19 μmol) in DMF. The solution was left to stir for 3 h at room temperature. The product was isolated as a golden oil following semipreparative HPLC (Method A). Yield (5.9 mg, 64%). HPLC (Method A): R_t = 16.1 min. ^{1}H NMR (600 MHz; $(CD_3)_2SO$): δ 8.50-8.48 (m, 1H), 7.79-7.77 (m, 1H), 7.63 (d, J = 8.1, 1H), 7.34-7.18 (m, 11H), 7.10 (d, J = 7.6, 2H), 6.91 (t, J = 0.9, 1H), 5.70-5.49 (m, 1H), 5.46-5.28 (m, 1H), 4.97-4.95 (m, 2H), 4.95-4.92 (m, 1H), 4.82 (d, J = 17.4, 1H), 4.36-4.32 (m, 2H), 4.27-4.07 (m, 1H), 3.57 (t, J = 6.4, 2H), 3.47-3.44 (m, 12H), 3.38-3.35 (m, 2H), 3.10-3.06 (m, 2H), 3.04-3.01 (m, 3H), 2.82 (t, J = 6.8, 1H), 2.33-2.32 (m, 6H), 2.29-2.25 (m, 3H), 1.90-1.79 (m, 4H), 1.64-1.53 (m, 5H), 1.41-1.24 (m, 5H). ^{13}C NMR (151 MHz; $(CD_3)_2SO$): δ 198.9, 171.3, 169.8, 168.1, 134.7, 132.5, 129.61, 129.58, 129.2, 128.27, 128.09, 127.76, 127.70, 127.55, 127.52, 126.3, 69.76, 69.74, 69.69, 69.65, 69.49, 69.1, 66.9, 66.7, 65.3, 56.04, 55.90, 38.2, 36.2, 29.1, 22.3, 19.3.

10-(3-Cyanophenyl)-5,5-difluoro-1,3,7,9-tetramethyl-5*H*-dipyrrolo[1,2-*c*:2',1'-*f*][1,3,2]diazaborinin-4-ium-5-uide (4.6) 3-Formylbenzonitrile (1.0 g, 7.6 mmol) was dissolved in anhydrous CH_2Cl_2 (100 mL) then 2,4-dimethylpyrrole (1.7 mL, 16.5 mmol), anhydrous CH_2Cl_2 (100 mL), and TFA (~ 4 drops) were added and the solution was left to stir for 30 min. A solution of 2,3-dichloro-5,6-dicyano-p-benzoquinone (1.7 g, 7.5 mmol) in

anhydrous CH_2Cl_2 (200 mL) was added, followed by the addition of DIPEA (15 mL, 86.1 mmol) and boron trifluoride diethyl etherate (8.9 mL, 72 mmol). The solution was left to stir overnight under a stream of argon. Afterwards water (100 mL) was added and the solution was extracted with CH_2Cl_2 (3 × 100 mL). The solvent was removed under reduced pressure. The desired product was isolated following flash chromatography (8%-66% EtOAc/Hexanes) and lyophilisation as a dark orange solid. Yield (520 mg, 20%). ^{1}H NMR (600 MHz; $(CD_3)_2SO$): δ 8.05 (td, J = 4.5, 1.8, 1H), 8.02 (d, J = 1.0, 1H), 7.79 (dd, J = 3.8, 1.3, 2H), 6.22 (s, 2H), 2.47 (s, 6H), 1.33 (s, 6H). ^{13}C NMR (151 MHz; $(CD_3)_2SO$): δ 155.9, 143.0, 139.5, 135.6, 133.64, 133.54, 132.2, 131.02, 130.89, 122.1, 118.6, 112.9, 14.7. HRMS Calcd. for $C_{20}H_{19}N_3F_2$ $[M+H]^+$: 350.1640. Found: 350.1657.

5,5-Difluoro-1,3,7,9-tetramethyl-10-(3-(6-methyl-1,2,4,5-tetrazin-3-yl)phenyl)-5*H*-dipyrrolo[1,2-*c*:2',1'-*f*][1,3,2]diazaborinin-4-ium-5-uide

(4.8) Colloidal sulphur (22.4 mg, 560 μmol) and **4.6** (97.8 mg, 280 μmol) were combined with anhydrous CH_3CN (146 μL) in a 5 mL microwave vial. A solution of hydrazine monohydrate (679 μL, 14.0 mmol) in absolute EtOH (2 mL) was added and left to stir 4 h at 85 °C. The solution was diluted with water (8 mL) and extracted with CH_2Cl_2 (3 × 10 mL). The solvent was removed under reduced pressure. The resultant residue was

dissolved in absolute EtOH (2 mL) and a solution of $NaNO_2$ (386 mg, 5.60 mmol) in water (5 mL) was added. The solution was adjusted to pH ~3 using 1N HCl and extracted with CH_2Cl_2 (3 × 10 mL). The combined organic extracts were extracted with brine (30 mL) and dried over $MgSO_4$. The solvent was removed under reduced pressure and the desired product was obtained as a red solid following semi-preparative HPLC. Yield (2.5 mg, 4%). HPLC (Method B) R_t = 17.8 min. ^{1}H NMR (600 MHz; $(CD_3)_2SO$): δ 8.63 (d, J = 8.1, 1H), 8.37 (s, 1H), 7.88 (t, J = 7.8, 1H), 7.75 (d, J = 7.6, 1H), 6.22 (s, 2H), 3.01 (s, 3H), 2.47 (s, 7H), 1.41 (s, 6H). ^{13}C NMR (151 MHz; $(CD_3)_2SO$): δ 167.2, 162.8, 155.4, 142.44, 142.41, 133.08, 132.98, 131.70, 131.66, 130.5, 128.0, 126.6, 121.5, 20.7, 14.1. HRMS Calcd. for $C_{22}H_{22}N_6OBF_2$ $[M+H]^+$: 419.1967. Found: 419.1974.

5-((4-(1,2,4,5-Tetrazin-3-yl)benzyl)carbamoyl)-2-(2,7-difluoro-3,6-dihydroxy-3*H*-xanthen-9-yl)benzoic acid (4.9) Oregon Green 488-X (1.3 mg, 2.5 μmol) was added to a 2 mL microwave vial containing benzylamino tetrazine hydrochloride (1.9 mg, 10 μmol) and anhydrous DMF (500 μL). Et_3N (1.4 μL) was added and the solution was shaken in the dark overnight. Afterwards water (1 mL) was added and the product was isolated as an orange film following semi-preparative HPLC (Method C) R^t = 14.0.

Radiolabelling Methods

^{125}I-Benzyl ((*S*)-1-(((*S*)-4-diazo-3-oxobutan-2-yl)amino)-3-(4-hydroxy-3-iodophenyl)-1-oxopropan-2-yl)carbamate (4.1) To an Eppendorf tube containing iodogen (20.0 μg, 0.046 μmol) and 10× phosphate buffered saline (PBS) (10 μL), [^{125}I]NaI (12.0 MBq) in 0.1% NaOH (10 μL), Z-YA-DMK (10 μg, 0.024 μmol) in EtOH (10 μL), and 10× PBS (15 μL) were added at 0 °C. After 15 min the reaction was quenched with 10× PBS (455 μL). The desired product was obtained following purification by analytical HPLC (Method A). RCY = 25 - 40% (n =3).

^{125}I-3-(5-Iodopyridin-2-yl)-6-(pyridin-2-yl)-1,2,4,5-tetrazine (4.10) To a tube containing 3-(pyridin-2-yl)-6-(5-(trimethylstannyl)pyridin-2-yl)-1,2-dihydro-1,2,4,5-tetrazine (500 μg, 1.24 μmol) iodogen (25 μg, 0.057 μmol) in 5% AcOH/CH_2CN (5 μL) and [^{125}I]NaI (14.9 MBq) in 0.1% NaOH (10 μL). After 5 min additional iodogen (140 μg, 0.32 μmol) in 5% AcOH/CH_2CN (28 μL) was added. After 15 min the reaction was quenched with 0.1M $Na_2S_2O_5$ (100 μL). CH_2Cl_2 (100 μL) was added and the solution was left to stand for 5 min. The organic layer was collected and the solvent removed under a stream of air. The residue was dissolved in CH_3CN (100 μL) and purified using analytical HPLC (Method D). RCY = 22-25% (n = 2).

Biological Assays

Determination of Inhibition Constants. The inhibition constant (K_i) and second order rate (k_i/K_i) constant for **4.5** were determined following the method previously described.[41]

Determination of Cathepsin B Activity in Cell and Tumor Lysates. (Performed by Nancy Janzen) Cell Assay was preformed using the Abcam Cathepsin B Activity Assay Kit (Fluorometric) and following the manufactures instructions. MDA-MB-231, u87-MG, MIA PaCa-2, BxPC-3, MeWo cells lysates and tumor xenograft homogenates were prepared using the CB lysis buffer. Lysates (50 μL) were transferred to a 96-well plate and the CB reaction buffer (50 μL) was added. The substrate, Ac-RR-AFC (2 μL, 10 mM), was added to give a final concentration of 200 μM. As a negative control lysates were pre-treated with the CB inhibitor. After incubation for 1 – 2 h at 37 °C fluorescence was measured (excitation $\lambda =$ 400 nm, emission $\lambda =$ 505 nm).

Active Protease Labelling in Whole Cells Using Fluorescent ABPs. MDA-MB231 and MeWo cells (6×10^4 cells/well) were seeded in a 96 well plate 1 d before the experiment. Cells were pretreated with CA-074 (100 μL, 260 μM) or 1% DMSO using DPBS with 10% FBS as the reaction buffer for 1 h at 37 °C. The cy5 labelled AOMK, **2.30** (50 μL, 20 μM) was added alongside CA-074 (50 μL, 520 μM) or 1% DMSO (50 μL) and

incubated for 3 h at 37 °C. The reaction buffer was removed and fresh buffer (100 μL) was added and fluorescence was measured (excitation $\lambda =$ 649 nm, emission $\lambda =$ 670 nm).

Turn on Ratios. Solutions of **4.8** in 1× PBS (50 μL) were added to a 96-well plate resulting in a final concentration of 400 nM. Solutions of **4.5** in 1× PBS (50 μL) were added to each well giving final concentrations of 0 nM, 1 μM, or 10 μM and the fluorescent emission spectra was measured (excitation $\lambda =$ 492 nm). The turn-on ratio was determined and reported as a ratio of the fluorescence intensity at 524 nm.

Labelling with Fluorescent Bioorthogonal ABPs in Whole Cells. MDA-MB231 and u87-MG cells (6×10^4 cells/well) were seeded in a 96 well plate 1 d before the experiment. Media was removed and cells were extracted with 1× PBS (3 × 100 μL). Cells were pretreated with CA-074 (100 μL, 260 μM) or PBS (100 μL) for 1 h at 37 °C. Inhibitors **4.5**, **2.6b** (100 μL, 20 μM) or *(E)*-cyclooct-4-enol (100 μL, 20 μM), or 1× PBS (100 μL) was added and incubated for 3 h at 37 °C. Cells were washed with 1× PBS (3 × 100 μL) and **4.8** (200 μL, 1 μM) or 1× PBS (100 μL) was added and fluorescence measured ($\lambda_{ex} =$ 500 nm, $\lambda_{em} =$ 512 nm). A similar method was applied for **4.9** using CA-074 (100 μL, 2.6 μM), Z-YA-DMK (100 μL, 26 μM) or 0.1% DMSO in PBS (100 μL) to pretreat cells. Inhbitors **4.5**,

2.6b (10 μL, 10 μM) or *(E)*-cyclooct-4-enol (10 μL, 10 μM), or 1× PBS (100 μL) were used to treat the cells. Fluorescence was measured (λ_{ex} = 492 nm, λ_{em} = 524 nm).

A similar method was applied for Tetrazine-5-FAM using CA-074 (100 μL, 65 μM) or 0.25% DMSO in growth media (100 μL) to pre-treat cells. Inhibitors **4.5**, **2.6b** (10 μL, 10 μM) or *(E)*-cyclooct-4-enol (10 μL, 10 μM), or 0.05% DMSO in growth media (100 μL) were used to treat the cells. Fluorescence was measured (λ_{ex} = 492 nm, λ_{em} = 517 nm).

Active Protease Labelling in Tumour Cell Lysates Using Radioactive ABPs. (Performed by Nancy Janzen) MDA-MB-231, u87-MG tumor xenograft homogenates, and human liver cathepsin B were prepared in the CB lysis buffer from abcam. Cells were pretreated with CA-074 (1 μL, 2.6 mM) or CB lysis buffer:CB loading buffer (1:1) (1 μL) for 1 h at 37 °C, then labelled with **4.1** or [^{125}I]**2.23** (1 × 10^6 c.p.m) for 2 h at 37 °C. The loading dye (9% SDS, 60% glycerol, 375 mM Tris 0.015% Bromophenol blue, 12% 2-mercaptoethanol) was added left to incubate for 30 min at room temperature. Samples were spun down by centrifugation and protein content was measured using a BCA assay. Equal amounts of protein were loaded to each lane of a 10% Mini-Protean TGX precast gel and analyzed

by SDS−PAGE. Gels were incubated overnight in gel-shrinking solution (65% methanol, 0.5% glycerol) while shaking at 4 °C. Gels were dried at room temperature using a commercial gel-drying kit and then exposed to a phosphor imaging screen which was subsequently scanned by a phosphorimager.

Biodistribution Study. (Performed by Nancy Janzen and CPDC Biologists) U87-MG cells were purchased from the American Type Culture Collection (ATCC) and cultured in accordance with supplier guidelines. Animal studies were approved by the Animal Research Ethics Board at McMaster University in accordance with Canadian Council on Animal Care (CCAC) guidelines. Female CD1 nu/nu mice (3−5 weeks old) were obtained from Charles River Laboratories (Senneville, QC) and were maintained under specific-pathogen-free (SPF) conditions with 12 h light/dark cycles and given food and water ad libitum. To create the tumor xenograft model, CD1 nu/nu female mice were injected with 2×10^6 u87-MG cells in 100 μL of PBS/Matrigel (1:1; BD Biosciences, Mississauga, ON, and Invitrogen, Burlington, ON, respectively) subcutaneously into the right flank. Tumours were allowed to grow for approximately 2 weeks prior to biodistribution studies. CD1 nu/nu mice (n = 15) were administered approximately 130 kBq of [^{125}I]**2.23a** (3.7 GBq/mL) in 10% EtOH in sterile PBS via tail vein injection. After 30 min, 5 h, and 23 h, groups of mice (n =

5) were anesthetized with 3% isoflurane and euthanized via exsanguination, and the indicated organs and tissues were collected by dissection and weighed. Activities were measured on a γ counter and reported as %ID/g of each organ, tissue, or fluid.

Analysis of Radioactive Bioorthogonal ABPs in Whole Cells. MDA-MB231 and u87-MG cells (4×10^5 cells/well) were seeded in a 6 well plate 1 d before the experiment. Media was removed and cells were washed with 1× PBS (3 × 1 mL). Cells were pre-treated with CA-074Me (1 mL, 65 μM) or 0.25% DMSO in growth media (1 mL) for 1 h at 37 °C. Inhibitors **4.4**, **2.6b** (100 μL, 10 μM) or *(E)*-cyclooct-4-enol (100 μL, 10 μM), was added and incubated for 3 h at 37 °C. Cells were washed with 1× PBS (3 × 1 mL) and **4.9** (1 mL, 74 KBq) was added and cells were incubated for 15 min at 37 °C. Cells were washed with 1× PBS (3 × 1 mL) and lysed with the addition of lysis buffer (50 mM sodium citrate, 50 mM sodium phosphate, 1% CHAPS, 0.5% Triton X-100) (500 μL) and incubated for 30 min at 37 °C. Protein content and radioactivity counts were measured for each sample.

Active Protease Labelling in Whole Cells Using Radioactive Bioorthogonal ABPs. MDA-MB231 and u87-MG cells (6×10^5 cells/well) were seeded in a 6 well plate 1 d before the experiment. Media was

removed and cells were washed with 1× PBS (3 × 1 mL). Cells were pretreated with CA-074, CA-074Me (1 mL, 65 μM) or 0.25% DMSO in growth media (1 mL) for 1 h at 37 °C. Inhibitors **4.4** or **2.6b** (100 μL, 10 μM) was added and incubated for 3 h at 37 °C. Cells were washed with 1× PBS (3 × 1 mL) and **4.10** (1 mL, 407 kBq) was added and cells were incubated for 15 min at 37 °C. Cells were washed with 1× PBS (3 × 1 mL) and cell dissociation buffer was added (500 μL). Cells were spun down and lysed with the addition of lysis buffer (50 mM sodium citrate, 50 mM sodium phosphate, 1% CHAPS, 0.5% Triton X-100) (50 μL) and incubated for 30 min at 37 °C. Protein content and radioactivity counts were measured for each sample. Equal amounts of protein were loaded to each lane of a 10% Mini-Protean TGX precast gel and analyzed by SDS−PAGE. Gels were incubated overnight in gel-shrinking solution (65% methanol, 0.5% glycerol) while shaking at 4 °C. Gels were dried at room temperature by use of a commercial gel-drying kit and then exposed to a phosphor imaging screen which was then scanned by a phosphorimager.

4.10 References

1. S. Lütje, M. Rijpkema, W. Helfrich, W. J. G. Oyen, and O. C. Boerman, *Mol. Imaging Biol.*, 2014, **16**, 747–755.

2. A. M. Sadaghiani, S. H. Verhelst, and M. Bogyo, *Curr. Opin. Chem. Biol.*, 2007, **11**, 20–28.

3. G. Ren, G. Blum, M. Verdoes, H. Liu, S. Syed, L. E. Edgington, O. Gheysens, Z. Miao, H. Jiang, S. S. Gambhir, M. Bogyo, and Z. Cheng, *PLoS One*, 2011, **6**, e28029.

4. J. L. Cutter, N. T. Cohen, J. Wang, A. E. Sloan, A. R. Cohen, A. Panneerselvam, M. Schluchter, G. Blum, M. Bogyo, and J. P. Basilion, *PLoS One*, 2012, **7**, e33060.

5. M. G. Paulick and M. Bogyo, *ACS Chem. Biol.*, 2011, **6**, 563–572.

6. D. Kato, K. M. Boatright, A. B. Berger, T. Nazif, G. Blum, C. Ryan, K. A. H. Chehade, G. S. Salvesen, and M. Bogyo, *Nat. Chem. Biol.*, 2005, **1**, 33–38.

7. K. B. Sexton, M. D. Witte, G. Blum, and M. Bogyo, *Bioorg. Med. Chem. Lett.*, 2007, **17**, 649–653.

8. M. Verdoes, L. E. Edgington, F. a Scheeren, M. Leyva, G. Blum, K. Weiskopf, M. H. Bachmann, J. A. Ellman, and M. Bogyo, *Chem. Biol.*, 2012, **19**, 619–628.

9. K. Oresic Bender, L. Ofori, W. a. van der Linden, E. D. Mock, G. K. Datta, S. Chowdhury, H. Li, E. Segal, M. Sanchez Lopez, J. a. Ellman, C. G. Figdor, M. Bogyo, and M. Verdoes, *J. Am. Chem. Soc.*, 2015, **137**, 4771–4777.

10. M. Verdoes, K. Oresic Bender, E. Segal, W. A. van der Linden, S. Syed, N. P. Withana, L. E. Sanman, and M. Bogyo, *J. Am. Chem. Soc.*, 2013, **135**, 14726–14730.

11. L. E. Edgington, M. Verdoes, A. Ortega, N. P. Withana, J. Lee, S. Syed, M. H. Bachmann, G. Blum, and M. Bogyo, *J. Am. Chem. Soc.*, 2013, **135**, 174–182.

12. G. Blum, G. von Degenfeld, M. J. Merchant, H. M. Blau, and M. Bogyo, *Nat. Chem. Biol.*, 2007, **3**, 668–677.

13. G. Blum, S. R. Mullins, K. Keren, M. Fonovic, C. Jedeszko, M. J. Rice, B. F. Sloane, and M. Bogyo, *Nat. Chem. Biol.*, 2005, **1**, 203–209.

14. E. M. Sletten and C. R. Bertozzi, *Angew. Chem. Int. Ed.*, 2009, **48**, 6974–6998.

15. T. Reiner and B. M. Zeglis, *J. Label. Compd. Radiopharm.*, 2014, **57**, 285–290.

16. M. R. Pratt, M. D. Sekedat, K. P. Chiang, and T. W. Muir, *Chem. Biol.*, 2009, **16**, 1001–1012.

17. H. C. Hang, J. Loureiro, E. Spooner, A. W. M. van der Velden, Y. Kim, A. M. Pollington, R. Maehr, M. N. Starnbach, and H. L. Ploegh, *ACS Chem. Biol.*, 2006, **1**, 713–723.

18. M. L. Blackman, M. Royzen, and J. M. Fox, *J. Am. Chem. Soc.*, 2008, **130**, 13518–13519.

19. D. L. Boger, *Chem. Rev.*, 1986, **86**, 781–794.

20. K. Lang, L. Davis, S. Wallace, M. Mahesh, D. J. Cox, M. L. Blackman, J. M. Fox, and J. W. Chin, *J. Am. Chem. Soc.*, 2012, **134**, 10317–10320.

21. A. Borrmann, S. Milles, T. Plass, J. Dommerholt, J. M. M. Verkade, M. Wießler, C. Schultz, J. C. M. van Hest, F. L. van Delft, and E. A. Lemke, *ChemBioChem*, 2012, **13**, 2094–2099.

22. K. Lang, L. Davis, J. Torres-Kolbus, C. Chou, A. Deiters, and J. W. Chin, *Nat. Chem.*, 2012, **4**, 298–304.

23. N. K. Devaraj, R. Weissleder, and S. A. Hilderbrand, *Bioconjug. Chem.*, 2008, **19**, 2297–2299.

24. D. N. Kamber, L. A. Nazarova, Y. Liang, S. A. Lopez, D. M. Patterson, H.-W. Shih, K. N. Houk, and J. A. Prescher, *J. Am. Chem. Soc.*, 2013, **135**, 13680–13683.

25. J. Yang, J. Šečkutė, C. M. Cole, and N. K. Devaraj, *Angew. Chem. Int. Ed.*, 2012, **51**, 7476–7479.

26. R. Rossin, P. R. Verkerk, S. M. van den Bosch, R. C. M. Vulders, I. Verel, J. Lub, and M. S. Robillard, *Angew. Chem. Int. Ed.*, 2010, **49**, 3375–3378.

27. J. C. T. Carlson, L. G. Meimetis, S. A. Hilderbrand, and R. Weissleder, *Angew. Chem. Int. Ed.*, 2013, **52**, 6917–20.

28. R. Rossin, P. R. Verkerk, S. M. van den Bosch, R. C. M. Vulders, I. Verel, J. Lub, and M. S. Robillard, *Angew. Chem. Int. Ed.*, 2010, **49**, 3375–8.

29. B. M. Zeglis, K. K. Sevak, T. Reiner, P. Mohindra, S. D. Carlin, P. Zanzonico, R. Weissleder, and J. S. Lewis, *J. Nucl. Med.*, 2013, **54**, 1389–1396.

30. B. Nichols, Z. Qin, J. Yang, D. R. Vera, and N. K. Devaraj, *Chem. Commun.*, 2014, **50**, 5215–5217.

31. N. K. Devaraj, G. M. Thurber, E. J. Keliher, B. Marinelli, and R. Weissleder, *P. Natl. Acad. Sci. USA*, 2012, **109**, 4762–4767.

32. R. Rossin, T. Lappchen, S. M. van den Bosch, R. Laforest, and M. S. Robillard, *J. Nucl. Med.*, 2013, **54**, 1989–1995.

33. R. Rossin and M. S. Robillard, *Curr. Opin. Chem. Biol.*, 2014, **21**, 161–169.

34. N. K. Devaraj, S. A. Hilderbrand, R. Upadhyay, R. Mazitschek, and R. Weissleder, *Angew. Chem. Int. Ed.*, 2010, **49**, 2869–2872.

35. A. W. Choi, K. K. Tso, V. M. Yim, H. Liu, and K. K. Lo, *Chem. Commun.*, 2015, **51**, 3442–3445.

36. H. Wu, J. Yang, J. Šečkutė, and N. K. Devaraj, *Angew. Chem. Int. Ed.*, 2014, **53**, 5805–5809.

37. L. G. Meimetis, J. C. T. Carlson, R. J. Giedt, R. H. Kohler, and R. Weissleder, *Angew. Chem. Int. Ed.*, 2014, **53**, 7531–7534.

38. A. M. Szpaderska and A. Frankfater, *Cancer Res.*, 2001, **61**, 3493–3500.

39. C. Crawford, R. W. Mason, P. Wikstrom, and E. Shaw, *Biochem. J.*, 1988, **253**, 751–758.

40. R. W. Mason, L. T. Bartholomew, and B. S. Hardwick, *Biochem. J.*, 1989, **263**, 945–949.

41. P. E. Edem, S. Czorny, and J. F. Valliant, *J. Med. Chem.*, 2014, **57**, 9564–9577.

42. H.-H. Otto and T. Schirmeister, *Chem. Rev.*, 1997, **97**, 133–172.

43. J. C. T. Carlson, L. G. Meimetis, S. A. Hilderbrand, and R. Weissleder, *Angew. Chem. Int. Ed.*, 2013, **52**, 6917–6920.

44. J. Yang, M. R. Karver, W. Li, S. Sahu, and N. K. Devaraj, *Angew. Chem. Int. Ed.*, 2012, **51**, 5222–5225.

45. M. O. Abdel, M. A. Kira, and M. N. Tolba, *Tetrahedron Lett.*, 1968, 3871–3872.

46. S. A. Albu, McMaster, 2014.

47. A. Darko, S. Wallace, O. Dmitrenko, M. M. Machovina, R. A. Mehl, J. W. Chin, and J. M. Fox, *Chem. Sci.*, 2014, **5**, 3770–3776.

48. N. K. Devaraj, S. A. Hilderbrand, R. Upadhyay, R. Mazitschek, and R. Weissleder, *Angew. Chem. Int. Ed.*, 2010, **49**, 2869–2872.

49. I. Nikić, J. H. Kang, G. E. Girona, I. V. Aramburu, and E. a Lemke, *Nat. Protoc.*, 2015, **10**, 780–791.

50. J. C. Krupa and J. S. Mort, *Anal. Biochem.*, 2000, **283**, 99–103.

51. A. M. Szpaderska and A. Frankfater, *Cancer Res.*, 2001, 3493–3500.

5 Synthesis of Radiolabelled Substrate Based Probes (SBPs)

5.1 Introduction

As stated previously, protease targeted imaging probes can be separated into two general classes: SBPs and ABPs.[1] The AOMK based probes discussed thus far are considered ABPs because they form covalent bonds with the active site of the protease. Because of this modification it is possible to measure, locate, and directly identify the protease targets involved.[1] One of the drawbacks of this approach is that the probe and enzyme interact via a one-to-one reaction, which prevents the opportunity for signal amplification.[1] Signal amplification is beneficial for a nuclear probe because it can lead to improved T:NT ratios, thereby improving image quality and maximizing radiation dose for radiotherapy. This is especially important in instances when target expression is low.

SBPs for proteases behave as substrates and when they are cleaved they emit a unique signal. An advantage of SBPs over ABPs is that they can allow for enzyme mediated signal enhancement.[1,2] Because one protease active site can hydrolyse more than one substrate molecule it can, for example, promote an increase in fluorescent signal over time.[2]

There are 3 general types of fluorogenic SPBs, the most common being a probe that contains a peptide sequence linked to chemically

modified fluorophore (Figure 5.1A).[1,3] The second class involves incorporating a fluorophore and a quencher on opposite sides of the scissile bond (Figure 5.1B)[4], while the third involves attaching multiple fluorophores to the substrate resulting in self-quenching due to the close proximity of the fluorophores (Figure 5.1C).[1,5] There are examples of these probes in the form of small molecules and nanoparticles.[2] In all three cases upon enzyme hydrolysis there is a measureable change in the fluorescence signal. Various examples of cathepsin B targeted SBPs have been used for cell and tumour imaging and a number of them have been translated for commercial use.[3,5–8]

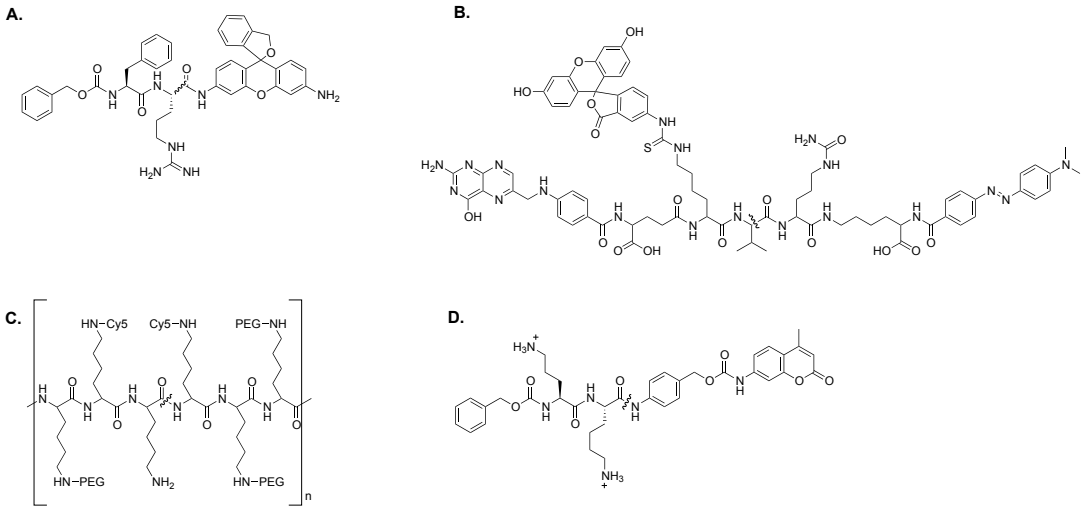

Figure 5.1 Cathepsin B targeted SBPs. (a) Z-Phe-Arg-HMRG, (b) FFCD (c) Graft co-polymer segment, and (d) Z-Lys-Lys-PABA-AMC.

An alternate strategy that is emerging involves using a self-immolative spacer where the fluorophore is released and “turned-on” upon enzymatic cleavage. This can be achieved by incorporating a para-aminobenzyloxycarbonyl (PABA) linker between the substrate and fluorescent portion of the molecule (Figure 5.1D).[2,3] In this case the enzyme hydrolysis initiates the self-destruction of the linker therefore releasing a highly fluorescent reporter molecule. Incorporation of this linker is believed to lead to increased serum stability and affinity toward cathepsin B when compared to probes lacking the linker.[2]

This approach was inspired by a class of cathepsin B targeted prodrugs where cytotoxic drugs such a doxorubicin and paclitaxel were conjugated to a substrate through the PABA linker.[4–8] Upon enzymatic cleavage the drugs are released at specific tumour sites for cancer treatment. These agents reduce the toxicity and side-effects associated with these anticancer drugs by only inducing cytotoxic effects in the cancer tissues.[6]

One of the disadvantages of SBPs when compared to ABPs is that they can be cleaved by a number of proteases.[1] Although a substrate may show higher affinity towards one protease or class it may be possible that other enzymes promote hydrolysis as well. Therefore it can be difficult to clearly identify the specific molecular targets for the SBP. Recently dual

targeting prodrugs have been developed where the SBP is designed to target cathepsin B as well as a secondary target that is also expressed at the site of the disease.[4,16] An example is the system involving a somatostatin targeting portion, a cathepsin B substrate, and either a fluorophore or an anticancer drug connected through the PABA linker. The construct allowed for selective imaging of cancer cells expressing both targets, while the anticancer drug led to specific cancer cell death.[16]

In comparison to fluorogenic probes, radioactive analogues are still preferred for clinical translation due to their high sensitivity, and signal penetration depth. However, in cases where a radiopharmaceutical has low affinity for the target or the target is not highly overexpressed, high T:NT ratios can be difficult to achieve without signal amplification. An opportunity for a signal amplification like approach in NMI can come from cellular internalization. This occurs when the radiopharmaceutical targets cell surface receptors which upon binding becomes internalized, or when the probe mimics a biomolecule that follows a specific metabolic pathway and gets trapped within the cell following active uptake.[17] Unfortunately a number of radiopharmaceuticals are not internalized when bound to their targets and probes that follow metabolic pathways can often be taken up by non-targeted cells. A SBP for cathepsin B linked to a known

radiopharmaceutical may achieve signal enhancement using the overexpression of the enzyme in tumor cells and the specificity of a known tracer.

Probe release has been applied to some radiopharmaceuticals. For example a 2,4-dinitrophenyl moiety was linked to [^{18}F]FDG such that the radiopharmaceutical was released following enzymatic hydrolysis. The resultant [^{18}F]FDG molecule was then able to react with the enzyme active site. This provided a method to label the β-glucocerebrosidase (GCase) enzyme which is found in Gaucher disease.[18] Another example of a radiopharmaceutal releasing probe was developed using 3`-deoxy-3`-[18F]- fluorothymidine ([^{18}F]FLT), which is a marker of tumor proliferation. [^{18}F]FLT uptake was directed by linking it to a peroxide triggering moiety that releases the agent in the presence of reactive oxygen species (ROS). The resultant dual targeting PET tracer only accumulates in cells that produce ROS, therefore improving the selectivity of [^{18}F]FLT.[19]

A similar radiopharmaceutical based dual targeting system can potentially be applied to cathepsin B with two potential outcomes. Firstly, cathepsin B positive tumours can be imaged with increased signal enhancement enabled by releasing an internalized probe. Secondly, cathepsin B can be used in combination with a primary target as a

secondary target to direct the uptake of known probe soley to the diseased tissue, therefore reducing non-target uptake.

One of the most common metabolic pathways that have been explored by radiotracers is the glucose transporter (GLUT) using [^{18}F]FDG, which resembles glucose and follows a similar metabolic pathway. Replacement of the hydroxyl group with a fluorine atom prevents complete metabolism, leading to intracellular trapping.[20] This mechanism has helped [^{18}F]FDG become one of the most successful PET agents for *in vivo* imaging of a variety cancers due to the increased glucose metabolism observed in nearly all tumours.[21] One of the limitations of [^{18}F]FDG is that it is not specific to tumour tissue; it will accumulate in other areas that exhibit increased glucose metabolism. This includes areas of inflammation, infection and hyperplasia, and in the brain.[22] The lack of specificity of [^{18}F]FDG can lead to increased background signal when other high glucose utilizing cells are present.

Another interesting class of probes that have the potential to be used to create new SBPs are the iodobenzamides used for imaging and treatment of malignant melanoma. Early detection of malignant melanoma is crucial for patient survival due to the propensity of the cancer cells to disseminate rapidly.[23] [^{18}F]FDG is effective in detecting late stage

melanoma however it is ineffective in discriminating melanoma metastases from other tumours.[24] Although there are treatment options for metastatic melanoma that impact median survival rates patients nearly always relapse.[25–27] An alternative that has been explored is to use radioiodinated benzamides, which as mentioned have been shown to image melanoma,[23,28–30] and be used as the basis for treatment via radiotherapy. Unfortunately as these probes bind melanin expressing tissues there are potential side effects associated with targeted radiotherapy.[24,30] These could be potentially mitigated using a cathepsin B activation strategy which should increase the concentration of the free tracer in the region where there are active tumor cells.

5.2 Objectives

The objective was to apply a prodrug strategy as a means to create a new class of nuclear SBPs targeting cathepsin B. This could be applied to improve the tumour selectivity exhibited by FDG and melanin binding iodobenzamides by using a dual targeting system. First an activated cathepsin B substrate was chosen and synthesized such that it can readily react with a free hydroxyl or amino group of a known radiopharmaceutical. Radiochemical methods were explored to conjugate [^{18}F]FDG to the activated substrate. For the second approach an iodinated melanoma

targeted probe was synthesized and radiochemical methods were explored to conjugate the probe with the activated substrate.

5.3 Synthesis of Activated Cathepsin B Substrate

The substrate of choice was based on the Z-Phe-Lys peptide, similar to what was described for the AOMKs. This derivative was chosen because it exhibited the fastest cathepsin B mediated release of doxorubicin when compared to other peptide motifs ($t_{½}$ = 8 min).[15] In addition to this construct, similar Phe-Lys based substrates have been successful in releasing other fluorophores and anticancer drugs when targeting cathepsin B.[11,13,16] The synthetic approach involved using the 4-methyltrityl (Mtt) protected lysine due to the mild conditions used for its deprotection (Scheme 5.1). This group can be removed under mildly acidic conditions without hydrolysing carbonate or carbamates conjugated through the PABA linker.

The synthetic strategy was similar to what was reported previously.[15] The commercially available, Fmoc-Lys(Mtt)-OH amino acid was treated with piperidine to remove the fluorenylmethyloxycarbonyl (Fmoc) group giving **5.1** in 72% yield (Scheme 5.1). Using a similar method employed in Chapter 2 the activated Z-Phe-Bt (**2.1**) was added to a solution of **5.1** giving the dipeptide **5.2** in 91% yield. The PABA linker was installed by

coupling 4-aminobenzyl alcohol with **5.2** using EEDQ to give **5.3** in 65% yield. The substrate was then activated using bis(4-nitrophenyl) carbonate giving the precursor for conjugation **5.4** in 64% yield. Compounds were characterized by ^{1}H and ^{13}C NMR, HRMS, and HPLC where indicated.

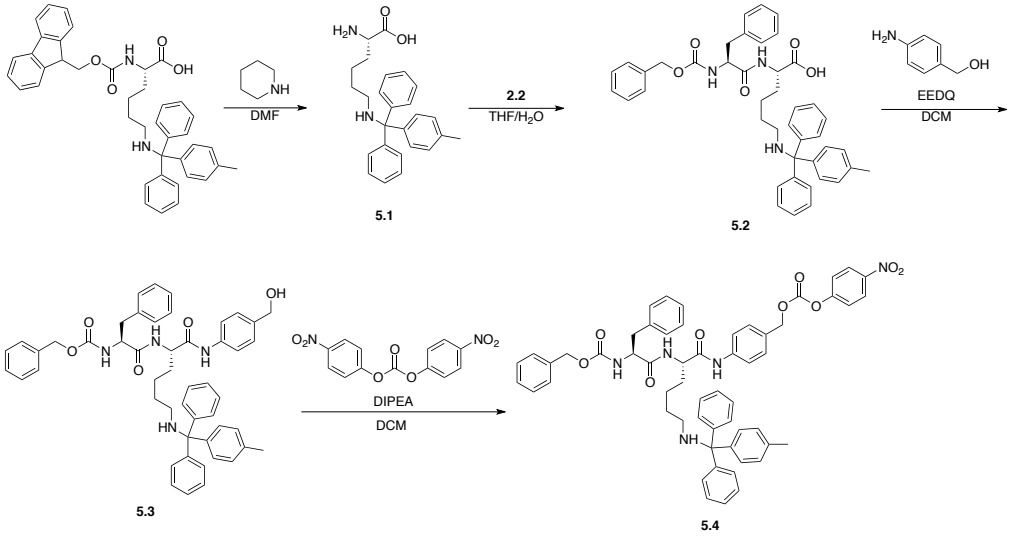

Scheme 5.1 Synthesis of **5.4**.

5.4 Synthesis of Glucose Linked Standard

The first radiopharmaceutical that was explored for conjugation with **5.4** was [^{18}F]FDG. In order to be efficient with cost, D-glucose was used in a model reaction with a simple p-nitrophenyl carbonate (Scheme 5.2). The reaction mixture was analysed using analytical HPLC before and after purification by reverse phase chromatography (Figure 5.2). The reaction mixture displayed excess 4-dimethylaminopyridine (DMAP), the desired product **5.5a**, and 4-nitrophenol (Figure 5.2B). The 4-nitrophenol was

identified by injecting the standard and correlating the retention time of the peaks (Figure 5.2D). The starting material was consumed and did not decompose since the benzyl alcohol side product was not observed (Figure 5.2A/C). Following purification the 4-nitrophenol leaving group was still present in the reaction mixture (Figure 5.2E) and ^{1}H NMR analysis revealed that it was the most abundant compound present. Because this was used solely as a model reaction, further efforts to purify **5.5a** further were not pursued.

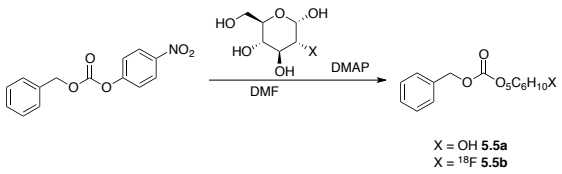

Scheme 5.2 Preparation of **5.5a** and **5.5b**.

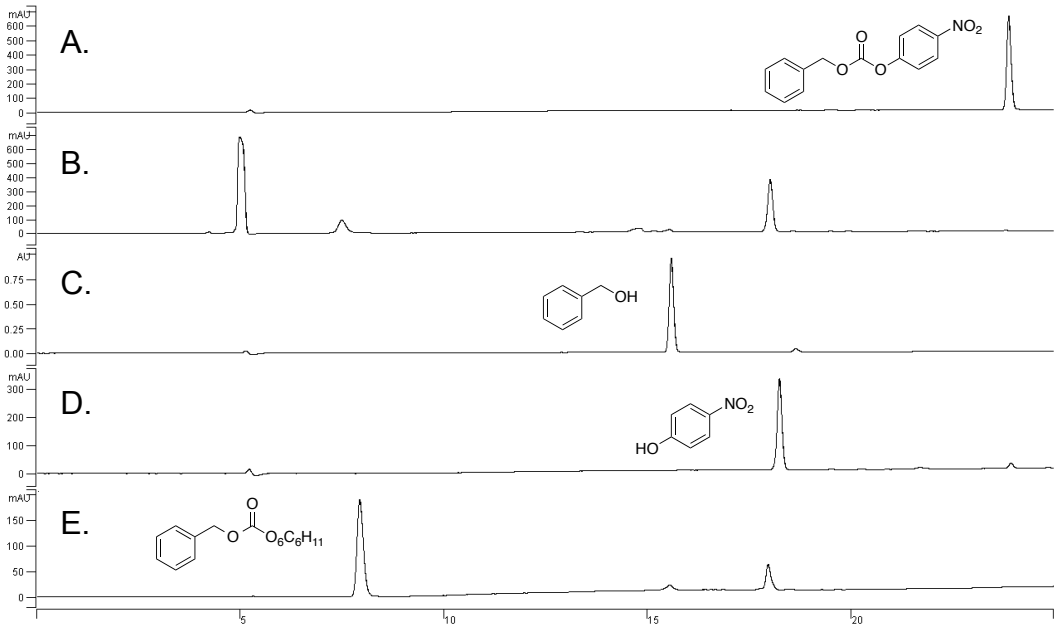

Figure 5.2 UV−visible (λ = 254 nm) HPLC chromatograms of (a) benzyl 4-nitrophenyl carbonate, (b) the reaction mixture, (c) benzyl alcohol, (d) 4-nitrophenol, and (e) **5.5a** after purification.

5.5 Synthesis of Glucose Linked Substrate

Using a similar approach used to synthesize **5.5a**, the cathepsin B substrate **5.4** was combined with D-glucose in place of FDG to make **5.7** as a model reaction (Scheme 5.3). Initial reaction conditions resulted in numerous side products in the reaction mixture; however the reaction time was reduced to optimize the amount of the desired product (Figure 5.3). The reaction mixture did contain a small amount of the alcohol **5.3** likely due to hydrolysis (Figure 5.3 B/C). This was not observed during the synthesis of **5.5a**. The protected probe was isolated using semipreparative

HPLC and showed a single peak following analytical HPLC analysis (Figure 5.3D).

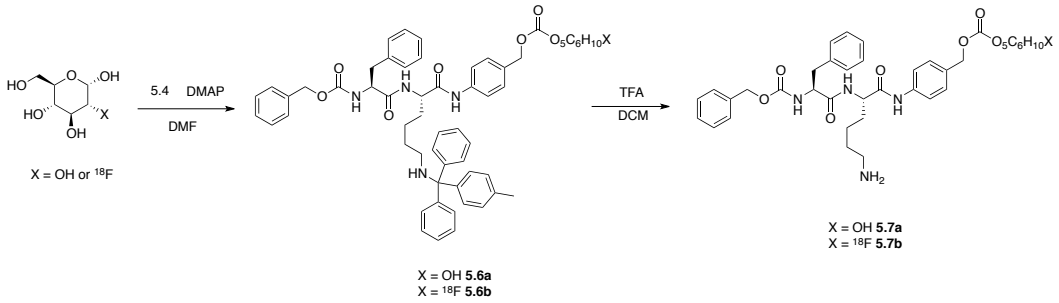

Scheme 5.3 Preparation of **5.7a** and **5.7b**.

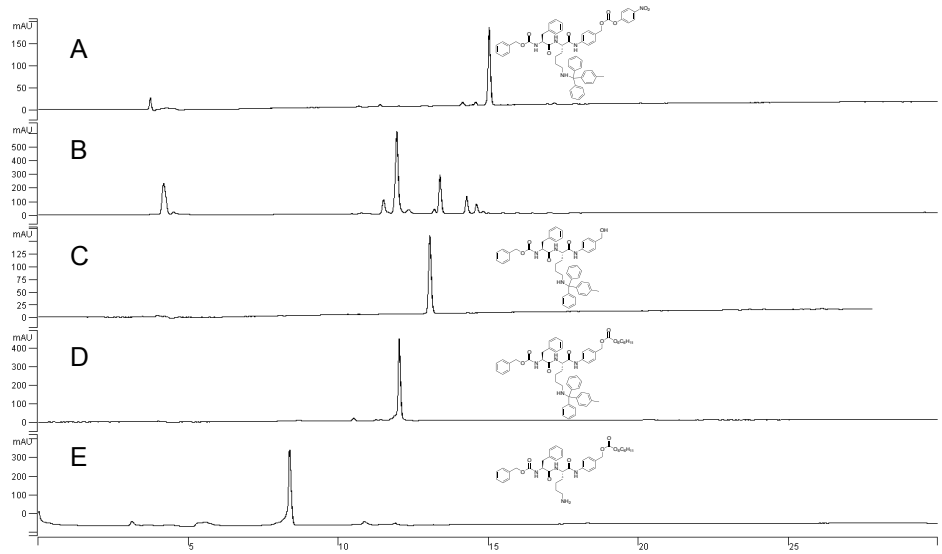

Figure 5.3 UV−visible (λ = 254 nm) HPLC chromatograms of (a) **5.4**, (b) reaction mixture, (c) **5.3**, (d) **5.6** following purification, and (e) **5.7** following deprotection.

A solution of 10% TFA in CH_2Cl_2 was used to remove the Mtt group. The desired product **5.7** was observed using analytical HPLC however following evaporation complete decomposition was observed. Although more dilute solutions could be explored for this deprotection to reduce this decomposition it was important to test the radiolabelling reaction to ensure this approach was feasible at the tracer level prior to investing more time.

5.6 Preparation of [^{18}F]FDG Linked Standard

The next step was to perform the corresponding radiochemical reactions using [^{18}F]FDG (Scheme 5.2 and Scheme 5.3). The radiopharmaceutical was obtained in its final formulation for clinical studies which was problematic because not only did the aqueous media have to removed so did any salts present in the formulation. In order to do this analytical HPLC was used to separate [^{18}F]FDG from any salts present using an amine functionalized column (Figure 5.4).

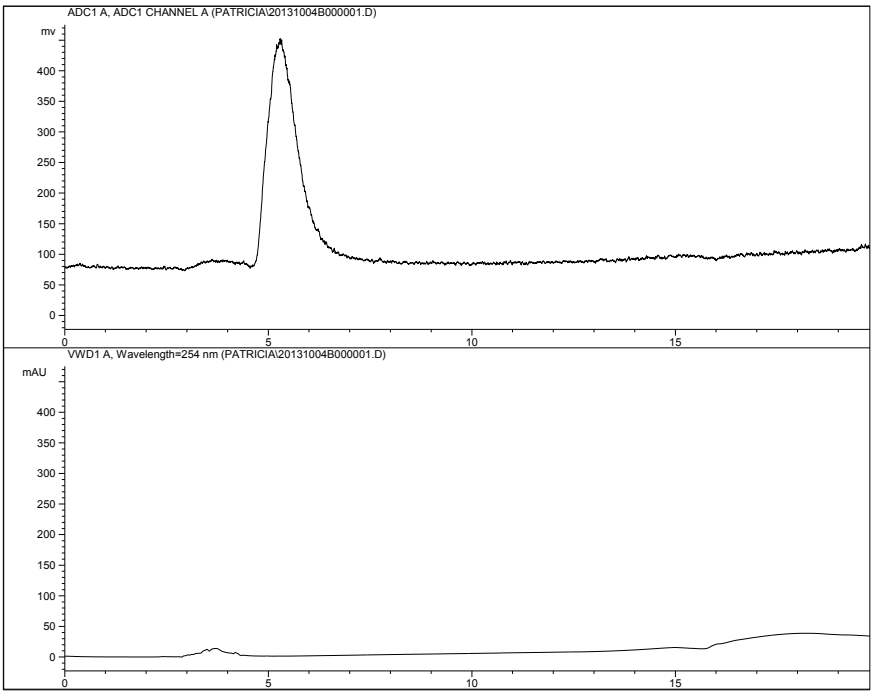

Figure 5.4 Radiochromatogram (upper trace) and UV−visible (λ = 254 nm) HPLC chromatogram (lower trace) of [^{18}F]FDG following HPLC purification.

[^{18}F]FDG was dried and transferred to a vial containing DMAP and benzyl 4-nitrophenyl carbonate using DMSO. After microwave irradiation the reaction was analysed using analytical HPLC (Figure 5.5). There were prominent peaks present in the radiochromatogram corresponding to unreacted [^{18}F]FDG and what may be functionalized [^{18}F]FDG. The UV chromatogram showed a peak at 15 min corresponding to the hydrolysis

product benzyl alcohol and a peak at 18 min corresponding to 4-nitrophenol.

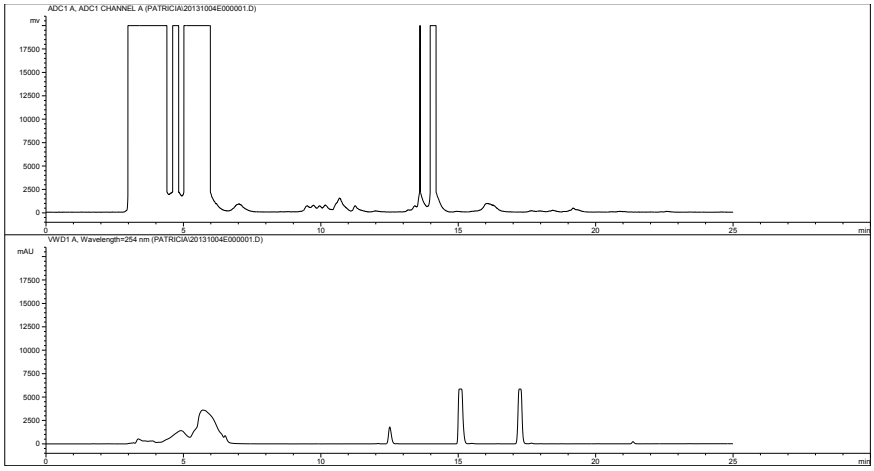

Figure 5.5 Radiochromatogram (upper trace) and UV−visible (λ = 254 nm) HPLC chromatogram (lower trace) of benzyl 4-nitrophenyl carbonate following incubation with [^{18}F]FDG.

Following HPLC purification 2 peaks were observed in the radiochromatogram (Figure 5.6). Without a non-radioactive FDG standard these peaks could not be identified. The 2 peaks, however, may in fact be due to functionalization of more than one hydroxyl group of [^{18}F]FDG. This experiment did indicate that [^{18}F]FDG can be used in a conjugation reaction following isolation from the standard formulation, however it may not be appropriate for use with this linker based on the challenges observed during attempted conjugation.

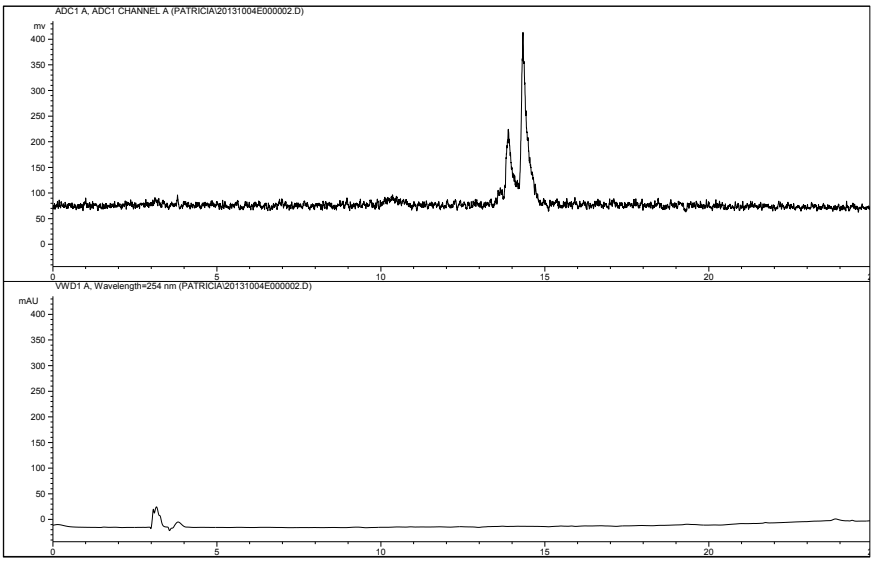

Figure 5.6 Radiochromatogram (upper trace) and UV−visible (λ = 254 nm) HPLC chromatogram (lower trace) of benzyl 4-nitrophenyl carbonate following incubation with [^{18}F]FDG.

5.7 Preparation of [^{18}F]FDG Linked Substrate

[^{18}F]FDG was dried and transferred to a vial containing DMAP and **5.4** using DMSO. After microwave irradiation the reaction was analysed using analytical HPLC (Figure 5.7). The majority of the radioactivity present was eluted at the solvent front, likely due to residual [^{18}F]FDG that did not react. There was a small radioactive peak that appeared at 11.9 min that may correspond to the desired compound **5.6b**; however without a non-radioactive standard this could not be confirmed. Interestingly there was a prominent peak in the UV chromatogram that had a similar retention time,

which could be the glucose analogue **5.6a**. This is possible since [^{18}F]FDG is often produced as a mixture containing glucose.[31] Alternatively this could be the alcohol intermediate **5.3** coming as a result of hydrolysis of **5.4**. Following purification and reinjection the peak at 11.9 min was no longer present and the radioactivity was observed at the solvent front. The procedures employed here were cumbersome and the resultant product was not stable during the purification procedures. As a result the focus shifted to using a simpler benzamide based agent.

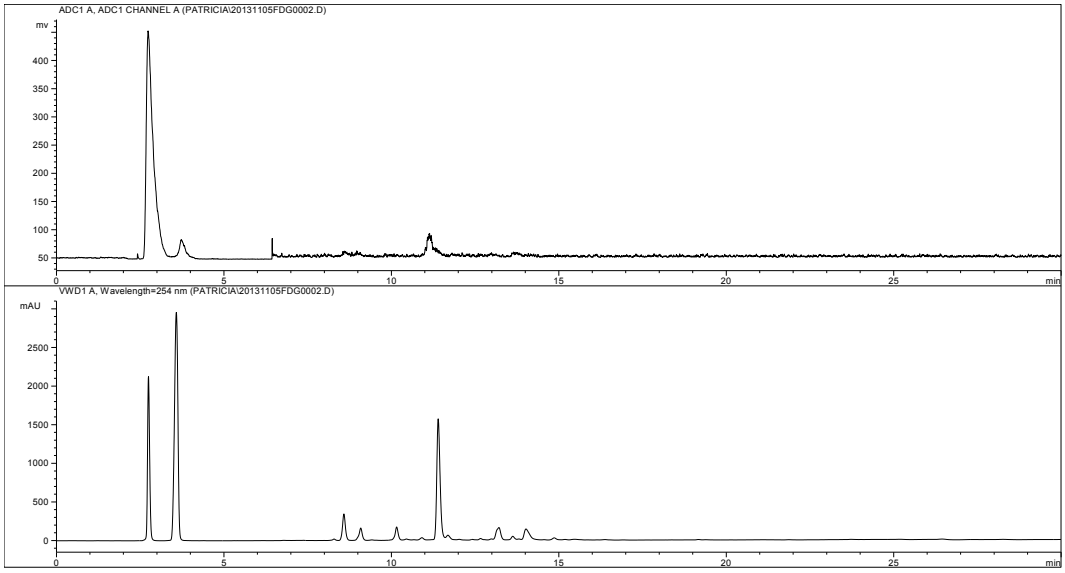

Figure 5.7 Radiochromatogram (upper trace) and UV−visible (λ = 254 nm) HPLC chromatogram (lower trace) of **5.4** following incubation with [^{18}F]FDG.

5.8 Synthesis and Radiolabelling of a Melanin Targeted Probe

The iodobenzamide, **5.9** was of particular interest for the releasing strategy because it showed high uptake in melanin expressing tumours with a T:NT ratio of 19 at 6 h p.i. in murine models.[23] Also it has a free amine that can be used for conjugation with **5.4** through a carbamate linkage. Similar compounds were prepared to explore the SAR for melanoma activity where modification of the amine with simple substituents often led to increased melanoma uptake; however incorporation of larger groups did result in decreased melanoma uptake.[23,30,32–34] Given its large size and steric bulk around the labeled unit, it is anticipated that the substrate linked probe will have poor melanin affinity until it has been released by active cathepsin B, which is overexpressed in malignant melanoma.[35–38]

The first step was to synthesize the melanin-targeting probe **5.9**. The procedure that was initially followed involved combining methyl 4-amino-2-methoxybenzoate with excess N,N-diethylethylenediamine and heating to 90 ºC for 12 h.[23] Following this procedure led to very little product (<10% yield). We have previously reported the formation of amides from reactive methyl esters in the presence of DIPEA in methanol and so a similar approach was applied here and the yield improved to 70% (Scheme 5.4).[39]

The next step was to perform a direct iodination using potassium iodate and sodium iodide in an acidic medium giving **5.9** in 22% yield. HPLC was used to determine the rentention time for **5.9** as the non-radioactive standard (R^t = 11 min) (Figure 5.8).

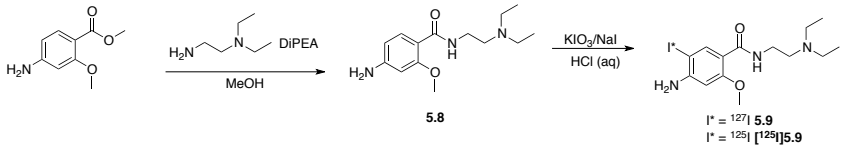

Scheme 5.4 Preparation of **5.9** and [^{125}I]**5.9**.

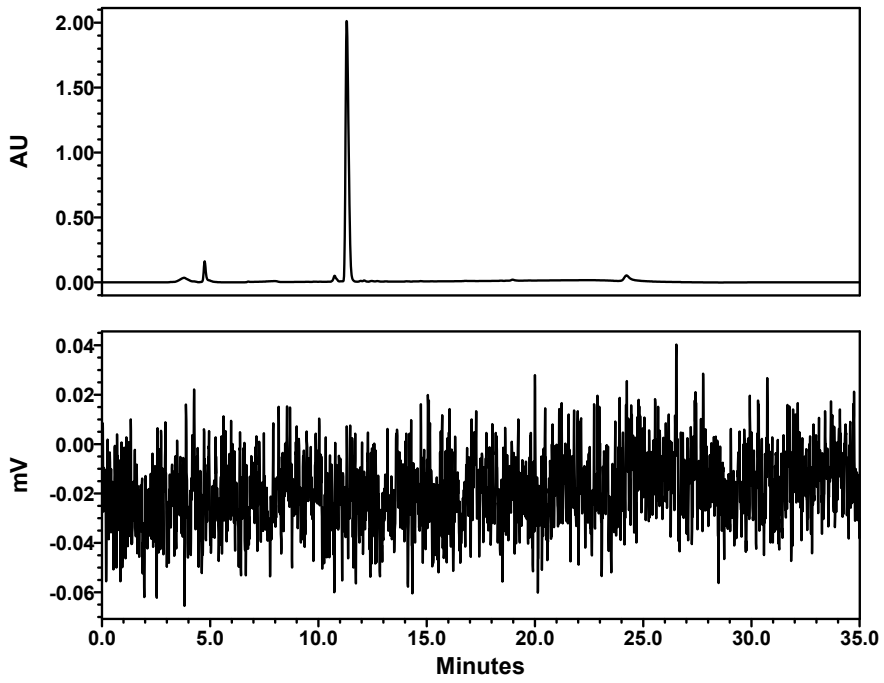

Figure 5.8 UV−visible (λ = 254 nm) HPLC chromatogram of (upper trace) **5.9**. Radiochromatogram (lower trace) was also collected by default.

To make the radioactive analogue, **5.8** was treated with [^{125}I]NaI in the presence of potassium iodate and hydrochloric acid in PBS. Following HPLC purification [^{125}I]**5.9** was obtained with a radiochemical purity >95% and isolated radiochemical yields between 20 – 40% (n = 3) (Figure 5.9).

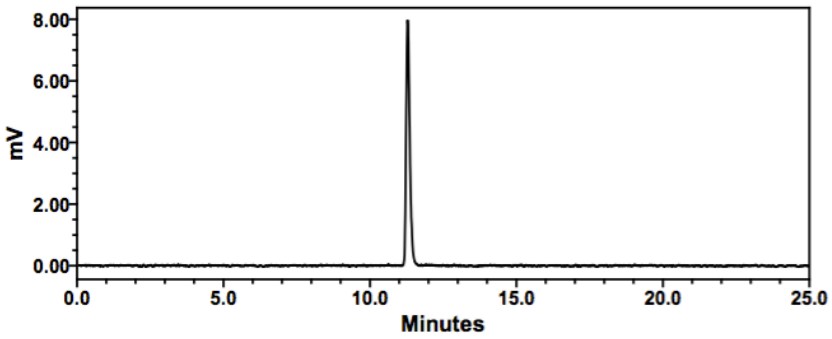

Figure 5.9 Radiochromatogram of [^{125}I]**5.9**.

5.9 Synthesis of Iodobenzamide Linked Substrate

Using a similar approach applied to synthesize **5.6a** the cathepsin B substrate **5.4** was combined with **5.9** to make the non-radioactive standard **5.10** (Scheme 5.5). The reaction mixture did contain a small amount of the starting material **5.4** but no other side products (Figure 5.10). The protected probe was isolated using semipreparative HPLC, yet some decomposition was observed (Figure 5.10).

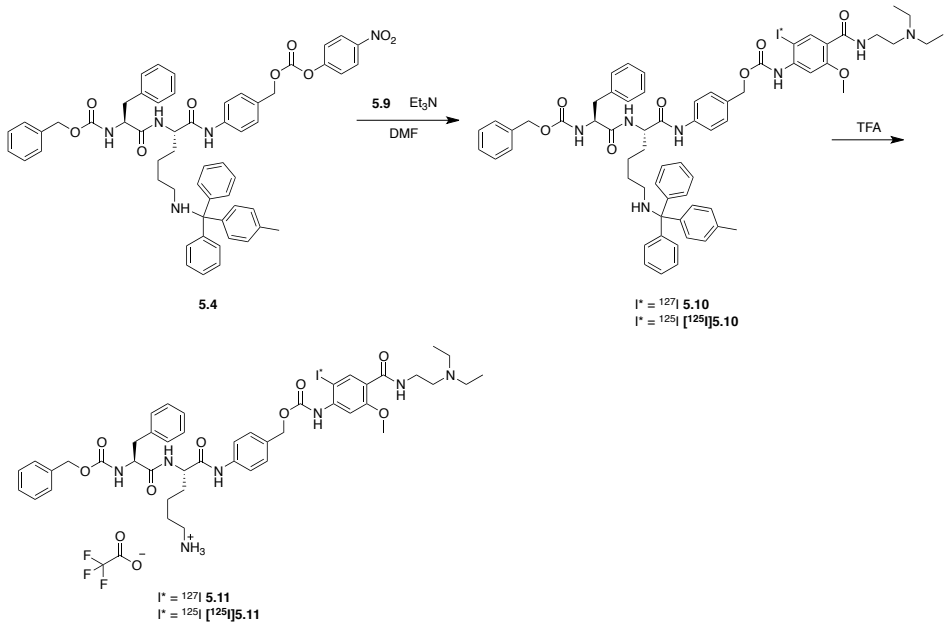

Scheme 5.5 Preparation of **5.11a** and [^{125}I]**5.11**.

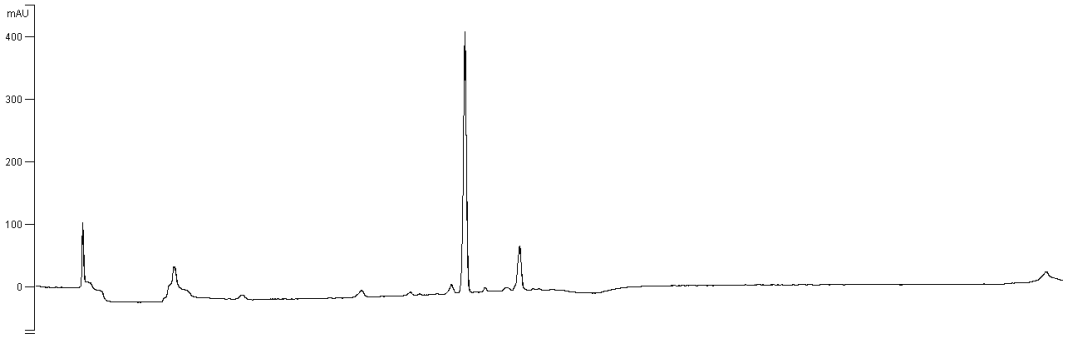

Figure 5.10 UV−visible (λ = 254 nm) HPLC chromatogram of reaction mixture forming **5.10**.

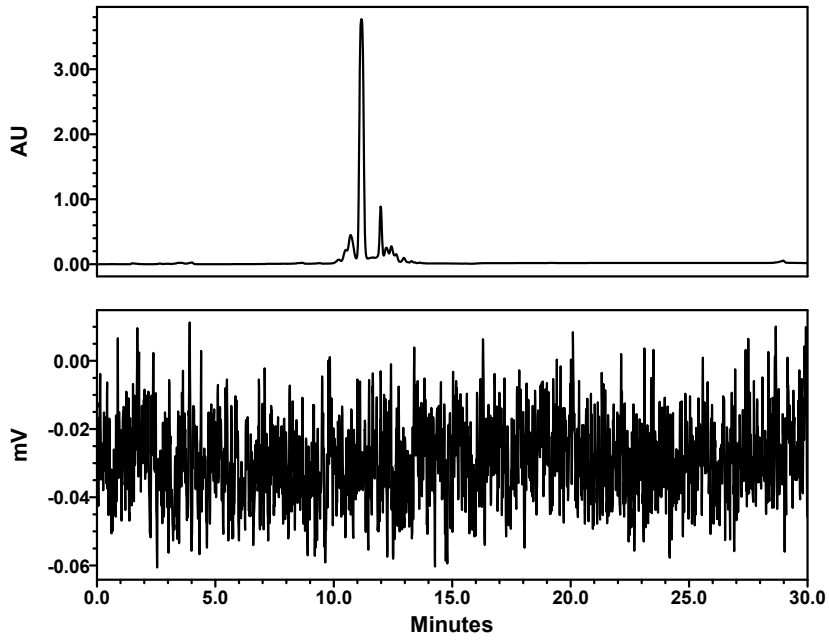

Figure 5.11 UV-visibe (λ = 254 nm) HPLC chromatogram (upper trace) of **5.10** following purification. Radiochromatogram (lower trace) was also collected by default.

Initial attempts to isolate **5.10** by HPLC showed a different result. When the elution solvent was not removed immediately a new peak was observed in the chromatogram (Figure 5.12). It was believed that this peak came as a result of removal of the Mtt group due to the TFA present in the elution solvent. This would be advantageous if the final product **5.11** could be isolated in this way without further steps. To explore the feasibility of this single step approach the radiochemical reaction was attempted.

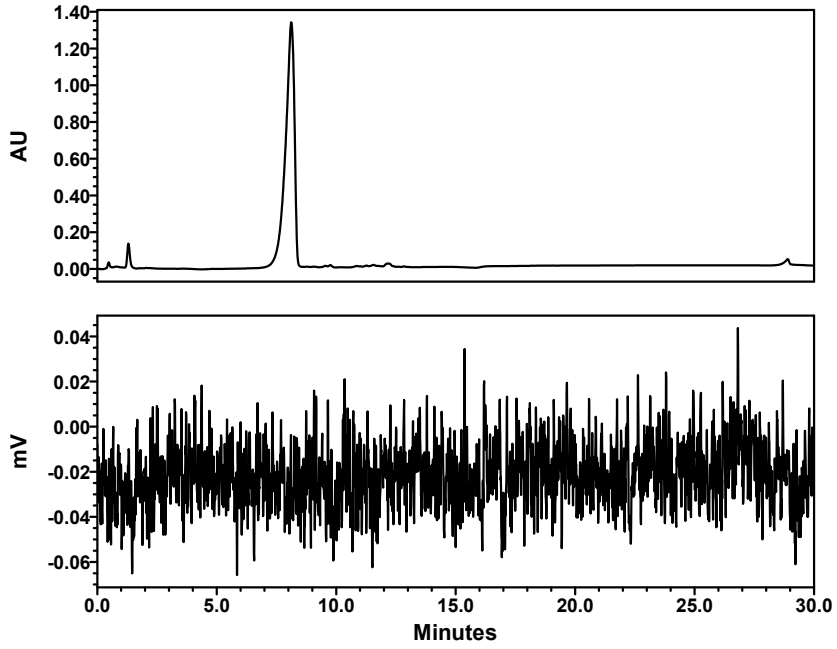

Figure 5.12 UV−visible (λ = 254 nm) HPLC chromatogram of initial reaction to form **5.10** following HPLC purification. Radiochromatogram (lower trace) was also collected by default.

5.10 Preparation of Radioiodobenzamide Linked Substrate

After drying, [^{125}I]**5.9** was transferred to a vial containing triethylamine and **5.4** using DMF. Due to the long half-life of ^{125}I ($t_{1/2}$ = 59.4 d)[40] microwave irradiation was not used to reduce the risk of contaminating the instrument. Instead, the reaction was shaken at room temperature for 30 min and analysed using analytical HPLC (Figure 5.13). The UV chromatogram showed a number of peaks the most prominent coming at ~11 min. This

corresponds to **5.10** based on its retention time with this instrument (Figure 5.11).

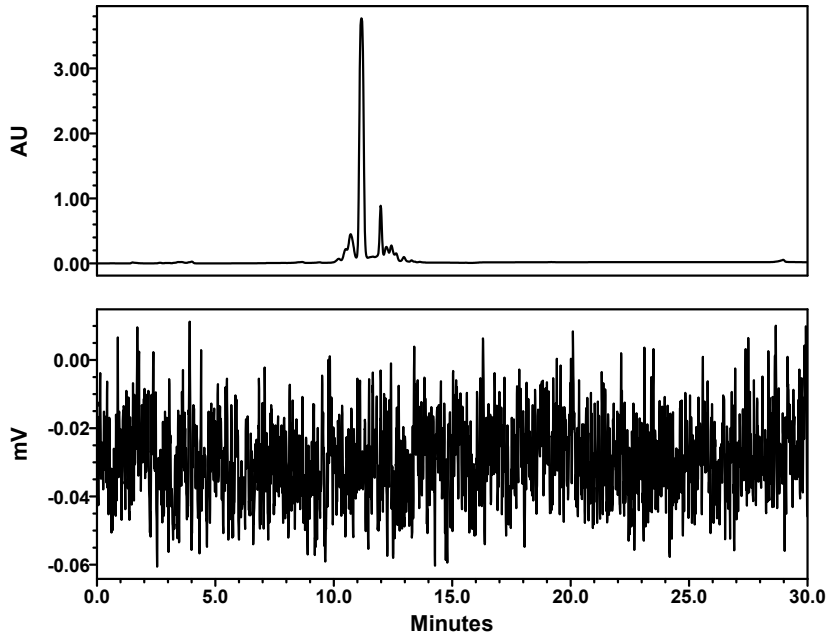

Figure 5.11 UV-visibe (λ = 254 nm) HPLC chromatogram (upper trace) of **5.10** following purification. Radiochromatogram (lower trace) was also collected by default.

Because [^{125}I]**5.9** was synthesized in the presence of ^{125}I and ^{127}I, it does have reduced specific activity therefore a certain amount of non-radioactive **5.10** is expected to form. This is not anticipated to be a problem for the probe overall since melanin is a non-saturable target.[23] The radiochromatogram showed a single peak at ~5 min but the retention

time did not correspond with the non-radioactive peak that was believed to come as a result of Mtt removal (Figure 5.12). Interestingly this peak also did not correspond to the iodobenzamide probe **5.9** when run with this method indicating this peak was not due to incomplete conjugation (Figure 5.14).

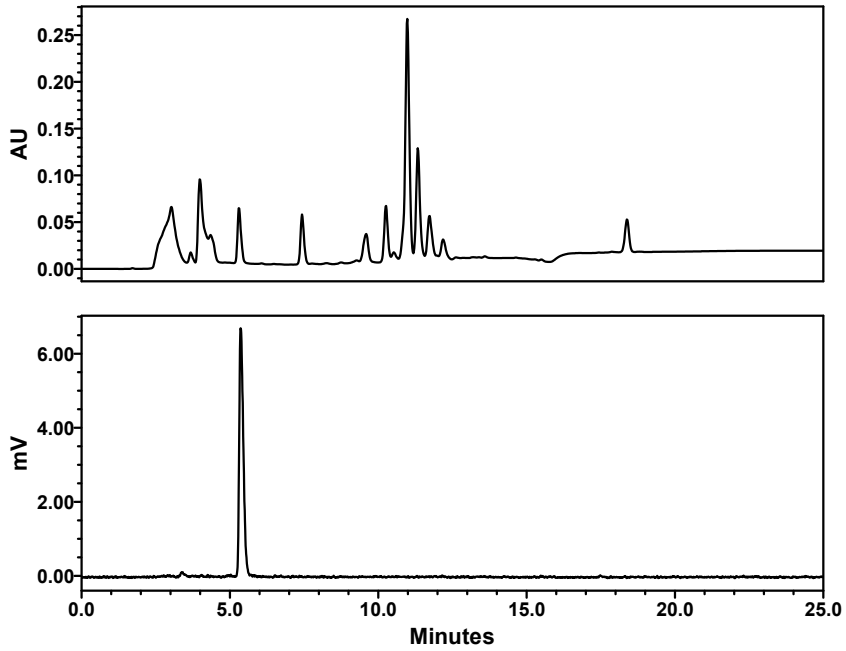

Figure 5.13 UV−visible (λ = 254 nm) HPLC chromatogram (upper trace) and radiochromatogram (lower trace) of **5.4** following incubation with [^{125}I]**5.9**.

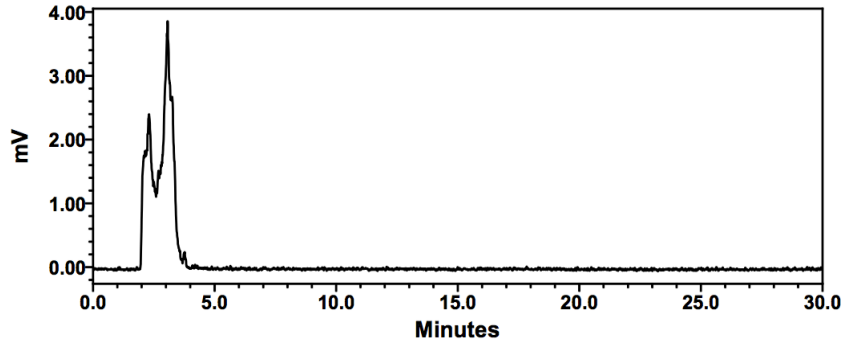

Figure 5.14 Radiochromatogram of [^{125}I]**5.9** using the same HPLC method as Figure 5.13.

The procedure employed here to synthesize the radioactive analogue [^{125}I]**5.11** was not similar to the preparation of **5.11** due to the constraints in working with ^{125}I. The reaction should be feasible using the shorter-lived isotope ^{123}I ($t_{1/2}$ = 13.2 h).[40] Further optimization of the radioactive and non-radioactive reactions is required to further explore this approach.

5.11 Summary and Conclusions

A new strategy was established to develop a class of substrate based probes that can deliver a known radiopharmaceutical to tumours with high cathepsin B expression. A known substrate was synthesized as precursor that could be linked to an amino or hydroxyl containing probe such as [^{18}F]FDG or [^{125}I]**5.9**. This approach is advantageous because it can be used to improve the selectivity of a known radiopharmaceutical. By using a

probe that requires the presence of two targets at the disease site, some of the non-tumour uptake can potentially be reduced.

A synthetic strategy was established to link the non-radioactive probe with the cathepsin B substrate. The reaction was optimized to improve the yield and reduce the production of side products. Radiochemical reactions proved problematic either because of incomplete conjugation or decomposition. The methods used for the non-radioactive probe were not easily translated to the radioactive analogues due to the nature of the formulation of the radiopharmaceutical or the half-life of the isotope involved. To further this approach alternate methods to produce the radiopharmaceutical need to be explored. Once this is established, the effectiveness of the releasing strategy can be tested *in vitro* and *in vivo*.

5.12 Experimental

General. All chemicals, unless otherwise stated, were purchased from Sigma−Aldrich. Fmoc-Lys(Mtt)-OH was obtained from EMD Biosciences. ^{1}H, ^{13}C, and 2D NMR spectra were recorded using either a Bruker AV600 spectrometer. ^{1}H NMR signals are reported in ppm measured relative to the residual proton signal of the deuterated solvent. Coupling constants (J) are reported in Hertz (Hz). ^{13}C signals are reported in ppm relative to the carbon signal from the solvent. High-resolution mass spectrometry

(HRMS) was preformed using a Waters/Micromass Q-Tof Ultima Global spectrometer. Analytical high performance liquid chromatography (HPLC) for non-radioactive compounds was performed using an Agilent/Varian Pro Star model 330 PDA detector, model 230 solvent delivery system. Analytical HPLC for radioiodinated compounds was performed using a Waters 1525 Binary (Midford, MA, USA) monitored simultaneously with 2489 UV/Visible detector and in-line radioactivity Bioscan gamma detector with NaI(Tl) scintillator. Analytical HPLC for radiofluorinated compounds was performed using an Agilent 1100 system equipped with an automatic liquid sampler, a variable wavelength UV detector and a Bioscan gamma detector connected in series. Analytical HPLC were preformed using either a Phenomenex Gemini (L × ID = 100 × 4.6 mm) column (5 μm C18) or a Phenomenex Luna (L × ID = 100 × 4.6 mm) column (5 μm NH2). Semi-preparative HPLC was performed using an Agilent/Varian Pro Star model 325 PDA detector, model 24 solvent delivery system and a Phenomenex Gemini (L × ID = 250 × 10 mm) column (5 μm C18). The elution conditions were as follows: **Method A**: Solvent A = CH_3CN (with 0.1% TFA), B = H_2O (with 0.1% TFA): Gradient: 10% A, 0 – 2 min; 10% A – 90%A, 2 – 20 min; 90% A, 20 – 22 min; 90% A to 10% A, 22 – 23 min; 10% A, 23 – 25 min. **Method B:** Solvent A = CH_3CN with 0.1% TFA, solvent B= H_2O with 0.1%

TFA. Gradient: 30% A to 100% A, 0−12 min; 100% A, 12−24 min; 100% A to 90% A, 24−28 min; 90% A to 30% A, 28−30 min. **Method C**: Solvent A = CH_3CN (with 0.1% TFA), B = H_2O (with 0.1% TFA): Gradient: 1% A, 0 – 3 min; 1% - 100% A, 3 – 10 min; 100% A, 10 – 15 min; 100 – 1% A, 15 – 20 min. **Method D:** Solvent A = CH_3CN (with 0.1% TFA), B = H_2O (with 0.1% TFA): Gradient: 10% A, 0 – 2 min; 10% A – 90%A, 2 – 20 min; 90% A, 20 – 22 min; 90% A to 10% A, 22 – 23 min; 10% A, 23 – 25 min. The flow rate was set at 1 mL/min for analytical methods and 4 mL/min for semi-preparative methods; monitoring occurred at 254 nm. Pharmaceutical grade fludeoxyglucose ([^{18}F]FDG), Glucovision) was obtained from The Centre of Probe Development and Commercialization formulated in phosphate buffer containing ethanol. [^{125}I]NaI (specific activity, 629 GBq/mg) was provided by the McMaster Nuclear Reactor. As this is a radioactive isotope, appropriate facilities, licenses, and procedures should be in place prior to use. Radioactivity measurements were made using a Wizard 1470 Automated Gamma Counter (PerkinElmer, Woodbridge ON).

Synthetic Methods

Synthesis of (*S*)-2-amino-6-((diphenyl(*p*-tolyl)methyl)amino)hexanoic acid (5.1). A solution of Fmoc-Lys(Mtt)-OH (2.5 g, 4.0 mmol) in 25% piperidine/DMF (16 mL) was stirred for 30 min at room temperature. The

reaction mixture was added to ethanol (125 mL). The precipitate was collected by vacuum filtered and lyophilized giving a white powder. Yield (1.16 g, 72%). TLC (20% MeOH/CH_2Cl_2): R_f = 0.65. ^{1}H NMR (600 MHz; CD_3OD): δ 7.44-7.42 (m, 4H), 7.30-7.28 (m, 2H), 7.26-7.23 (m, 4H), 7.17-7.15 (m, 2H), 7.07 (d, J = 8.0, 2H), 3.73 (t, J = 6.7), 3.48 (dd, J = 7.0, 5.2, 1H), 2.29 (s, 3H), 2.16 (t, J = 7.2, 2H), 1.88-1.81 (m, 2H), 1.78-1.72 (m, 1H), 1.58-1.53 (m, 2H), 1.45-1.39 (m, 2H). ^{13}C NMR (151 MHz; $((CD_3)_2SO)$: δ 169.6, 146.4, 143.2, 134.9, 128.3, 128.2, 127.6, 125.9, 54.3, 43.4, 31.2, 30.1, 23.2, 20.5. HRMS Calcd. for $C_{26}H_{31}N_2O_2$ $[M+H]^+$: 403.2386. Found: 403.2400.

(*S*)-2-((*S*)-2-(((benzyloxy)carbonyl)amino)-3-phenylpropanamido)-6-((diphenyl(*p*-tolyl)methyl)amino)hexanoic acid (5.2). To a solution of Et_3N (170 μL, 1.22 mmol) in 50% THF/water (20 mL), **5.1** (439 mg, 1.09 mmol) was added. After which **2.2** (481 mg, 1.20 mmol) was added and the solution was left to stir 3 h. The organic solvent was removed by rotary evaporation and 1N HCl (15 mL) was added and the solution extracted with EtOAc (3 × 15 mL). The combined organic extracts were then extracted with 6N HCl (3 × 15 mL), brine (3 × 15 mL), and dried over $MgSO_4$. The solvent was removed by rotary evaporation and the residue was precipitated from EtOAc/hexanes giving **5.2** as a white solid. Yield

(677 mg, 91%). TLC (5% MeOH/CH_2Cl_2): R_f = 0.29. ^{1}H NMR (600 MHz; ($(CD_3)_2SO$): δ 12.65-12.60 (m, 1H), 10.34-10.27 (m, 2H), 8.27-8.24 (m, 1H), 7.48-7.38 (m, 10H), 7.36-7.19 (m, 14H), 4.92-4.86 (m, 2H), 4.29-4.26 (m, 1H), 4.19-4.14 (m, 1H), 2.75-2.68 (m, 3H), 2.33-2.30 (m, 3H), 1.77-1.68 (m, 2H), 1.68-1.49 (m, 3H), 1.32-1.19 (m, 4H). ^{13}C NMR (151 MHz; ($(CD_3)_2SO$): δ 173.3, 171.7, 155.7, 138.1, 138.0, 137.0, 129.2, 129.1, 128.9, 128.8, 128.5, 128.5, 128.3, 128.1, 128.0, 127.7, 127.5, 127.4, 126.2, 79.2, 75.3, 72.2, 65.1, 55.9, 51.6, 45.2, 37.3, 30.9, 30.4, 25.5, 20.5.

Benzyl ((*S*)-1-(((*S*)-6-((diphenyl(*p*-tolyl)methyl)amino)-1-((4-(hydroxymethyl)phenyl)amino)-1-oxohexan-2-yl)amino)-1-oxo-3-phenylpropan-2-yl)carbamate (5.3). 4-Aminobenzyl alcohol (97.5 mg, 790 mmol) was added to a solution of **5.2** (451 mg, 660 mmol) in CH_2Cl_2 (10 mL) under a stream of Ar. 2-Ethoxy-1-ethoxycarbonyl-1,2-dihydroquinoline (EEDQ) (245 mg, 990 mmol) was added and the solution left to stir for 16 h at room temperature. The solvent was removed by rotary evaporation and the residue was triturated with Et_2O (25 mL). After sonication for 30 min the solution was left to stand and room temperature, where upon a precipitate formed that was collected by vacuum filtration and dried by rotary evaporation with CH_2Cl_2/Et_2O giving a white solid. Yield (338 mg, 65%). TLC (5% MeOH/CH_2Cl_2): R_f = 0.42. ^{1}H NMR (600 MHz; ($(CD_3)_2SO$): δ 10.22-10.09 (m, 2H), 10.00 (s, 1H), 8.22 (d, J = 7.9,

1H), 7.56-7.15 (m, 28H), 4.93-4.88 (m, 2H), 4.44-4.42 (m, 2H), 4.39-4.35 (m, 1H), 4.31-4.27 (m, 1H), 3.02-2.99 (m, 1H), 2.75-2.69 (m, 4H), 2.31-2.29 (m, 3H), 1.76-1.49 (m, 4H). HRMS Calcd. for $C_{50}H_{53}N_4O_5$ $[M+H]^+$: 789.4016. Found:789.4051.

Benzyl ((*S*)-1-(((*S*)-6-((diphenyl(*p*-tolyl)methyl)amino)-1-((4-((((4-nitrophenoxy)carbonyl)oxy)methyl)phenyl)amino)-1-oxohexan-2-yl)amino)-1-oxo-3-phenylpropan-2-yl)carbamate (5.4). Bis(4-nitrophenyl) carbonate (281 mg, 925 μmol) and **5.3** (146 mg, 185 μmol) were combined in CH_2Cl_2 (10 mL) under Ar. DIPEA (99.1 μL, 569 mmol) was added and the solution was left to stir for 3 d. The solvent was removed by rotary evaporation. The residue was dissolved in EtOAc (20 mL), extracted with 10% (w/v) citric acid (3 × 20 mL), brine (3 × 20 mL), and dried over Na_2SO_4. The solvent was removed by rotary evaporation and the residue was triturated with Et_2O (30 mL). After sonication for 30 min the solution was left to stand and room temperature. The precipitate was collected by vacuum filtration and dried by rotary evaporation. Yield (112 mg, 64%). TLC (5% MeOH/CH_2Cl_2): R_f = 0.55. ^{1}H NMR (600 MHz; ($(CD_3)_2SO$): δ 10.16 (s, 1H), 8.33-8.31 (m, 2H), 8.16 (dd, J = 38.7, 8.4, 1H), 7.67-7.05 (m, 32H), 5.26 (s, 2H), 4.92 (s, 2H), 4.43-4.42 (m, 1H), 4.34-4.30 (m, 1H), 3.03-3.00 (m, 1H), 2.74 (dd, J = 13.6, 10.9, 1H), 2.22

(s, 3H), 1.97-1.92 (m, 2H), 1.71-1.59 (m, 3H), 1.51-1.48 (m, 2H), 1.41-1.32 (m, 2H). ^{13}C NMR (151 MHz; $((CD_3)_2SO)$: δ 171.5, 170.7, 155.8, 155.3, 151.9, 146.5, 146.4, 145.2, 143.2, 139.3, 138.8, 138.0, 137.0, 134.9, 129.5, 129.2, 128.6, 128.3, 128.3, 128.2, 128.0, 127.6, 127.6, 127.4, 126.2, 125.9, 125.4, 122.6, 119.1, 70.2, 65.2, 56.0, 53.5, 43.2, 37.4, 32.3, 29.9, 23.4, 20.4.

Benzyl (((2*R*,3*S*,4*S*,5*R*,6*S*)-3,4,5,6-tetrahydroxytetrahydro-2*H*-pyran-2-yl)methyl) carbonate (5.5). Benzyl 4-nitrophenyl carbonate (273 mg, 1 mmol)**,** D-(+)-glucose (180 mg, 1 mmol), and 4-dimethylaminopyridine (244 mg, 2 mmol) were added to a 2 mL microwave vial and DMF (2 mL) was added. The reaction was heated to 80 ºC in a microwave for 15 min. The product was collected following reverse phase SP1 purification (10-90% CH_3CN/H_2O). HPLC (method A) R^t = 6.2 min.

Benzyl ((*S*)-1-(((*S*)-6-amino-1-oxo-1-((4-((((((2*R*,3*S*,4*S*,5*R*,6*S*)-3,4,5,6-tetrahydroxytetrahydro-2*H*-pyran-2-yl)methoxy)carbonyl)oxy)methyl)phenyl)amino)hexan-2-yl)amino)-1-oxo-3-phenylpropan-2-yl)carbamate (5.7). 5.4 (19 mg, 20 μmol)**,** D-(+)-glucose (24 mg, 20 μmol) and 4-dimethylaminopyridine (49 mg, 40 μmol) were added to a 2 mL microwave vial and DMF (2 mL) was added. The reaction was heated to 80 ºC by microwave irradiation for 10 min. The

product was collected following semipreparative HPLC (method B) giving **5.6a**. HRMS Calcd. for $C_{57}H_{63}N_4O_{12}$ $[M+H]^+$: 995.4442. Found: 995.4449. HPLC (method B) R^t = 11.9 min. **5.6** was treated with 10% TFA/CH_2Cl_2 (5 mL) for 30 min giving **5.7**. HRMS Calcd. for $C_{37}H_{47}N_4O_{12}$ $[M]^+$: 739.3190. Found: 739.3196. HPLC (method B) R^t = 8.4 min. ^{1}H NMR (600 MHz; $((CD_3)_2SO)$: δ 9.98 (s, 1H), 8.15-8.13 (m, 1H), 7.53 (d, J = 8.5, 2H), 7.47-7.03 (m, 28H), 5.09 (t, J = 5.7, 1H), 4.92-4.87 (m, 2H), 4.43 (d, J = 5.5, 2H), 4.42-4.38 (m, 1H), 4.32-4.28 (m, 1H), 3.51-3.46 (m, 1H), 3.01-2.98 (m, 1H), 2.74-2.70 (m, 1H), 2.43-2.37 (m, 1H), 2.21-2.20 (m, 3H), 1.96-1.90 (m, 2H), 1.68-1.65 (m, 1H), 1.59-1.55 (m, 1H), 1.50-1.45 (m, 2H), 1.39-1.35 (m, 1H), 1.32-1.26 (m, 1H), 1.25-1.21 (m, 2H).

4-Amino-*N*-(2-(diethylamino)ethyl)-2-methoxybenzamide (5.8). Methyl 4-amino-2-methoxybenzoate (1.40 g, 7.73 mmol) was dissolved in methanol (10 mL). N,N-Diethylethylenediamine (5.31 mL, 37.1 mmol) and DIPEA (3.91 mL, 22.4 mmol) were added and the solution was heated to reflux at 90 ºC for 3 d. The solvent was removed by rotary evaporation and CH_2Cl_2 (20 mL) was added. The solution was extracted with water (3 × 20 mL) and brine (3 × 20 mL), and dried over Na_2SO_4. The solvent was removed by rotary evaporation and the product was isolated following SP1 purification (5-40% MeOH/CH_2Cl_2). Yield (1.42 g, 69%). TLC (20%

MeOH/CH_2Cl_2): R_f = 0.45. ^{1}H NMR (600 MHz; $CDCl_3$): δ 8.20 (s, 1H), 7.91 (d, J = 8.5, 1H), 6.23 (dd, J = 8.5, 2.0, 1H), 6.14 (d, J = 2.0, 1H), 4.22 (s, 2H), 3.79 (s, 3H), 3.46 (q, J = 5.7, 2H), 2.60 (t, J = 6.2, 2H), 2.54 (q, J = 7.1, 4H), 1.00 (t, J = 7.1, 6H). ^{13}C NMR (151 MHz; $CDCl_3$): δ 165.9, 159.5, 151.6, 133.8, 111.5, 107.5, 97.3, 55.7, 51.9, 47.0, 37.4, 11.9. HRMS Calcd. for $C_{14}H_{24}N_3O_2$ $[M+H]^+$: 266.1869. Found: 266.1877.

4-Amino-*N*-(2-(diethylamino)ethyl)-5-iodo-2-methoxybenzamide (5.9a). To a solution of **5.8** (122 mg, 460 mmol) in 1 N HCl (8.5 mL) 0.5 M $KIO_{3(aq)}$ (1.65 mL) was added. 1 M $NaI_{(aq)}$ (825 μL) was added in 165 μL portions over 30 min. 1 M $Na_2S_2O_{5(aq)}$ (825 μL) was added and after 10 min 1 M NaOH (~10 mL) was added to raise the pH to 12. The mixture was extracted with Et_2O (3 × 20 mL), extracted with brine (15 mL), and dried over Na_2SO_4. The solvent was removed by rotary evaporation and the product was precipitated from EtOAc/hexanes. Yield (39 mg, 22%). TLC (20% MeOH/CH_2Cl_2): R_f = 0.60. ^{1}H NMR (600 MHz; $CDCl_3$): δ 8.45 (s, 1H), 8.16 (s, 1H), 6.27 (s, 1H), 4.42 (s, 2H), 3.87 (s, 3H), 3.48 (m, J = 5.6, 2H), 2.61 (t, J = 6.1, 2H), 2.56 (q, J = 7.1, 4H), 1.04 (t, J = 7.1, 7H). ^{13}C NMR (151 MHz; $CDCl_3$): δ 163.8, 159.0, 150.0, 142.3, 113.9, 96.5, 73.2, 51.3, 46.5, 37.2. HRMS Calcd. For $C_{14}H_{23}N_3O_2I$ $[M+H]^+$: 392.0835. Found: 392.0840.

[^{125}I]4-Amino-*N*-(2-(diethylamino)ethyl)-5-iodo-2-methoxybenzamide (5.9b). To a solution of **5.8** (53 μg, 0.2 μmol) in 1 N HCl (20 μL) 50 mM $KIO_{3(aq)}$ (5 μL) was added followed by [^{125}I]NaI (7.1 MBq) in 0.1% NaOH (5 μL). After 10 min 10× PBS (170 μL) was added and the desired product was obtained following purification by analytical HPLC (Method C). RCY = 20 – 40% (n = 3).

Benzyl ((*S*)-1-(((*S*)-1-((4-((((4-((2-(diethylamino)ethyl)carbamoyl)-2-iodo-5-methoxyphenyl)carbamoyl)oxy)methyl)phenyl)amino)-6-((diphenyl(*p*-tolyl)methyl)amino)-1-oxohexan-2-yl)amino)-1-oxo-3-phenylpropan-2-yl)carbamate (5.10). 5.4 (14 mg, 15 μmol) and **5.9** (6 mg, 15 μmol) were added to a 2 mL microwave vial and dissolved in DMF (1 mL) in the presence of Et_3N (2.0 μL, 15 μmol). The reaction was heated to 80 ºC by microwave irradiation for 20 min. The solution was diluted with CH_3CN (1 mL) and purified using semipreparative HPLC (method C). HPLC (method C) R^t = 12.3 min. ^{1}H NMR (600 MHz; $(CD_3)_2SO$): δ 8.31 (d, J = 8.7, 2H), 7.65-7.63 (m, 2H), 7.57-7.55 (m, 2H), 7.48-7.04 (m, 33H), 5.25 (s, 2H), 4.91 (s, 2H), 4.43-4.35 (m, 1H), 4.33-4.27 (m, 1H), 3.02-2.95 (m, 1H), 2.75-2.71 (m, 3H), 2.31 (s, 2H), 2.21 (s, 2H), 1.96-1.93 (m, 1H), 1.72-1.65 (m, 2H), 1.58-1.56 (m, 1H), 1.50-1.48 (m, 1H), 1.44-1.33 (m, 1H), 1.24-1.20 (m, 2H).

5.13 References

1. L. E. Edgington, M. Verdoes, and M. Bogyo, *Curr. Opin. Chem. Biol.*, 2011, **15**, 798–805.

2. R. Löser and J. Pietzsch, *Front. Chem.*, 2015, **3**, 1–36.

3. T. Fujii, M. Kamiya, and Y. Urano, *Bioconjugate Chem.*, 2014, **25**, 1838–1846.

4. R. Tian, M. Li, J. Wang, M. Yu, X. Kong, Y. Feng, Z. Chen, Y. Li, W. Huang, W. Wu, and Z. Hong, *Org. Biomol. Chem.*, 2014, **12**, 5365–5374.

5. R. Weissleder, C.-H. Tung, U. Mahmood, and A. J. Bogdanov, *Nat. Biotechnol.*, 1999, **17**, 375–378.

6. H. Y. Hu, D. Vats, M. Vizovisek, L. Kramer, C. Germanier, K. U. Wendt, M. Rudin, B. Turk, O. Plettenburg, and C. Schultz, *Angew. Chem. Int. Ed.*, 2014, **53**, 7669–7673.

7. D. Caglič, A. Globisch, M. Kindermann, N. H. Lim, V. Jeske, H. P. Juretschke, E. Bartnik, K. U. Weithmann, H. Nagase, B. Turk, and K. U. Wendt, *Bioorganic Med. Chem.*, 2011, **19**, 1055–1061.

8. J. H. Ryu, S. A. Kim, H. Koo, J. Y. Yhee, A. Lee, J. H. Na, I. Youn, K. Choi, I. C. Kwon, B.-S. Kim, and K. Kim, *J. Mater. Chem.*, 2011, **21**, 17631–17634.

9. M. A. Chowdhury, I. A. Moya, S. Bhilocha, C. C. McMillan, B. G. Vigliarolo, I. Zehbe, and C. P. Phenix, *J. Med. Chem.*, 2014, **57**, 6092–6104.

10. J. A. Richard, Y. Meyer, V. Jolivel, M. Massonneau, R. Dumeunier, D. Vaudry, H. Vaudry, P. Y. Renard, and A. Romieu, *Bioconjug. Chem.*, 2008, **19**, 1707–1718.

11. K. A. Ajaj, M. L. Biniossek, and F. Kratz, *Bioconjugate Chem.*, 2009, **20**, 390–396.

12. K. Hochdörffer, K. Abu Ajaj, C. Schäfer-Obodozie, and F. Kratz, *J. Med. Chem.*, 2012, **55**, 7502–7515.

13. L.-H. Shao, S.-P. Liu, J.-X. Hou, Y.-H. Zhang, C.-W. Peng, Y.-J. Zhong, X. Liu, X.-L. Liu, Y.-P. Hong, R. a Firestone, and Y. Li, *Cancer*, 2012, **118**, 2986–96.

14. R. Satchi, T. A. Connors, and R. Duncan, *Br. J. Cancer*, 2001, **85**, 1070–1076.

15. G. M. Dubowchik, R. A. Firestone, L. Padilla, D. Willner, S. J. Hofstead, K. Mosure, J. O. Knipe, S. J. Lasch, and P. A. Trail, *Bioconjugate Chem.*, 2002, **13**, 855–869.

16. X. Tian, K.-H. Baek, and I. Shin, *Chem. Sci.*, 2013, **4**, 947.

17. S. J. Mather, *Mol. Biosyst.*, 2007, **3**, 30–35.

18. C. P. Phenix, B. P. Rempel, K. Colobong, D. J. Doudet, M. J. Adam, L. A. Clarke, and S. G. Withers, *P. Natl. Acad. Sci. USA*, 2010, **107**, 10842–10847.

19. V. Carroll, B. W. Michel, J. Blecha, H. VanBrocklin, K. Keshari, D. Wilson, and C. J. Chang, *J. Am. Chem. Soc.*, 2014.

20. B. M. Gallagher, J. S. Fowler, N. I. Gutterson, R. R. MacGregor, and A. P. Wolf, *J. Nucl. Med.*, 1978, **19**, 1154–1161.

21. L. Kostakoglu and S. J. Goldsmith, *J. Nucl. Med.*, 2003, **44**, 224–239.

22. J. W. Fletcher, B. Djulbegovic, H. P. Soares, B. a Siegel, V. J. Lowe, G. H. Lyman, R. E. Coleman, R. Wahl, J. C. Paschold, N. Avril, L. H. Einhorn, W. W. Suh, D. Samson, D. Delbeke, M. Gorman, and A. F. Shields, *J. Nucl. Med.*, 2008, **49**, 480–508.

23. M. Eisenhut, W. E. Hull, A. Mohammed, W. Mier, D. Lay, W. Just, K. Gorgas, W. D. Lehmann, and U. Haberkorn, *J. Med. Chem.*, 2000, **43**, 3913–22.

24. A. Maisonial, B. Kuhnast, J. Papon, R. Boisgard, M. Bayle, A. Vidal, P. Auzeloux, L. Rbah, M. Bonnet-Duquennoy, E. Miot-Noirault, M.-J. Galmier, M. Borel, S. Askienazy, F. Dollé, B. Tavitian, J.-C. Madelmont, N. Moins, and J.-M. Chezal, *J. Med. Chem.*, 2011, **54**, 2745–66.

25. M. Maio, J.-J. Grob, S. Aamdal, I. Bondarenko, C. Robert, L. Thomas, C. Garbe, V. Chiarion-Sileni, A. Testori, T.-T. Chen, M. Tschaika, and J. D. Wolchok, *J. Clin. Oncol.*, 2015, **33**, 1191–1196.

26. T. Straetemans, C. Berrevoets, M. Coccoris, E. Treffers-Westerlaken, R. Wijers, D. K. Cole, V. Dardalhon, A. K. Sewell, N. Taylor, J. Verweij, and R. Debets, *Mol. Ther.*, 2014, **23**, 396–406.

27. M. a Henderson, B. H. Burmeister, J. Ainslie, R. Fisher, J. Di Iulio, B. M. Smithers, A. Hong, K. Shannon, R. a Scolyer, S. Carruthers, B. J. Coventry, S. Babington, J. Duprat, H. J. Hoekstra, and J. F. Thompson, *Lancet Oncol.*, 2015, **2045**, 1–12.

28. N. Moins, J. Papon, H. Seguin, D. Gardette, M. F. Moreau, P. Labarre, M. Bayle, J. Michelot, J. C. Gramain, J. C. Madelmont, and a Veyre, *Nucl. Med. Biol.*, 2001, **28**, 799–808.

29. J. M. Michelot, M. F. Moreau, P. G. Labarre, J. C. Madelmont, a J. Veyre, J. M. Papon, D. F. Parry, J. F. Bonafous, J. Y. Boire, and G. G. Desplanches, *J. Nucl. Med.*, 1991, **32**, 1573–80.

30. J. L. Joyal, J. a Barrett, J. C. Marquis, J. Chen, S. M. Hillier, K. P. Maresca, M. Boyd, K. Gage, S. Nimmagadda, J. F. Kronauge, M. Friebe, L. Dinkelborg, J. B. Stubbs, M. G. Stabin, R. Mairs, M. G. Pomper, and J. W. Babich, *Cancer Res.*, 2010, **70**, 4045–53.

31. S. Yu, *Biomed. Imaging Interv. J.*, 2006, **2**, e57.

32. T. Q. Pham, I. Greguric, X. Liu, P. Berghofer, P. Ballantyne, J. Chapman, F. Mattner, B. Dikic, T. Jackson, C. Loc'h, and A. Katsifis, *J. Med. Chem.*, 2007, **50**, 3561–72.

33. W. Mier, C. Kratochwil, J. C. Hassel, F. L. Giesel, B. Beijer, J. W. Babich, M. Friebe, M. Eisenhut, A. Enk, and U. Haberkorn, *J. Nucl. Med.*, 2014, **55**, 9–14.

34. M. Friebe, A. Mahmood, H. Spies, R. Berger, B. Johannsen, A. Mohammed, M. Eisenhut, C. Bolzati, A. Davison, and A. G. Jones, *J. Med. Chem.*, 2000, **43**, 2745–52.

35. P. Matarrese, B. Ascione, L. Ciarlo, R. Vona, C. Leonetti, M. Scarsella, A. M. Mileo, C. Catricalà, M. G. Paggi, and W. Malorni, *Mol. Cancer*, 2010, **9**, 207.

36. R. A. Craven, A. J. Stanley, S. Hanrahan, N. Totty, D. P. Jackson, R. Popescu, A. Taylor, J. Frey, P. J. Selby, P. M. Patel, and R. E. Banks, *Proteomics*, 2004, **4**, 3998–4009.

37. B. Sloane, K. Honn, J. Sadler, W. Turner, J. Kimpson, and J. D. Taylor, *Cancer Res.*, 1981, **42**, 980–986.

38. F. Qian, A. S. Bajkowski, D. F. Steiner, S. J. Chan, and A. Frankfater, *Cancer Res.*, 1989, **49**, 4870–4875.

39. A. Darwish, M. Blacker, N. Janzen, S. M. Rathmann, S. Czorny, S. M. Hillier, J. L. Joyal, J. W. Babich, and J. F. Valliant, *ACS Med. Chem. Lett.*, 2012, **3**, 313–316.

40. M. Eisenhut and W. Mier, *Handbook of Nuclear Chemistry*, Springer US, Boston, MA, 2011.

6 Conclusion and Future Directions

Cancer is a devastating disease that affects people all over the world. Extensive research in the field of oncology has led to breakthroughs in treatment development and understanding the underlying mechanism in cancer progression. Despite the progress in the field, there are still mechanisms that are not well understood. In addition to improving early detection and better characterization of tumors in patients, MI serves as a tool to give new insights in to the biological mechanisms involved in cancer. Cancer (as well as other diseases) can progress very differently from one patient to another. MI can be used to monitor the biochemical makeup and progression of the disease in individual patients to determine the best course of treatment and to assess the effectiveness of the chosen treatment. This is a foundation of personalized medicine.[1]

As the study of mechanisms of cancer aggressiveness and progression continues to grow the search for new targets that can be imaged clinically grows as well. Proteases are a class of enzymes that have been studied extensively in terms of their biochemical role in cancer processes such as metastasis, yet the number of imaging probes developed to target proteases is limited.

Developing the ideal probe for protease targeting can be difficult as there are a number of criteria that need to be met. The probes must: posses high affinity, such that they are reactive to the target site yet not so reactive that they bind to the enzyme in non-targeted tissues; be able to detect activity not just expression; bind to the active enzyme and distinguish it from other enzymes; emit distinctive signals for *in vivo* imaging, possess high stability and be able to access the target *in vivo* (i.e. be cell permeable).[2]

Over the course of this study an irreversible inhibitor and a substrate have been explored as synthons to develop imaging probes for the cysteine protease cathepsin B, a protease frequently implicated in cancer metastasis. Many of these criteria were met when developing these probes yet achieving all within a single compound proved challenging. A series of iodinated prosthetic groups were used to modify a known cathepsin B inhibitor (**2.6a** and **2.6b**) in such a way to maintain affinity for cathepsin B (Chapter 2). A new probe was identified (**2.23a**) and was used to detect the isolated active enzyme; however high *in vivo* stability was not established preventing the agent from accessing the target in sufficient quantities. Not all derivatives were tested *in vivo* because they had lower cathepsin B affinity than **2.23a**; however they may poses greater *in vivo* stability, which is yet to be explored. Iodotriazoles such as **2.24** or *m*-

iodobenzamides such as **2.23b** could have reduced *in vivo* deiodination[3,4] and may be worth testing *in vivo* despite their slightly slower binding affinity.

This early work led to the development of probes with more stable prosthetic groups, featuring the tricarbonyl rhenium core (Chapter 3). This was applied to a direct labelling strategy as well as multimeric dendrimer probes. Although this strategy did not yield probes with high affinity, the moderate affinity may be suitable for *in vivo* imaging, especially if there is improved stability.

Due to the challenge in producing high affinity probes with stable prosthetic groups a bioorthogonal strategy was employed (Chapter 4). Using this strategy, a chemical reporter (**4.5**) was developed that maintained good affinity for the target enzyme. When used with a suitable bioorthogonal partner, intracellular active cathepsin B was detected in whole cells; however a related cysteine protease was also labelled. This approach resulted in the most promising results toward meeting the required criteria for protease probe development. Further *in vivo* assessment is required to realize the true potential of this approach.

The last approach that was explored involved the use of a cathepsin B substrate (Chapter 5). A preliminary attempt was made to link known

radiopharmaceuticals, FDG and an iodobenzamide to the Z-Phe-Lys substrate through a PABA linker. The goal was to develop a means to improve the T:NT ratios in tumor cells through signal enhancement while decreasing non-target uptake through dual targeting. One of the potential challenges with this approach is that the probe release at the target site must occur rapidly and efficiently to prevent premature washout. Once the construct is developed the release rate and tumor uptake would need to be compared with non-cathepsin B targeted analogues.

The importance of proteases in cancer progression is undeniable yet there are no imaging agents in clinical use, despite the numerous preclinical studies that indicate proteases are a viable target for assessing metastatic potential. This thesis explored new approaches and preclinical studies to meet this goal and in doing so contributes to furthering the field of molecular imaging.

6.1 References

1. M. A. Hamburg and F. S. Collins, *N. Engl. J. Med.*, 2010, **363**, 301–304.

2. L. E. Edgington, M. Verdoes, and M. Bogyo, *Curr. Opin. Chem. Biol.*, 2011, **15**, 798–805.

3. R. Yan, K. Sander, E. Galante, V. Rajkumar, A. Badar, M. Robson, E. El-Emir, M. F. Lythgoe, R. B. Pedley, and E. Årstad, *J. Am. Chem. Soc.*, 2013, **135**, 703–9.

4. D. M. Wieland, J. Wu, L. E. Brown, T. J. Mangner, D. P. Swanson, and W. H. Beierwaltes, *J. Nucl. Med.*, 1980, **21**, 349–353.